

Politecnico di Torino

Master of Science Degree in Civil Engineering

Structural Engineering



***Developing an expeditious protocol for a simplified assessment
of the seismic risk in seismic zones***

Supervisors:

Prof. Bernardino Chiaia

Prof. Marco Civera

Matteo Dalamasso

Candidate:

Zahra Haqi

July 2025

Abstract

This thesis explores how we can better understand and assess earthquake risks in some of Italy's most seismically active regions. The focus is on evaluating how vulnerable buildings are to earthquakes by developing empirical fragility curves for typical residential structures, focusing on reinforced concrete and masonry buildings. These curves are based on extensive post-earthquake damage data collected from events between 1976 and 2012, sourced from the Da.D.O. platform, which offers detailed records on building locations, construction types, and the extent of observed damage.

The research uses the Rosti framework to refine the fragility curves for reviewing and validating the input data to ensure consistency and quality. Municipalities with incomplete surveys were excluded, leaving the Irpinia 1980 and L'Aquila 2009 earthquake datasets as the most complete and reliable case studies.

The modeling process links Peak Ground Acceleration (PGA) values taken (from Da.D.O. shakemaps) to each building's location and damage report. Damage levels are based on the EMS-98 classification system, which outlines six levels of structural damage. These levels are further adapted to distinguish between structural elements and infill wall damage, giving a more accurate picture of building performance during earthquakes.

A key innovation in this thesis is shifting from traditional lognormal distributions to the Generalized Extreme Value (GEV) distribution for fragility modeling, aiming to produce more conservative damage predictions. This change, implemented through custom Python tools, leads to more neat, accurate, and realistic predictions of how buildings will likely respond to seismic events.

The result is a set of redefined fragility curves that can estimate the probability of damage to buildings based on their design level, building height, and the ground motion intensity they experience. These predictive models are valuable for seismic design and planning and offer practical benefits for the insurance industry, allowing for more informed risk assessments and resilience planning.

Key Words: Seismic Hazard, Vulnerability, Italy, DaDO, PGA, GEV Distribution, Risk Assessment.

Acknowledgment

The past few years have been a journey filled with lessons, growth, joy, and challenges. I have learned, succeeded, stumbled, and grown again. Along the way, I have been lucky to have people who offered their help, guidance, and kindness.

I want to sincerely thank my professors for their support and for the knowledge they shared with me.

To my parents, my mom and dad, my Rafat and my Masoud, and to my sisters, my Maryam and my Zahra, firstly, thank you for everything. Even when we were far apart, you were with me every step of the way, giving me courage, assurance, hope, and love. Though we may have been separated by distance, our souls were never apart. My heart always belongs to you. Thank you again for being my family and for being my reason.

To my friends, you made life much easier and more enjoyable. You were a light in my dark days. Thank you for your patience and for believing in me even when I struggled to believe in myself.

Lastly, to my younger self, for being bold enough and brave enough to make hard decisions, for believing that good things come with effort, and for picking herself up over and over again to keep moving forward.

This thesis is as much yours as it is mine, and I am grateful beyond words to all who have walked this path with me.

Table of Contents	
Abstract	2
Table of figures	6
Introduction	10
Description and History of the Topic	10
Statement of the Research Subject	11
Importance of the Research	12
Novelty and significance of this work and the Literature Review	13
Novelty and Significance	13
Dynamic analysis	13
Demand and Response Spectra	13
Related Studies	14
Fragility Curves	15
Empirical Seismic Vulnerability Model	16
Masonry Paper (Unreinforced Masonry Buildings - URM) (Annalisa Rosti, Rota, and Penna 2021)	16
RC Paper (Reinforced Concrete Buildings) (A Rosti et al. 2021).....	17
Methodology/Analysis Framework	21
Data Collection and Validation	21
Sources of Seismic Data	21
Quality Control and Validation of Post-Earthquake Survey Data	22
Completeness Analysis	22
Selection of Focus Events	22
Seismic Intensity Measures and Damage Classification	25
Introduction to Typology Classification	26
Development of Fragility Curves	36
Distributions	36
Lognormal distribution	36
Generalized extreme value distribution	38
Results and Analysis	40
Histogram and Lognormal Distribution	40
Concrete buildings	41
Masonry buildings	70
Comparison between methods	96

Histograms and GEV Distribution:	97
Concrete buildings:	98
Masonry buildings	125
Study case	156
Modelling	156
Fragility curves	159
Conclusion	160
References	162

Table of figures

Figure 1. Components of Risk and Their Interrelation	11
Figure 2. Spectral curve with yield, ultimate points, and damage levels.....	14
Figure 3. Probability curve showing expected damage levels based on shaking intensity and spectral response	16
Figure 4. Classification of damage grades based on EMS98, Hazus definitions, and Eurocode 8 limit states	20
Figure 5. Visual classification of earthquake damage grades for masonry and reinforced concrete buildings, from slight damage to destruction.....	21
Figure 6. Map of completeness ratio for surveyed municipalities near the earthquake epicenter	23
Figure 7. Map showing the L'Aquila input data and locations of surveyed structures.....	24
Figure 8. Abruzzo and Campania regions showing surveyed structures in L'Aquila and Irpinia provinces	24
Figure 9. Comparison of Concrete damage scales for vertical structures and infills/partitions from the 1980 Irpinia and 2009 L'Aquila earthquakes	25
Figure 10. Comparison of masonry damage scales from the 1980 Irpinia and 2009 L'Aquila earthquakes, based on EMS-98 descriptions and extent of damage	26
Figure 11. Irpinia construction year distribution based on the percentage of surveyed reinforced concrete buildings	27
Figure 12. Irpinia design level distribution by reinforced concrete building height and structural category	27
Figure 13. L'Aquila construction year distribution based on the percentage of surveyed reinforced concrete buildings	28
Figure 14. L'Aquila design level distribution by reinforced concrete building height and structural category	28
Figure 15. Irpinia reinforced concrete building height distribution by percentage of low-, medium-, and high-rise structures	29
Figure 16. Irpinia floor distribution showing the percentage of reinforced concrete buildings by number of floors, 29	
Figure 17. L'Aquila reinforced concrete building height distribution by percentage of low-, medium-, and high-rise structures.....	30
Figure 18. L'Aquila floor distribution showing the percentage of reinforced concrete buildings by number of floors, 30	
Figure 19. Irpinia construction year distribution based on the percentage of surveyed masonry buildings.....	32
Figure 20. L'Aquila construction year distribution based on the percentage of surveyed masonry buildings.....	33
Figure 21. Irpinia masonry building height distribution by percentage of low-, medium-, and high-rise structures	33
Figure 22. Irpinia floor distribution showing the percentage of masonry buildings by number of floors, 34	
Figure 23. L'Aquila masonry building height distribution by percentage of low-, medium-, and high-rise structures.....	34

Figure 24. L'Aquila floor distribution showing the percentage of masonry buildings by number of floors	35
Figure 25. Number of masonry buildings by category and height, showing the distribution across low-rise, medium-rise, and high-rise structures.....	36
Figure 26. Generalized Extreme Value (GEV) distribution curves for different shape parameters (ξ), illustrating variations in density behavior	39
Figure 27. Comparison of lognormal and GEV distributions against Monte Carlo (MC) simulation results, shown through probability density function (PDF) and cumulative distribution function (CDF) plots	40
Figure 28. Low-rise gravity load building response for all damage levels, showing frequency distribution and comparison between lognormal PDF (input) and lognormal PDF (Rosti input) for each damage state	43
Figure 29. Low-rise Seismic pre81 building response for all damage levels, showing frequency distribution and comparison between lognormal PDF (input) and lognormal PDF (Rosti input) for each damage state	46
Figure 30. Low-rise Seismic post81 building response for all damage levels, showing frequency distribution and comparison between lognormal PDF (input) and lognormal PDF (Rosti input) for each damage state	49
Figure 31. medium-rise gravity load building response for all damage levels, showing frequency distribution and comparison between lognormal PDF (input) and lognormal PDF (Rosti input) for each damage state	52
Figure 32. medium-rise Seismic pre81 building response for all damage levels, showing frequency distribution and comparison between lognormal PDF (input) and lognormal PDF (Rosti input) for each damage state	55
Figure 33. medium-rise Seismic post81 building response for all damage levels, showing frequency distribution and comparison between lognormal PDF (input) and lognormal PDF (Rosti input) for each damage state	58
Figure 34. high-rise gravity load building response for all damage levels, showing frequency distribution and comparison between lognormal PDF (input) and lognormal PDF (Rosti input) for each damage state	61
Figure 35. high-rise Seismic pre81 building response for all damage levels, showing frequency distribution and comparison between lognormal PDF (input) and lognormal PDF (Rosti input) for each damage state	64
Figure 36. medium-rise Seismic post81 building response for all damage levels, showing frequency distribution and comparison between lognormal PDF (input) and lognormal PDF (Rosti input) for each damage state	67
Figure 37. Cumulative distribution functions (CDFs) for low-rise, medium-rise, and high-rise buildings under gravity load, seismic pre-81, and seismic post-81 design levels, comparing input and Rosti lognormal curves across all damage states (DS1–DS5).	68
Figure 38. IRR-F-NCD damage level distributions (DS1–DS5) for masonry buildings.....	72
Figure 39. IRR-F-CD damage level distributions (DS1–DS5) for masonry buildings.....	75
Figure 40. IRR-R-NCD damage level distributions (DS1–DS5) for masonry buildings	78
Figure 41. IRR-R-CD damage level distributions (DS1–DS5) for masonry buildings	81

Figure 42. REG-F-NCD damage level distributions (DS1–DS5) for masonry buildings	84
Figure 43. REG-F-CD damage level distributions (DS1–DS5) for masonry buildings	87
Figure 44. REG-R-NCD damage level distributions (DS1–DS5) for masonry buildings	89
Figure 45. REG-R-CD damage level distributions (DS1–DS5) for masonry buildings	92
Figure 46. IRR-F-NCD cumulative distribution functions (CDFs) and comparison between input data and Rosti figures	92
Figure 47. IRR-F-CD cumulative distribution functions (CDFs) and comparison between input data and Rosti figures	93
Figure 48. IRR-R-NCD cumulative distribution functions (CDFs) and comparison between input data and Rosti figures	93
Figure 49. IRR-R-CD cumulative distribution functions (CDFs) and comparison between input data and Rosti figures	94
Figure 50. REG-F-NCD cumulative distribution functions (CDFs) and comparison between input data and Rosti figures	94
Figure 51. REG-F-CD cumulative distribution functions (CDFs) and comparison between input data and Rosti figures	95
Figure 52. REG-R-NCD cumulative distribution functions (CDFs) and comparison between input data and Rosti figures	95
Figure 53. REG-R-CD cumulative distribution functions (CDFs) and comparison between input data and Rosti figures	96
Figure 54. GEV distribution for low-rise gravity load concrete buildings across all damage levels	100
Figure 55. GEV distribution for low-rise seismic pre-81 concrete buildings across all damage levels	103
Figure 56. GEV distribution for low-rise seismic post-81 concrete buildings across all damage levels	106
Figure 57. GEV distribution for medium-rise gravity load concrete buildings across all damage levels	109
Figure 58. GEV distribution for medium-rise seismic pre-81 concrete buildings across all damage levels	112
Figure 59. GEV distribution for medium-rise seismic post-81 concrete buildings across all damage levels	115
Figure 60. GEV distribution for high-rise gravity load concrete buildings across all damage levels	118
Figure 61. GEV distribution for high-rise seismic pre-81 concrete buildings across all damage levels	121
Figure 62. GEV distribution for high-rise seismic post-81 concrete buildings across all damage levels	124
Figure 63. GEV distribution for IRR-F-CD masonry buildings across all damage levels	127
Figure 64. GEV distribution for IRR-F-NCD masonry buildings across all damage levels	130
Figure 65. GEV distribution for IRR-R-NCD masonry buildings across all damage levels	133
Figure 66. GEV distribution for REG-F-CD masonry buildings across all damage levels	136
Figure 67. GEV distribution for REG-F-NCD masonry buildings across all damage levels	139

Figure 68. GEV distribution for REG-R-NCD masonry buildings across all damage levels.....	142
Figure 69. GEV distribution for IRR-R-CD masonry buildings across all damage levels.....	145
Figure 70. GEV distribution for REG-R-CD masonry buildings across all damage levels	147
Figure 71. Cumulative distribution functions (CDFs) of the GEV distribution for concrete buildings with shape parameter $\xi = -0.5$	148
0.145	
Figure 73. Cumulative distribution functions (CDFs) of the GEV distribution for concrete buildings with shape parameter $\xi = 0.5$	150
Figure 74. Adjusted Generalized Extreme Value (GEV) and lognormal CDFs for concrete buildings.....	151
Figure 75. Cumulative distribution functions (CDFs) of the GEV distribution for masonry buildings with shape parameter $\xi = -0.5$	153
0.148	
Figure 77. Cumulative distribution functions (CDFs) of the GEV distribution for masonry buildings with shape parameter $\xi = 0.5$	154
Figure 78. Adjusted Generalized Extreme Value (GEV) for masonry buildings	155
Figure 79. Building location distribution in Torino and Piemonte, Italy.....	156
Figure 80. Map of input building data across Torino, Italy, showing spatial distribution of surveyed structures used in the analysis.....	157
Figure 81. Torino construction year distribution based on the percentage of surveyed buildings	158
Figure 82. Torino building height distribution by percentage of low-, medium-, and high-rise structures	158
Figure 83. Fragility curves of Torino using the Generalized Extreme Value (GEV) distribution for reinforced concrete (RC) buildings across all heights, design levels, and damage levels.....	160

Introduction

Description and History of the Topic

Earthquakes are among the most devastating natural disasters, which can cause huge damage to buildings and infrastructure, disrupting lives, and leaving lasting social and economic impacts. While they may not happen often, when they do, their effects can be long-lasting, leading to injuries, loss of life, displacement, and long, difficult recovery periods.

Because earthquakes can have devastating impacts, assessing seismic risk has become a top priority for researchers, city planners, and policymakers. These assessments are crucial in emergency response plans, strengthening at-risk buildings, and helping communities prepare for future quakes. They also ensure that limited resources are used wisely, focusing attention and funding on the places that need it most, to minimize damage and build resilience.

In the face of such devastating impacts, the need for better tools, more reliable data, and smarter methods to make earthquake risk predictions more accurate and useful has never been more urgent. Governments, city planners, and the insurance world rely on solid data and accurate models to determine the risk level, set fair insurance premiums, and design coverage that can truly protect people and their property. This growing need is a call to action for all of us to work towards a safer, more resilient future.

In recent years, many studies have focused on understanding the impact of earthquakes and finding ways to reduce future damage. Italy, with its long history of seismic activity, has played a major role in the progression of this research. One of the country's most valuable contributions is the Da.D.O. platform—a national database that collects detailed information from post-earthquake building surveys. With its comprehensive records of how buildings were damaged, their structural features, and the intensity of the ground shaking, this platform has become a crucial resource for researchers working to improve seismic risk assessments and develop more accurate models for predicting earthquake damage.

Researchers, the driving force behind progress, have used data from the Da.D.O. platform to develop new and more effective ways to assess earthquake risk. This rich dataset, a testament to their dedication, makes it possible to build empirical fragility curves and vulnerability models, while also helping to identify patterns and trends in how buildings respond to earthquakes. As a result, Da.D.O. has become a resource for deepening our understanding of seismic risk and shaping better strategies to protect both lives and property.

Statement of the Research Subject

Seismic risk is a complex, multi-faceted concept that reflects the combination of three key factors: the intensity of potential earthquakes (seismic hazard), how vulnerable buildings and infrastructure are (structural vulnerability), and how many people and assets are at risk (exposure). In simple terms, seismic risk represents the chance that earthquake-related losses—such as damage, injuries, or economic costs—will exceed a certain level within a specific area and time frame. Probabilistic models often measure this to estimate how likely serious impacts will occur.

This kind of calculation often looks at the combined losses from multiple earthquakes over time, making it essential to create smart, long-term strategies to manage and reduce seismic risk effectively.



Figure 1. Components of Risk and Their Interrelation

A key component of seismic risk assessment is the development of fragility curves—tools that estimate the probability of different levels of damage occurring in buildings under specific seismic conditions. Traditionally, these curves have been modeled using the lognormal distribution, but recent advancements have introduced new approaches, such as the Generalized Extreme Value (GEV) distribution.

This study looks at how we model earthquake damage using the GEV (Generalized Extreme Value) distribution to redefine fragility curves, building on earlier methods like the Rosti framework. GEV is better at handling extreme cases than the more commonly used lognormal model, which is especially important when discussing earthquakes. It does a much better job estimating the chances of rare but catastrophic events, like a building collapsing during a major quake. These extreme scenarios might not happen often, but the consequences are huge when they do. That is why capturing them accurately is important for creating realistic and trustworthy risk assessments.

Using the GEV distribution in fragility modeling, this study aims to make seismic risk assessments more accurate and dependable. This improved method gives a clearer picture of how buildings will likely behave during earthquakes, which helps guide smarter decisions about where to focus resources. In the long run, it supports more effective planning for earthquake preparedness, risk reduction, and building stronger, more resilient communities.

Importance of the Research

Earthquakes pose a serious risk to people, infrastructure, and the overall stability of communities. That is why accurately assessing seismic risk and understanding the most vulnerable structures is so important. This research offers a new and improved way to make evaluations more precise and dependable.

The importance of this research lies in the following key areas:

1. Improved Risk Prediction:

By applying the Generalized Extreme Value (GEV) distribution to fragility modeling, this research offers a better way to predict earthquake damage. Unlike the traditional lognormal model, GEV is more effective at capturing rare but devastating events, which are the scenarios that matter most when preparing for major earthquakes and planning effective disaster responses.

2. Data-Driven Insights:

This study draws on the rich data from the Da.D.O. platform, ensuring the findings are rooted in real-life experiences from past earthquakes. By using detailed information about how buildings were damaged, it becomes possible to understand better which structures are most vulnerable and to refine the models we use to predict future damage more accurately.

3. Support for Policy and Decision-Making:

Accurate seismic risk assessments are crucial for helping policymakers, urban planners, and engineers make smart, informed decisions. This research supports efforts to identify which buildings need retrofitting most urgently, use available resources best, and strengthen communities to better prepare for future earthquakes.

4. Applications in Insurance and Reinsurance:

Predicting potential losses more accurately is valuable for the insurance and reinsurance industries. This research offers tools to estimate the chances of buildings failing during an earthquake and helps to calculate the financial risks involved.

Novelty and significance of this work and the Literature Review

Novelty and Significance

This study takes seismic risk assessment further by incorporating site-specific response spectra that reflect local conditions and seismic activity. This approach allows for more accurate predictions of how structures respond during an earthquake (Khatiwada et al. 2023). It also applies advanced statistical tools like the Generalized Extreme Value (GEV) distribution to better model rare, high-impact seismic events. This makes the assessment more reliable, especially for critical infrastructure, such as hospitals, bridges, and power plants (Rohmer et al. 2020).

Additionally, using probabilistic demand spectra helps account for the uncertainties in seismic hazards and how structures respond, offering a stronger and more flexible foundation for retrofitting strategies and disaster preparedness (Shahi and Baker 2011). By drawing on real-world data from the 2009 L'Aquila earthquake, this study connects theoretical advancements with practical applications by making a meaningful contribution to performance-based design approaches and developing more accurate fragility curves (A. Rosti et al. 2021).

Dynamic analysis

Dynamic analysis evaluates how a structure responds to time-dependent forces, like those caused by earthquakes. It helps predict how buildings will behave during seismic events. A key part of this is modal analysis, which looks at a structure's natural vibration characteristics like its frequencies, mode shapes, and how it absorbs energy (damping). Understanding these properties is essential for designing buildings that can safely withstand earthquake forces. Recent studies have highlighted the benefits of using site-specific response spectra. By tailoring seismic input to match local soil and ground conditions, engineers can optimize structural designs for better performance during earthquakes.

Demand and Response Spectra

The response spectrum is a key tool in earthquake engineering. It shows the maximum response, such as displacement, velocity, or acceleration, of a simple structure (or oscillator) across a range of natural frequencies when exposed to a specific earthquake. This helps engineers understand how different buildings with their natural frequencies might respond to the same seismic event. We get the demand spectrum from the response spectrum, representing the force or displacement a structure is expected to experience during an earthquake. This is especially important in performance-based seismic design, where the goal is to match a building's performance to the demands of a likely earthquake.

One widely used approach is the Capacity Spectrum Method (CSM). It compares the demand spectrum with the building's capacity curve, which shows how much force the structure can handle. The two curves intersect at the performance point—a key indicator of how much damage or deformation the building will likely suffer in an earthquake.

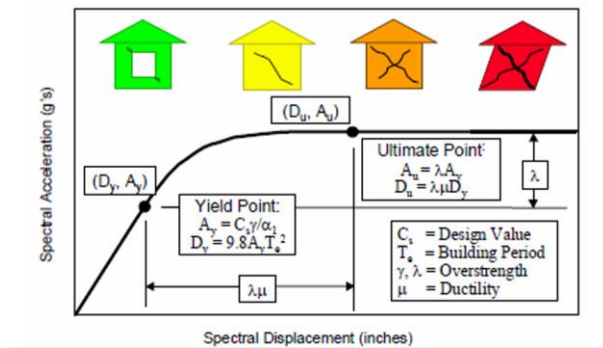


Figure 2. Spectral curve with yield, ultimate points, and damage levels

Several studies have highlighted the importance of customizing demand and response spectra to reflect site-specific seismic conditions. Factors like local soil type, ground motion characteristics, and regional seismic activity can significantly affect the shape and intensity of these spectra. By accounting for these local variations, advanced models have been developed to provide more accurate and reliable predictions of how structures will respond during earthquakes.

Furthermore, recent research has focused on probabilistic demand spectra, which account for uncertainties in both seismic hazard and how structures respond. Unlike traditional approaches that provide a single estimated value, these spectra offer a range of possible outcomes, making them especially useful for risk assessments. By incorporating this variability, probabilistic spectra give a more complete picture of potential structural demands during an earthquake. Their use in fragility analysis helps better identify building vulnerabilities and supports more informed decisions when planning retrofitting and mitigation strategies.

Related Studies

Many studies have contributed valuable insights into using response spectra in seismic design, particularly regarding inelastic behavior, ductility demand, and performance-based approaches. The study focuses on ductility demand response spectra, showing how different ground motion records affect the ductility demands of structures with varying stiffness. This highlights the importance of considering inelastic structural behavior when evaluating seismic performance and designing buildings to match it (Cheikh 1992).

A 2015 study from Geoscience World examines earthquake energy demand spectra, calculating input and plastic energy to assess a building's ability to dissipate energy and maintain resilience under different soil conditions (Lee, Johnson, and Kibble 2017). Another Geoscience World (2017) study proposes the drift spectrum as an alternative to traditional modal analysis, particularly for near-fault earthquakes with strong velocity pulses (Chopra and Chintanapakdee 2001).

For far-field earthquakes, identifies gaps in existing seismic codes and introduces improved response spectrum models that better capture long-period responses, especially for flexible soil profiles (Nabilah et al. 2023). A related study evaluates hysteretic energy and response spectra from the Turkey-Syria earthquake, offering insights into how different ductility levels affect energy dissipation (Shao 2024).

Lastly, combines nonlinear static pushover analysis with response spectra to predict seismic displacement demands, presenting a simplified yet effective method for performance-based seismic design (Elaiwi 2023).

Together, these studies enhance the understanding of how response spectra can be applied to more accurately model structural demands and support safer, more resilient seismic design strategies.

Fragility Curves

Fragility curves play a central role in seismic risk assessment, offering a probabilistic view of how likely structures are to experience different levels of damage during earthquakes. Over the years, many studies have advanced the methodology and application of fragility curve development.

Naumovski et al. (2023) used pushover analysis and the Capacity Spectrum Method (CSM) to develop fragility curves for the Philippine General Hospital Spine Building. Their work demonstrated the building's seismic resilience and emphasized the importance of fragility curves in safeguarding essential infrastructure (Naumovski et al. 2023)

Baylon et al. (2022) reinforced these insights by assessing critical healthcare infrastructure, emphasizing the fragility-based evaluation for emergency facilities in seismic zones (Baylon et al. 2022).

Banerjee et al. (2022) introduced a numerical simulation approach that incorporates probabilistic modeling to account for uncertainties in material properties, structural variations, and modeling assumptions. Their research showed the necessity of accurately defining parameters for trustworthy seismic vulnerability assessments (Banerjee, Das, and Roy 2022).

Zentner et al. (2008) supported this by demonstrating how material and model uncertainties significantly impact fragility curve reliability, particularly in nuclear structures (Zentner, Humbert, and Viallet 2008).

Caruso et al. (2023) compared generic fragility curves to site-specific ones, revealing that generalized models could misrepresent local vulnerabilities. Their study highlights the value of using localized seismic inputs and structural conditions to improve fragility accuracy (Caruso, Di Ludovico, and Prota 2023).

Milutinovic et al. (2018) compiled a set of fragility curves for various European buildings and advocated for standardized methods to enhance international comparability (Milutinovic, Trendafiloski, and Scherbaum 2018).

Wang et al. (2024) challenged the traditional lognormal model by applying ordinal regression to real bridge damage data from the Wenchuan earthquake, improving accuracy in complex seismic scenarios (Wang, Zhang, and Li 2024).

Together, these studies mark a step forward in fragility curve research. By tackling common challenges like uncertainty, limited data, and long computation times, they help keep fragility curves a key part of seismic risk analysis. More importantly, they open the door to broader, more practical applications, from designing safer buildings and retrofitting older ones to guiding disaster preparedness on both local and global levels.

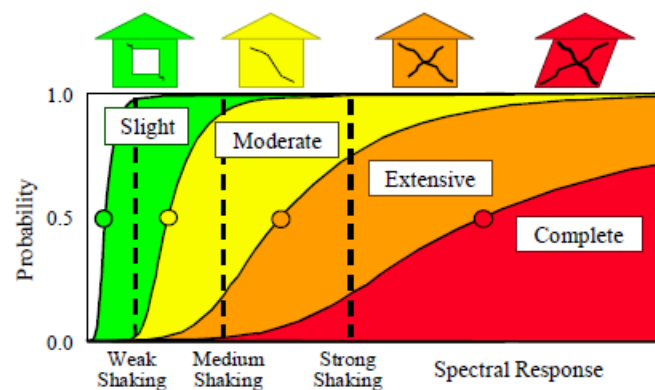


Figure 3. Probability curve showing expected damage levels based on shaking intensity and spectral response

Empirical Seismic Vulnerability Model

Masonry Paper (Unreinforced Masonry Buildings - URM)(Annalisa Rosti, Rota, and Penna 2021)

This study is about how Italian masonry buildings—especially older ones not built to withstand earthquakes—respond when the ground shakes. The authors wanted to find a way to predict the chances of different levels of damage, from minor cracks to total collapse. Moreover, they did not rely on computer simulations or lab tests to do that. Instead, they turned to real-life data from two big Italian earthquakes: Irpinia in 1980 and L’Aquila in 2009.

After those earthquakes, engineers had gone out and inspected thousands of buildings. That data in the Da.D.O. database includes not just whether a building was damaged, but also details like its height, age, construction materials, and design quality. The authors cleaned up this data to make sure it was reliable. For example, in some places, only buildings with visible damage were inspected, which would skew the numbers if undamaged buildings were left out. So the team included data from areas with very little shaking, assuming those buildings had no damage, to balance the picture.

The buildings were grouped by key features that affect how they perform in earthquakes, like whether their walls were made from good-quality stone or not, whether they had wooden floors (which are flexible and tend to shake more), and whether they had tie rods or beams to hold the structure together. These categories helped the researchers see which building types were more likely to get damaged.

Then, using a statistical technique, they built “fragility curves.” Imagine these as charts showing, for each building type, how likely it is to reach or exceed a certain level of damage when the ground shakes at a certain strength. The shaking is measured in terms of “PGA,” the strongest peak ground acceleration felt during the earthquake.

One of the interesting things is that buildings with irregular stone walls and no seismic devices (like tie rods) are far more likely to get damaged than those made with regular, high-quality masonry and some basic strengthening. Also, buildings with rigid floors (like concrete) did better than those with flexible ones (like wood). Furthermore, low-rise buildings (1–2 stories) generally performed better than taller ones, which makes sense because they are lighter and sway less.

To make these results usable for national planning, they sorted the buildings into three broader vulnerability classes: A (highly vulnerable), B (medium), and C1 (lower vulnerability). Then they matched these classes to census categories of buildings across Italy, so the results could be plugged into the IRMA risk platform—a tool that generates seismic risk maps for the country.

In short, the paper gives Italy a much better way to estimate which types of older masonry homes will most likely be damaged in future quakes.

RC Paper (Reinforced Concrete Buildings)(A Rosti et al. 2021).

This paper focuses on a different part of the building stock: residential buildings made with reinforced concrete (RC). These became more common in Italy in the mid-20th century, but not all were designed to handle earthquakes. Many older ones were built before seismic codes were even a thing.

Like the masonry paper, the researchers used real-world damage data from post-earthquake surveys, relying mainly on the Irpinia 1980 and L’Aquila 2009 events. They looked at about 24,000 RC buildings in total. However, they were careful—they did not just take all the data at face value. Instead, they filtered out towns where only damaged buildings had been inspected, because that would skew the results. Only data from towns where most buildings were checked (more than 90%) were kept for analysis. They also added buildings from areas with very weak shaking and assumed those had no damage, to help round out the data.

The authors focused on two key features of RC buildings:

1. **How they were designed:** were they built to resist earthquakes or only gravity loads
2. **How tall they are:** taller buildings tend to be more flexible and are more affected by seismic waves.

They used a consistent method to turn observed damage into a 6-level damage scale (from "no damage" to "collapse"), using official European criteria. They also included damage to things like infill walls and interior partitions—not just the structural frame, which is important because those can fail first and lead to costly repairs even if the main structure holds up.

Then, using the same kind of statistical modeling as in the masonry study, they created fragility curves for various building types, showing the likelihood of damage at different levels of shaking. These curves clearly show that buildings built only for gravity loads are far more fragile than those designed according to seismic codes. Interestingly, even among seismically designed buildings, newer codes (post-1981) made a noticeable difference in performance.

They also grouped these buildings into two vulnerability classes:

- **C2** for older RC buildings that might have followed some basic seismic principles but are not up to modern standards.
- **D** for newer, code-compliant buildings that are much more resistant.

They further broke down the fragility curves within each class by building height.

It is visible that if an RC building was built after Italy updated its seismic codes in 1981 and it is low-rise, it is much less likely to suffer heavy damage in a typical quake. However, older, taller buildings designed only for gravity loads could be at serious risk.

Again, all this feeds into the national IRMA platform, allowing planners to assess seismic risk block by block and street by street using actual observed performance, not just estimates or lab tests.

Over the years, researchers have made major progress in understanding and applying fragility curves, essential for assessing how structures might be damaged during earthquakes. One such study by Rohmer et al. (2020) applied a new approach using non-stationary extreme value theory, specifically the Generalized Extreme Value (GEV) distribution, to analyze how nuclear power plant components respond to seismic activity. Their method tackled uncertainties in how these structures behave under earthquake forces and helped improve risk assessments for critical infrastructure (Rohmer et al. 2020).

In a similar line of work, Zentner and Guéguen (2008) used Monte Carlo simulations to estimate fragility curves for nuclear facilities. They showed that relying on various statistical models—like the GEV distribution—can better reflect how different structures respond to earthquakes (Zentner, Humbert, and Viallet 2008).

Building on this, the U.S. Nuclear Regulatory Commission (2017) compared fragility models that use lognormal and GEV distributions. They found that GEV-based models often provide a more accurate picture of structures' behavior under extreme seismic forces and recommended their use in certain cases (Commission, Dasgupta, and Antonio 2017).

In Italy, Lucantoni et al. (2001) were pioneers in creating fragility curves for unreinforced masonry (URM) and reinforced concrete (RC) buildings. They used real earthquake damage data to reflect local construction types and vulnerabilities (Lucantoni, Dolce, and Moroni 2001).

Later, Di Pasquale et al. (2005) developed a vulnerability index system based on the EMS-98 scale to map potential earthquake damage across regions, laying the groundwork for Italy's broader seismic risk strategies (Di Pasquale, Orsini, and Romeo 2005).

Globally, researchers like Crowley et al. (2004) worked on integrating empirical damage data with probabilistic models, helping create better loss estimation tools by combining hazard, exposure, and vulnerability data (Crowley, Pinho, and Bommer 2004).

Meanwhile, Bernardini et al. (2010) emphasized the importance of having standardized damage surveys after earthquakes. Their work improved the data quality going into Italy's national seismic risk system, IRMA (Bernardini, Dolce, and Goretti 2010).

Rota et al. (2011) focused on how fragility curves are affected by peak ground acceleration (PGA) and seismic intensity. They tested their models against real earthquake data and confirmed the importance of ground motion in damage predictions (Rota et al. 2011).

On a larger scale, Silva (2014) helped develop the OpenQuake engine—software that allows engineers and researchers to assess seismic risk on a regional or national level. It combines uncertainty in hazard, vulnerability, and building exposure into a unified, probabilistic framework (Silva 2014).

From a policy perspective, the Philippines' National Disaster Risk Reduction and Management Council (2011) stressed fragility curves in disaster planning. They encouraged cooperation between institutions to improve data-sharing and long-term resilience ("National Disaster Risk Reduction and Management Plan (NDRRMP)" 2011).

In Italy, Dolce et al. (2021) thoroughly reviewed how vulnerability is assessed nationwide, blending historical damage data with newer analytical methods. They also pushed for policy updates to better prepare for future earthquakes (Masi et al. 2021).

Later, Del Gaudio et al. (2020) advanced fragility modeling by incorporating nonlinear dynamic analysis, especially for RC and masonry buildings in high-risk areas. Their study offered practical recommendations for choosing which buildings should be prioritized for retrofitting (Del Gaudio et al. 2020).

Finally, Rosti et al. (2021) updated empirical fragility curves tailored to Italy's unique seismic landscape, using damage data from recent earthquakes to reflect the country's evolving understanding of structural risk (A. Rosti et al. 2021).

These studies show how fragility curves have evolved from simple empirical tools into advanced, data-rich, and probabilistic models. Fragility curves play a vital role in seismic risk assessment by integrating methods like GEV modeling, improving data quality, addressing structural uncertainties, and tailoring outputs to local and global needs.

Damage level

The EMS-98 (European Macroseismic Scale 1998) is a widely used system for classifying earthquake damage to buildings, dividing structural damage into six clearly defined levels:

- D0 – No Damage: No visible damage to structural or non-structural elements.
- D1 – Slight Damage: Small cracks in plaster or superficial finishes; minor, non-structural issues.
- D2 – Moderate Damage: Visible cracks in load-bearing elements like walls; some deformation; moderate non-structural damage.
- D3 – Heavy Damage: Large cracks in structural components; partial collapse of non-structural elements; noticeable loss of integrity.
- D4 – Very Heavy Damage: Extensive cracking and deformation; severe damage to structural elements; localized collapses.
- D5 – Destruction: Near or total collapse of the building; structure is no longer usable.

This classification is essential for understanding how buildings perform under seismic loading, capturing structural and non-structural damage. Non-structural damage, like damage to facades, internal walls, or utility systems, is crucial for assessing a building's post-earthquake usability, even if the main structure remains standing.

In fragility analysis, D0 is usually excluded, as the focus lies on modeling the probability of reaching or exceeding damage levels D1 through D5. Fragility functions describe the likelihood of a structure reaching a specific damage state based on a seismic intensity measure (IM), such as Peak Ground Acceleration (PGA). This probabilistic approach allows for more accurate earthquake loss predictions, better-informed retrofitting strategies, and more efficient allocation of resources for seismic risk management.

The EMS-98 scale is the basis for many national and international seismic assessment frameworks and aligns with standards like Eurocode 8 (EC8). These frameworks promote consistent methods for damage classification and fragility curve development, making risk assessments more reliable and comparable across different regions. Integrating real-world damage data with seismic inputs, EMS-98 helps bridge the gap between theory and practice, strengthening earthquake preparedness and resilience strategies (Nabilah et al. 2023).

DM	EMS98 damage grades (D_k)	Other definition (Hazu)	Limit states (EC8)
1	Negligible to slight	Slight	Fully operational
2	Moderate	Moderate	Damage limitation
3	Substantial to heavy	Extensive	Significant damage
4	Very heavy	Complete	Near collapse
5	Destruction	–	–

Figure 4. Classification of damage grades based on EMS98, Hazus definitions, and Eurocode 8 limit states


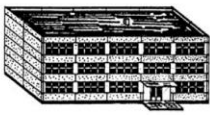

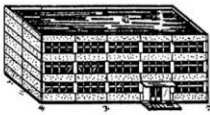






Masonry buildings	Reinforced concrete buildings	Classification of damages
		Grade 1: Negligible to slight damage (no structural damage, slight non-structural damage)
		Grade 2: Moderate damage (slight structural damage, moderate non-structural damage)
		Grade 3: Substantial to heavy damage (moderate structural damage, heavy non-structural damage)
		Grade 4: Very heavy damage (heavy structural damage, very heavy non-structural damage)
		Grade 5: Destruction (very heavy structural damage)

Figure 5. Visual classification of earthquake damage grades for masonry and reinforced concrete buildings, from slight damage to destruction

Methodology/Analysis Framework

Data Collection and Validation

Sources of Seismic Data

The Da.D.O. platform is a detailed online archive that collects and organizes damage data from buildings affected by earthquakes in Italy. As Dolce et al. (2021) described, it offers valuable insights into structural and non-structural damage observed after seismic events. The platform is built on data from inspections of more than 300,000 residential buildings carried out following Italian earthquakes that occurred between 1976 and 2012, making it one of the most comprehensive resources for studying how buildings perform during earthquakes (Masi et al. 2021).

The Da.D.O. database provides a rich source of information that helps researchers better understand how earthquakes affect buildings. It includes detailed data on:

- Building characteristics: The year of construction, number of floors, and structural type (e.g., unreinforced masonry or reinforced concrete).
- Building usage: Mostly focused on residential buildings, though some data from other types are included.
- Seismic parameters: In many cases, the database records values like peak ground acceleration (PGA) and peak ground velocity (PGV)—key indicators of how strong the shaking was in specific areas.
- Post-earthquake inspections: Damage is carefully documented through on-site surveys, using the EMS-98 damage scale to classify the severity. This creates a consistent and standardized view of how buildings perform during seismic events.

Quality Control and Validation of Post-Earthquake Survey Data

Reliable post-earthquake survey data is the foundation of accurate seismic risk assessments. A thorough review of all datasets from the Da.D.O. platform was carried out to ensure the data used in this study was trustworthy and consistent. The goal was to clean and standardize the data, ensuring it reflects how buildings respond to earthquakes. This process included:

Completeness Analysis

- A completeness ratio (CR) was calculated for each municipality, defined as the ratio of inspected buildings to the total number of residential buildings based on census data (ISTAT, 2001).
- Municipalities with low CR values (below 90%) were excluded. A higher CR ensures that damaged and undamaged buildings are represented, mitigating the risk of overestimating fragility due to focusing only on damaged structures.

Selection of Focus Events

- The datasets for the Irpinia 1980 and L'Aquila 2009 earthquakes were selected as the most reliable due to their high completeness ratios.
- For the 2009 L'Aquila earthquake, a selected group of municipalities reached a completeness ratio (CR) greater than 90%, meaning the post-earthquake surveys in these areas were representative. The municipalities with high CR include:

Acciano, Barisciano, Castel di Ieri, Castelvechio Calvisio, Caporciano, Carapelle Calvisio, Castel del Monte, Calascio, Campotosto, L'Aquila, Lucoli, Fontecchio, Fossa, Collepietro, Fagnano Alto, Goriano Sicoli, Castelvechio Subequo, Gagliano Aterno, Prata d'Ansidonia, Rocca di Mezzo, San Demetrio ne' Vestini, Rocca di Cambio, Pizzoli, Ocre, Poggio Picenze, Ofena, San Pio delle Camere, Navelli, San Benedetto, Villa Sant'Angelo, Scoppito, Santo Stefano di Sessanio, Villa Santa Lucia degli Abruzzi, Tione degli Abruzzi, Sant'Eusanio Forconese, Tornimparte.

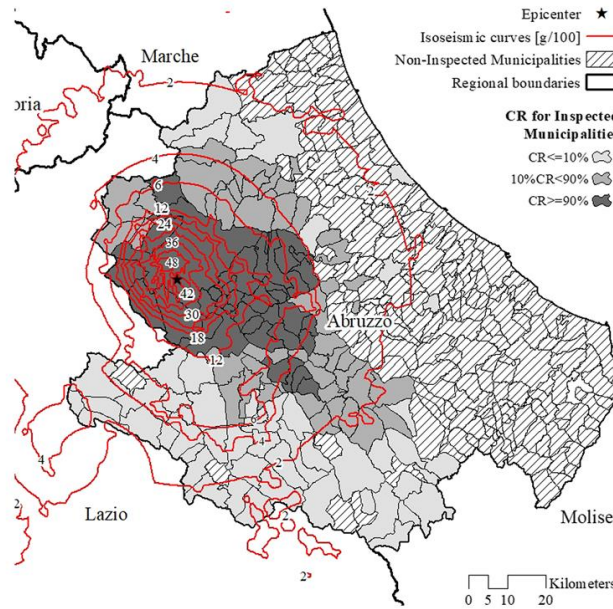


Figure 6. Map of completeness ratio for surveyed municipalities near the earthquake epicenter

These municipalities provided especially valuable data for fragility analysis, as the surveyed buildings represent the majority of the residential structures in the area.

Data Filtering and Refinement

The original Da.D.O. database underwent filtering to focus on structural typologies and usage categories:

- Only residential buildings were included, excluding structures with non-residential uses.
- Buildings with vertical load-bearing structures other than moment-resisting frames (MRF), such as structural walls or mixed systems, were removed.
- Databases from events with negligible representation of reinforced concrete (RC) buildings (e.g., Umbria-Marche 1997; Emilia 2003) or lacking damage data for infills and partitions (e.g., Friuli 1976; Abruzzo 1984) were removed.



Figure 7. Map showing the L'Aquila input data and locations of surveyed structures

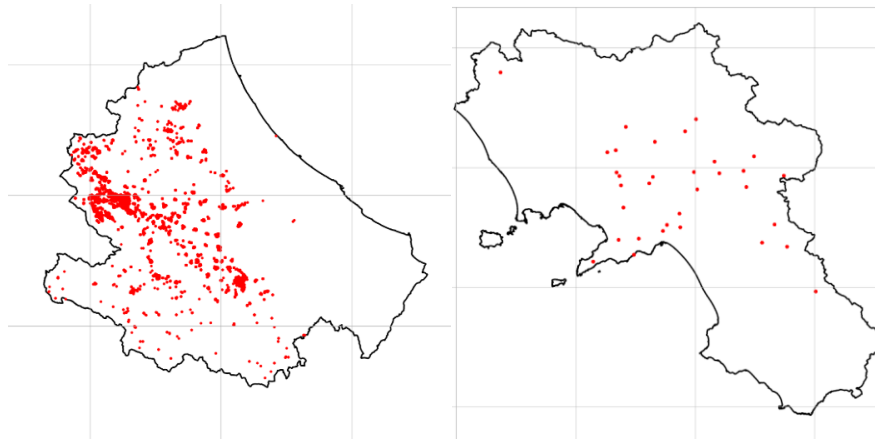


Figure 8. Abruzzo and Campania regions showing surveyed structures in L'Aquila and Irpinia provinces

Seismic Intensity Measures and Damage Classification

- Use of Peak Ground Acceleration (PGA) as an Intensity Measure

Peak Ground Acceleration (PGA) is a key indicator in seismic risk analysis, capturing the highest level of ground acceleration during an earthquake. This study uses PGA as a standard measure of earthquake intensity to assess building fragility across different datasets. To maintain consistency, only buildings with PGA values greater than 0.06g were included in the L'Aquila and Irpinia datasets. This threshold ensures that only structures exposed to significant ground motion are analyzed, making comparing the two earthquake events more reliable.

- Application of the EMS-98 Damage Scale for Classifying Structural and Non-Structural Damage

The European Macroseismic Scale (EMS-98) is applied in this study to classify building damage levels. It distinguishes between structural damage (affecting load-bearing elements) and non-structural damage (such as damage to infills and partition walls). This classification is used for masonry and reinforced concrete (RC) buildings. Damage data for the Irpinia 1980 and L'Aquila 2009 earthquakes are presented using this scale.

	Irpinia 1980		L'Aquila 2009	
	Vertical structures	Infills/partitions	Vertical structures	Infills/partitions
DS0	No damage	No damage	D0	D0
DS1	Insignificant Negligible	Insignificant Negligible	D1-< 1/3	D1-< 1/3
			D1-1/3-2/3	D1-1/3-2/3
			D1-> 2/3	D1-> 2/3
DS2	Considerable Serious	Considerable Serious	D2-D3-< 1/3	D2-D3-< 1/3
				D2-D3-1/3-2/3
				D2-D3-> 2/3
DS3	Very serious	Very serious Partially-collapsed Collapsed	D2-D3-1/3-2/3	D4-D5-< 1/3
			D2-D3-> 2/3	D4-D5-1/3-2/3
				D4-D5-> 2/3
DS4	Partially-collapsed		D4-D5-< 1/3	
			D4-D5-1/3-2/3	
DS5	Collapsed		D4-D5-> 2/3	

○

Figure 9. Comparison of Concrete damage scales for vertical structures and infills/partitions from the 1980 Irpinia and 2009 L'Aquila earthquakes

EMS-98	Damage Description		
	Irpinia (1980)	L'Aquila (2009)	
		Damage level	Extent
DS0	No damage	No damage (D0)	
DS1	Insignificant Slight	Slight (D1)	$e < 1/3$
		Slight (D1)	$1/3 < e < 2/3$
		Slight (D1)	$e > 2/3$
DS2	Considerable Serious	Medium-severe (D2-D3)	$e < 1/3$
DS3	Very serious	Medium-severe (D2-D3)	$1/3 < e < 2/3$
		Medium-severe (D2-D3)	$e > 2/3$
DS4	Partially-collapsed	Very heavy (D4-D5)	$e < 1/3$
		Very heavy (D4-D5)	$1/3 < e < 2/3$
DS5	Collapsed	Very heavy (D4-D5)	$e > 2/3$

○

Figure 10. Comparison of masonry damage scales from the 1980 Irpinia and 2009 L'Aquila earthquakes, based on EMS-98 descriptions and extent of damage

Building Typology Classification

Introduction to Typology Classification

This process involves grouping structures based on key characteristics such as construction age, number of floors, structural systems, and overall design approach. By organizing buildings this way, researchers can better understand how different types perform during earthquakes and identify where mitigation efforts should be focused.

The Irpinia 1980 and L'Aquila 2009 datasets offer detailed information on masonry and reinforced concrete (RC) buildings. These structures are categorized according to their vulnerability-related features, capturing changes in construction practices and seismic design standards over time.

Reinforced Concrete (RC) Buildings

Construction Age:

Irpinia 1980 Dataset: Nearly all RC buildings were constructed before the municipality's seismic classification in 1981 (Ministerial Decree 7/3/1981). These buildings were designed for gravity loads, making them highly vulnerable to seismic events.

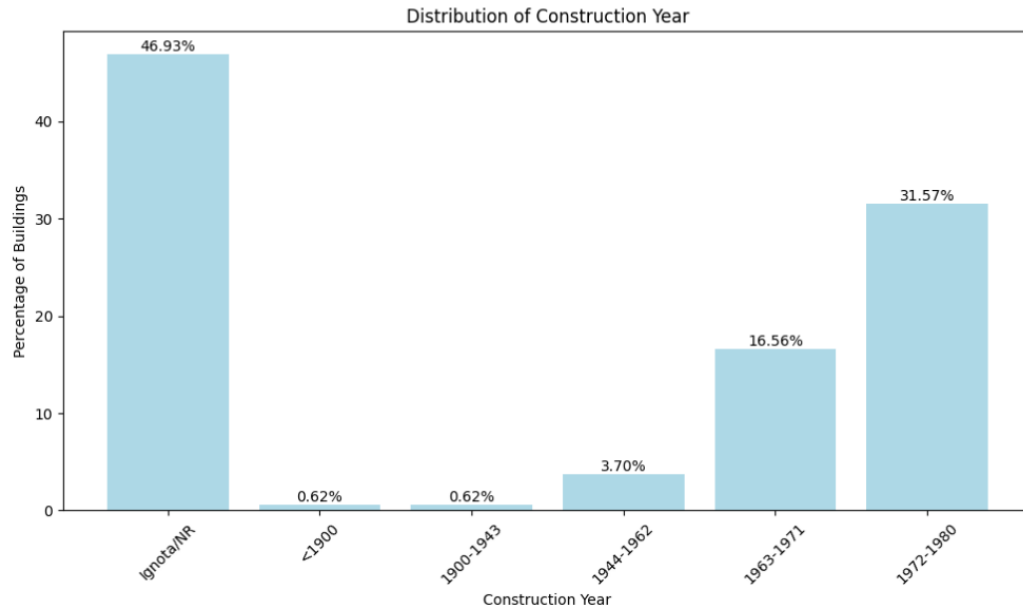


Figure 11. Irpinia construction year distribution based on the percentage of surveyed reinforced concrete buildings

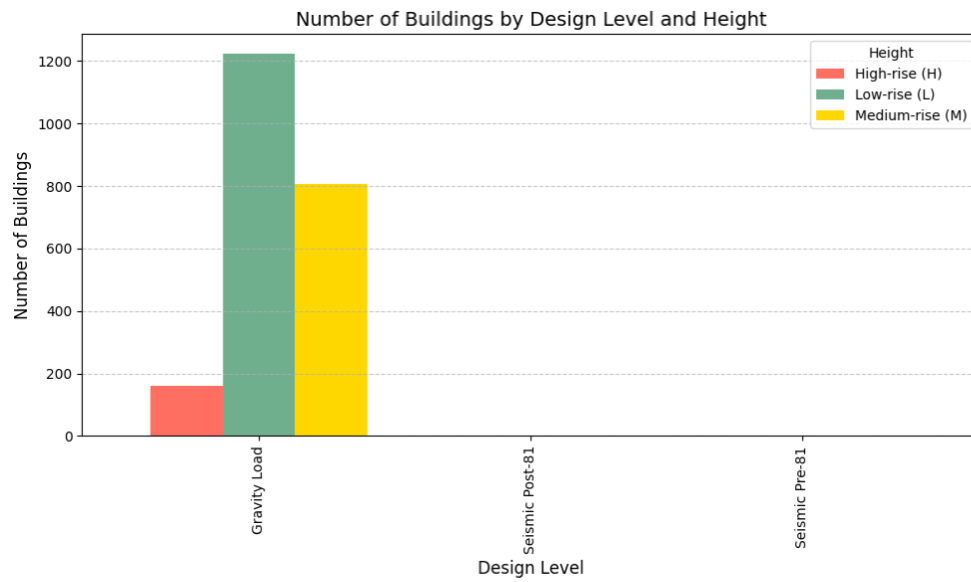


Figure 12. Irpinia design level distribution by reinforced concrete building height and structural category

L'Aquila 2009 Dataset: Most buildings were constructed after the seismic classification introduced by Royal Law n.573 (1915). These buildings were seismically designed to resist earthquakes.

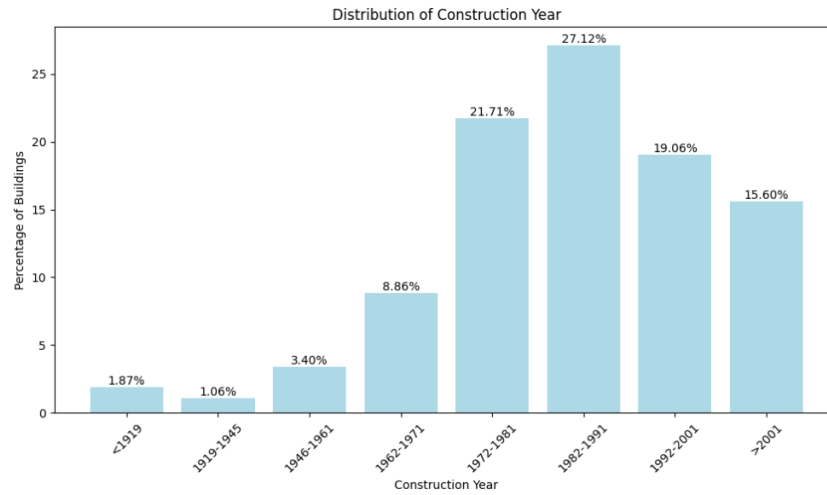


Figure 13. L'Aquila construction year distribution based on the percentage of surveyed reinforced concrete buildings

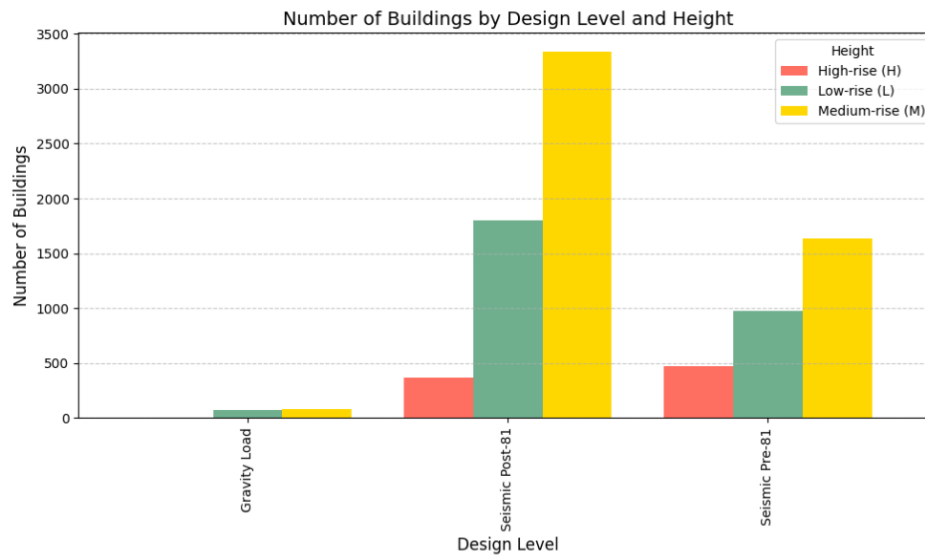


Figure 14. L'Aquila design level distribution by reinforced concrete building height and structural category

Irpinia 1980 Dataset: Predominantly low-rise structures:

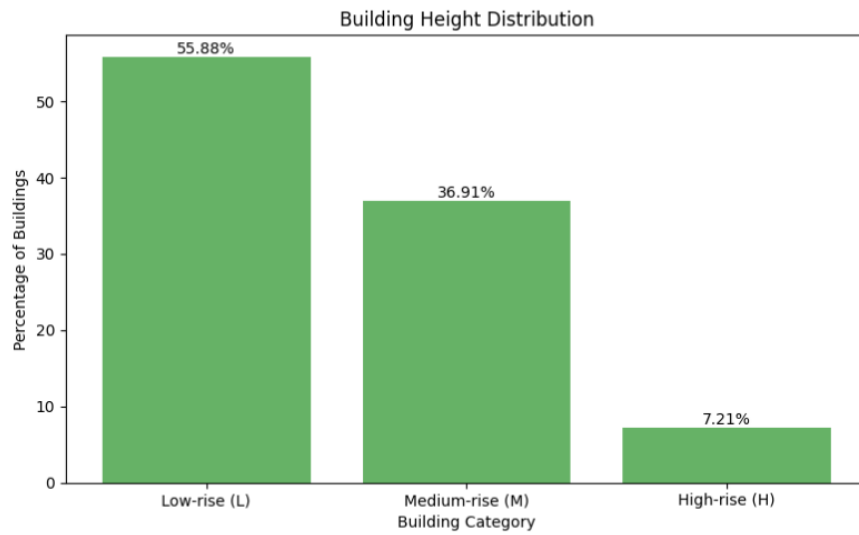


Figure 15. Irpinia reinforced concrete building height distribution by percentage of low-, medium-, and high-rise structures

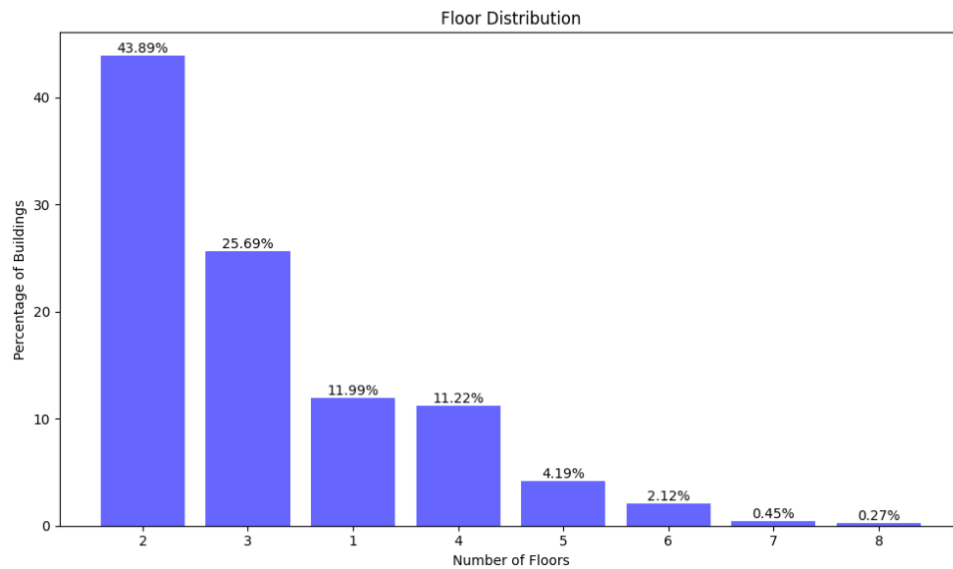


Figure 16. Irpinia floor distribution showing the percentage of reinforced concrete buildings by number of floors

L'Aquila 2009 Dataset: Taller buildings dominate:

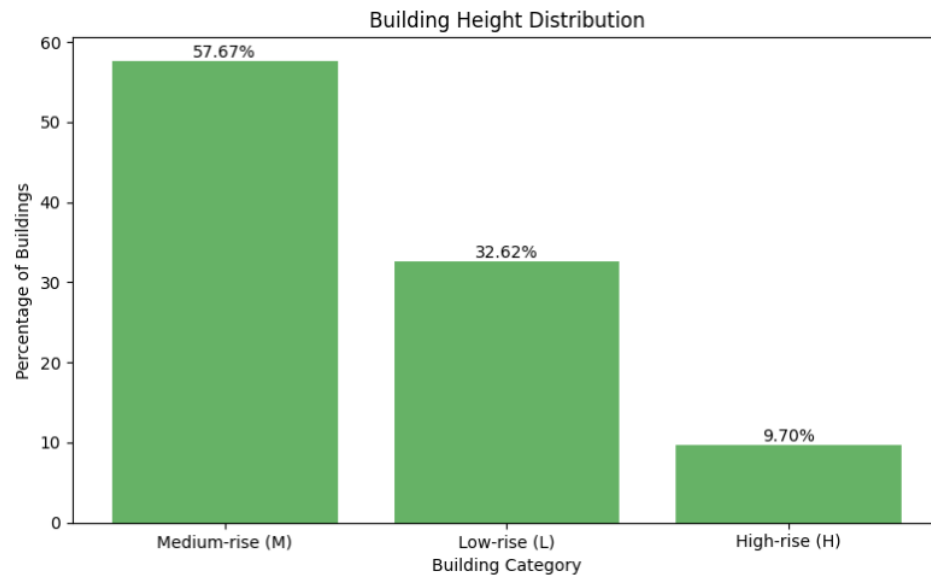


Figure 17. L'Aquila reinforced concrete building height distribution by percentage of low-, medium-, and high-rise structures

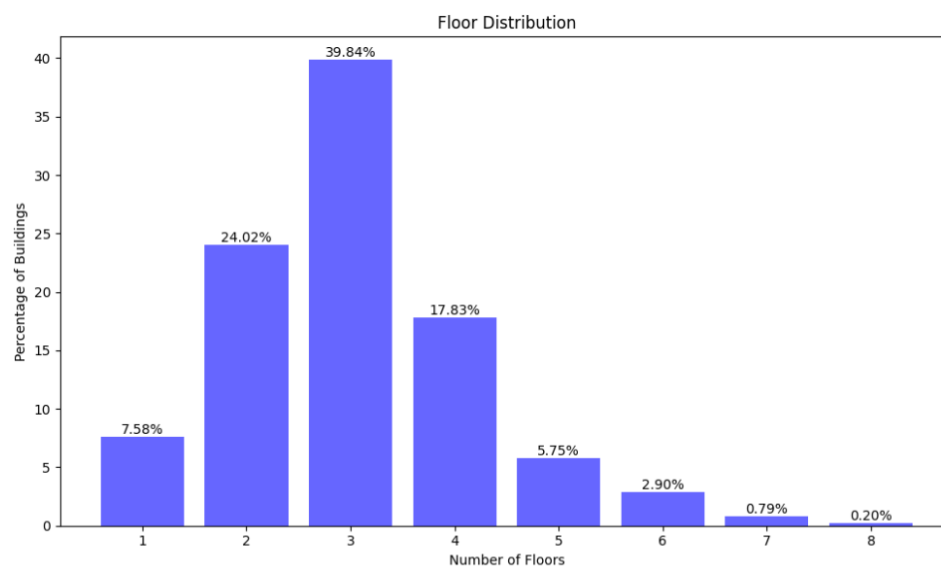


Figure 18. L'Aquila floor distribution showing the percentage of reinforced concrete buildings by number of floors

Masonry Buildings

Wall Texture (Material Quality):

- Irregular/Poor-Quality Masonry (IRR): Typically found in older buildings, this type of masonry uses uneven materials and shows poor quality, resulting in lower structural integrity.
- Regular/Good-Quality Masonry (REG): Common in more recent constructions, this masonry features uniform materials and better construction quality, improving strength and performance.

Horizontal Structure (Diaphragm Rigidity):

- Flexible Diaphragms (F): These are usually made from traditional wood or lightweight materials. While common in older buildings, they cannot transfer lateral forces during earthquakes.
- Rigid Diaphragms (R): Made from materials like reinforced concrete, these structures provide better horizontal stiffness and are more effective at resisting seismic loads.

Presence of Connecting Devices:

- With Connecting Devices (CD): These buildings include tie rods, tie beams, or other elements that improve the connection between structural components, enhancing overall stability and reducing earthquake vulnerability.
- Without Connecting Devices (NCD): Lacking such reinforcement, these structures are more susceptible to the separation of elements and higher levels of damage during seismic events.

Statistics of Masonry Buildings

Construction Age:

Irpinia Dataset:

37% of masonry buildings were built before 1900, reflecting a significant presence of vulnerable structures.

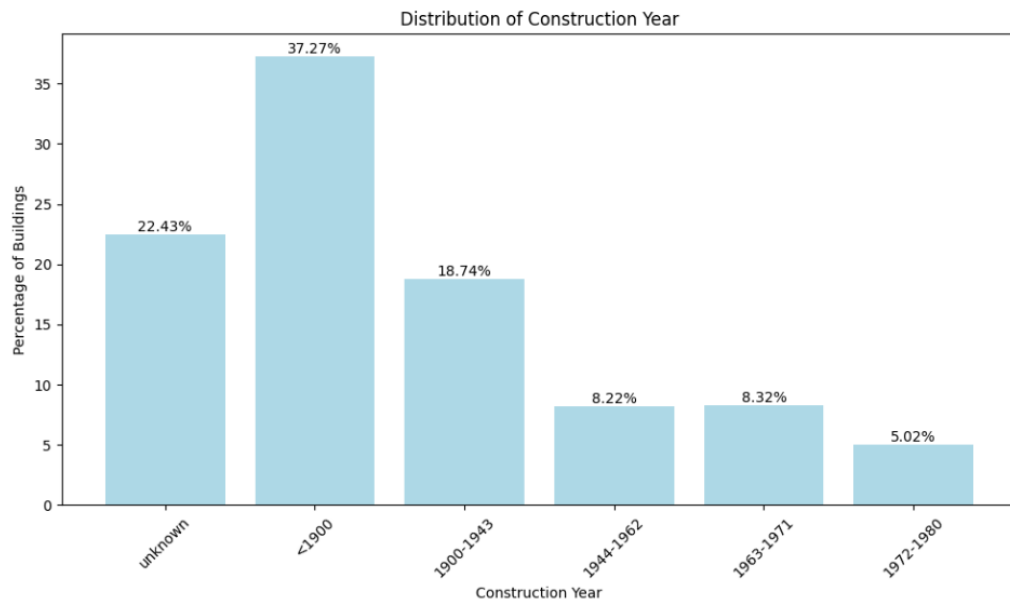


Figure 19. Irpinia construction year distribution based on the percentage of surveyed masonry buildings

L'Aquila Dataset:

57% of masonry buildings were constructed before 1919, indicating a larger proportion of older constructions than in Irpinia.

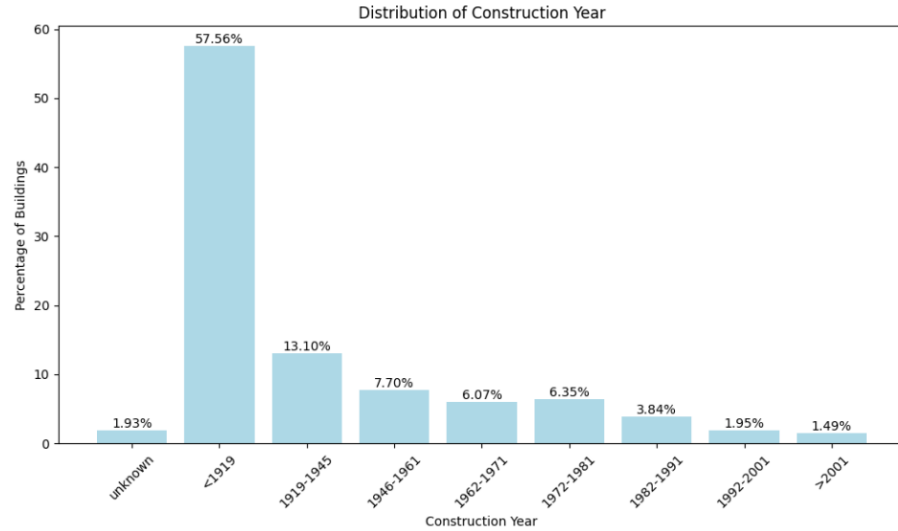


Figure 20. L'Aquila construction year distribution based on the percentage of surveyed masonry buildings

Number of Floors:

Irpinia 1980 Dataset: Low-rise (1–2 floors) masonry buildings are 80.9% of the dataset.

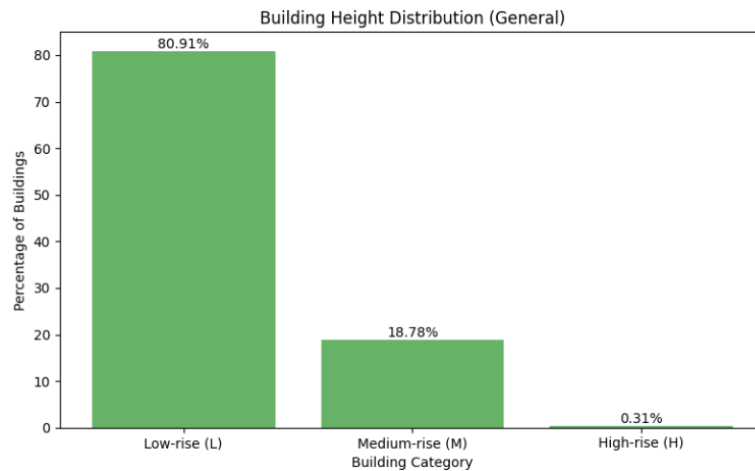


Figure 21. Irpinia masonry building height distribution by percentage of low-, medium-, and high-rise structures

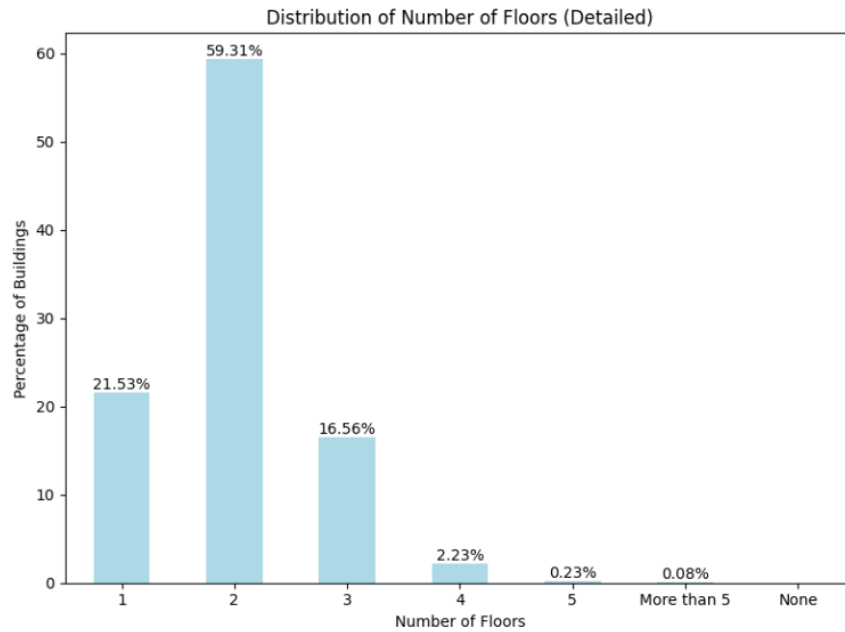


Figure 22. Irpinia floor distribution showing the percentage of masonry buildings by number of floors

L'Aquila 2009 Dataset: Low-rise buildings make up 59%, indicating a shift toward taller structures.

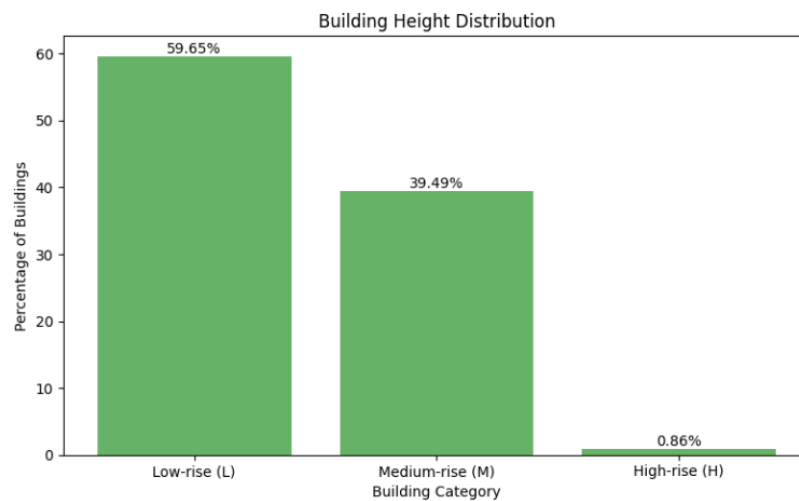


Figure 23. L'Aquila masonry building height distribution by percentage of low-, medium-, and high-rise structures

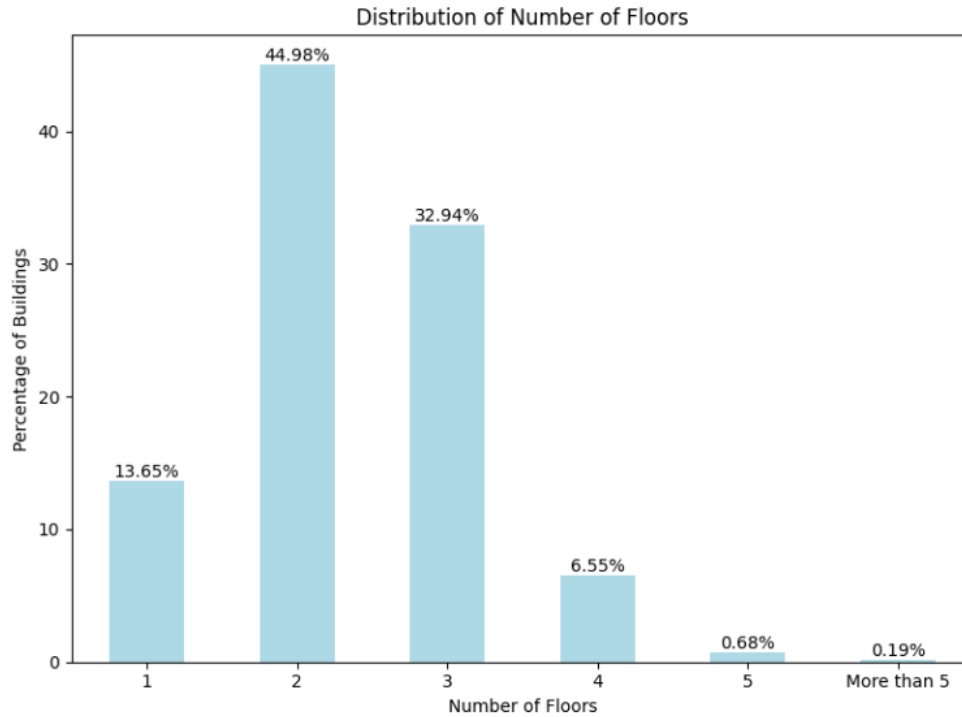


Figure 24. L'Aquila floor distribution showing the percentage of masonry buildings by number of floors

The classification is further detailed in Table 1, which presents a masonry building taxonomy based on key parameters such as wall texture, diaphragm rigidity, and the presence of connecting devices.

Category	Description
IRR-F-NCD	Irregular texture, Flexible diaphragm, No connecting devices
IRR-F-CD	Irregular texture, Flexible diaphragm, with connecting devices
IRR-R-NCD	Irregular texture, Rigid diaphragm, No connecting devices
IRR-R-CD	Irregular texture, Rigid diaphragm, with connecting devices
REG-F-NCD	Regular texture, Flexible diaphragm, No connecting devices
REG-F-CD	Regular texture, Flexible diaphragm, with connecting devices
REG-R-NCD	Regular texture, Rigid diaphragm, No connecting devices
REG-R-CD	Regular texture, Rigid diaphragm, with connecting devices

Table 1. Masonry building typology taxonomy

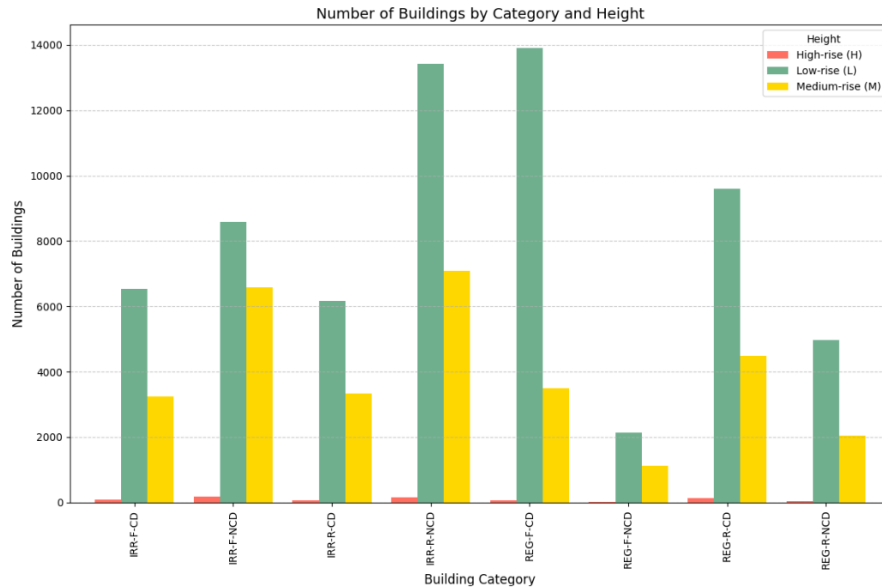


Figure 25. Number of masonry buildings by category and height, showing the distribution across low-rise, medium-rise, and high-rise structures

Development of Fragility Curves

- Traditional lognormal distribution models
- Integration and benefits of the Generalized Extreme Value (GEV) distribution

Distributions

Lognormal distribution

In probability theory, a log-normal distribution describes a continuous random variable whose logarithm follows a normal (Gaussian) distribution. In other words, if you take the natural log of a log-normally distributed variable, the result will be normally distributed. This type of distribution is commonly used to model positively skewed variables that cannot take on negative values, such as income levels, stock prices, or, in engineering, certain types of structural responses to stress or load. This means that if a random variable follows a log-normal distribution, its natural logarithm $Y=\ln(X)$ follows a normal distribution (Weisstein, n.d.).

Similarly, if Y has a normal distribution, then the exponential function of Y , given by $X=\exp(Y)$, follows a log-normal distribution. A random variable that is log-normally distributed assumes only positive real values, reflecting the fact that the exponential function maps all real numbers to positive values (Everitt and Skrondal 2010).

A log-normal process is a statistical model representing the result of multiplying many independent, positive random variables. This behavior can be explained using the central limit theorem, but applied in the logarithmic domain. When you take the logarithm of these variables,

their product turns into a sum, and the central limit theorem illustrates that the sum of many independent variables tends to follow a normal distribution. As a result, the original (non-logged) variable follows a log-normal distribution. This concept is often known as **Gibrat's law**, which suggests that proportional growth rates—like in economics, biology, or engineering—lead to log-normal outcomes. According to this law, combining many independent, multiplicative processes, the result follows a log-normal distribution (Park and Bera 2009).

The log-normal distribution is the maximum entropy distribution for a random variable X when the mean and variance of $\ln(X)$ are fixed. In simpler terms, among all possible distributions with a given mean and variance of the logarithm, the log-normal is the most "unbiased" or "least informative" choice—it represents the highest level of uncertainty consistent with the known constraints (Wikipedia contributors, n.d.).

A log-normal distribution is defined by a random variable $X=e^{\mu+\sigma Z}$ where Z is a standard normal variable, and μ and σ are real numbers, with $\sigma>0$. The distribution of X is log-normal with parameters μ and σ , representing the mean and standard deviation of the natural logarithm of X , not X itself.

If $Y=\mu+\sigma Z$ is normally distributed, then $X=e^Y$ is log-normally distributed. The relationship holds for any logarithmic base.

To produce a log-normal distribution with desired mean μ_X and variance σ_X^2 , use:

$$\mu = \ln \left(\frac{\mu_X^2}{\sqrt{\mu_X^2 + \sigma_X^2}} \right)$$

$$\sigma = \ln \left(1 + \frac{\sigma_X^2}{\mu_X^2} \right)$$

Alternatively, the "multiplicative" or "geometric" parameters $\mu^*=e^\mu$ and $\sigma^*=e^\sigma$ can be used. These parameters have a more direct interpretation: μ^* represents the median of the distribution, while σ^* is useful for determining the "scatter" or variability of the distribution.

The probability density function (PDF) of a log-normal distribution, where $X \sim \text{Lognormal}(\mu, \sigma^2)$, is derived from the fact that the natural logarithm of X is normally distributed with mean μ and variance σ^2 . Mathematically, if $\ln(X) \sim N(\mu, \sigma^2)$, then the PDF of the log-normal distribution is:

$$f_x(x) = \frac{1}{x\sigma\sqrt{2\pi}} \exp \left(-\frac{(\ln(x) - \mu)^2}{2\sigma^2} \right)$$

Where:

- $x>0$ (since X is positive)
- μ and σ are the parameters of the underlying normal distribution of $\ln(X)$

This formula describes the likelihood of observing a value x from a log-normal distribution (Johnson, Kotz, and Balakrishnan 1994).

(Weisstein, n.d.).

The cumulative distribution function (CDF of a log-normal random variable X is: $f_x(x) = \Phi\left(\frac{\ln(x)-\mu}{\sigma}\right)$

- Φ is the standard normal distribution
- μ is the median of the logarithm of X .
- σ is the standard deviation of the logarithm of X (Wikipedia contributors, n.d.).

Generalized extreme value distribution

The Generalized Extreme Value (GEV) distribution brings together three types of extreme value distributions—Gumbel (Type I), Fréchet (Type II), and Weibull (Type III)—into a single, unified model. It is commonly used in extreme value theory to describe the behavior of the maximum values in sequences of identically distributed variables (de Haan and Ferreira 2007).

In studies, the PDF of the standardized GEV distribution is (de Haan and Ferreira 2007).

(Coles 2001)

$$f(s; \xi) = \begin{cases} e^{-s} \exp(-e^{-s}), & \text{if } \xi = 0, \\ (1 + \xi s)^{-(1+1/\xi)} \exp(-(1 + \xi s)^{-1/\xi}), & \text{if } \xi \neq 0 \text{ and } \xi s > -1, \\ 0, & \text{otherwise.} \end{cases}$$

The CDF of the GEV distribution is defined as:

$$F(s; \xi) = \begin{cases} \exp(-e^{-s}), & \text{if } \xi = 0, \\ \exp(-(1 + \xi s)^{-1/\xi}), & \text{if } \xi \neq 0 \text{ and } \xi s > -1, \\ 0, & \text{if } \xi > 0 \text{ and } s \leq -\frac{1}{\xi}, \\ 1, & \text{if } \xi < 0 \text{ and } s \geq -\frac{1}{\xi}. \end{cases}$$

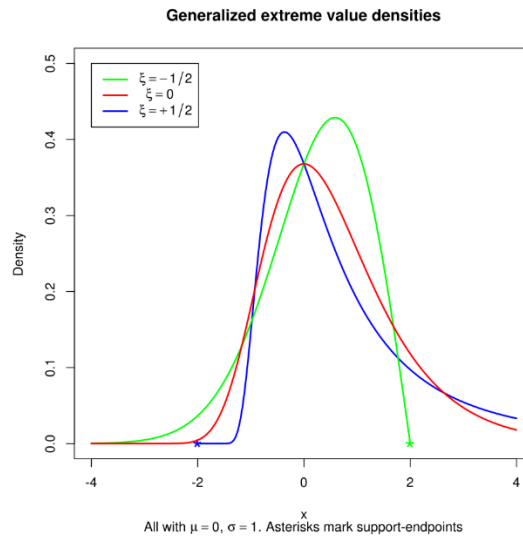


Figure 26. Generalized Extreme Value (GEV) distribution curves for different shape parameters (ξ), illustrating variations in density behavior: numerator, minus mu, and density behavior: numerator, minus mu, and numerator and denominator, minus mutorand $\frac{\mu}{\sigma}$ is the standardized variable.

- μ : Specifies the central value or location.
- σ : Controls the spread or scale.
- ξ : Determines the tail behavior:
 - $\xi > 0$: Heavy-tailed (Fréchet).
 - $\xi = 0$: Exponential tail (Gumbel).
 - $\xi < 0$: Bounded tail (Weibull).

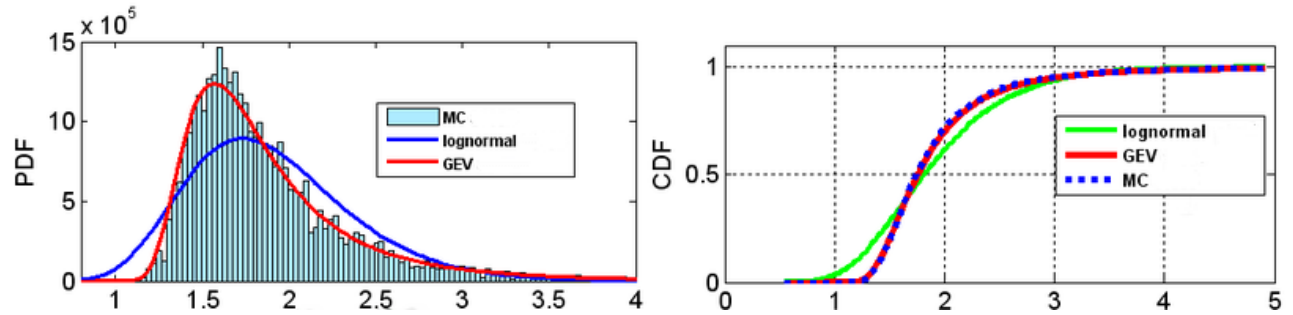


Figure 27. Comparison of lognormal and GEV distributions against Monte Carlo (MC) simulation results, shown through probability density function (PDF) and cumulative distribution function (CDF) plots

Results and Analysis

This chapter compares the lognormal fragility curves from the filtered dataset with those from Rosti et al. The goal is to evaluate how data filtering affects the curve shape and damage state progression across typologies.

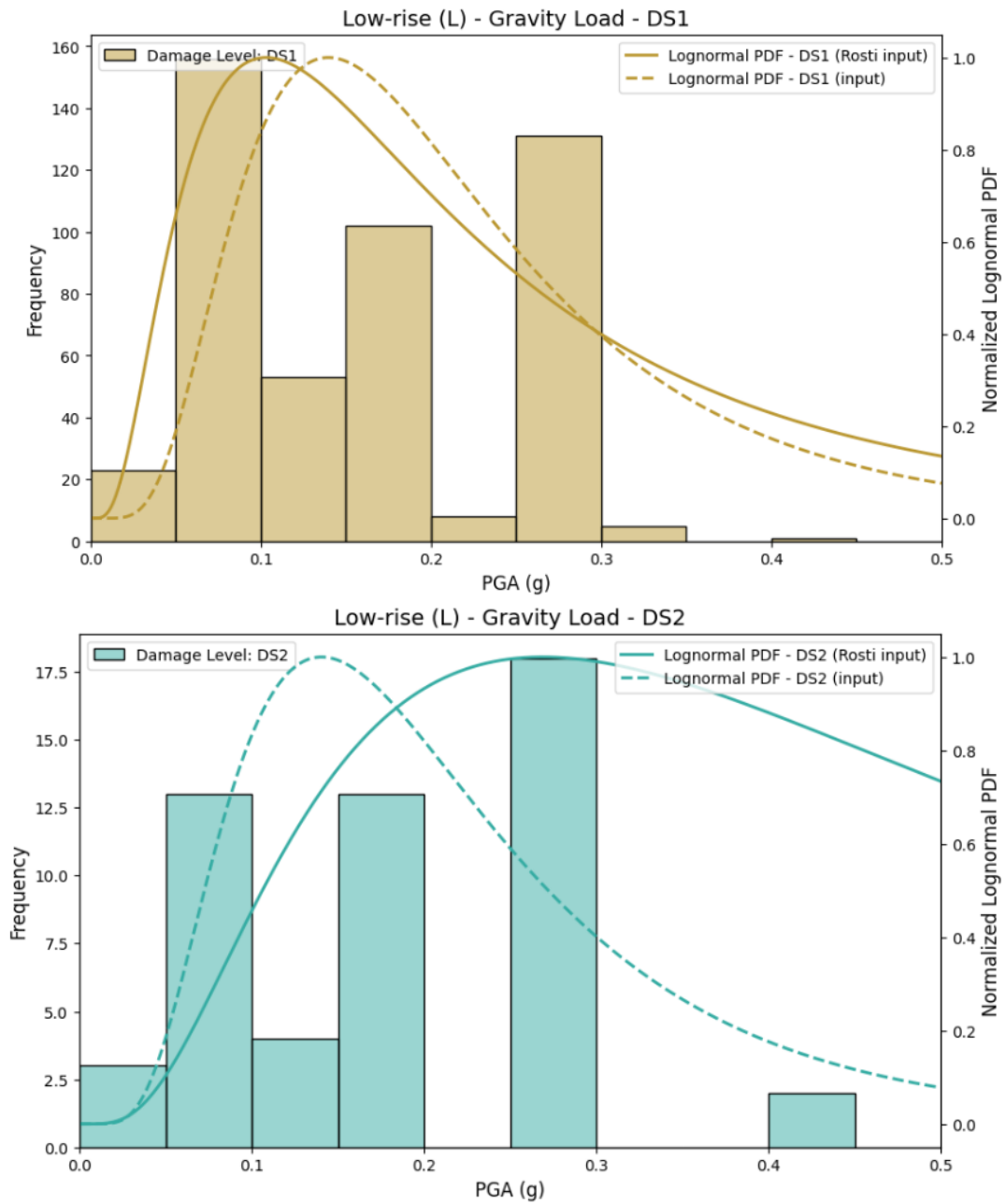
Histogram and Lognormal Distribution

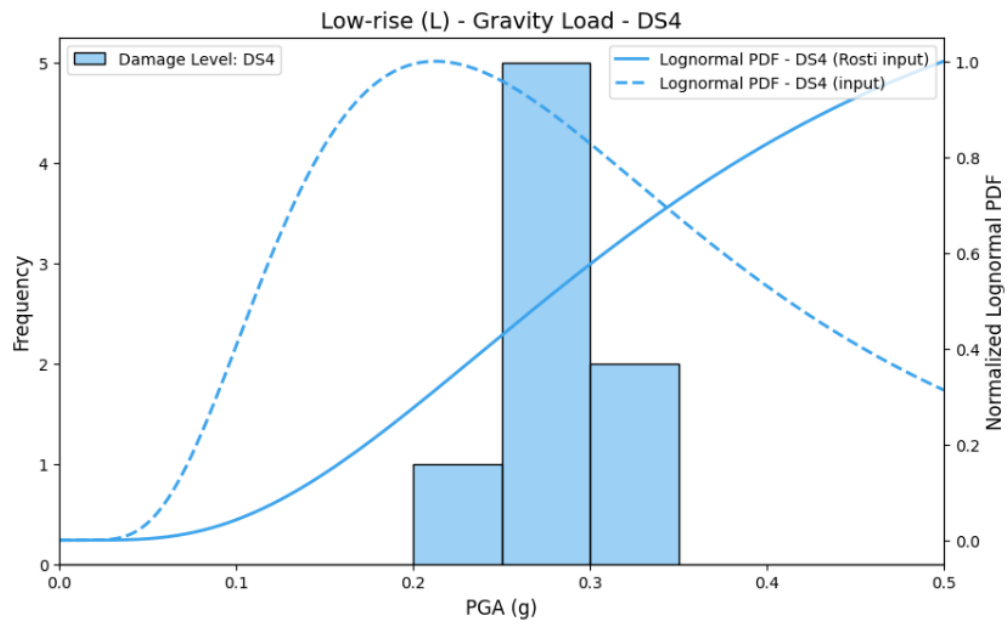
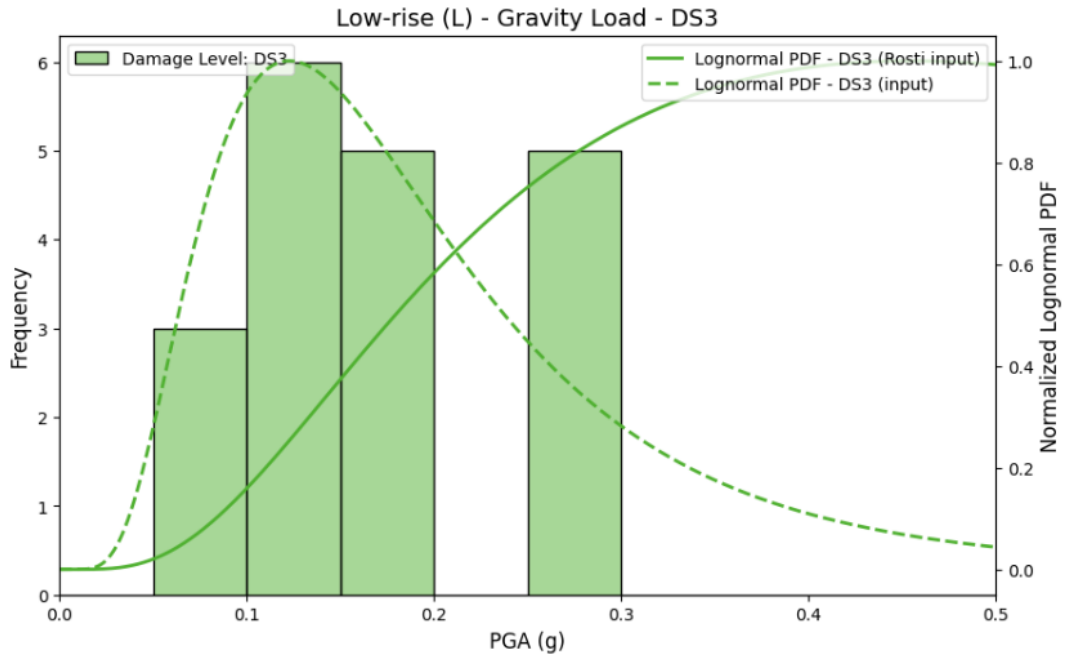
Histograms were created using the input data, and the lognormal distribution's Probability Density Function (PDF) was overlaid for comparison. These results were then evaluated against the fitted lognormal distribution in the Rosti paper. While the overall trends and shapes of the distributions appear similar, there are noticeable differences between the two.

One key factor behind these differences is the lack of transparency regarding the data filtering process used in the Rosti study. Their methodology for filtering the data is not clearly explained. This lack of detail makes it difficult to replicate their results or fully understand the adjustments they applied.

Concrete buildings

For concrete inputs, we can summarize the data as follows:





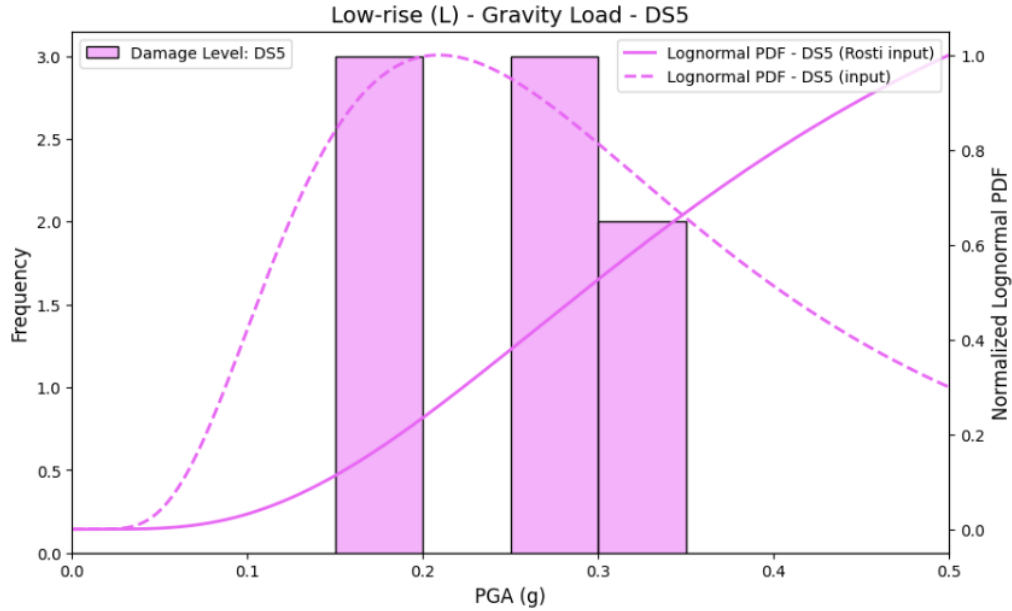
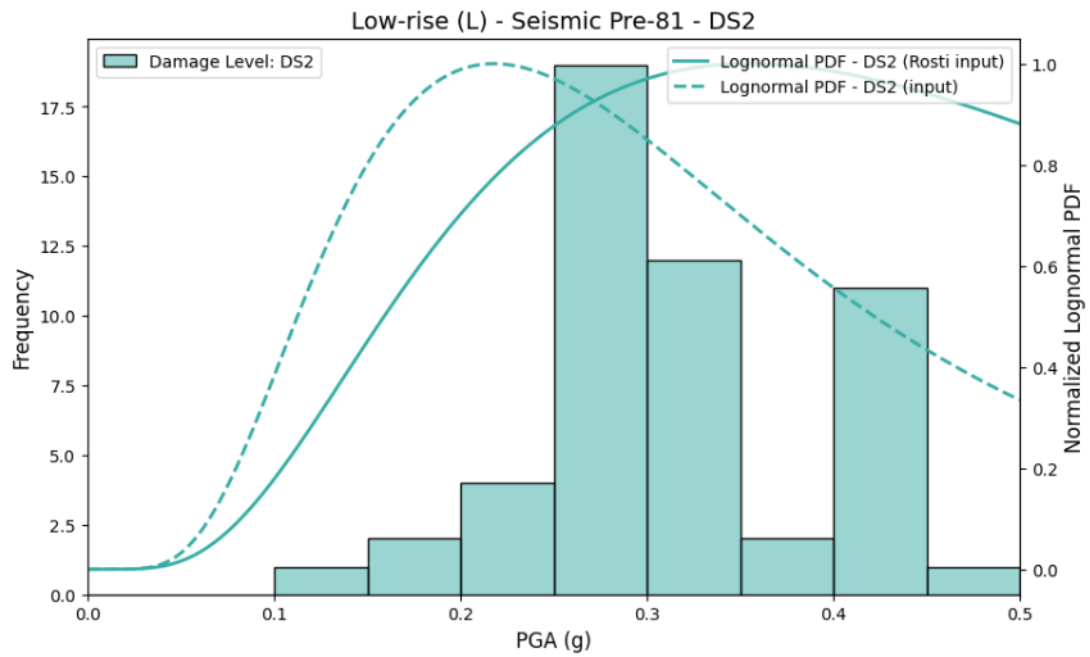
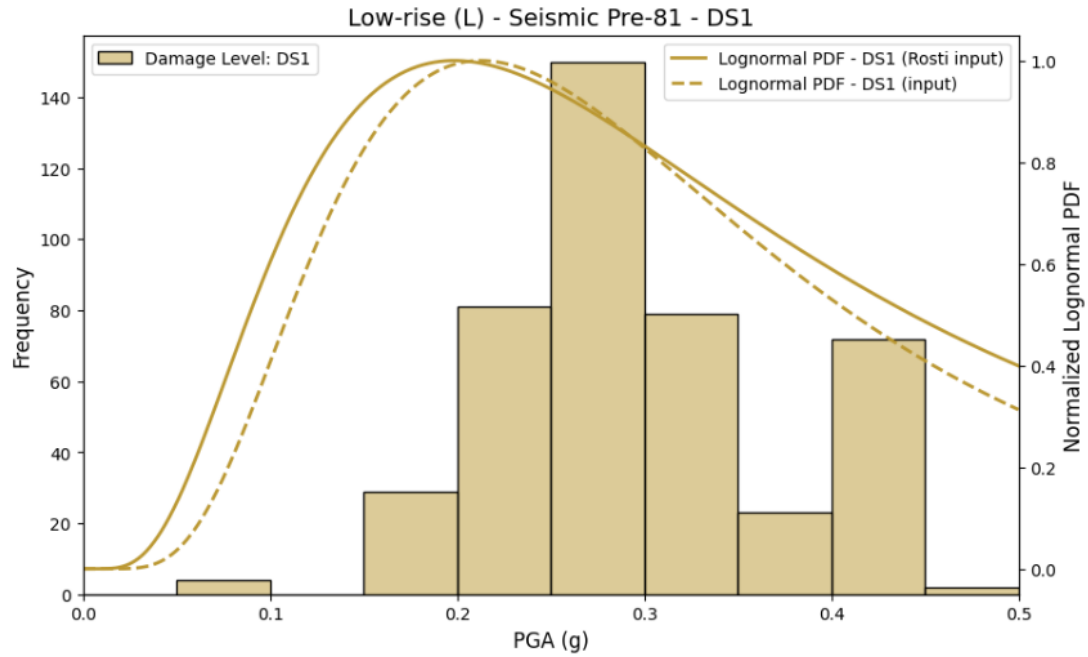
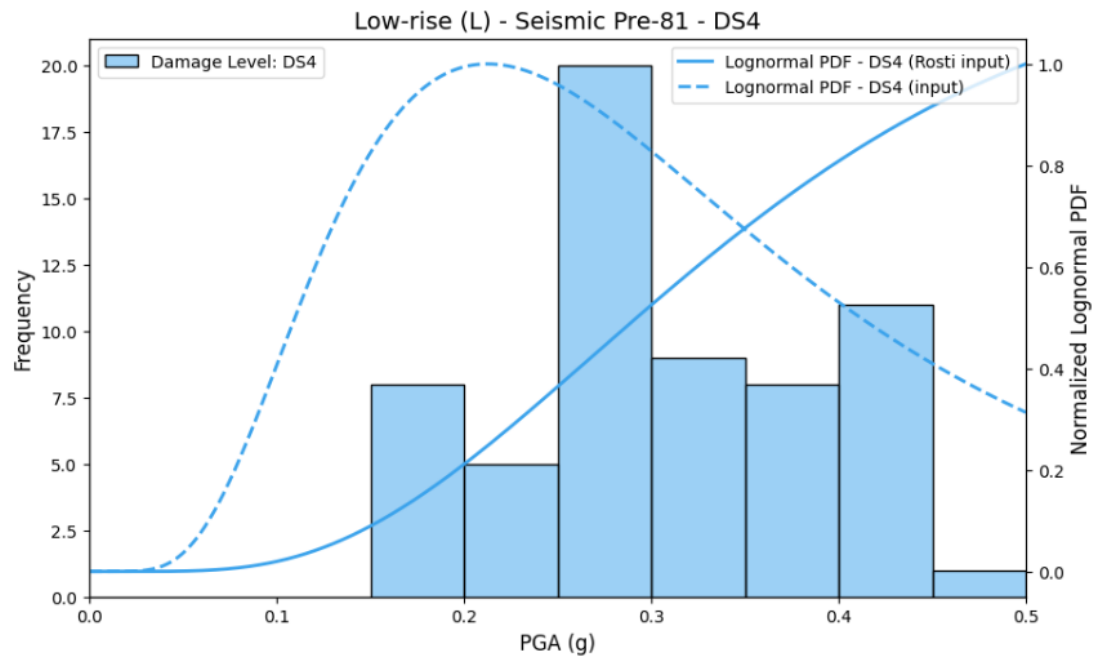
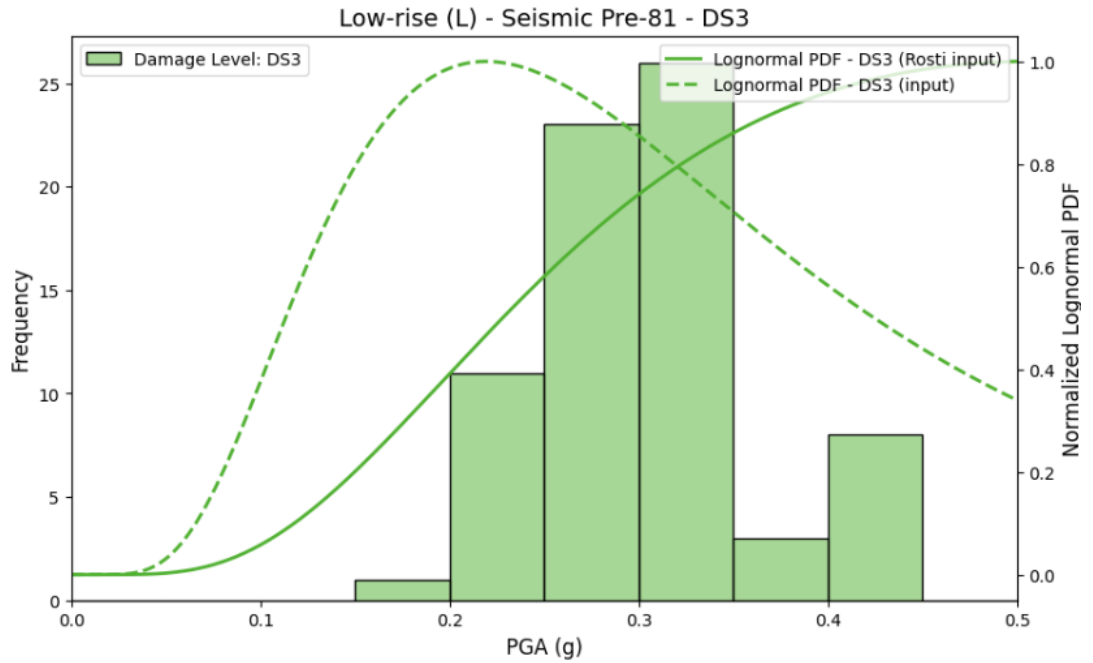


Figure 28. Low-rise gravity load building response for all damage levels, showing frequency distribution and comparison between lognormal PDF (input) and lognormal PDF (Rosti input) for each damage state

When analyzing low-rise reinforced concrete buildings designed only for gravity loads, the comparison between my lognormal curves and those of Rosti reveals a consistent trend: while the general shape and progression remain similar across damage states, the difference between the curves becomes more obvious as the damage state increases. This pattern also appears in low-rise buildings designed with seismic criteria. However, at higher damage states—particularly DS5—the differences become much more significant, with the curves diverging despite following the same overall direction.





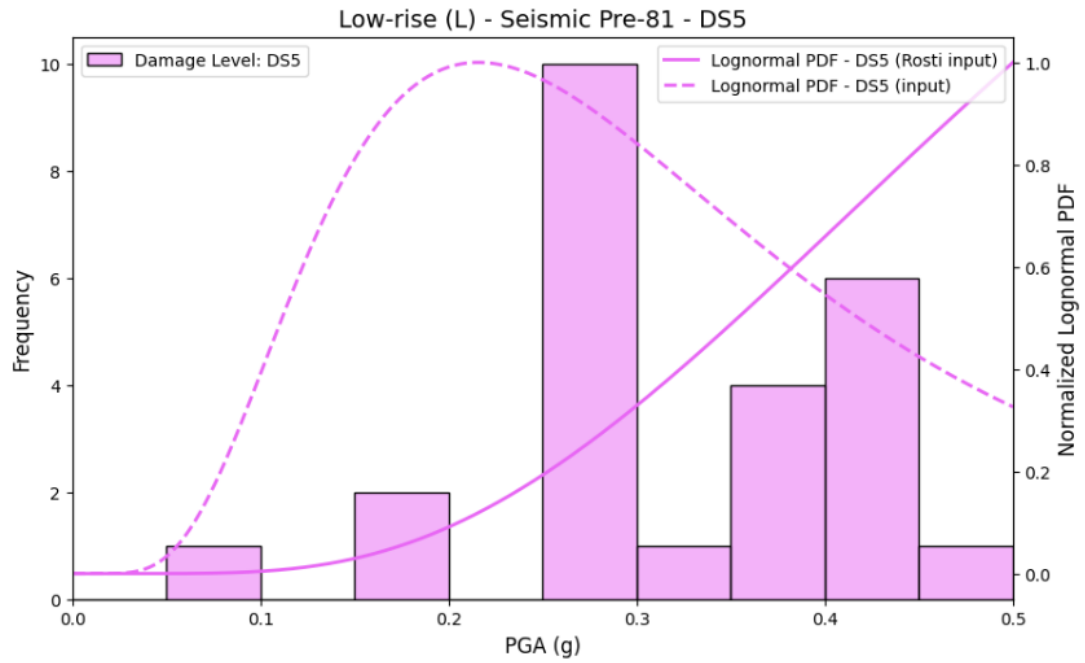
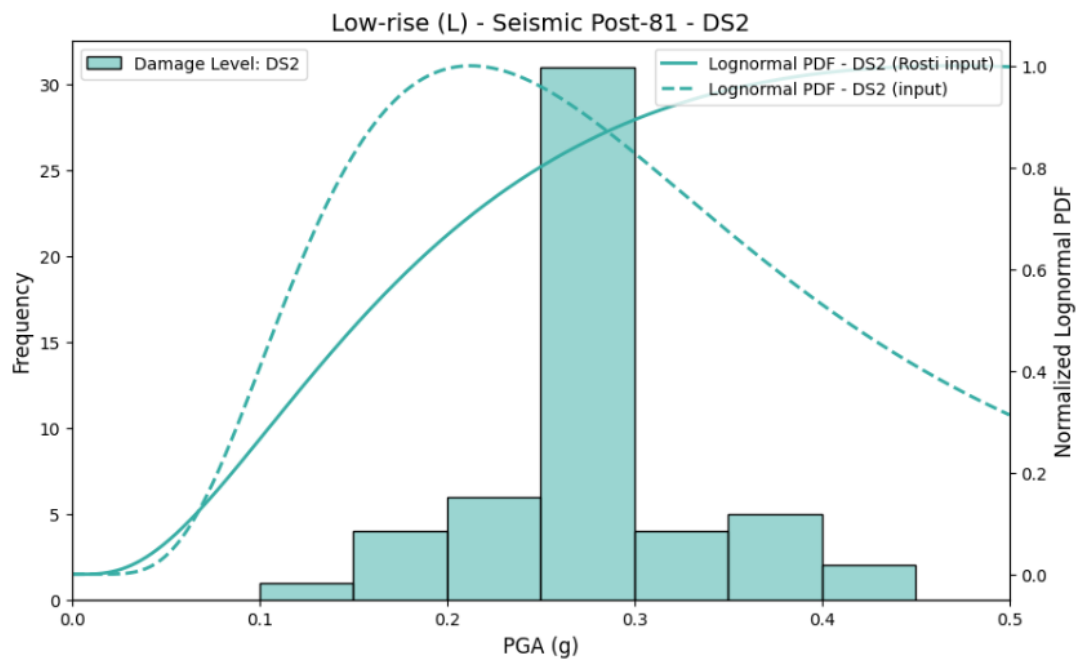
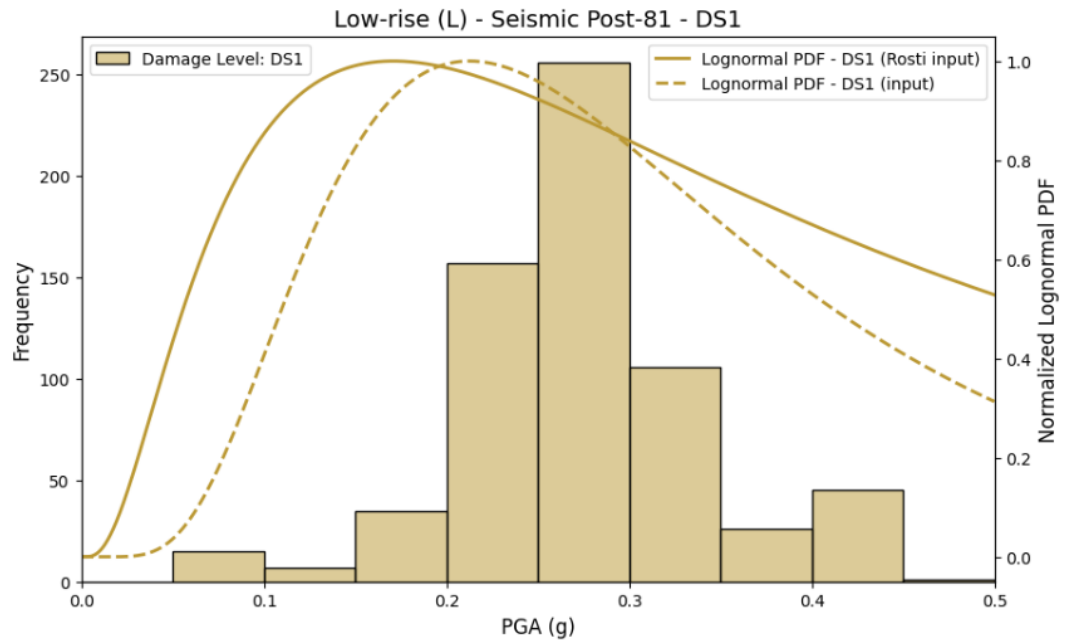
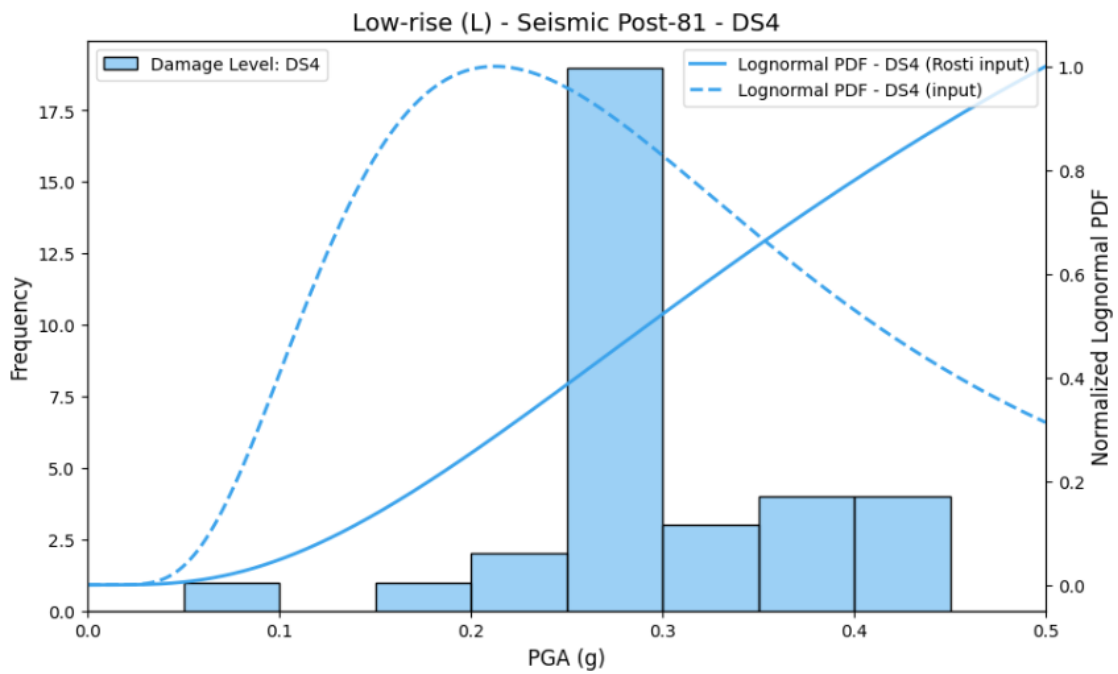
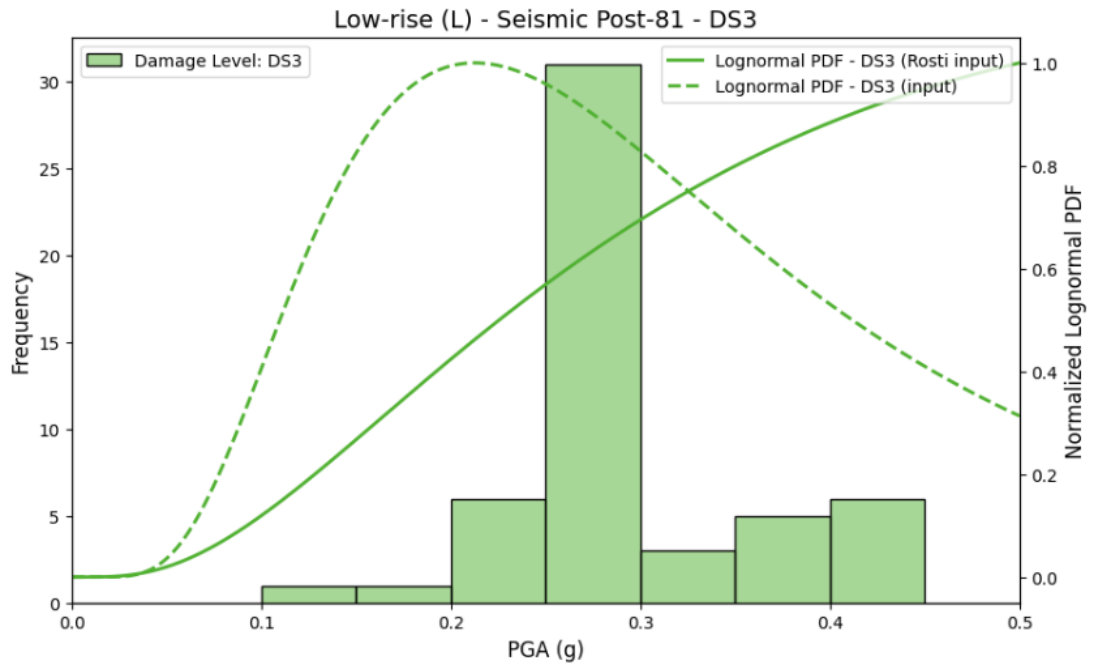


Figure 29. Low-rise Seismic pre81 building response for all damage levels, showing frequency distribution and comparison between lognormal PDF (input) and lognormal PDF (Rosti input) for each damage state





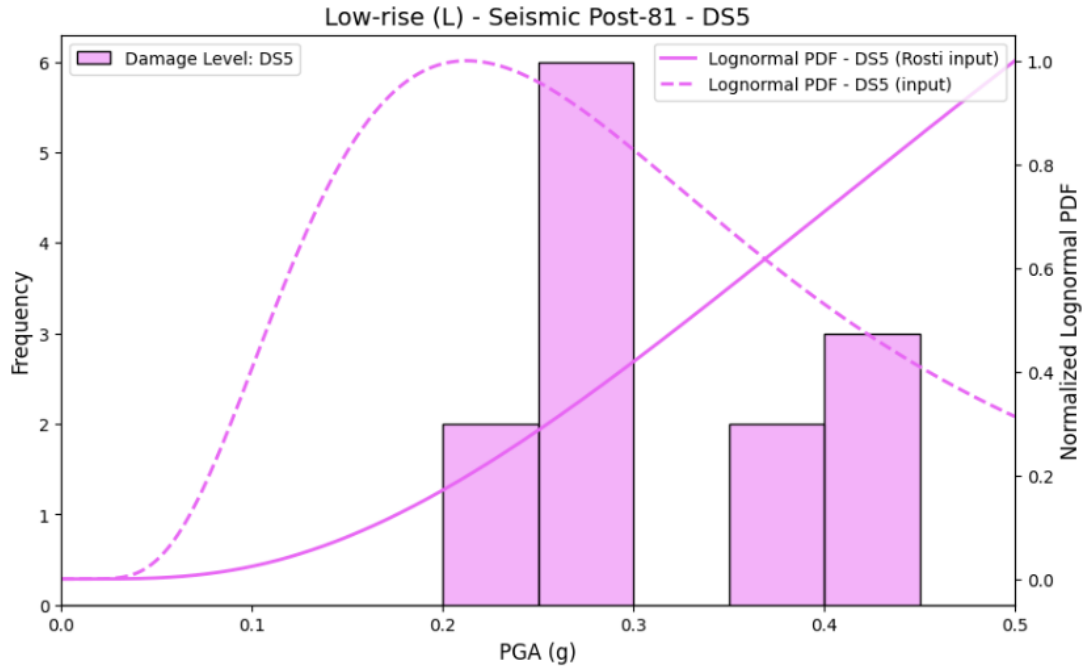
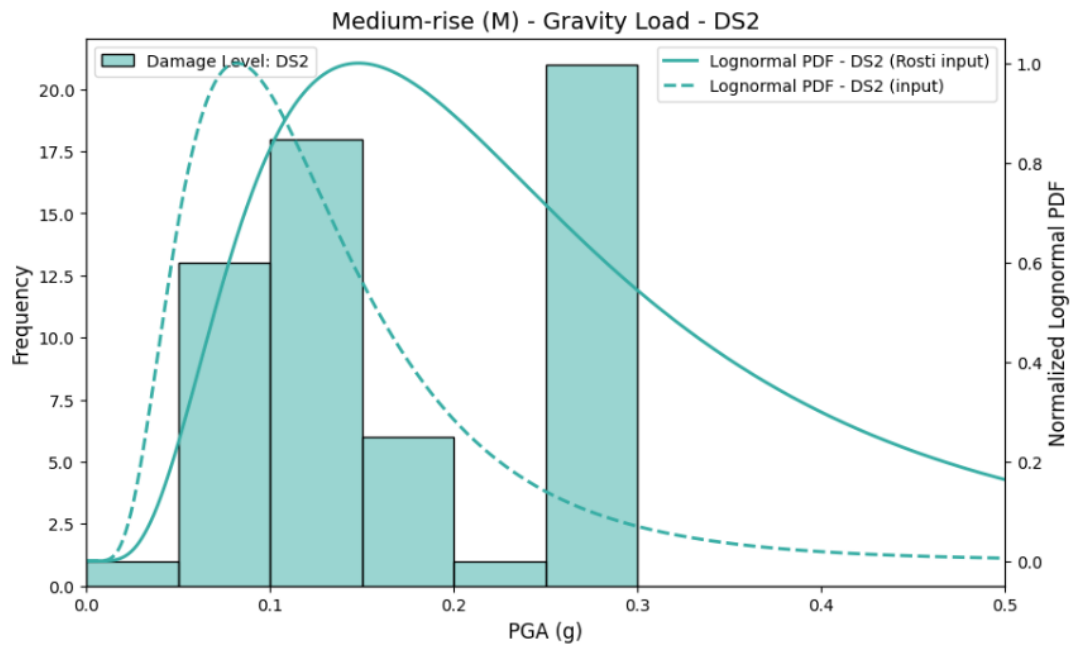
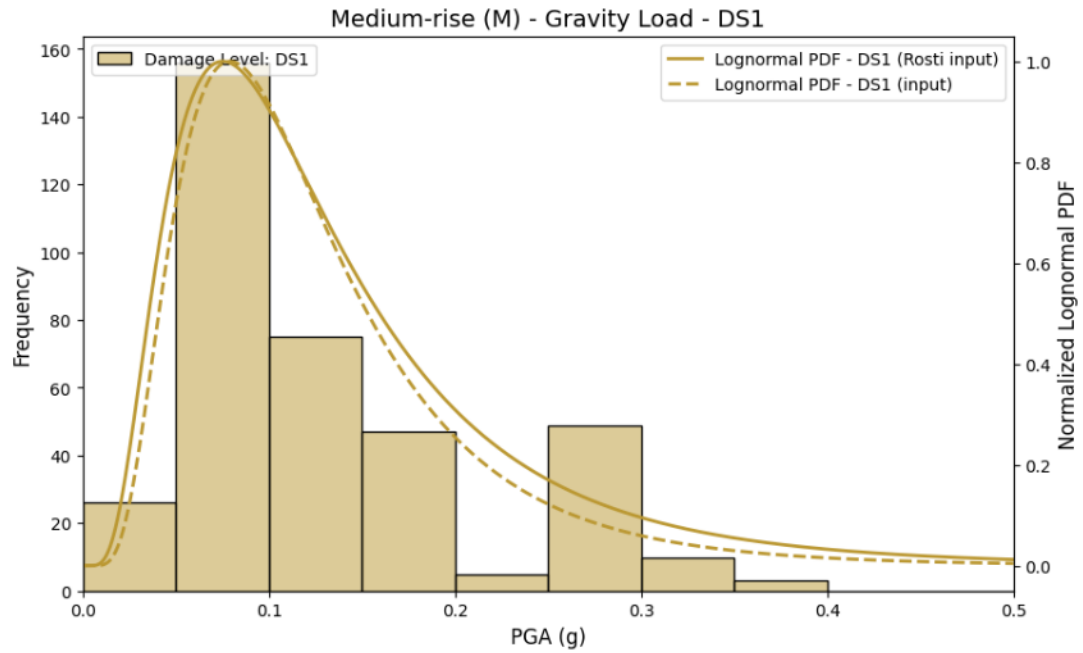
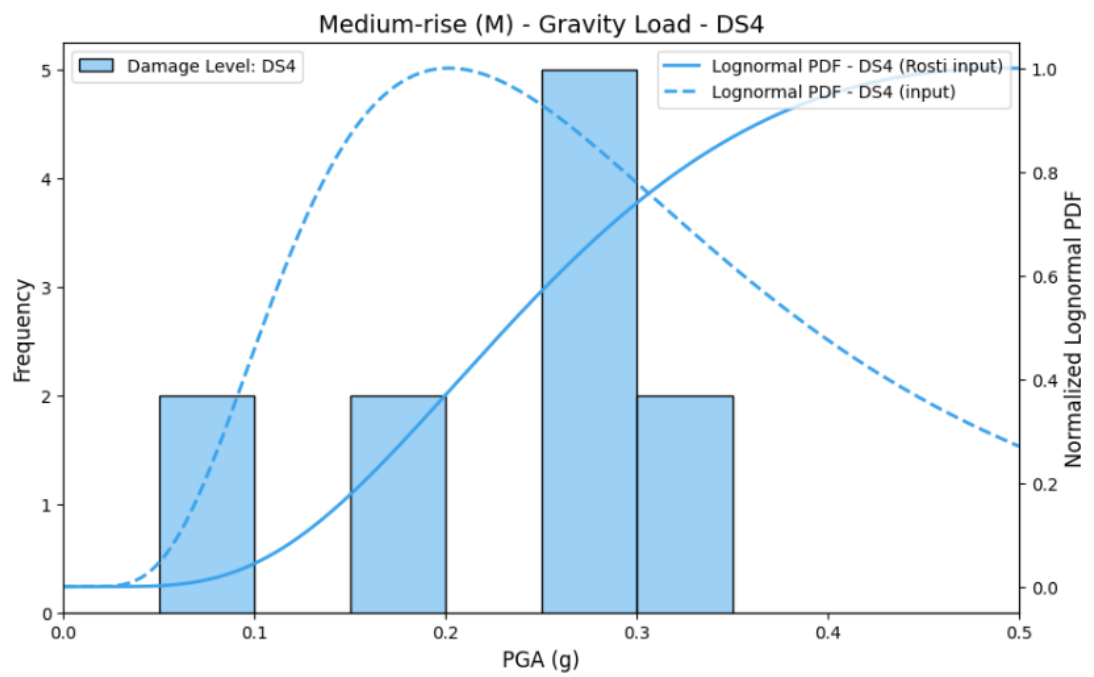
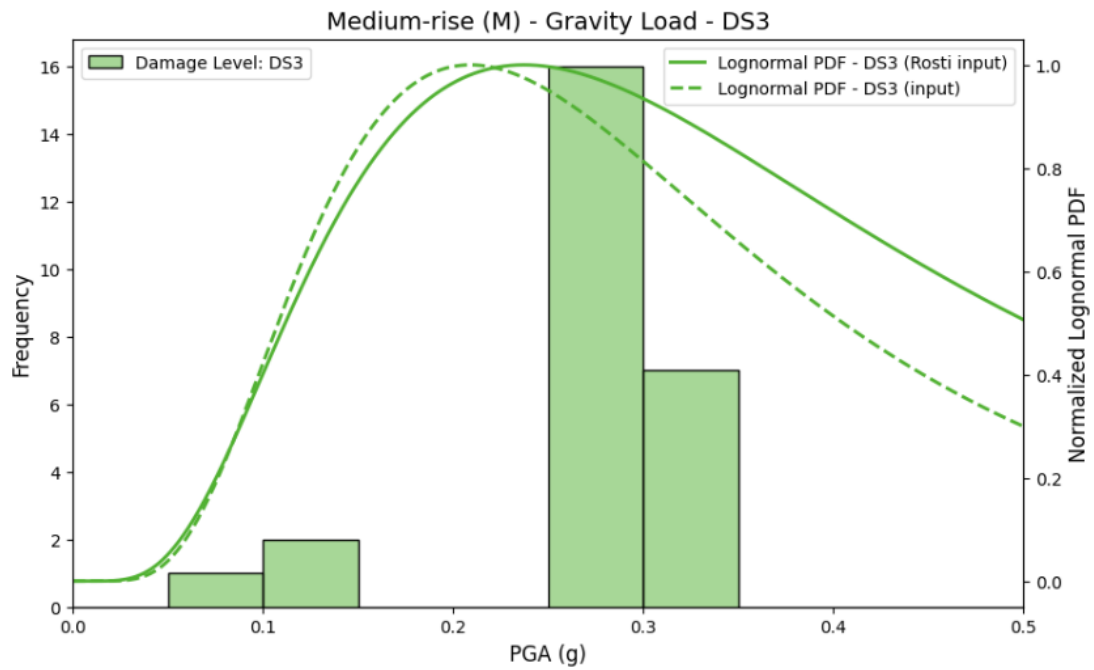


Figure 30. Low-rise Seismic post81 building response for all damage levels, showing frequency distribution and comparison between lognormal PDF (input) and lognormal PDF (Rosti input) for each damage state

A similar trend is observed in post-1981 code-compliant low-rise buildings, where the curves stay relatively aligned at lower damage levels but begin to deviate more sharply as damage severity increases. This suggests that, while both models agree on the initial damage behavior of low-rise reinforced concrete structures, their estimates diverge when predicting the likelihood of extensive or near-collapse damage.





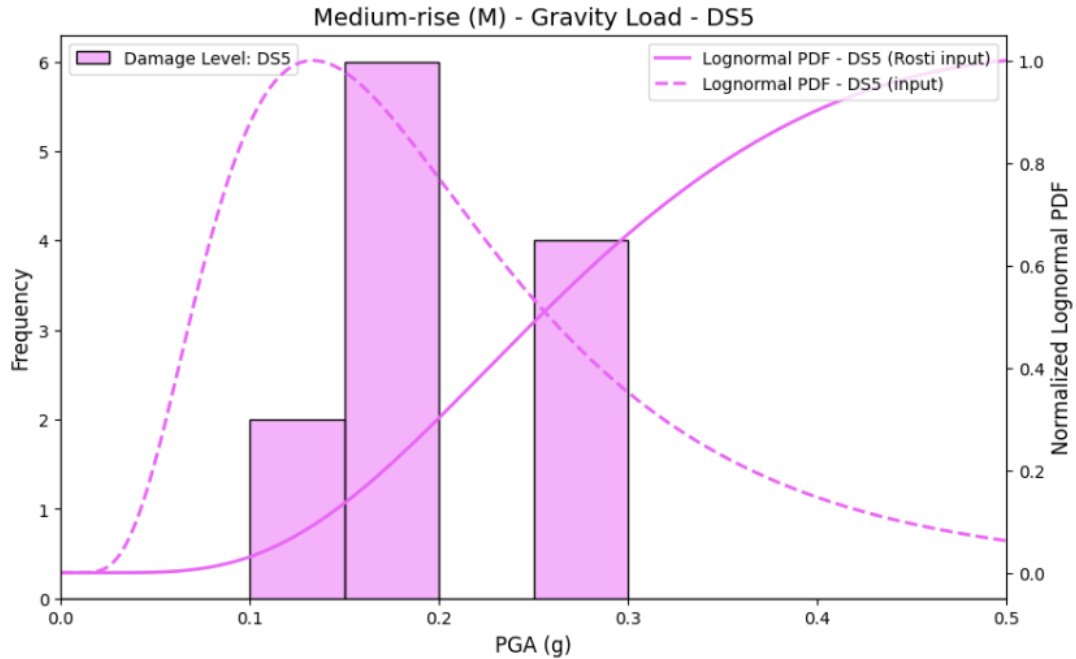
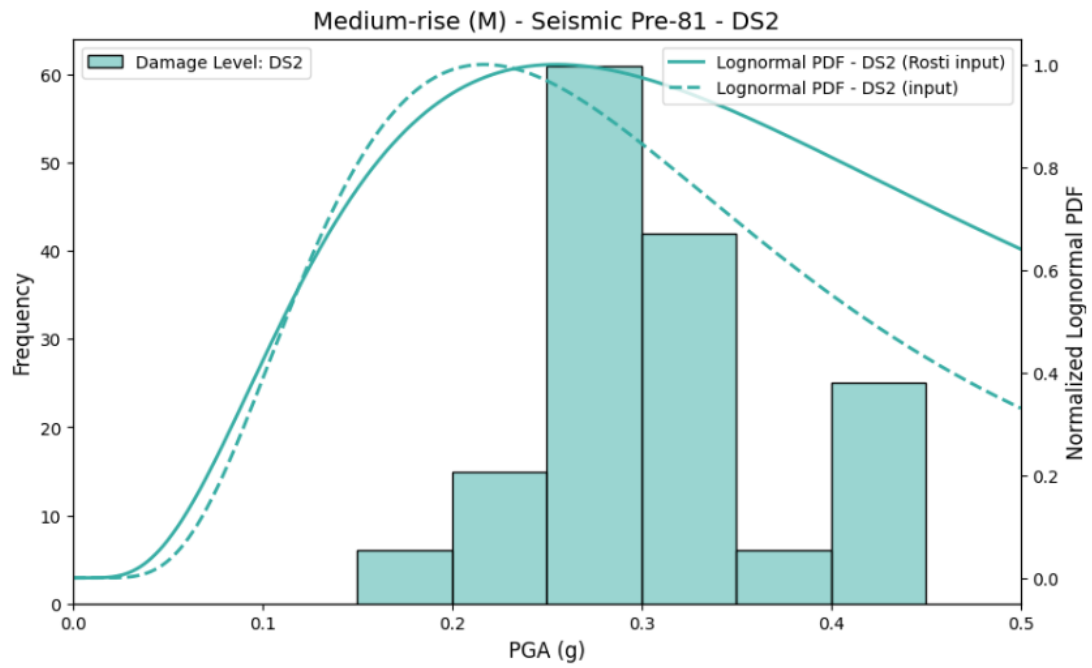
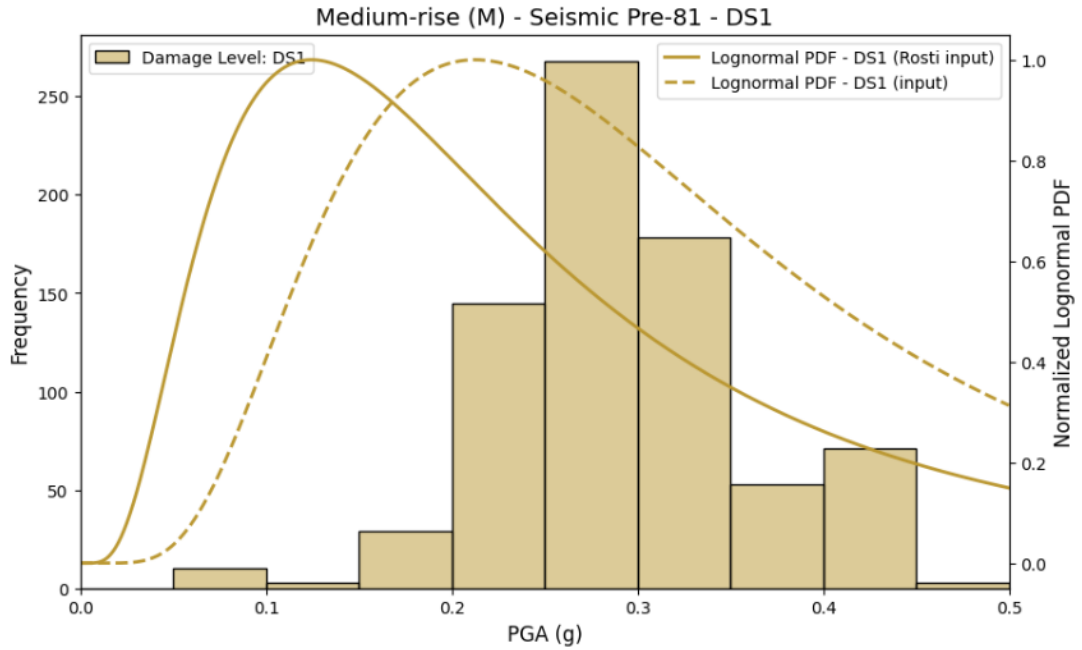
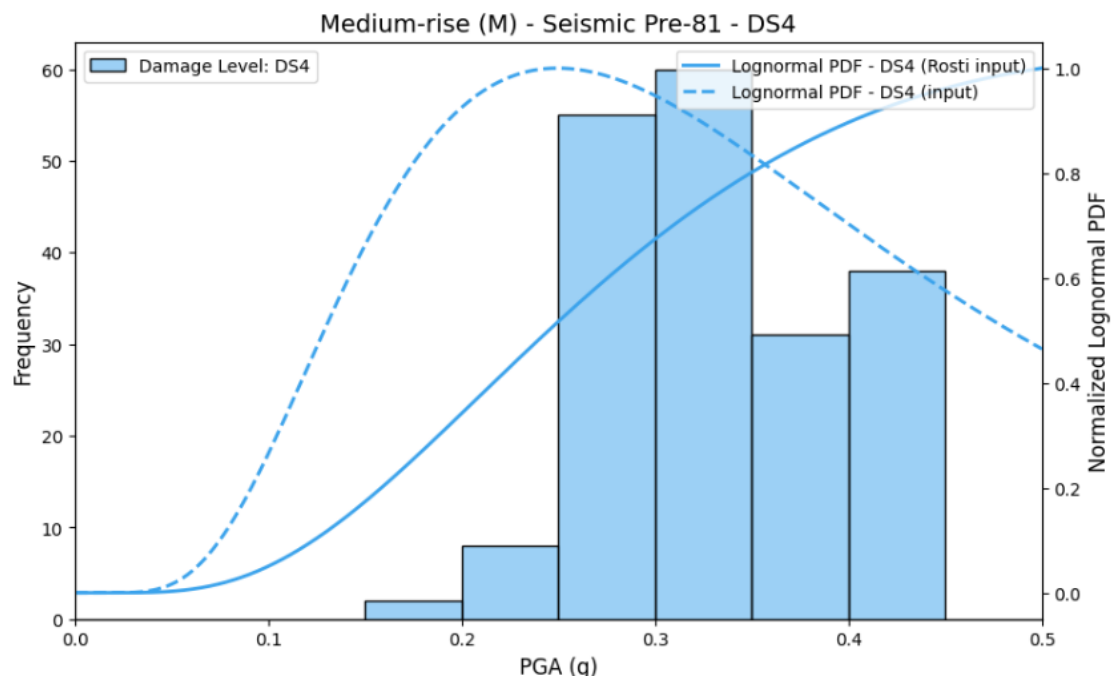
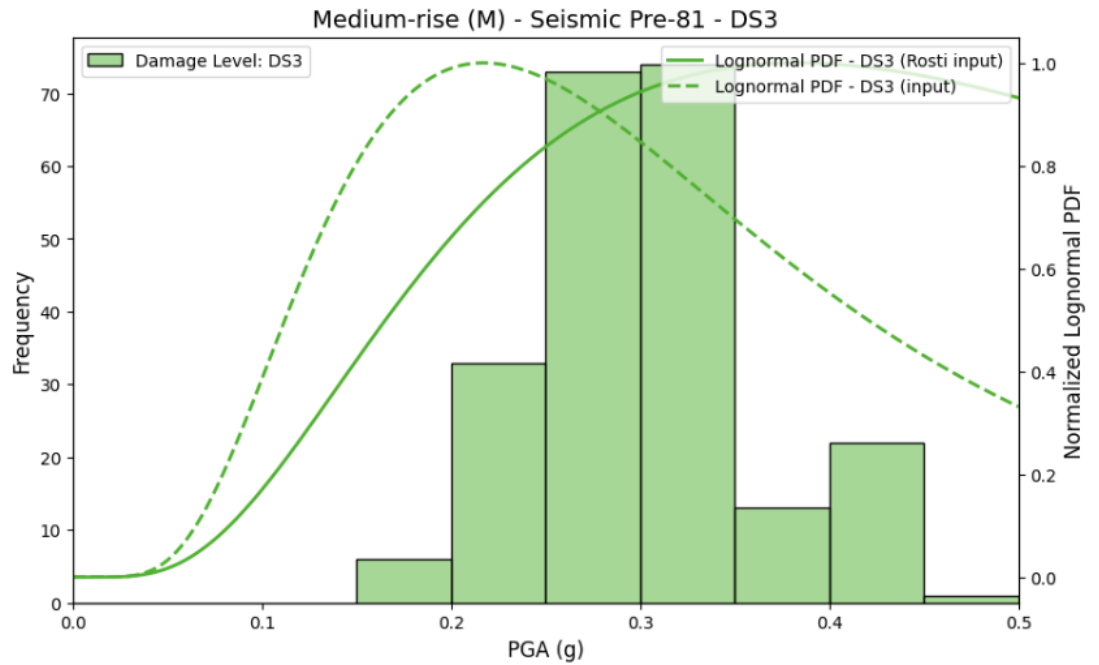


Figure 31. medium-rise gravity load building response for all damage levels, showing frequency distribution and comparison between lognormal PDF (input) and lognormal PDF (Rosti input) for each damage state

The curves of mid-rise reinforced concrete buildings designed for gravity loads show good agreement at lower damage states, indicating a shared understanding of the initial vulnerability however, as we move toward DS3 and beyond, the curves diverge, reflecting increasing differences in how the models estimate the structure's performance under stronger shaking.





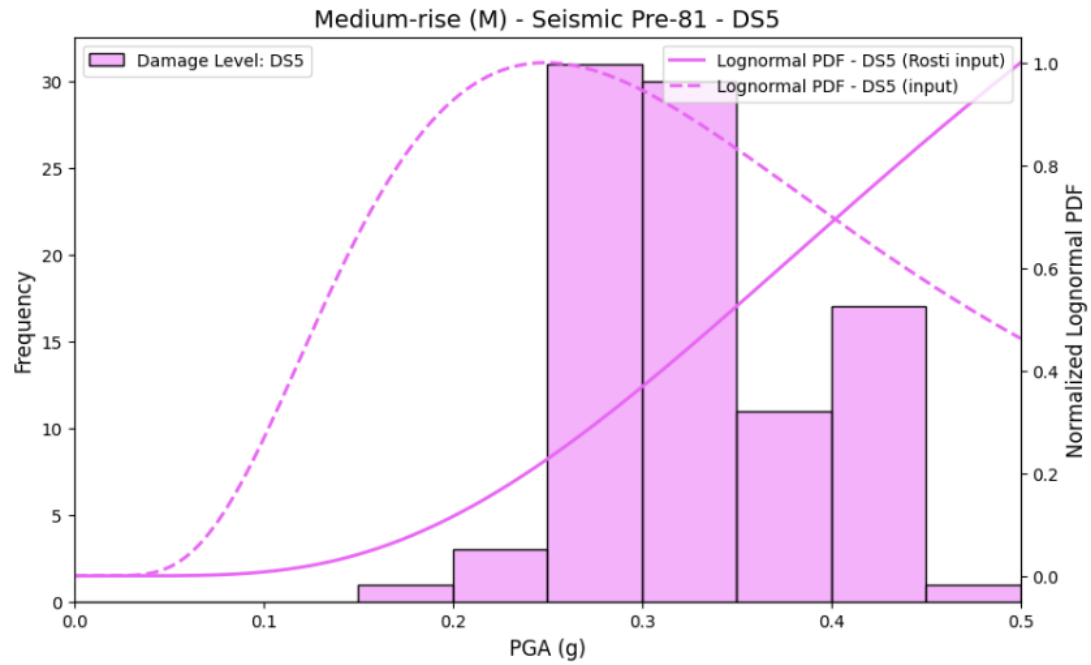
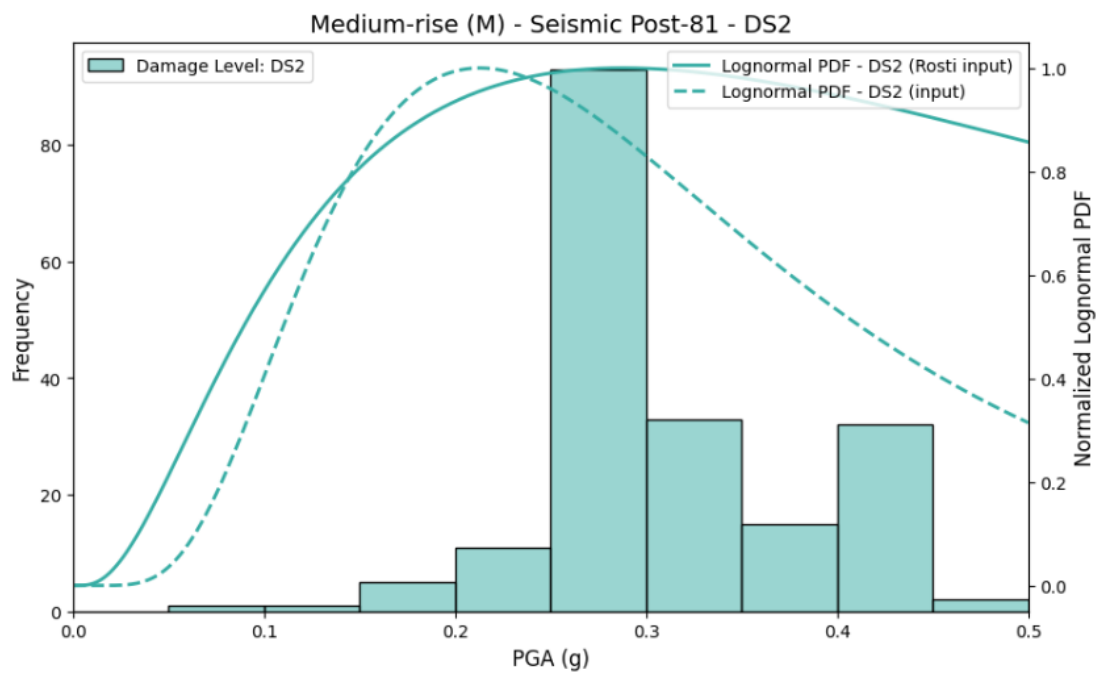
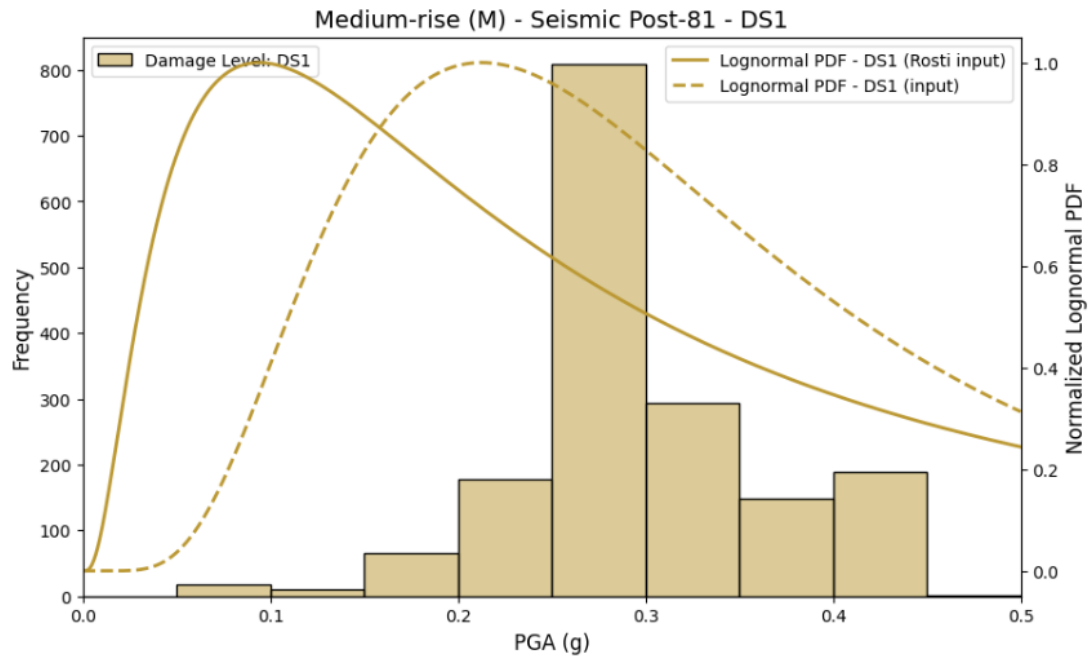
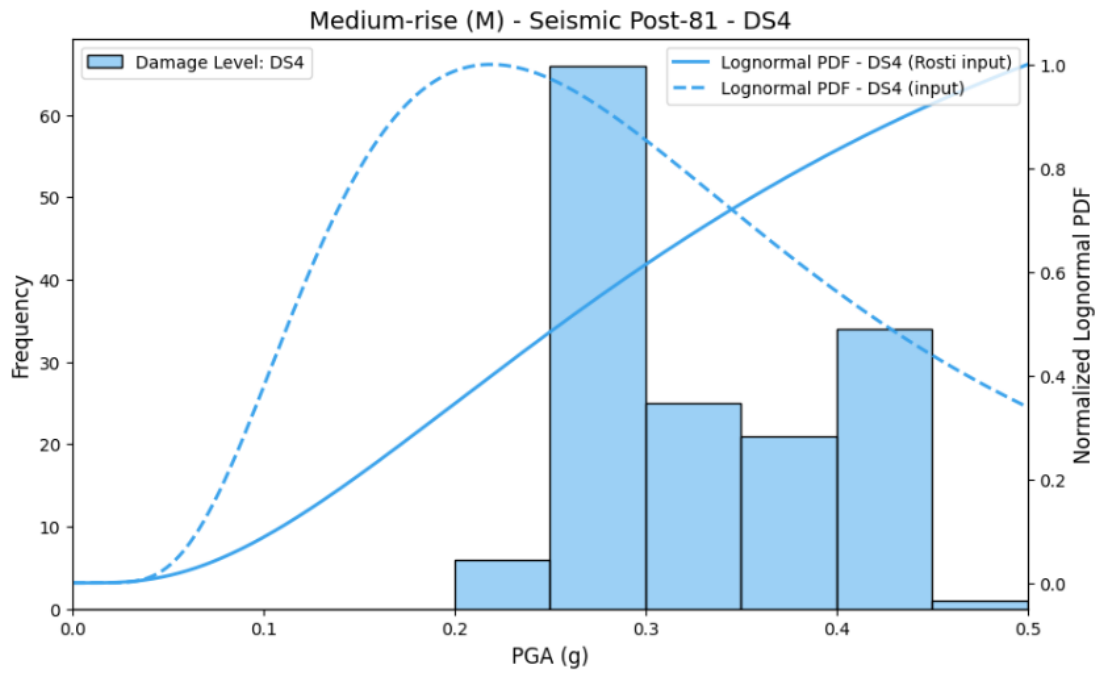
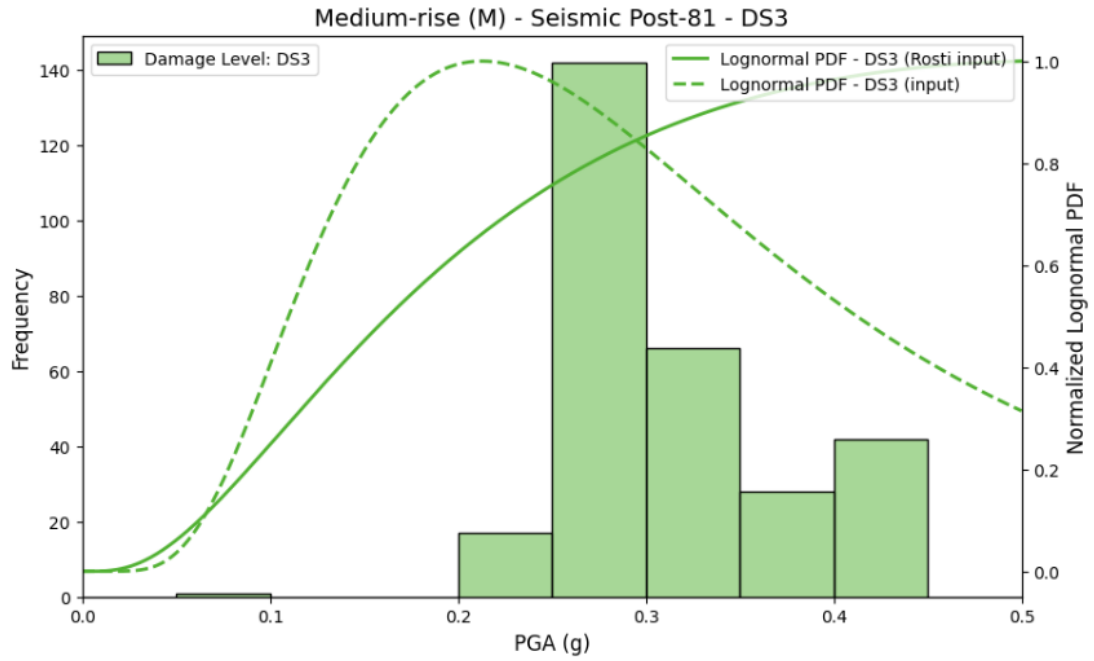


Figure 32. medium-rise Seismic pre81 building response for all damage levels, showing frequency distribution and comparison between lognormal PDF (input) and lognormal PDF (Rosti input) for each damage state





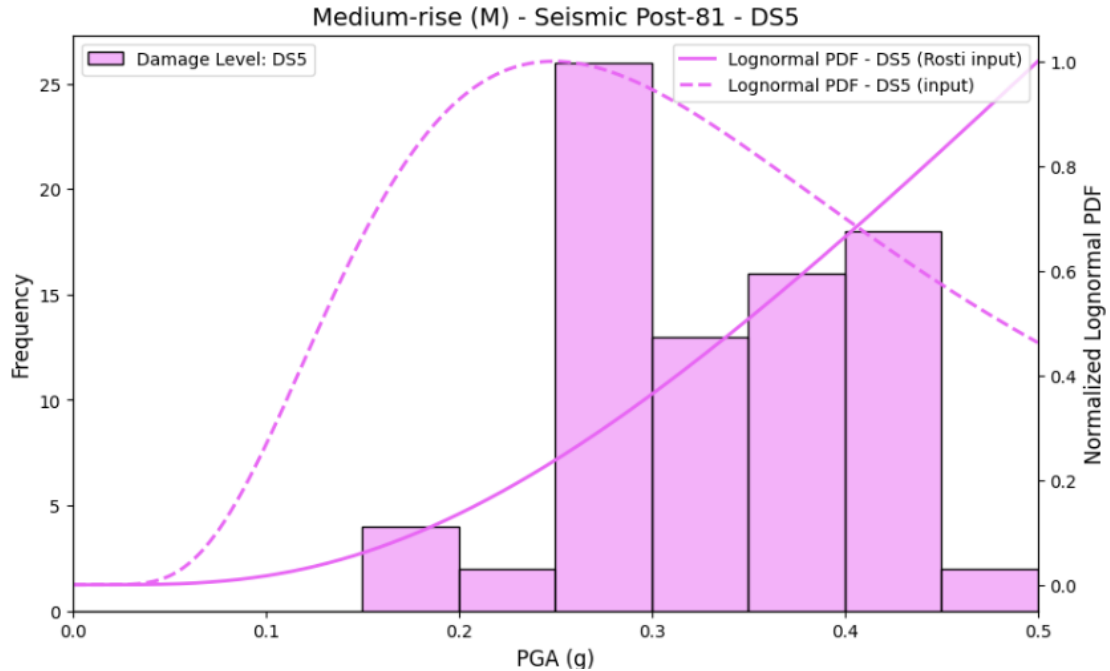
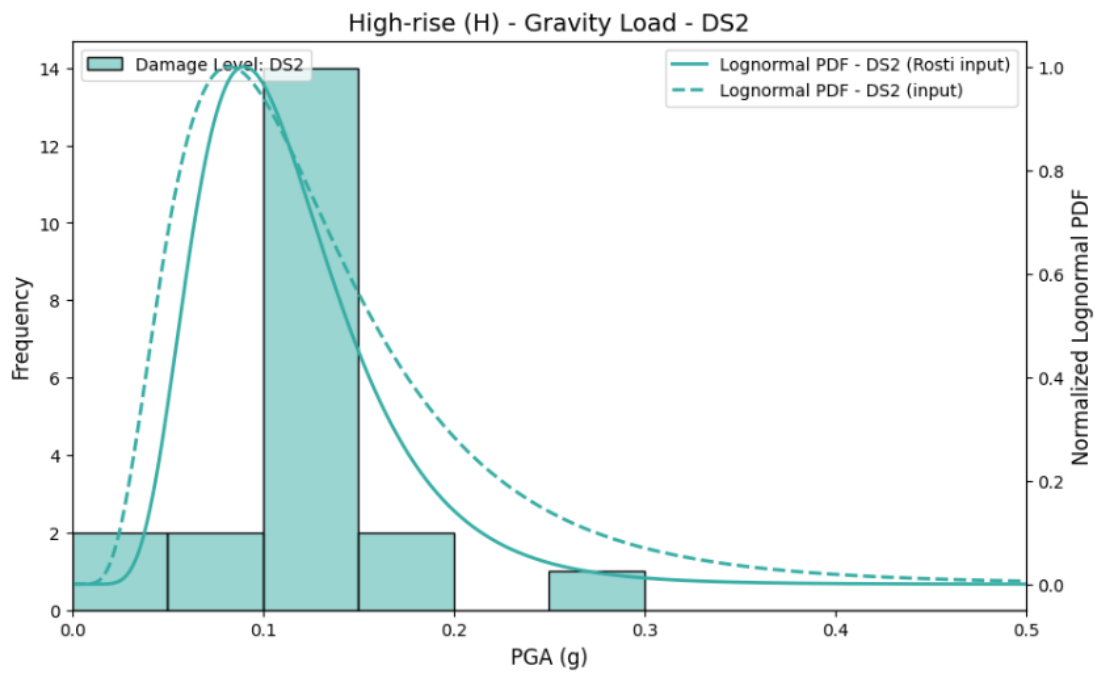
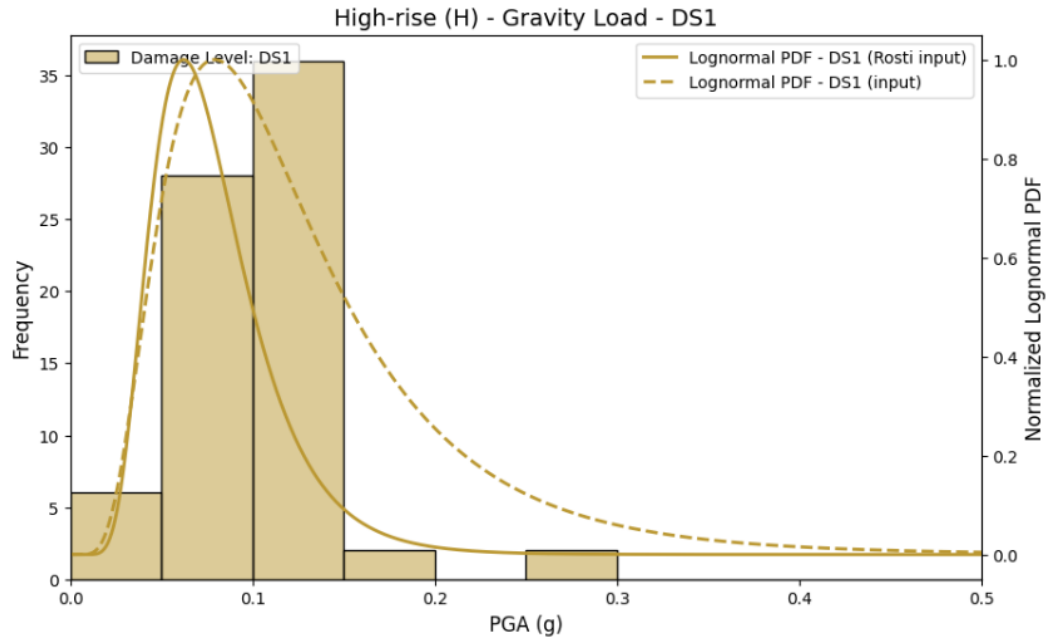
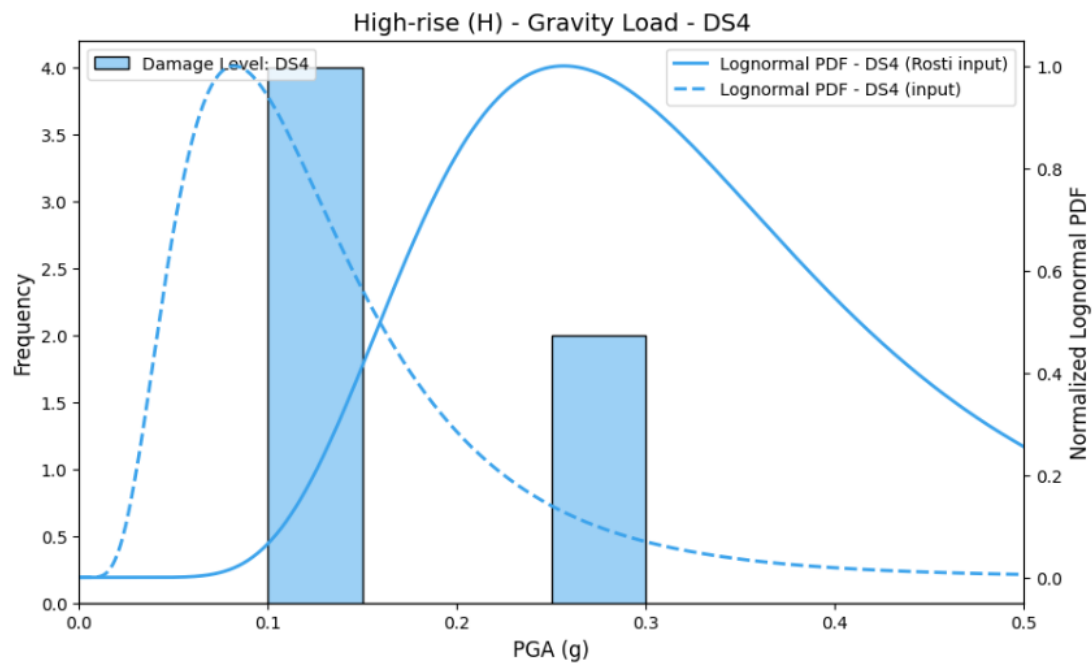
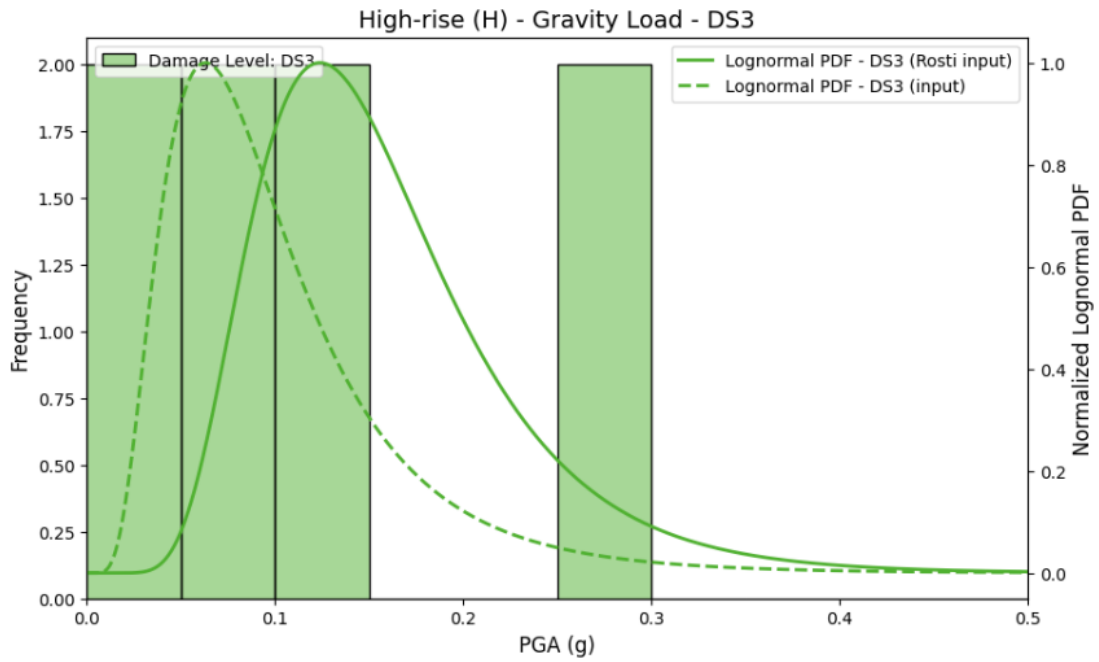


Figure 33. medium-rise Seismic post81 building response for all damage levels, showing frequency distribution and comparison between lognormal PDF (input) and lognormal PDF (Rosti input) for each damage state

A similar trend is visible for pre-code seismic reinforced concrete buildings (constructed before 1981) in the mid-rise category: alignment at lower damage levels, followed by increasing divergence at higher ones. However, in this case, the overall similarity remains better than the low-rise cases, possibly due to more consistent structural behavior or better representation in the filtered dataset. The post-code mid-rise buildings (constructed after 1981) show a nearly identical trend, with good agreement in DS1 and DS2 but growing differences as the severity of damage increases, though again, with slightly better consistency than their low-rise counterparts.





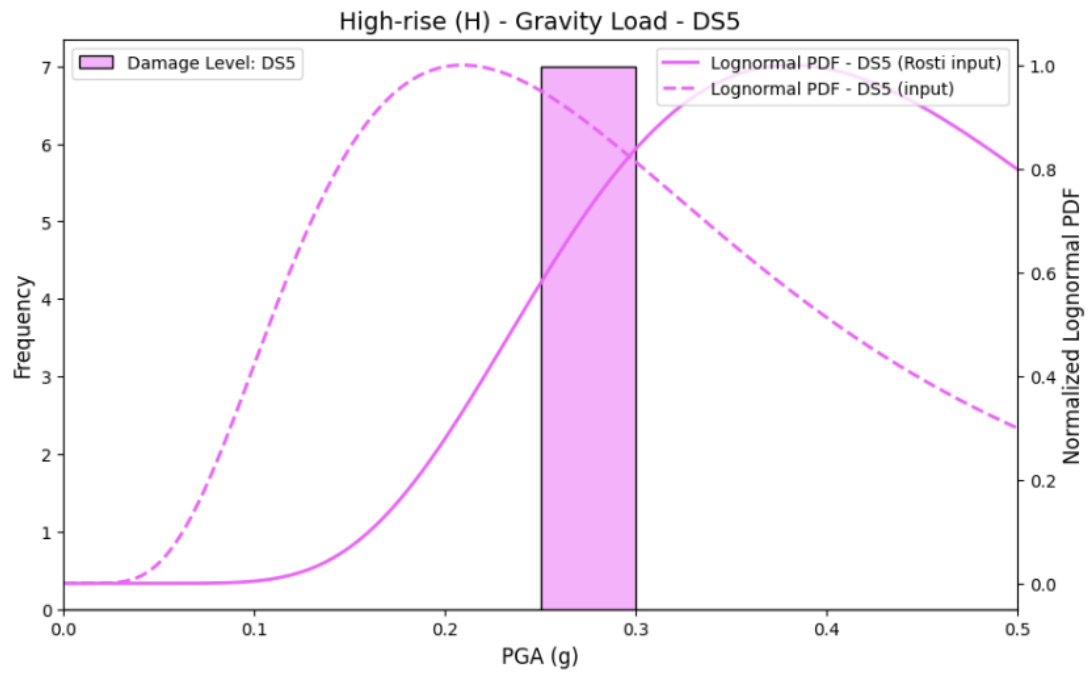
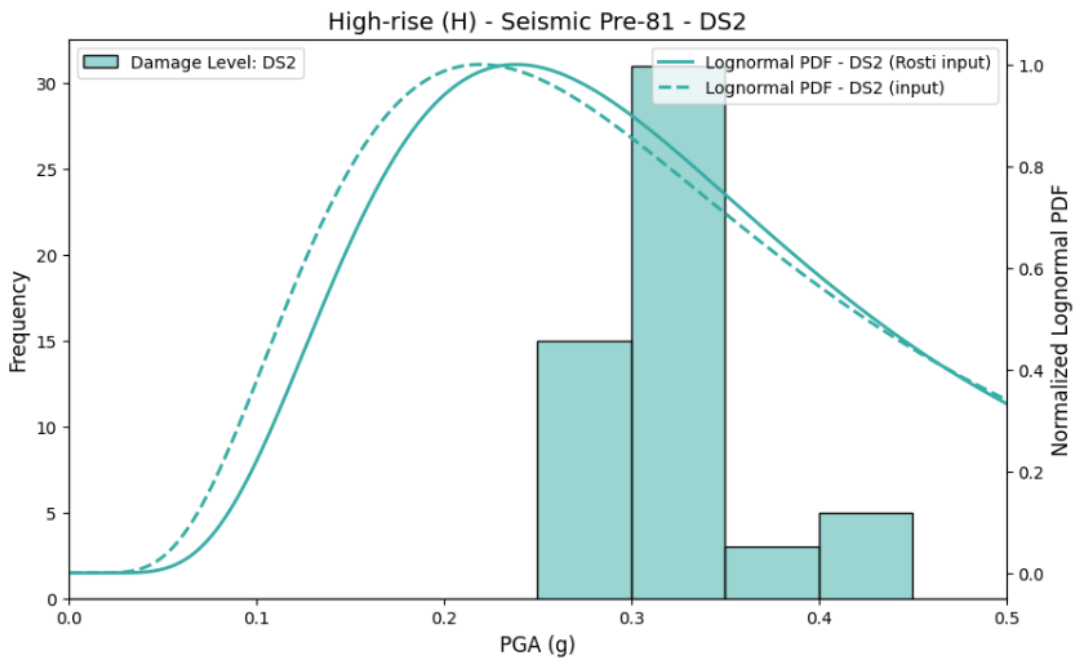
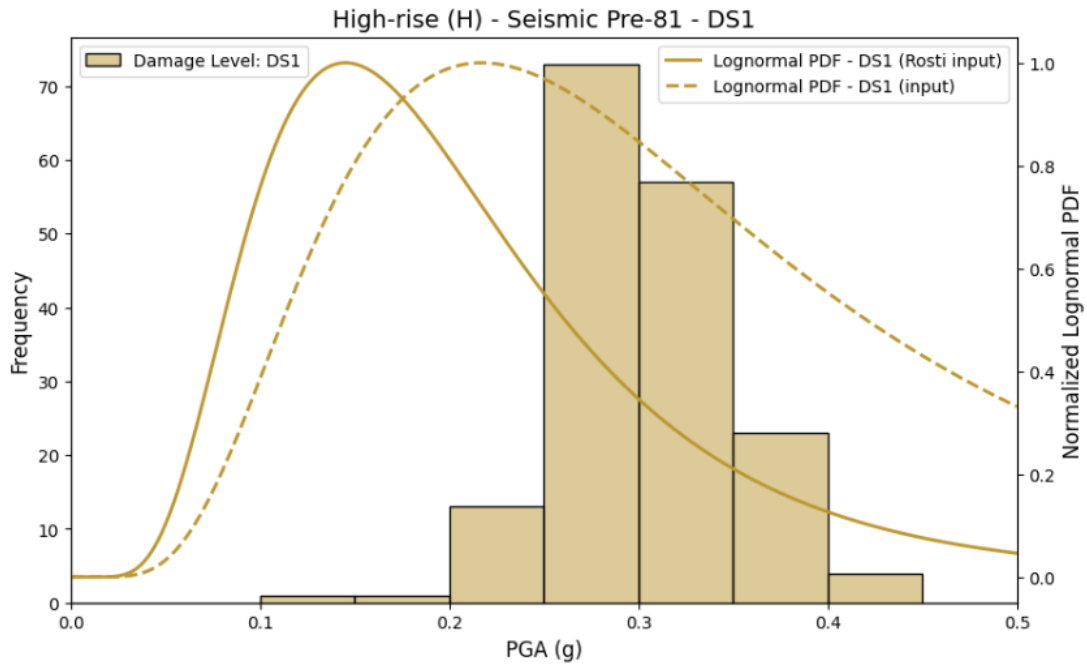
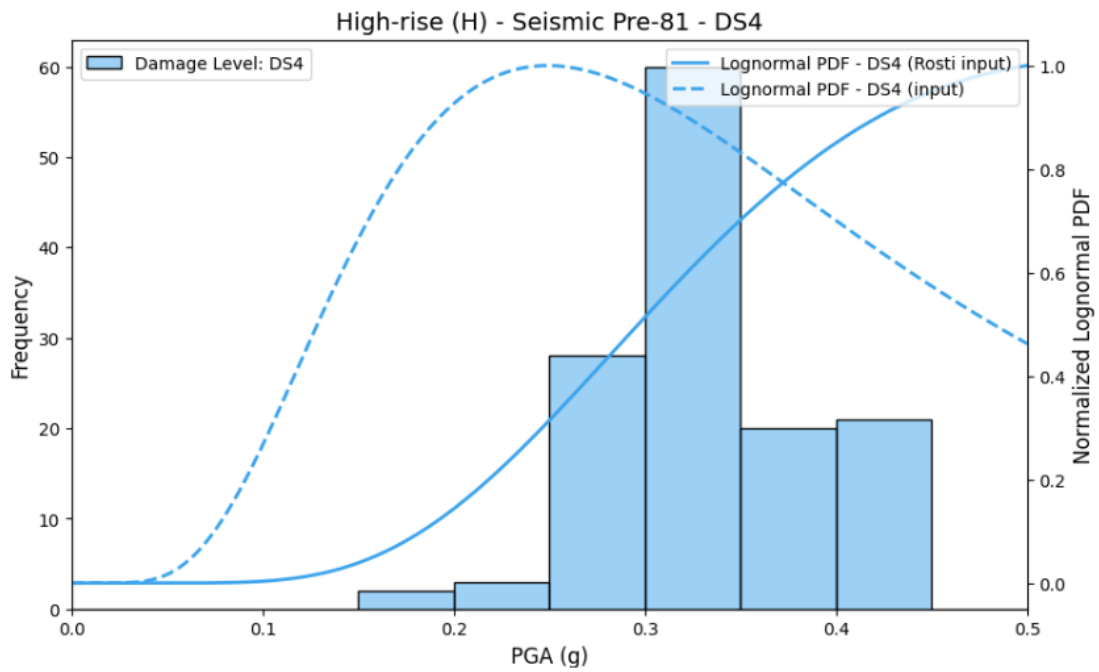
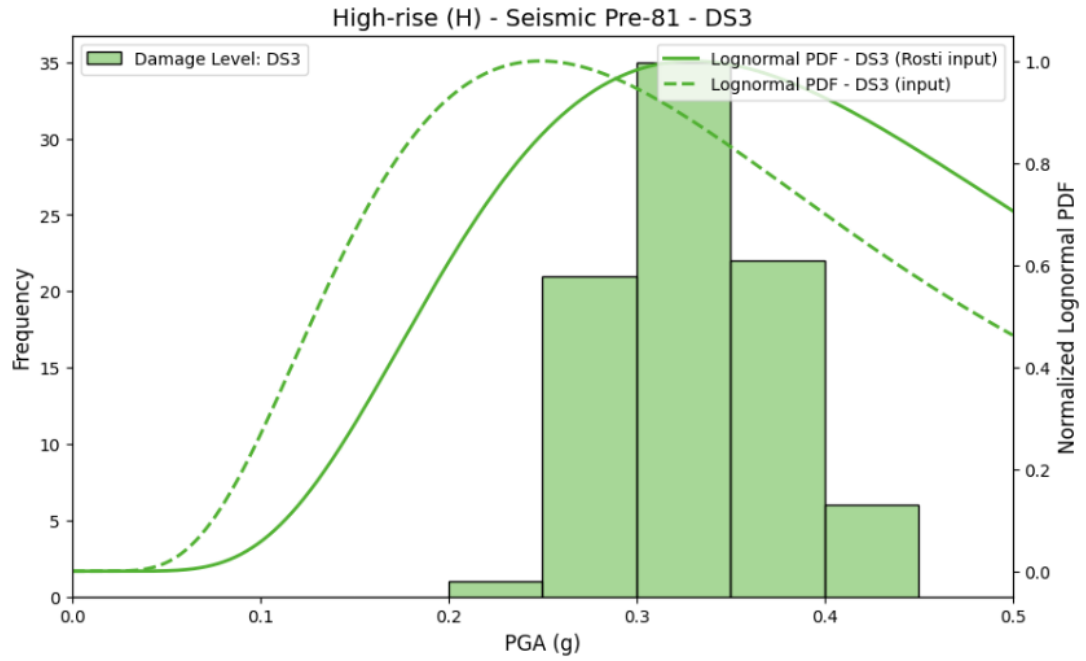


Figure 34. high-rise gravity load building response for all damage levels, showing frequency distribution and comparison between lognormal PDF (input) and lognormal PDF (Rosti input) for each damage state





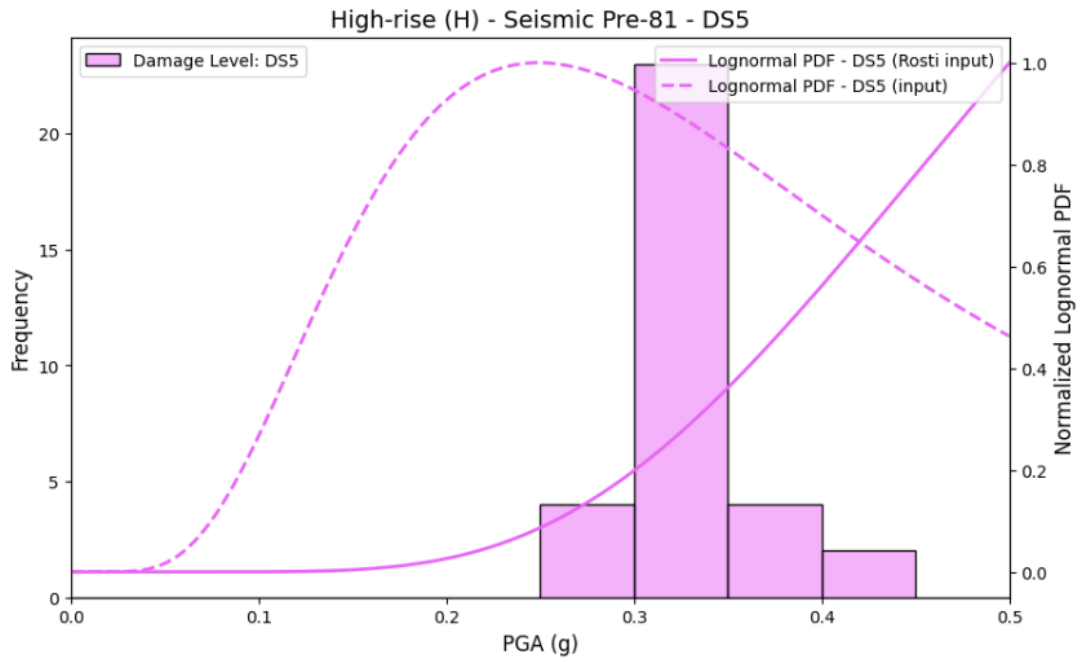
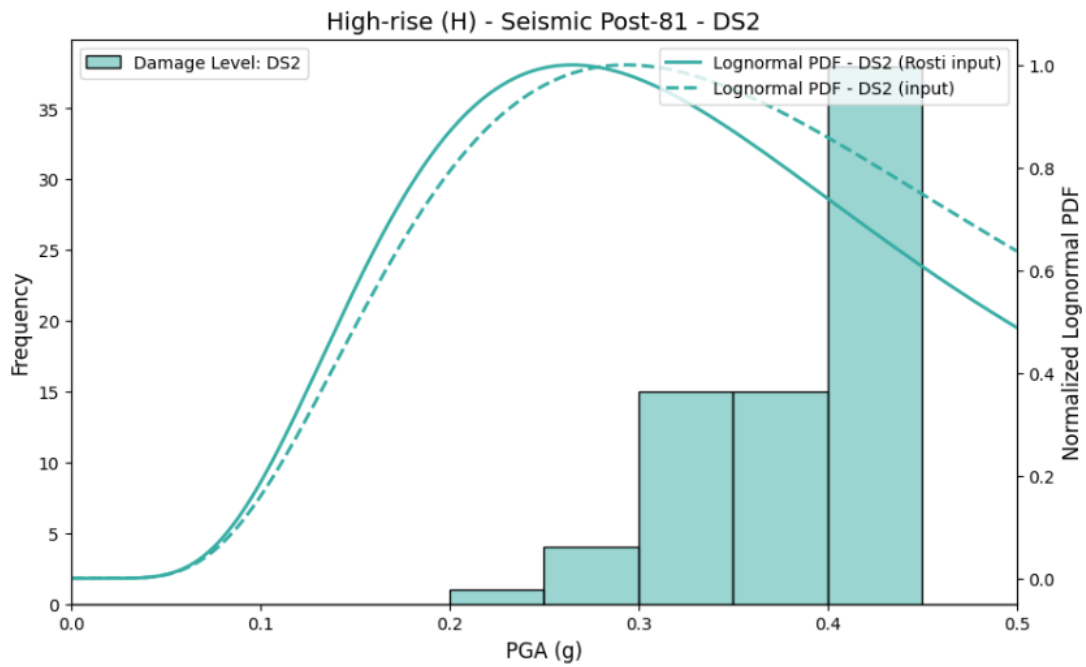
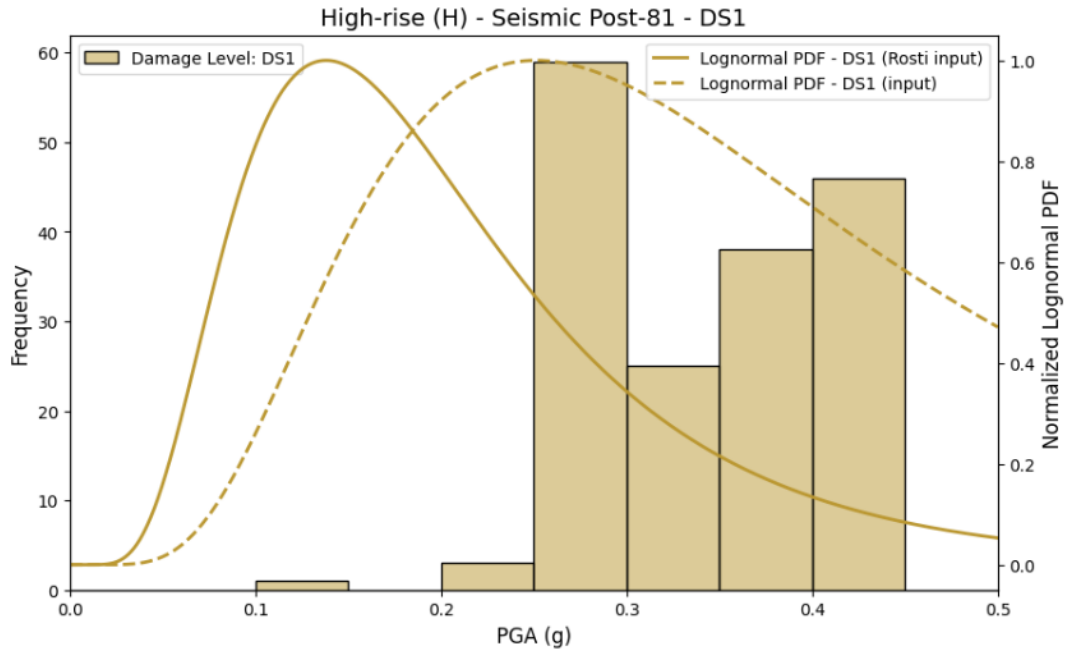
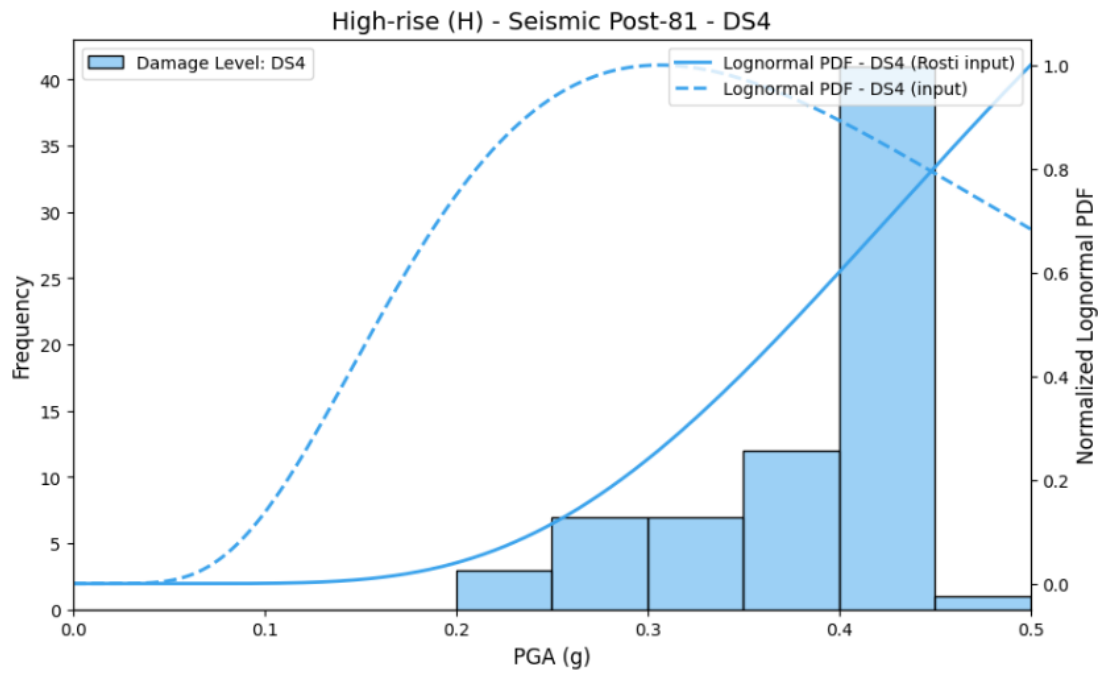
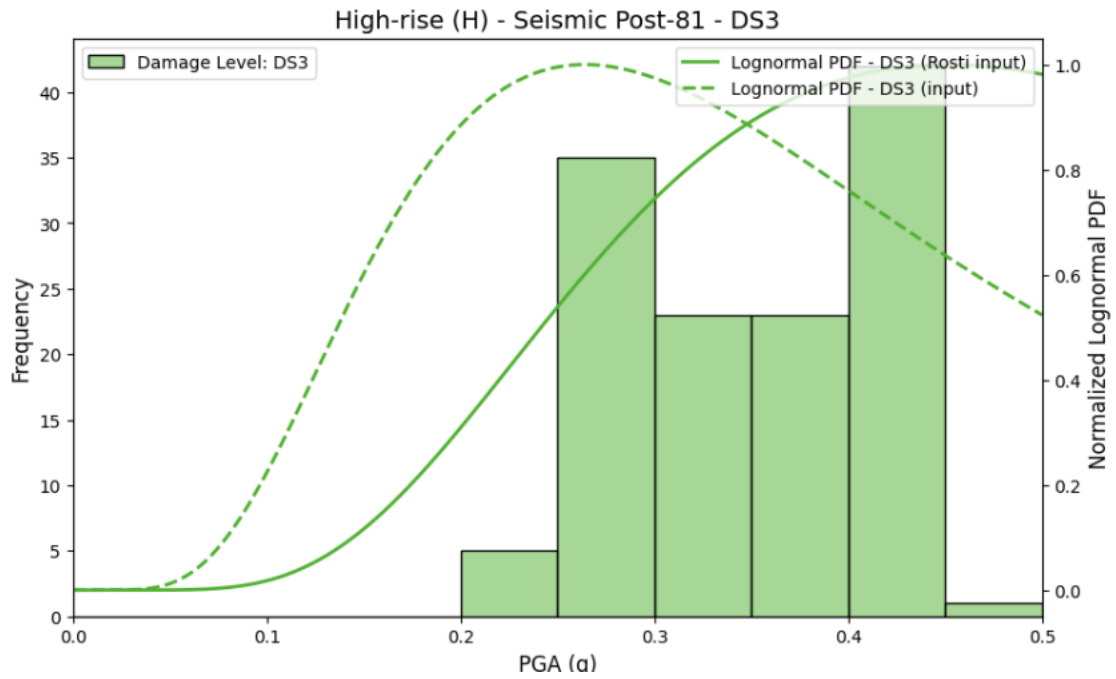


Figure 35. high-rise Seismic pre81 building response for all damage levels, showing frequency distribution and comparison between lognormal PDF (input) and lognormal PDF (Rosti input) for each damage state





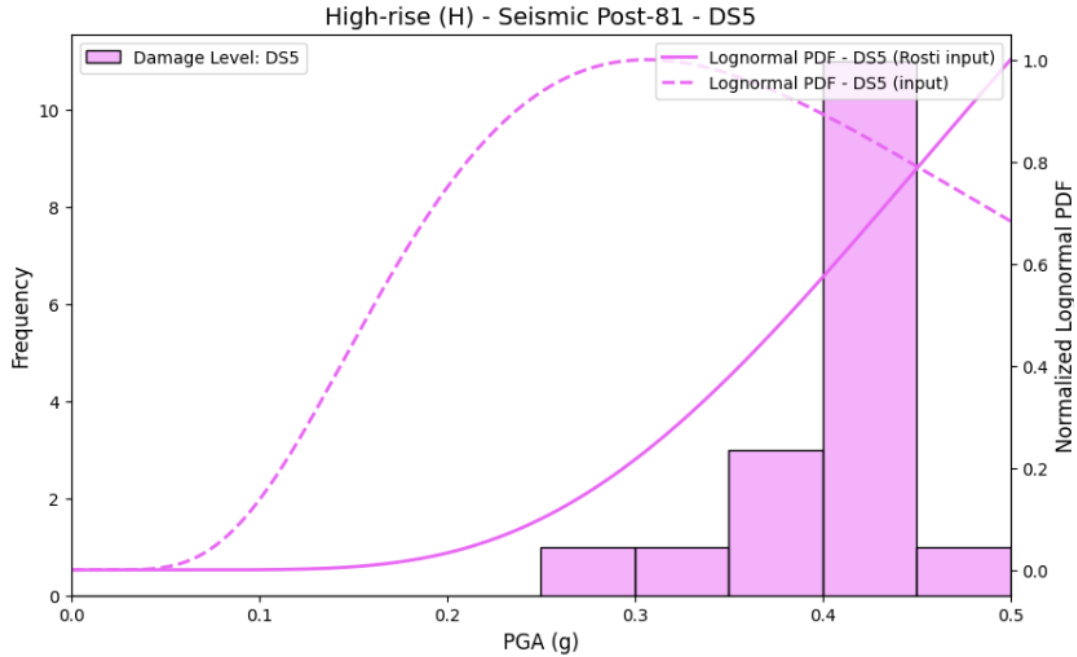


Figure 36. medium-rise Seismic post81 building response for all damage levels, showing frequency distribution and comparison between lognormal PDF (input) and lognormal PDF (Rosti input) for each damage state

When looking at high-rise structures, a noticeable shift of the curves to the right is observed in my results, indicating that higher PGA values are needed to reach the same probability of damage as estimated by Rosti. However, despite this horizontal shift, the overall trend remains similar, and especially at lower damage states, the curves show matched behavior, suggesting a shared understanding of how high-rise buildings begin to respond under seismic loading.

The comparison of the Rosti model's Cumulative Distribution Function (CDF) with the input data can be visualized as follows:

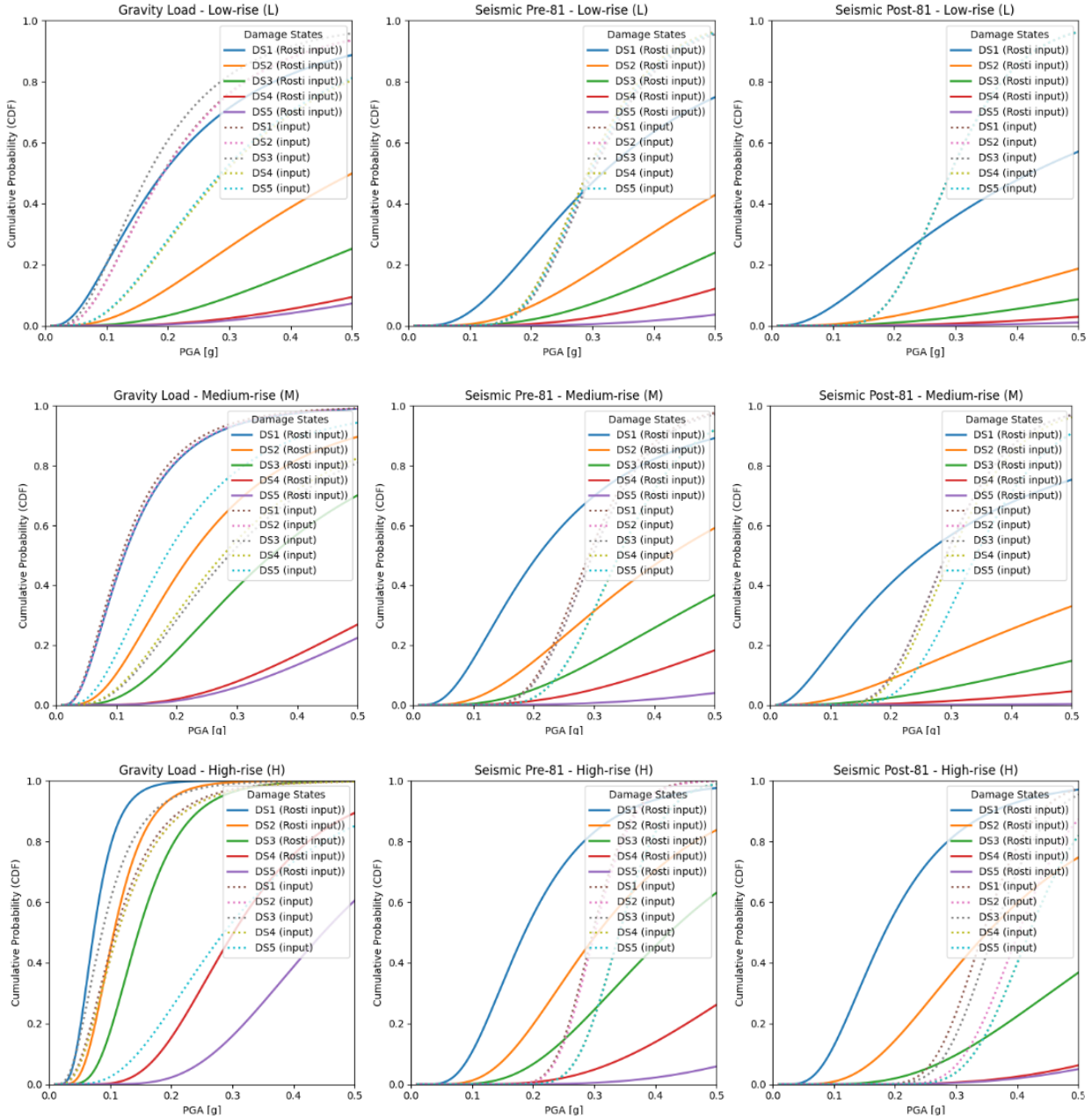


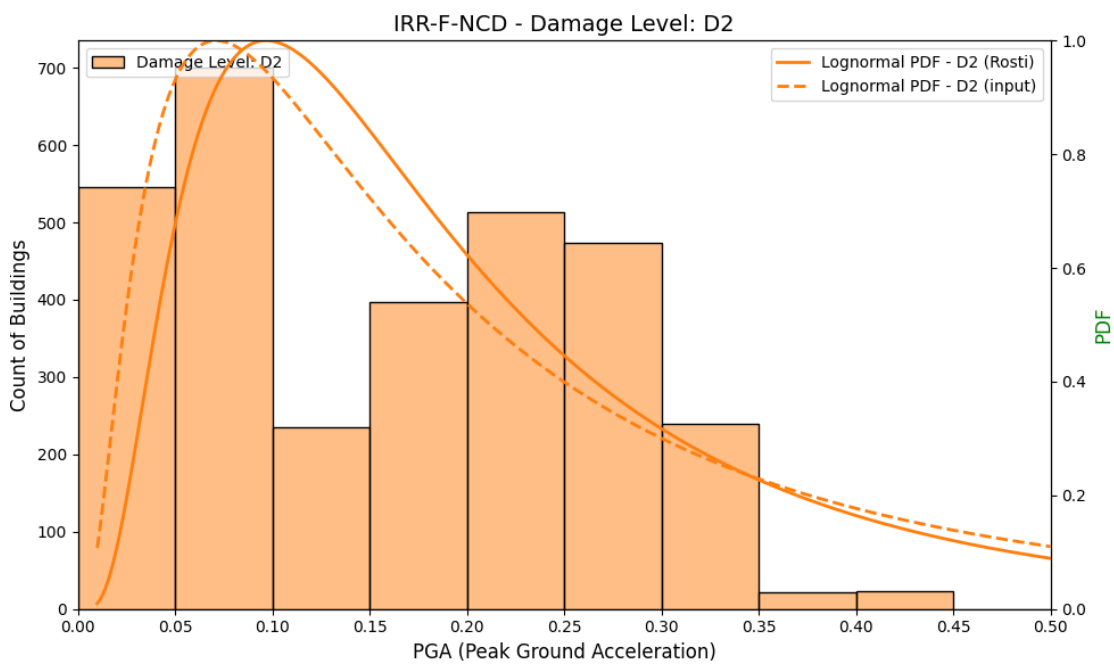
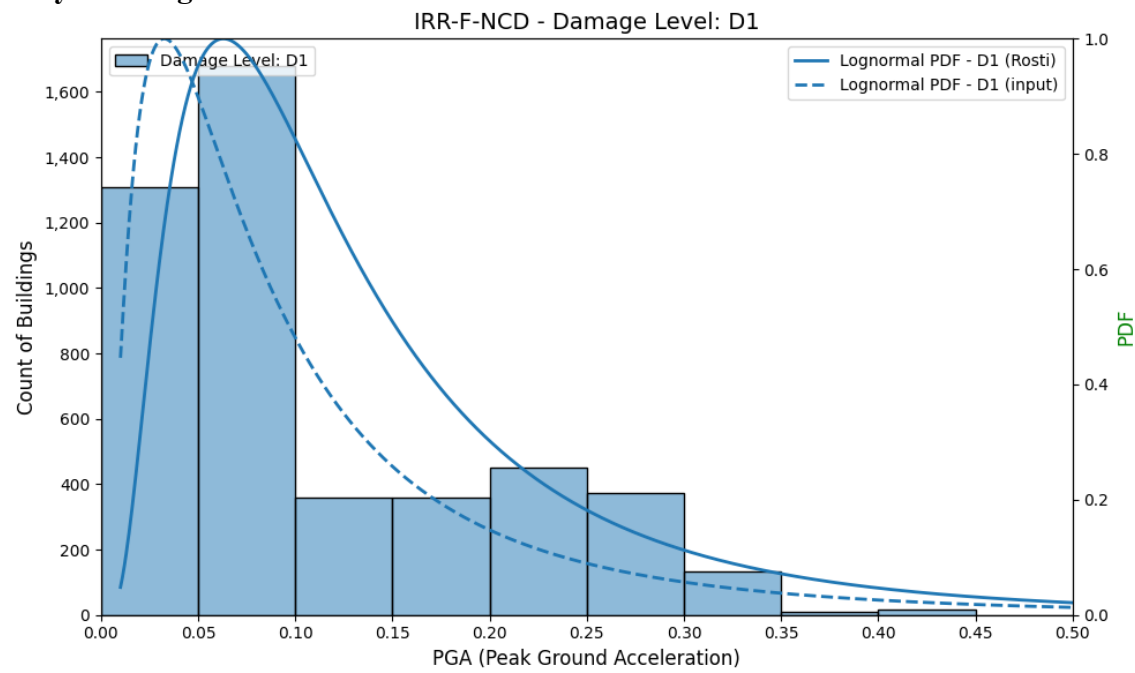
Figure 37. Cumulative distribution functions (CDFs) for low-rise, medium-rise, and high-rise buildings under gravity load, seismic pre-81, and seismic post-81 design levels, comparing input and Rosti lognormal curves across all damage states (DS1–DS5).

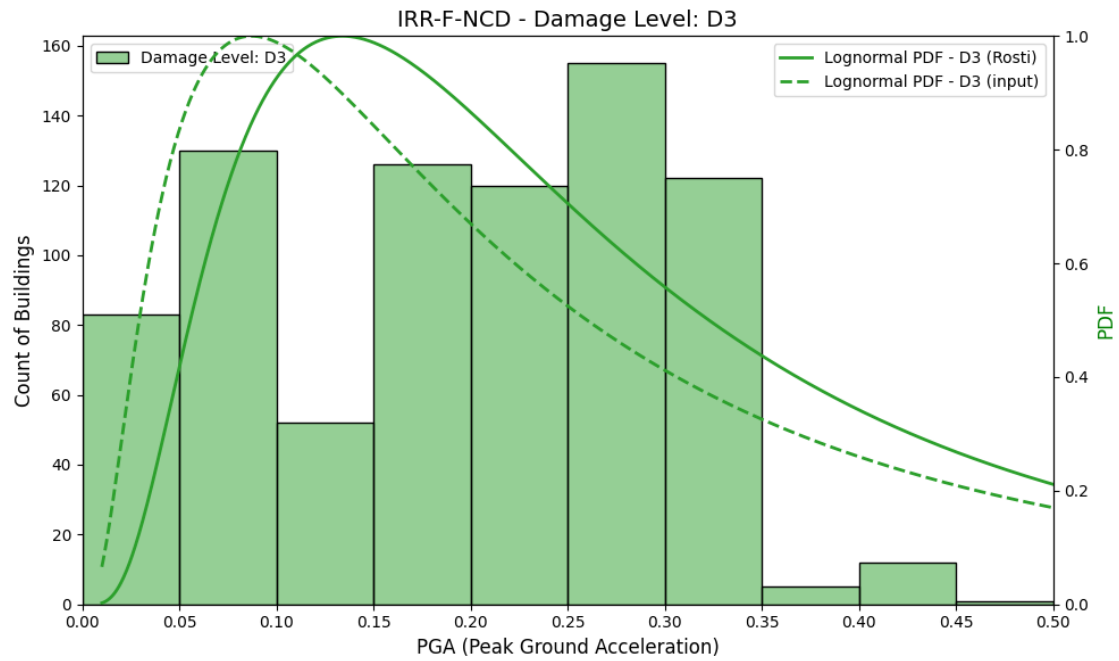
In almost all cases, the expected trend of increasing probability with higher damage states and a clear separation between damage levels is not well captured in the input curves derived from my dataset and filtering approach. This pattern, however, is visible in the original curves presented by

Rosti. In Rosti's model, the progression from DS1 to DS5 follows a logical and smooth increase in probability, with consistent spacing between each damage level. In contrast, my curves often show overlapping or irregular transitions between damage states, making it more difficult to distinguish the progression of structural degradation as seismic intensity increases.

The exception is in the gravity load case, where the figures show relatively good similarity between the input data and Rosti's model. In the other typologies, however, my results exhibit a sharper change between damage states, especially in the higher ones, while Rosti's curves maintain a more gradual and continuous increase. This difference suggests that while my filtering method may have improved data quality by removing inconsistencies, it may also have reduced the smoothness and continuity of the damage progression visible in the original model.

Masonry buildings





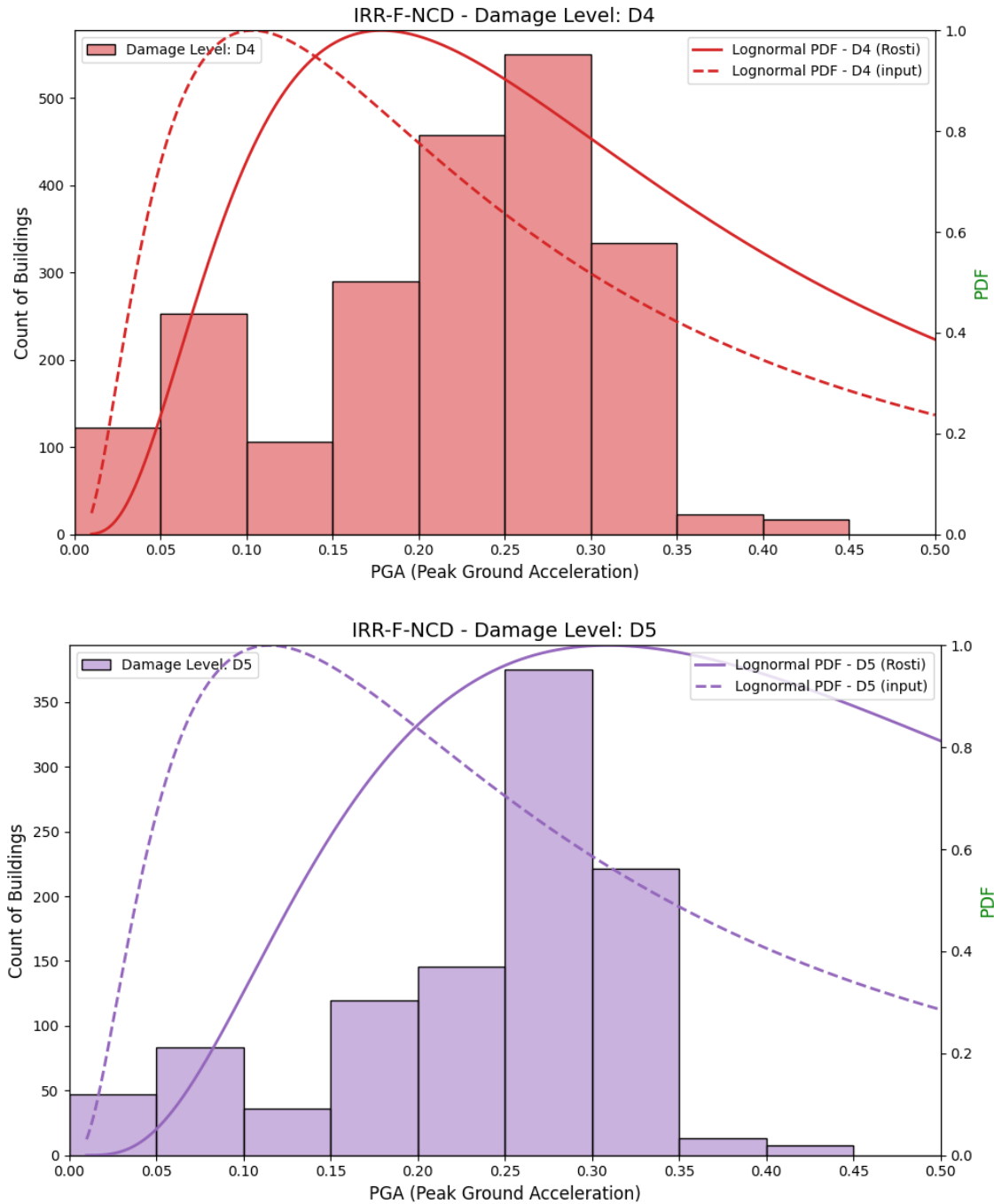
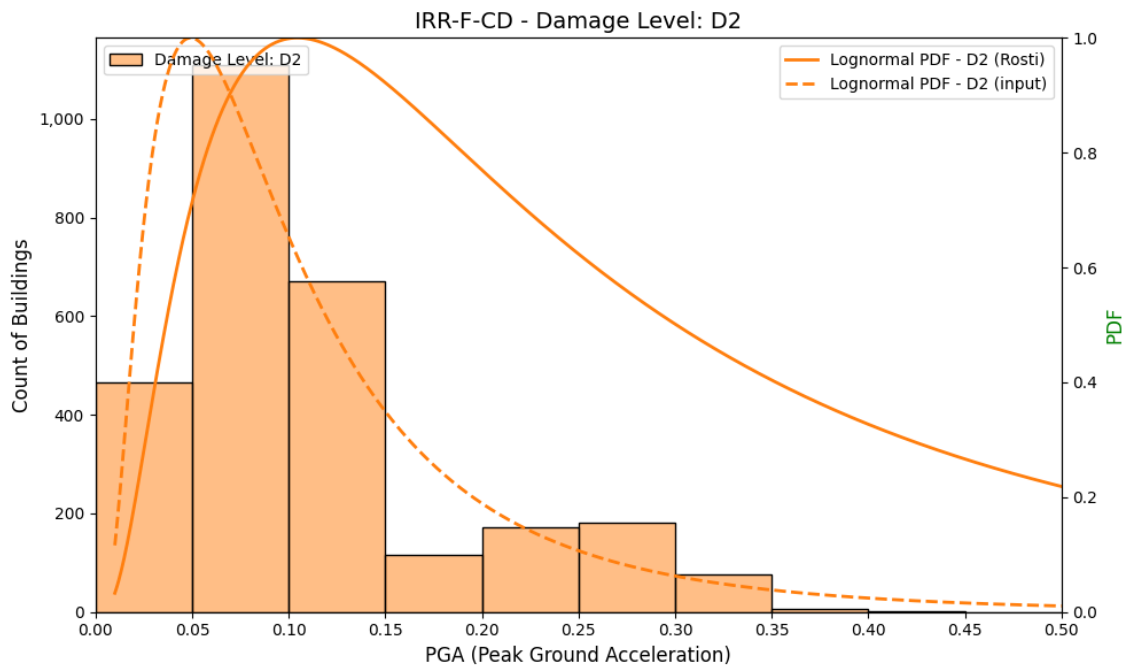
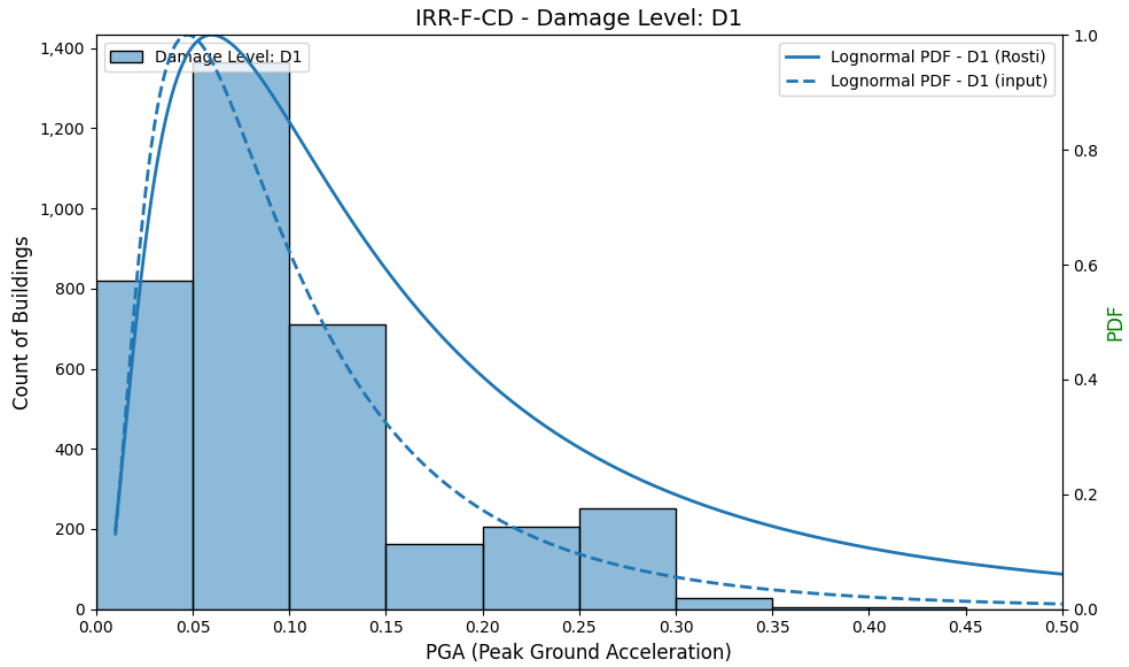
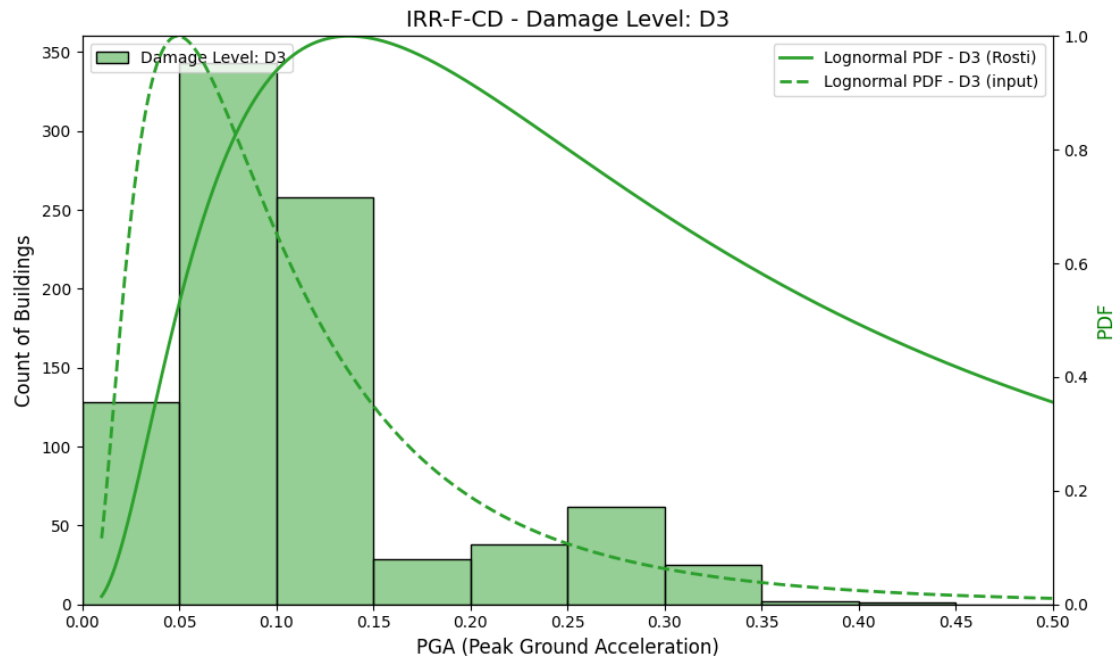


Figure 38. IRR-F-NCD damage level distributions (DS1–DS5) for masonry buildings

For the IRR-F-NCD class, there is a clear increase in the gap between the input data and Rosti's curves as the damage level increases. However, in the lower damage states, particularly DS1 and DS2, the two models display a similar trend, although with a noticeable shift to the left in the input curve, indicating a higher estimated vulnerability at lower PGA levels.





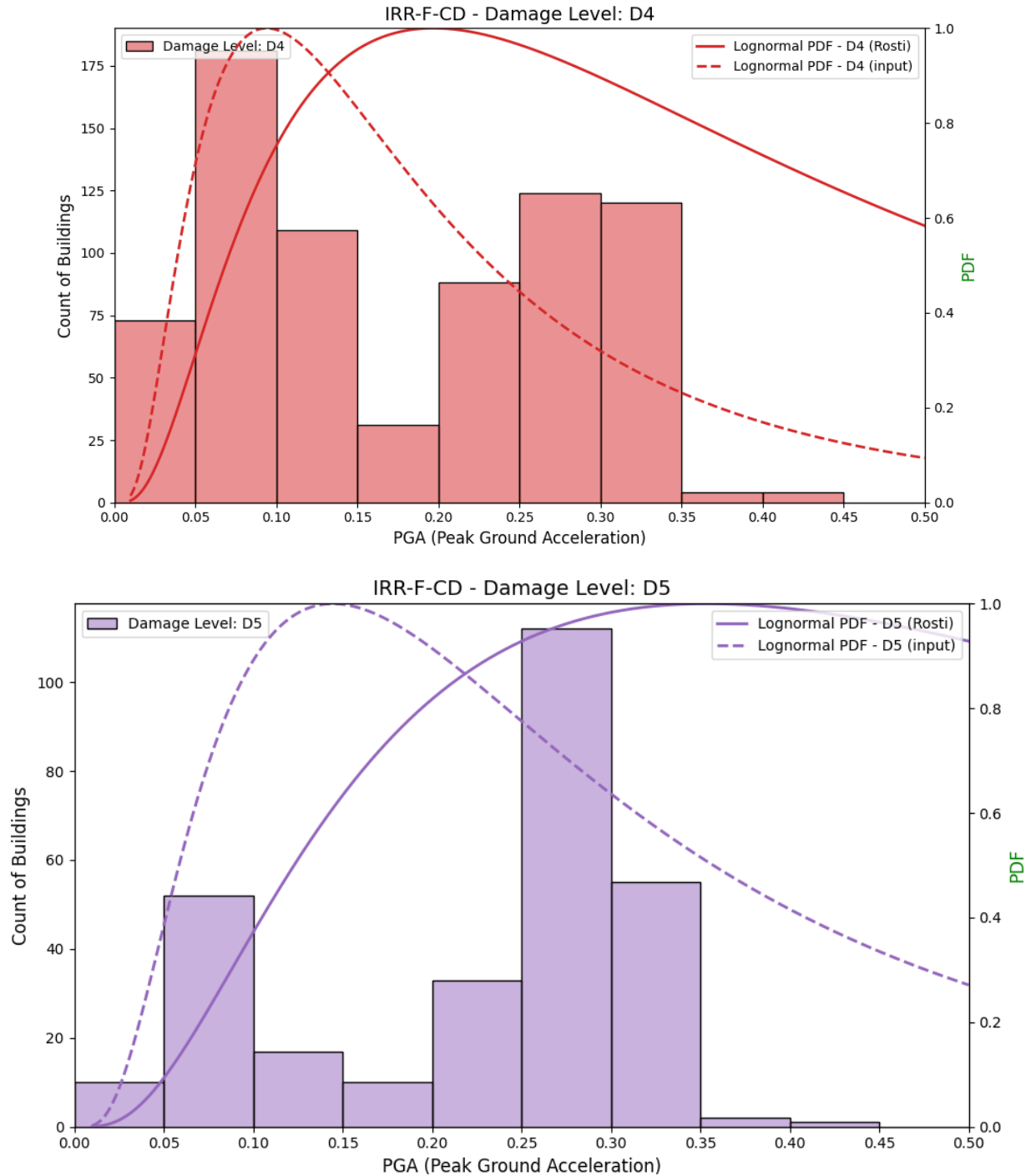
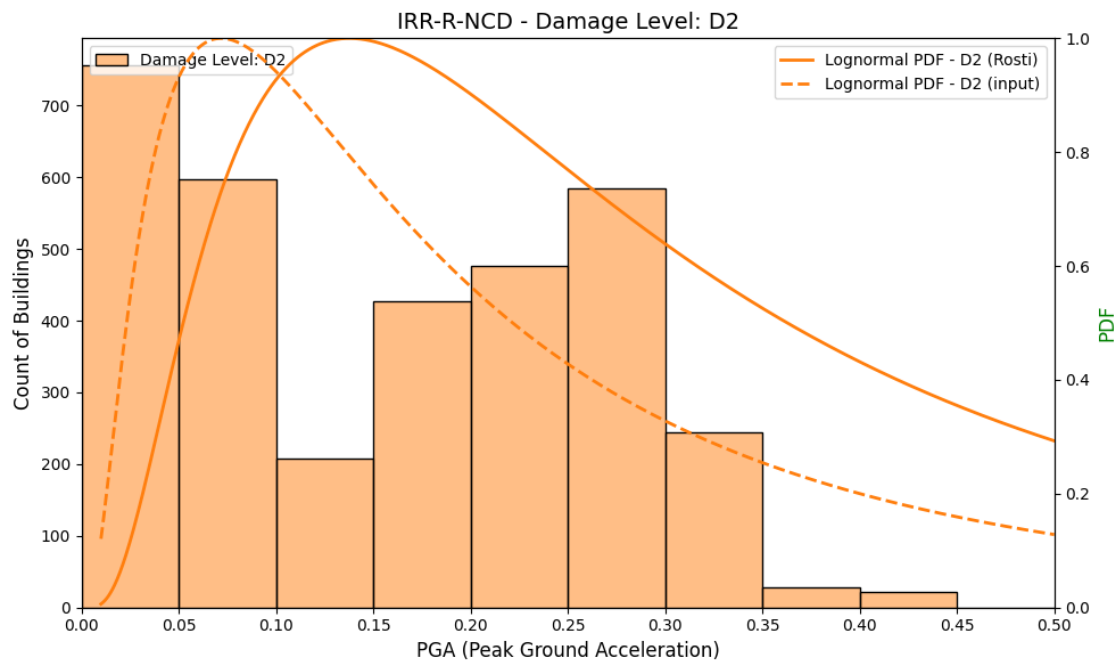
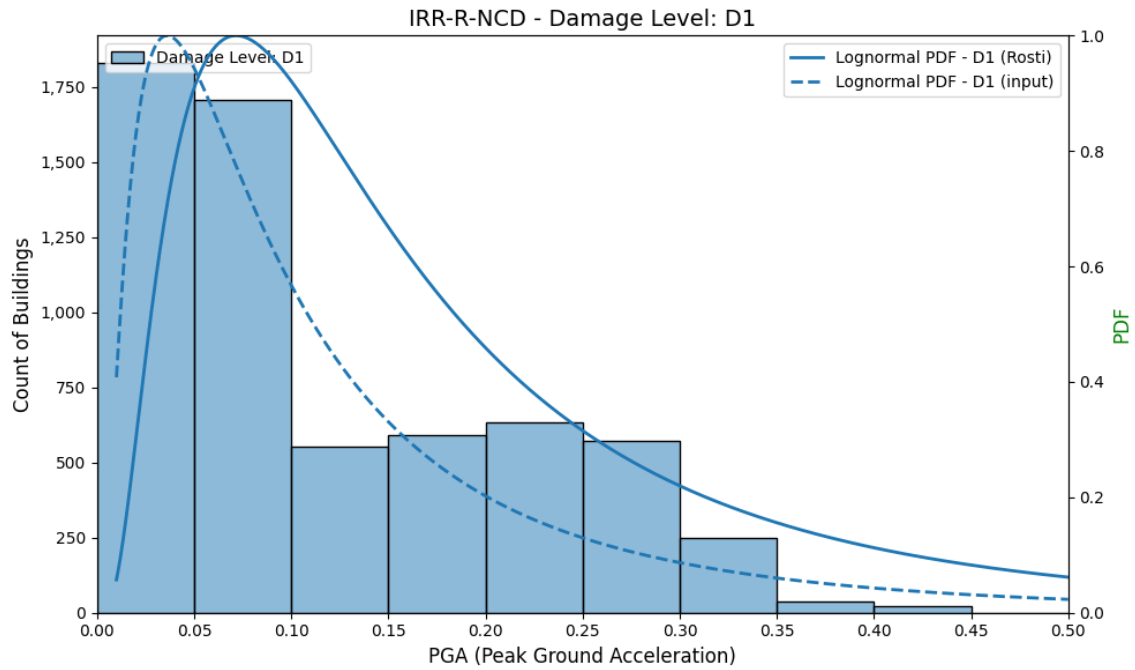
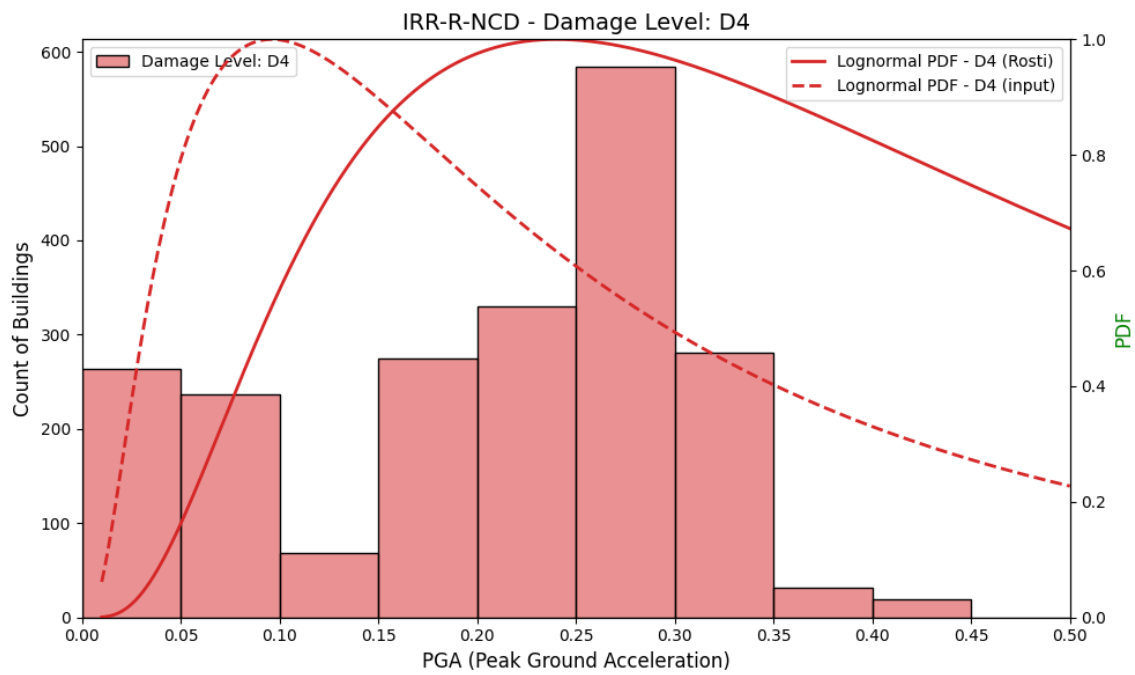
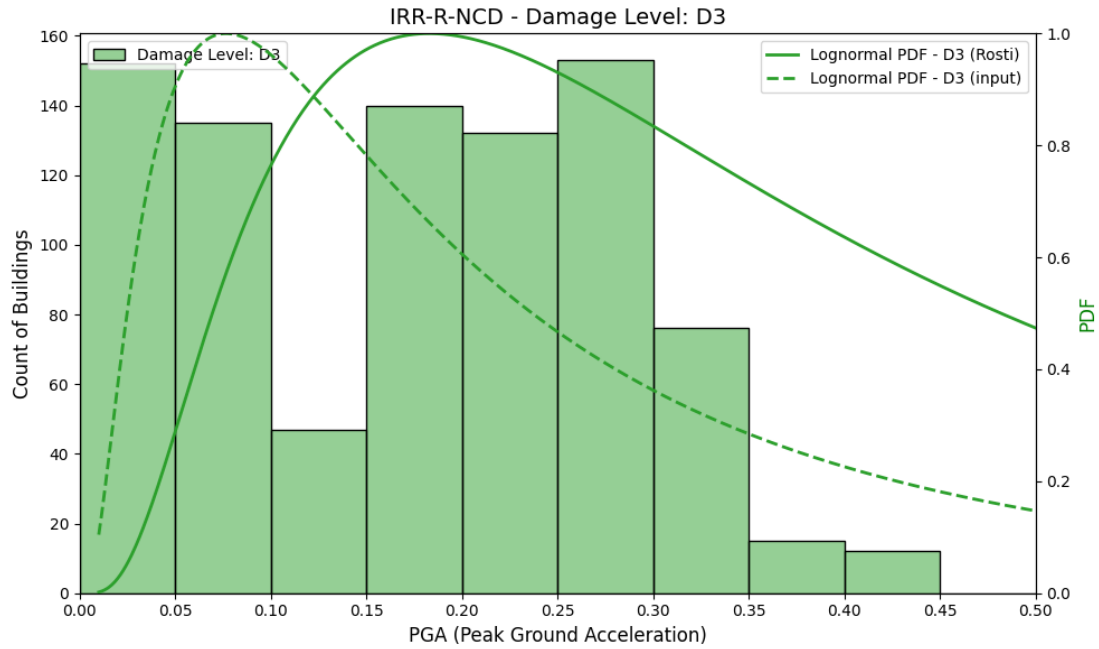


Figure 39. IRR-F-CD damage level distributions (DS1–DS5) for masonry buildings

In the IRR-F-CD typology, the match is strong in the early damage states, with DS1 and DS2 closely matching Rosti's results. However, the similarity drops significantly at DS5, where the input curve diverges, suggesting a much different prediction of collapse probability. A similar pattern is observed in IRR-R-NCD: while the lower damage levels align well, the higher damage states show growing differences, with a steeper increase in the input model.





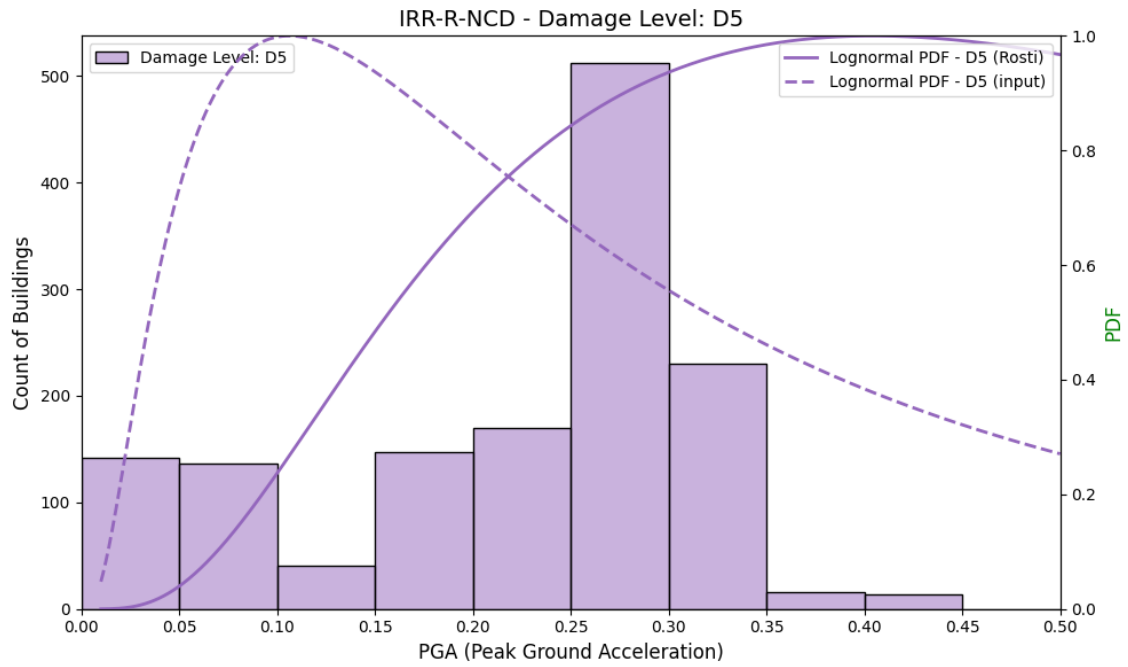
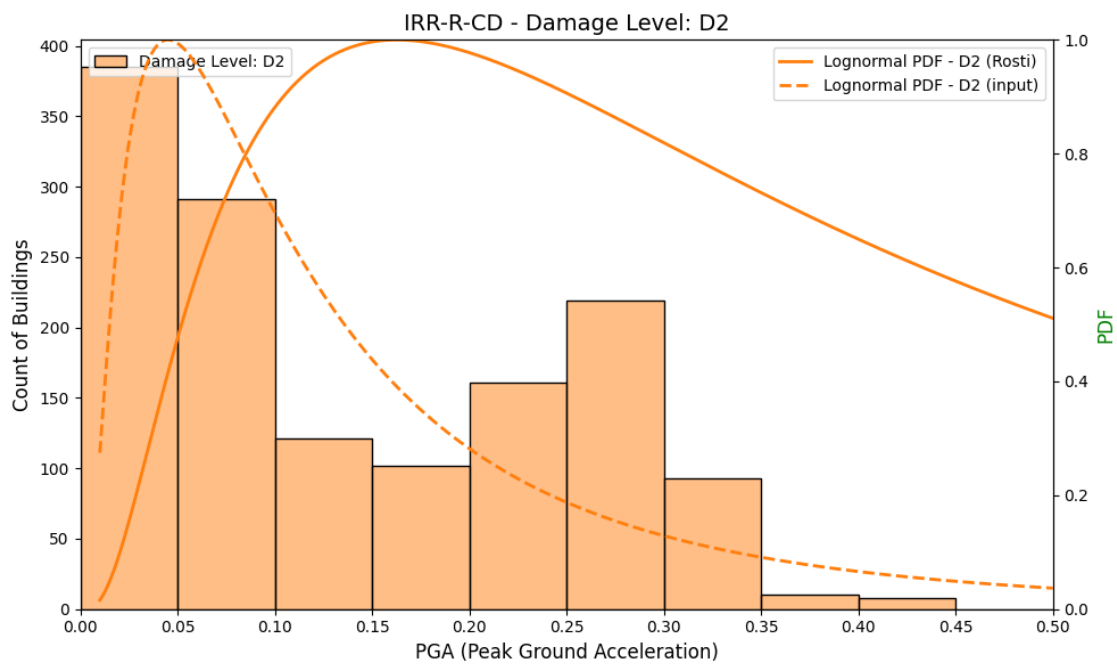
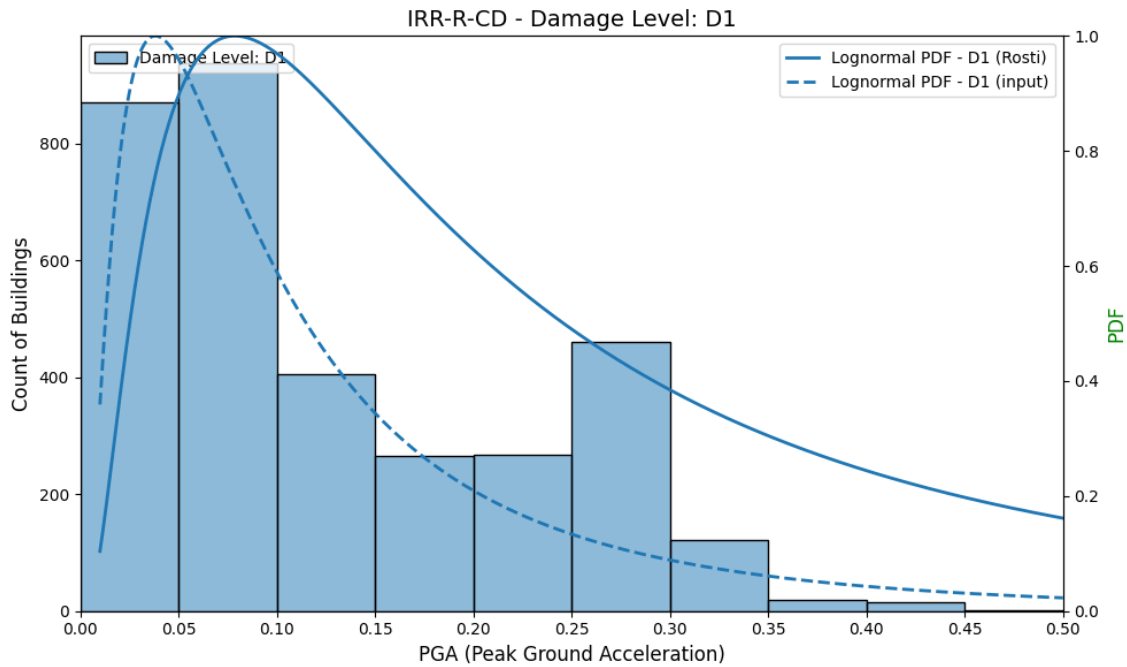
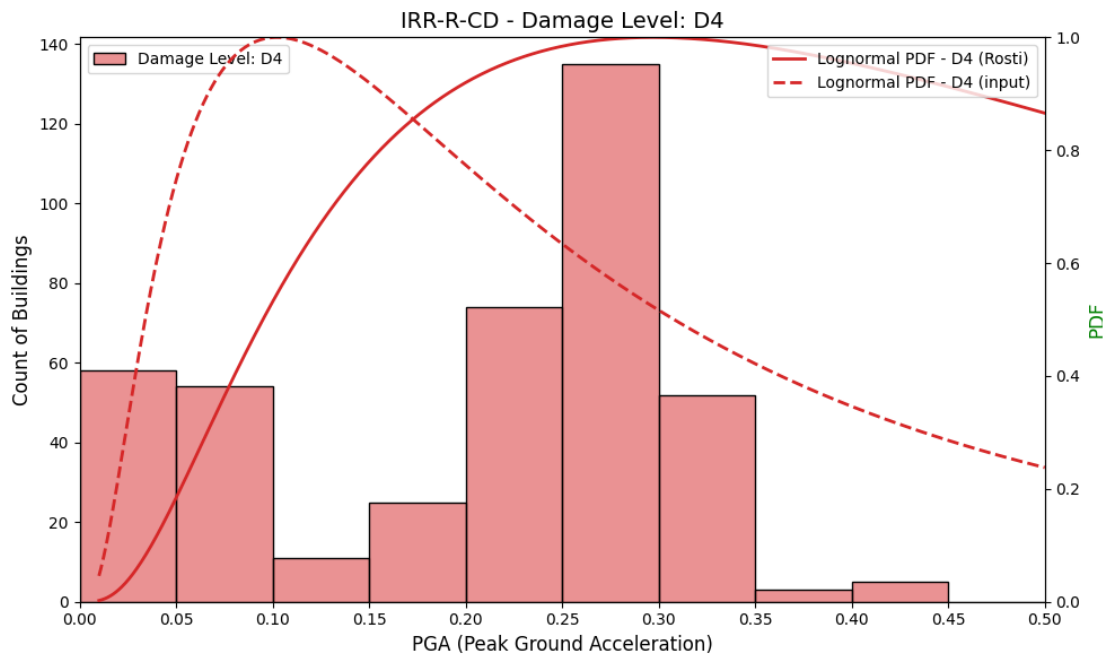
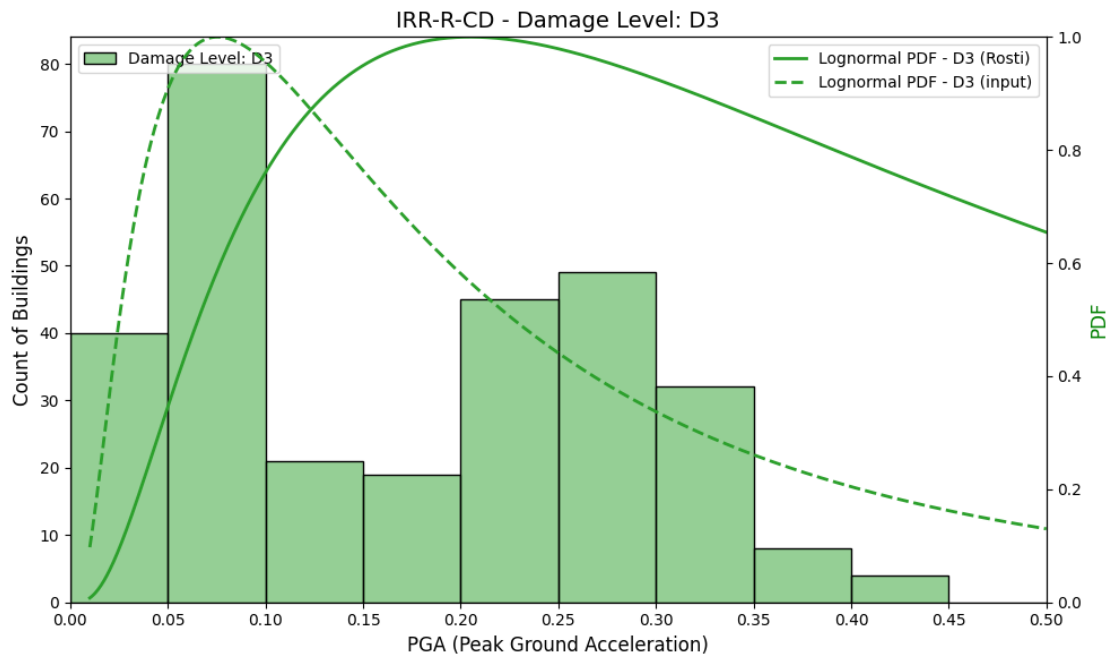


Figure 40. IRR-R-NCD damage level distributions (DS1–DS5) for masonry buildings





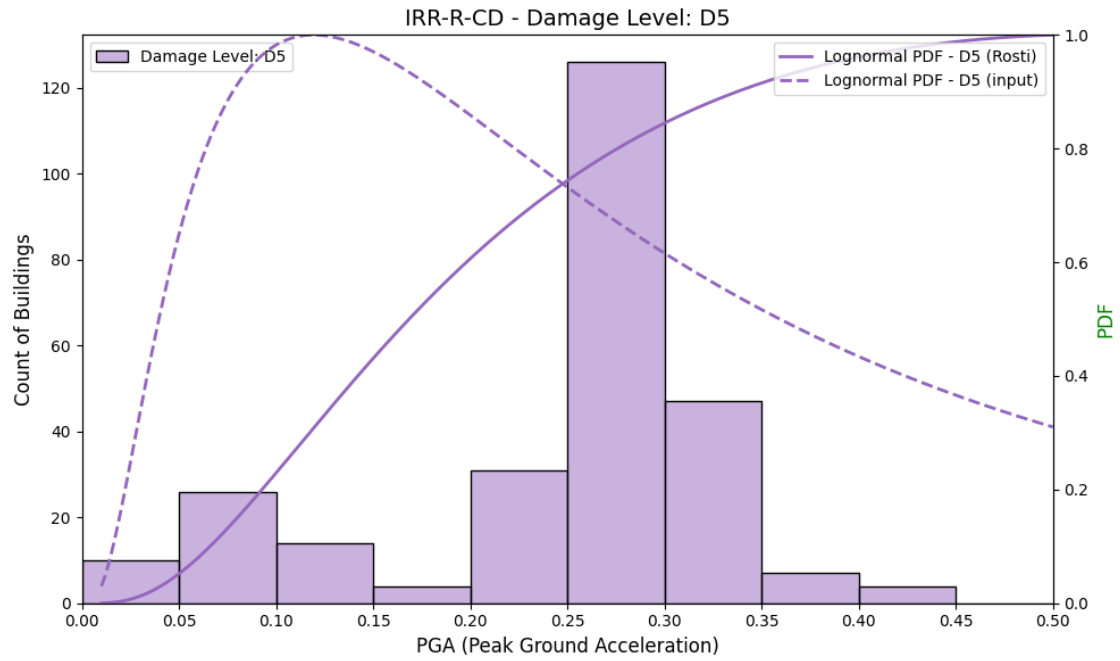
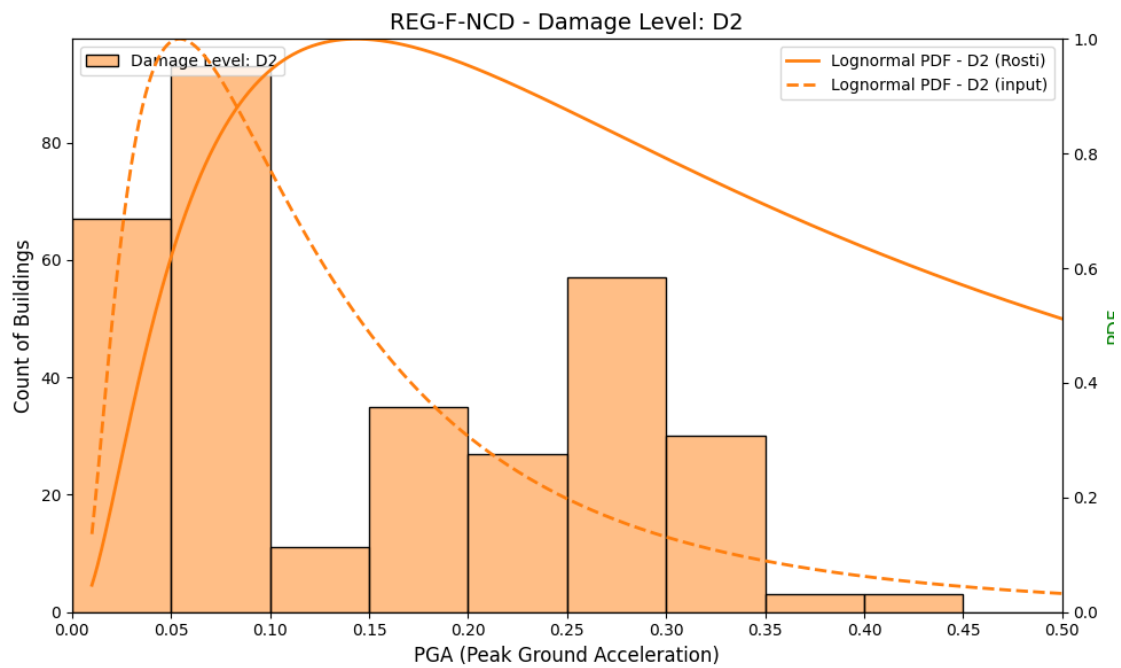
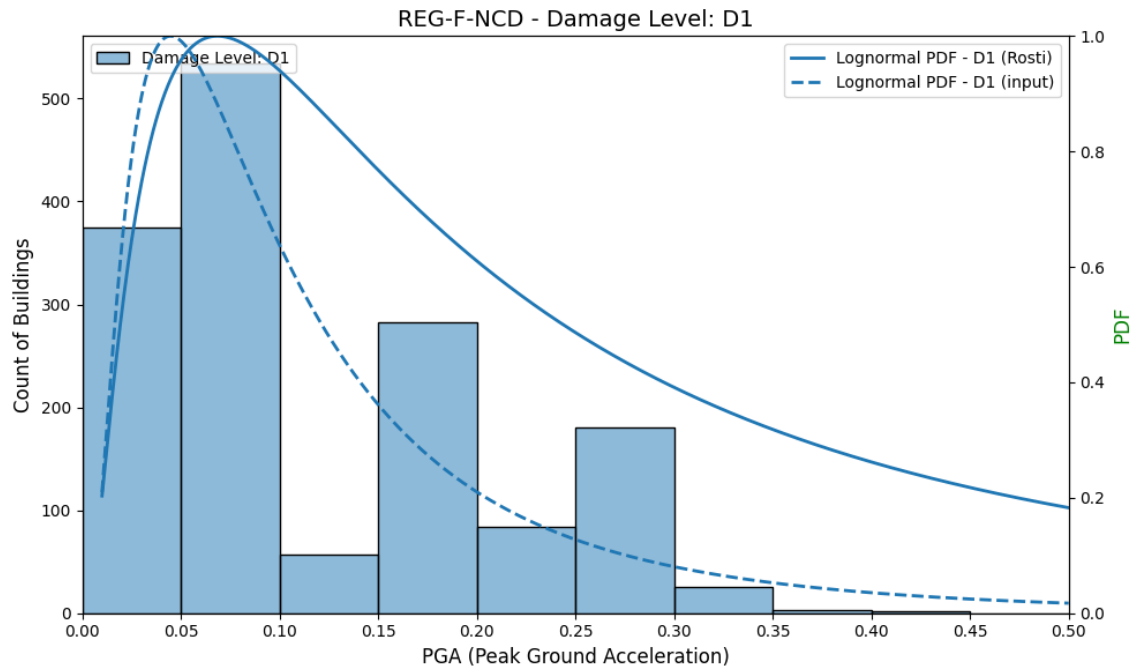
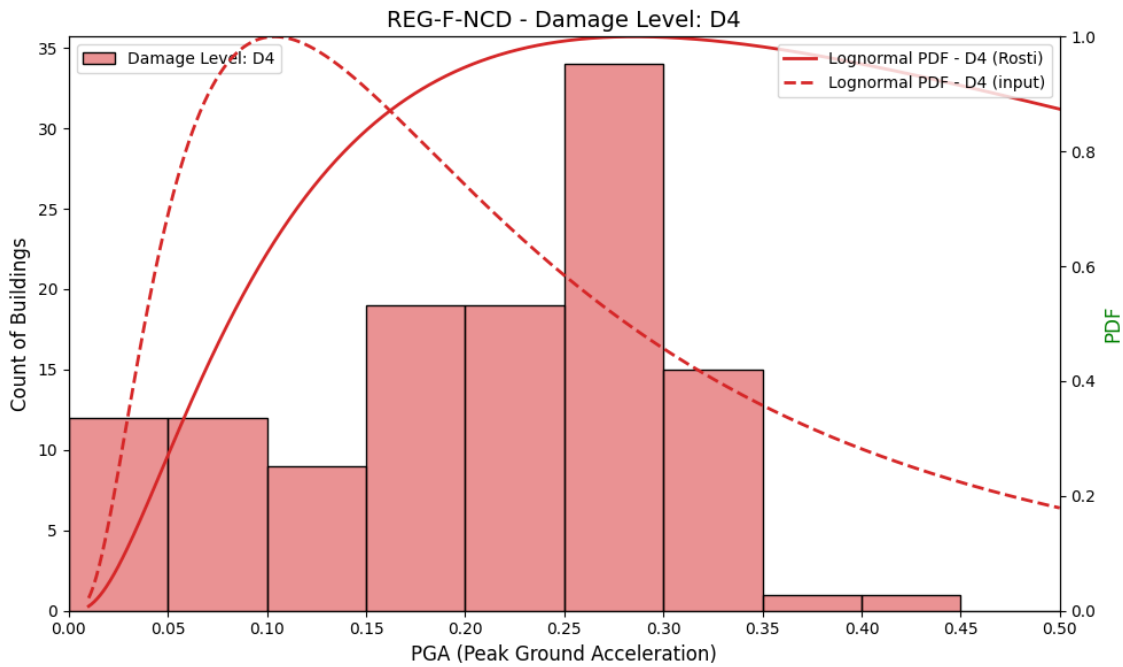
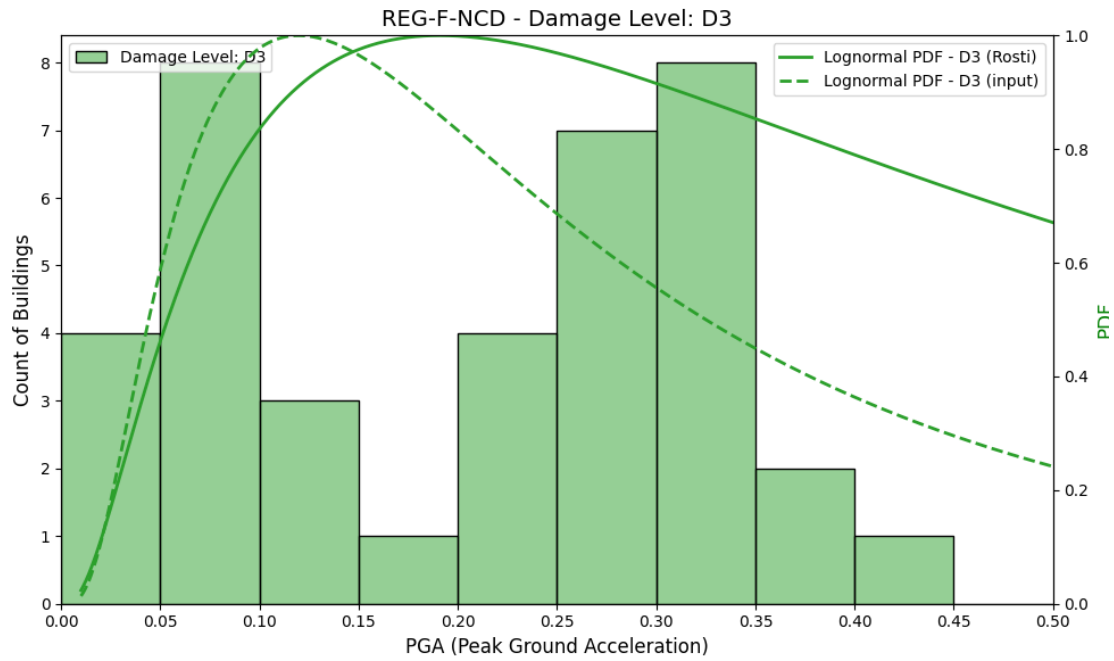


Figure 41. IRR-R-CD damage level distributions (DS1–DS5) for masonry buildings





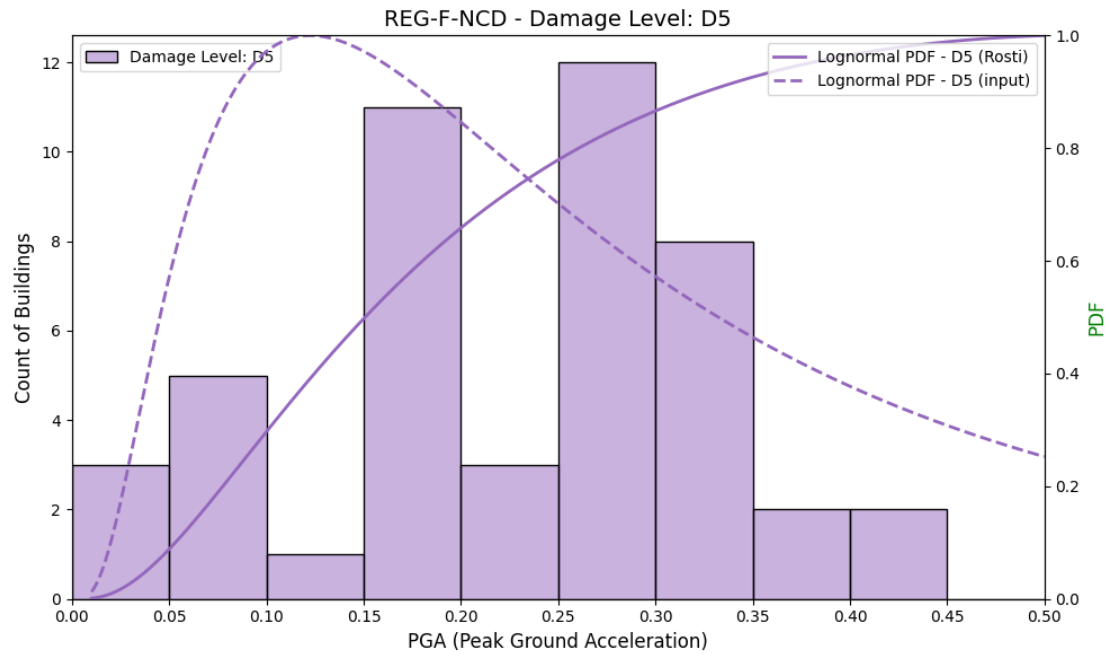
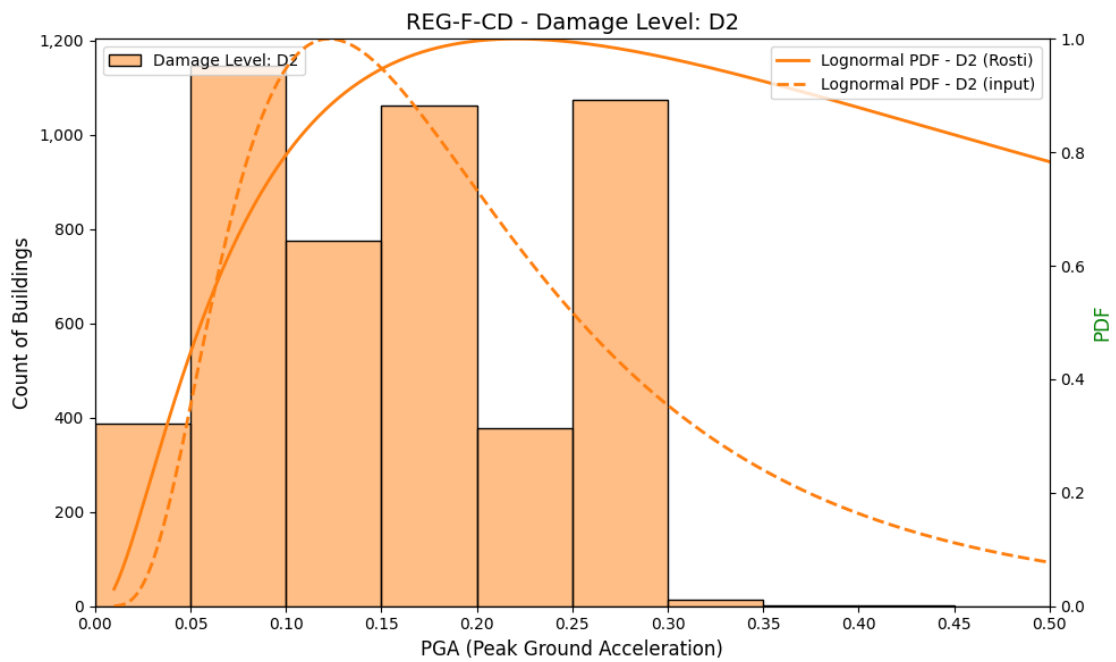
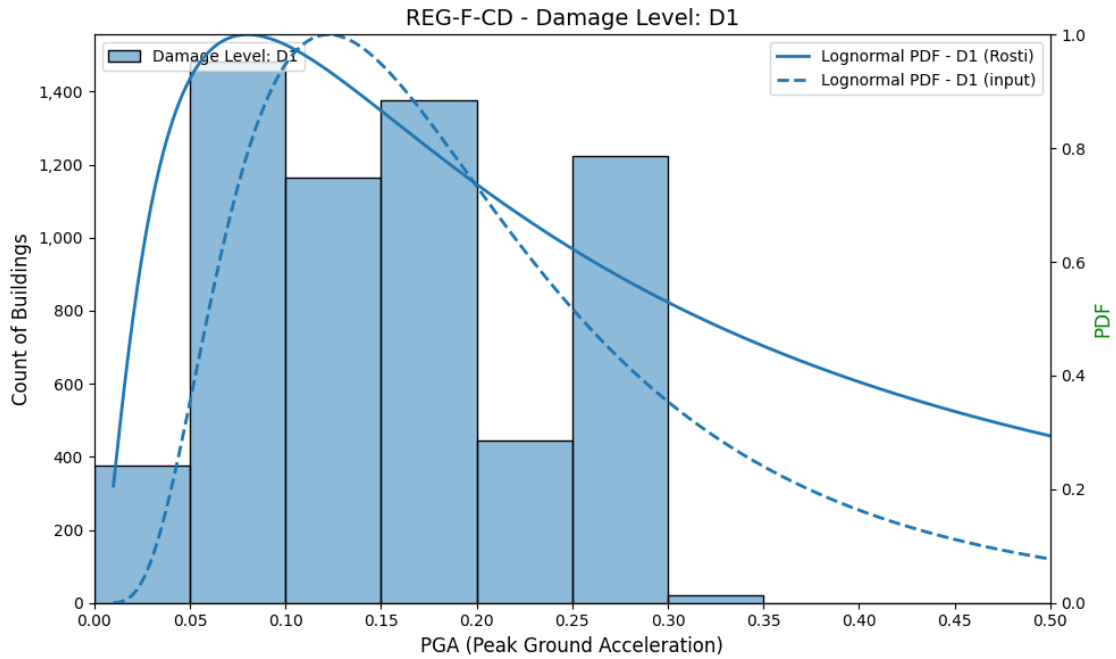
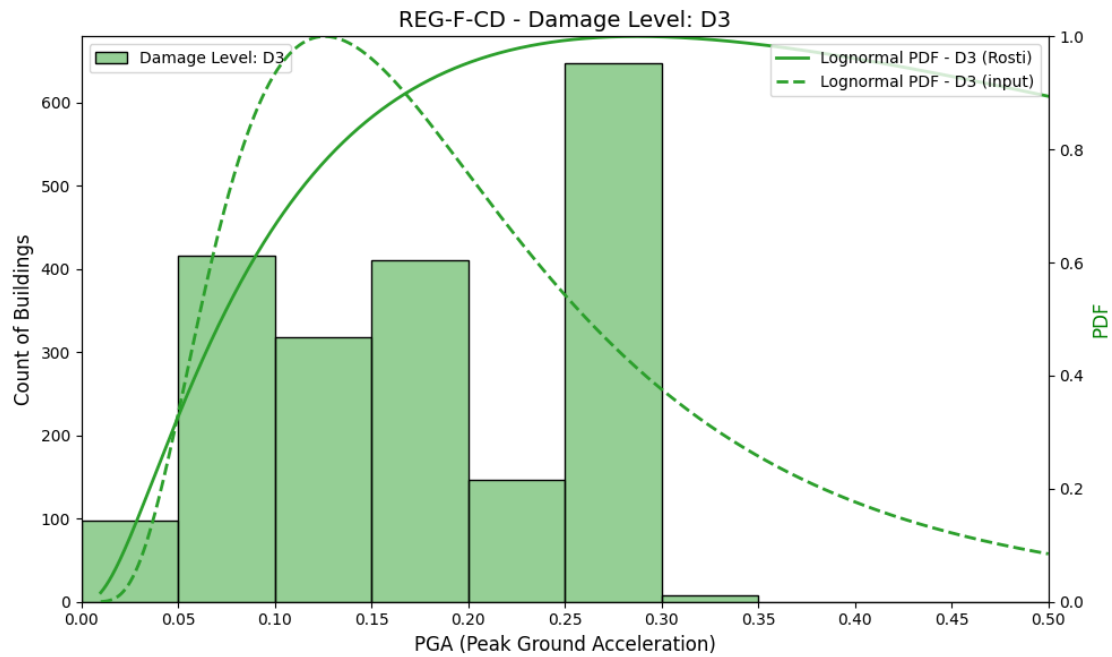
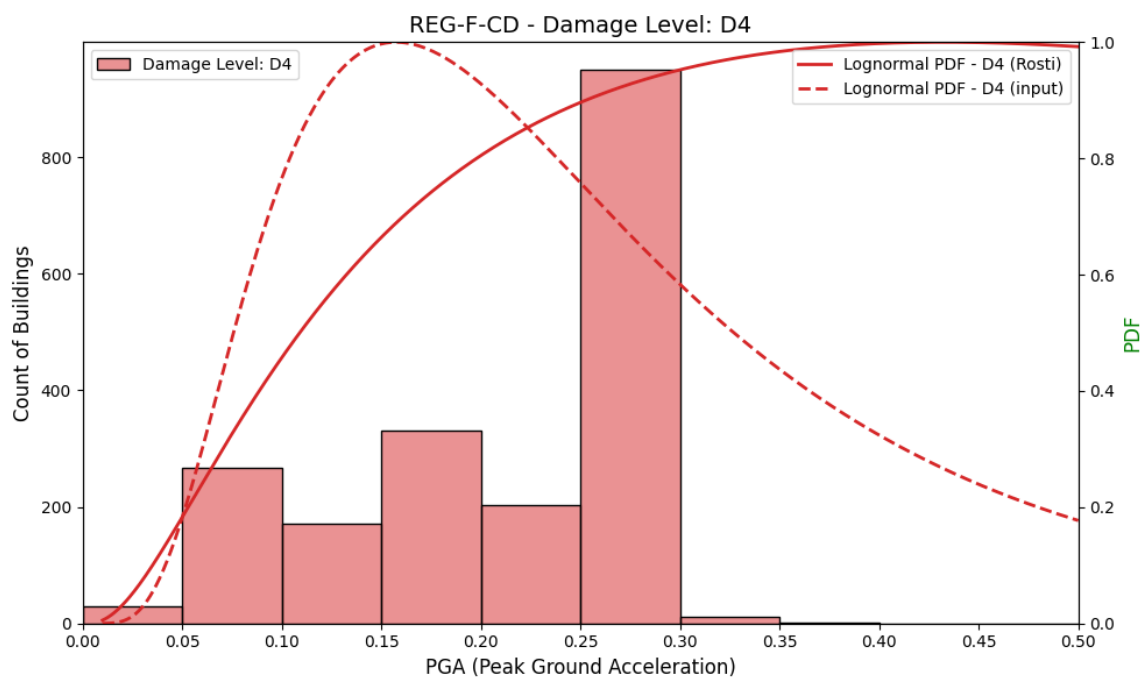


Figure 42. REG-F-NCD damage level distributions (DS1–DS5) for masonry buildings





47



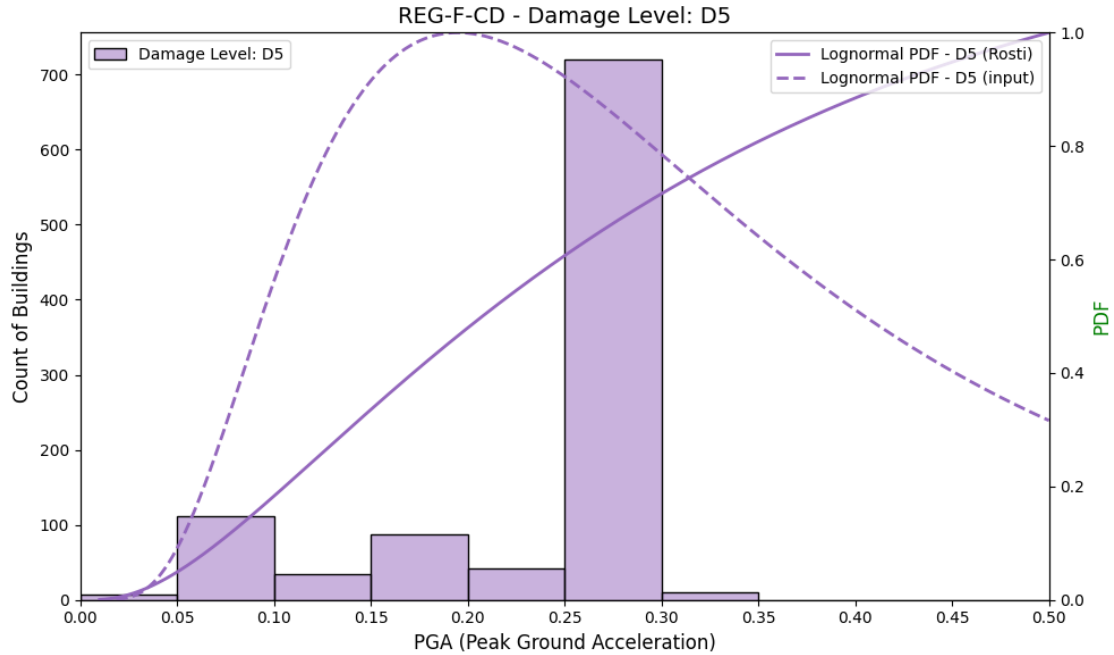
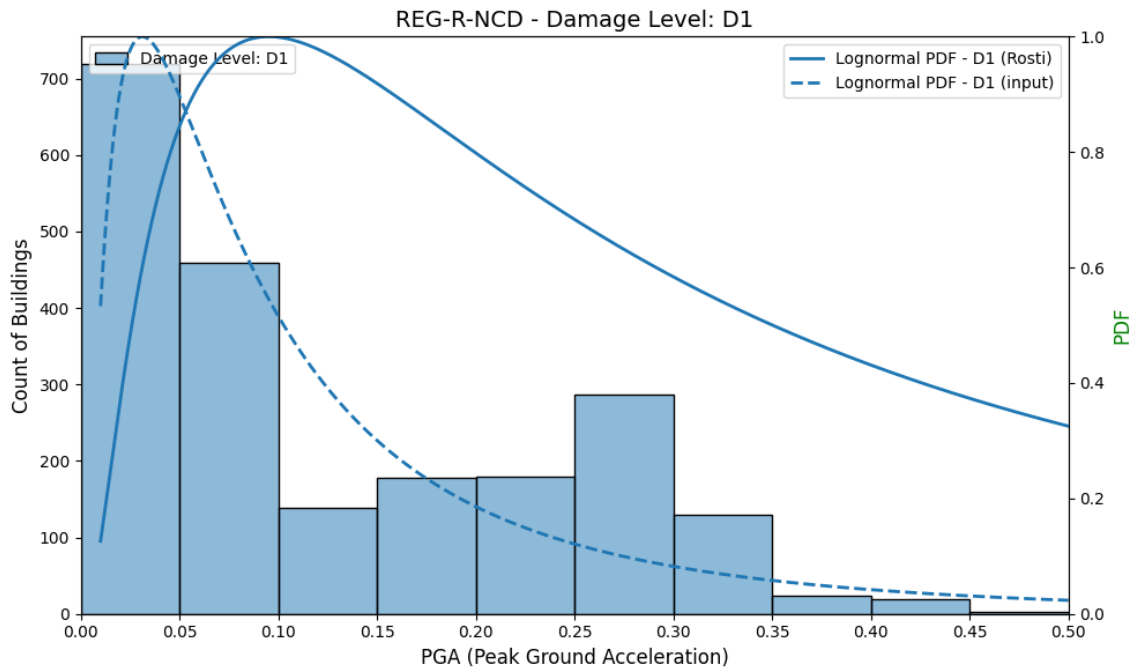
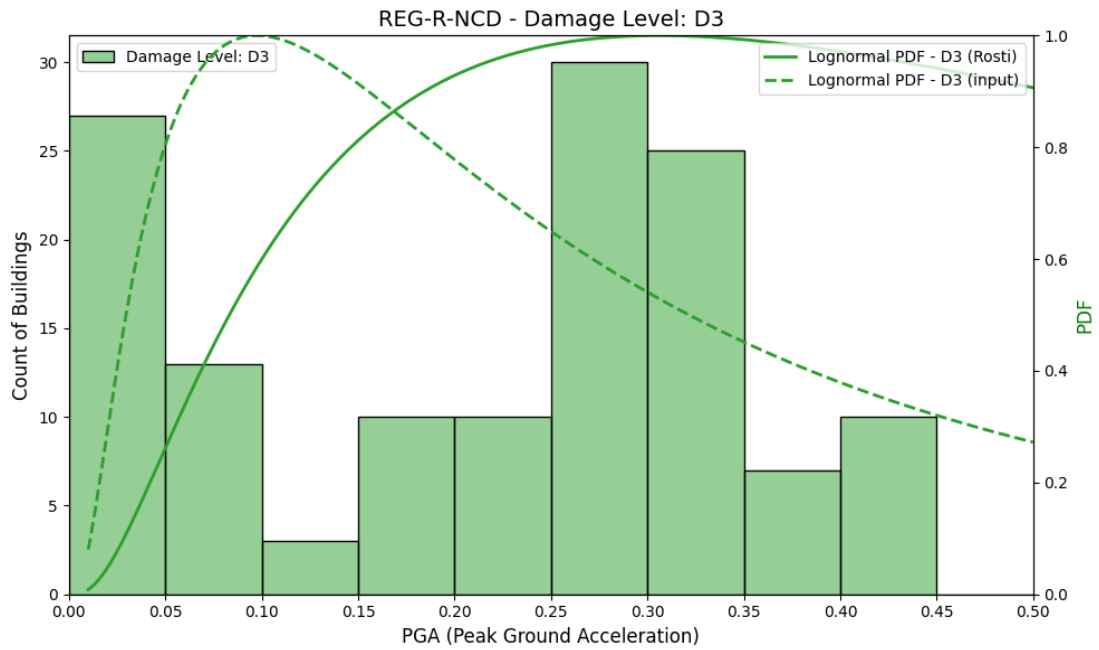
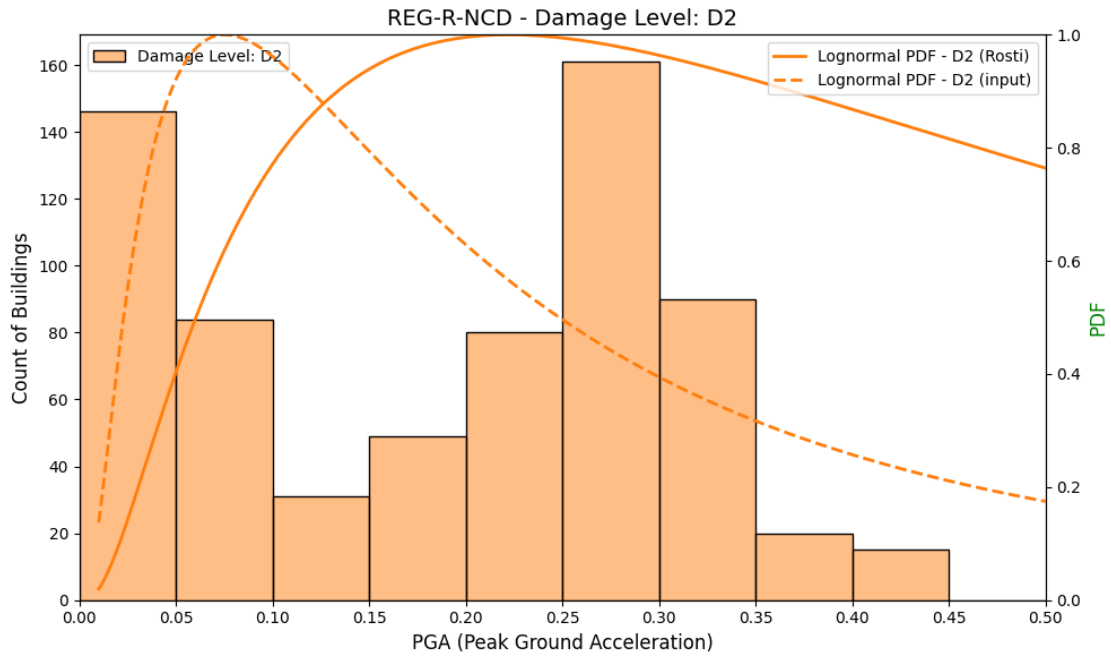


Figure 43. REG-F-CD damage level distributions (DS1–DS5) for masonry buildings

For IRR-R-CD, REG-F-NCD, and REG-F-CD typologies, the initial damage state DS1 matches the two models. Nevertheless, beyond DS1, the differences become substantial, particularly at DS4 and DS5, where the input curves rise too sharply or fail to follow the gradual increase observed in Rosti's curves.





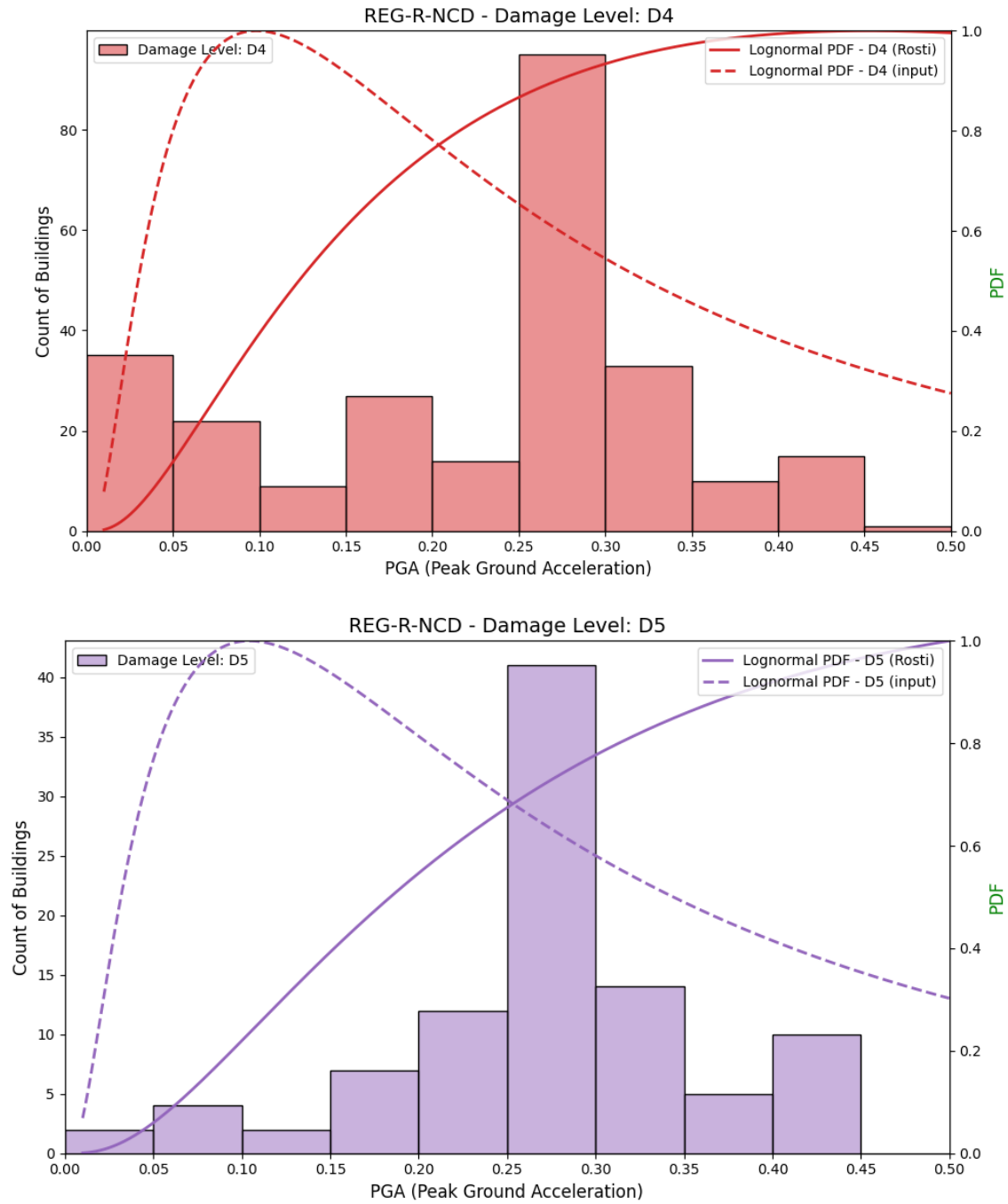
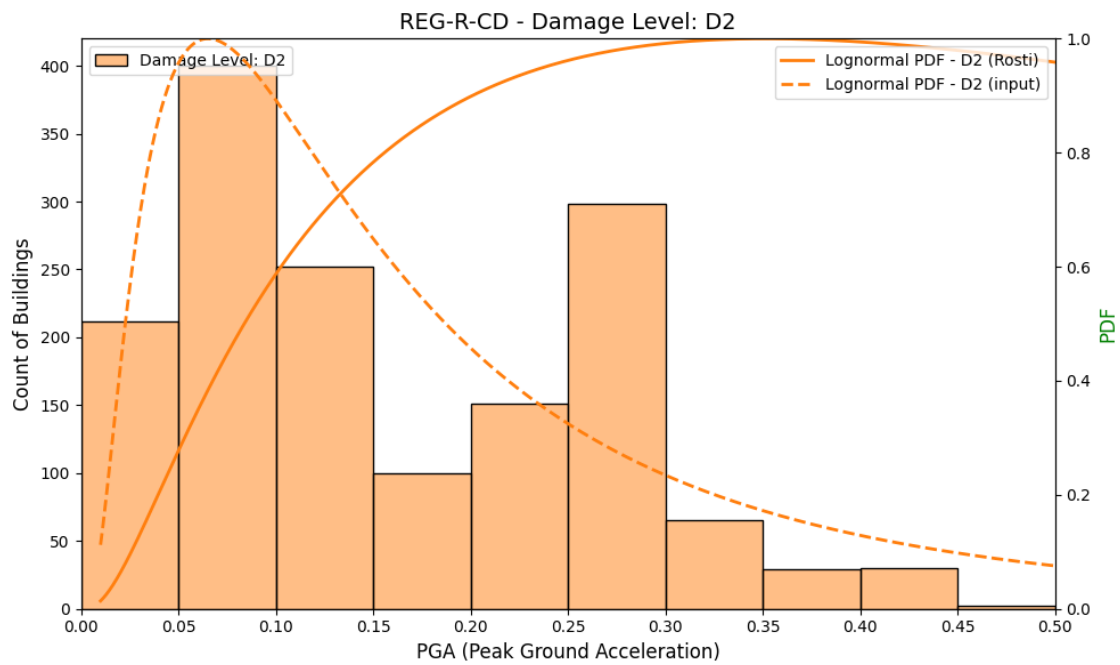
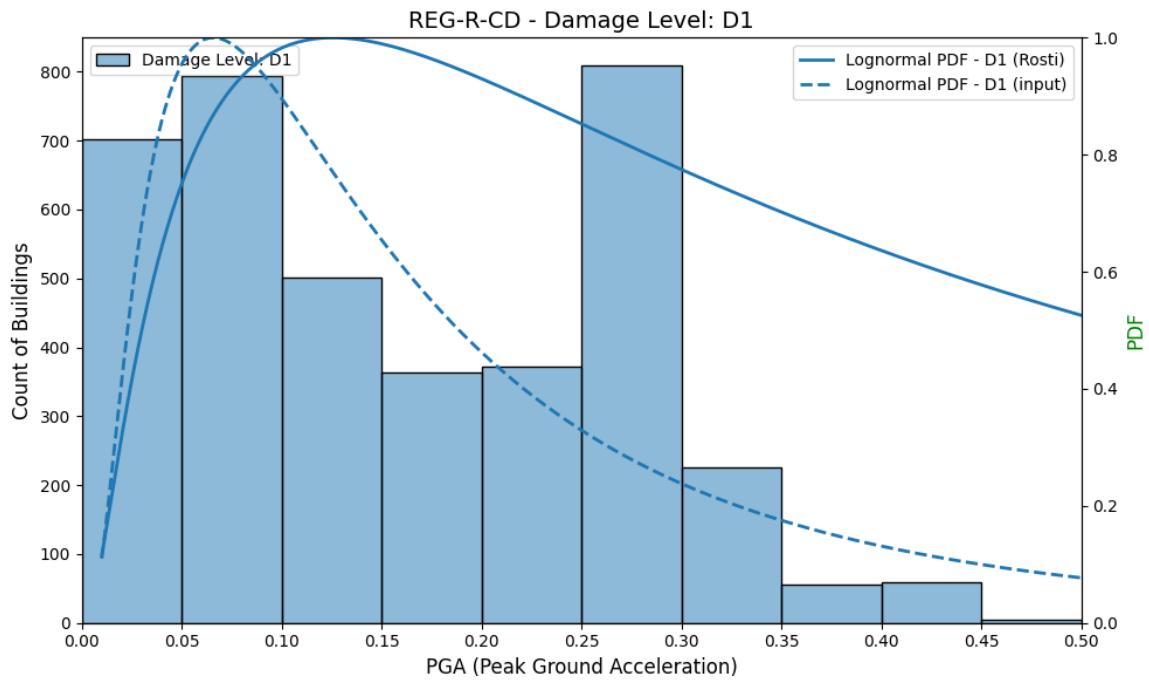
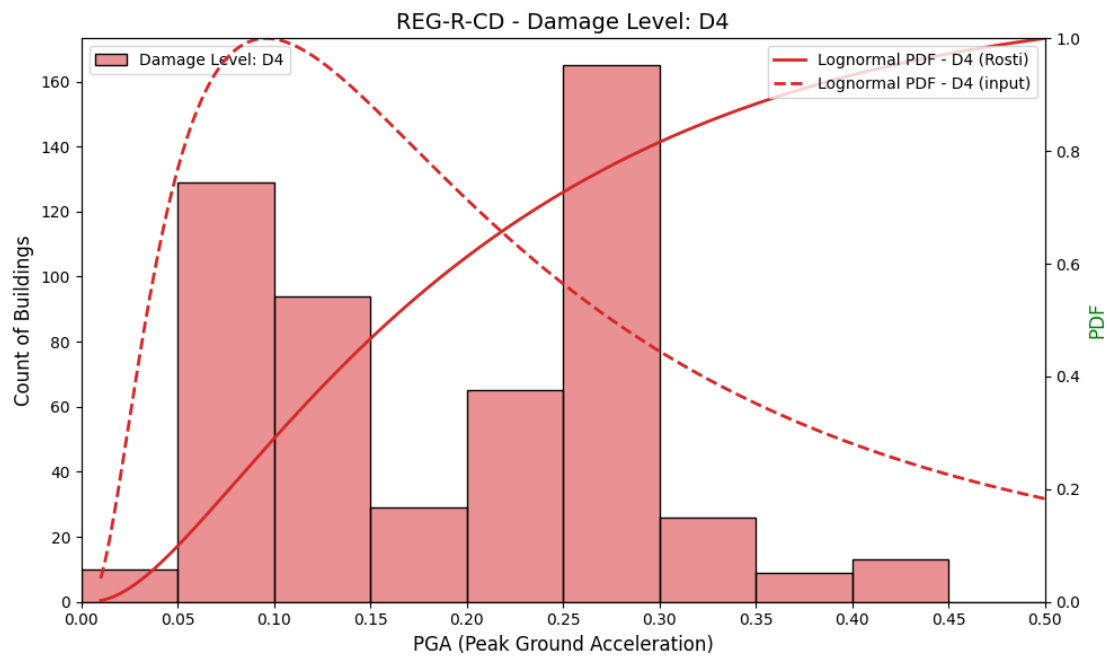
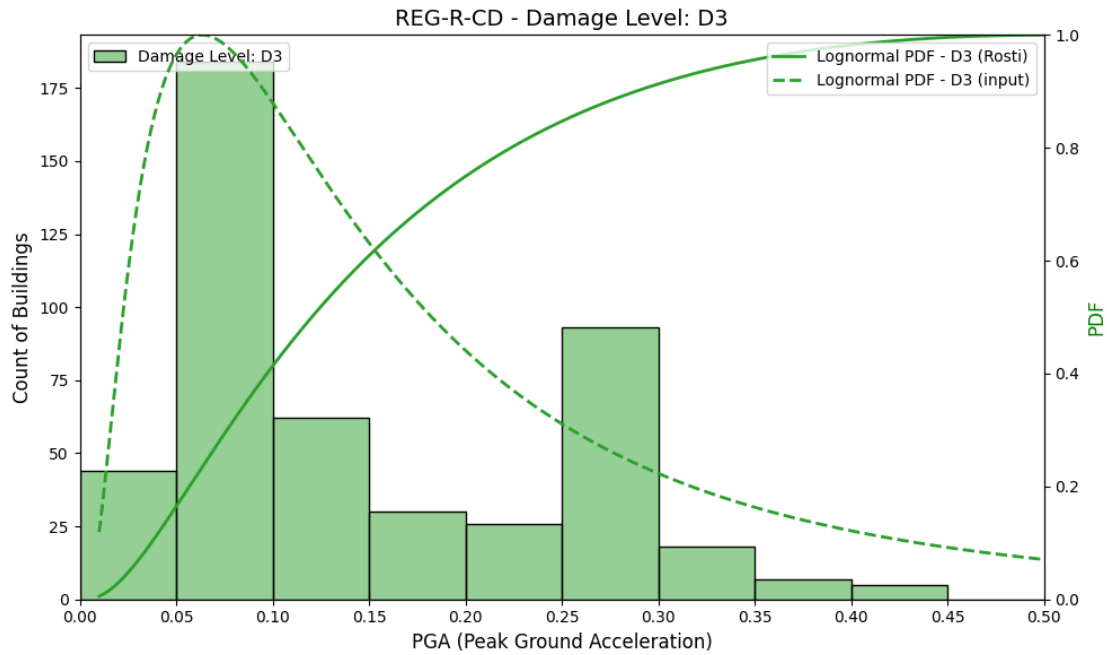


Figure 44. REG-R-NCD damage level distributions (DS1–DS5) for masonry buildings





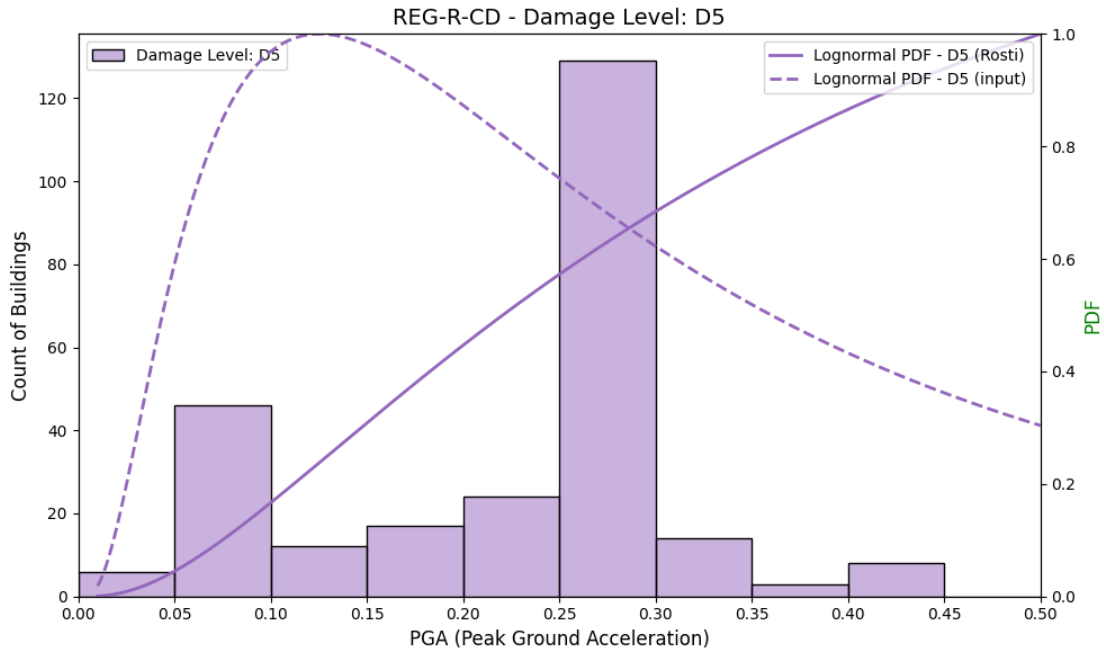


Figure 45. REG-R-CD damage level distributions (DS1–DS5) for masonry buildings

In the cases of REG-R-NCD and REG-R-CD, the input model shows a consistent leftward shift compared to Rosti's, particularly in the higher damage states. While DS1 still demonstrates some similarity, this alignment vanishes progressively as the damage level increases.

The CDF distribution of the masonry buildings can be presented as below for both Rosti and input data:

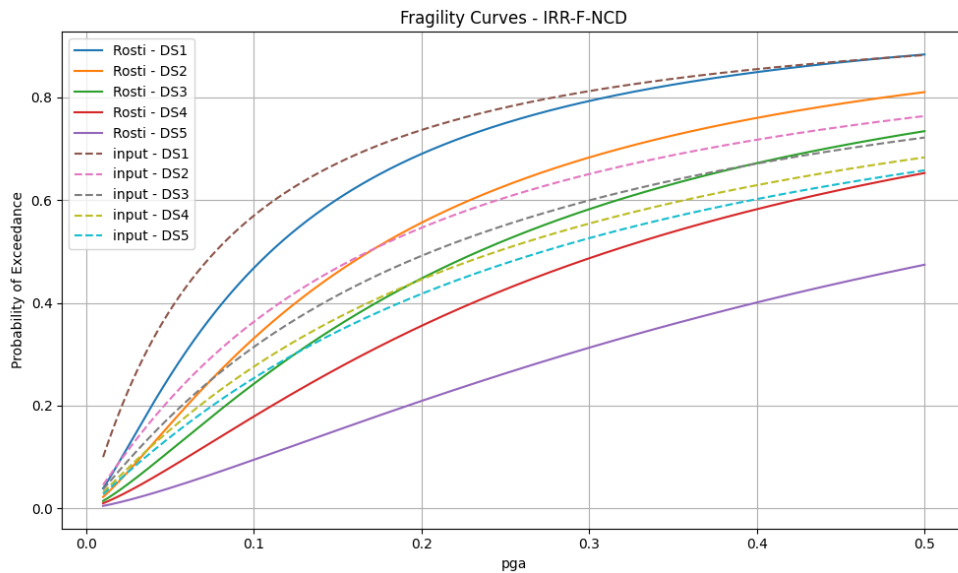


Figure 46. IRR-F-NCD cumulative distribution functions (CDFs) and comparison between input data and Rosti figures

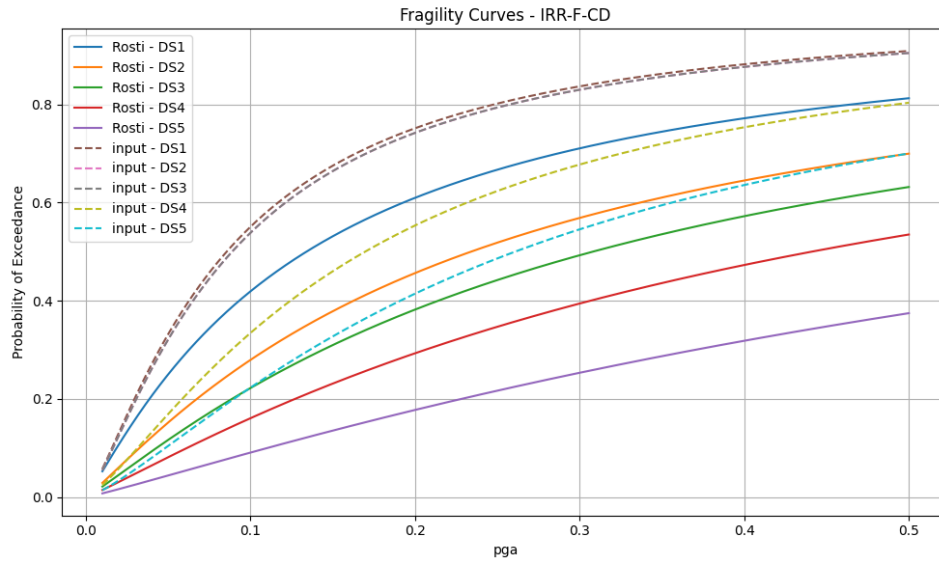


Figure 47. IRR-F-CD cumulative distribution functions (CDFs) and comparison between input data and Rosti figures

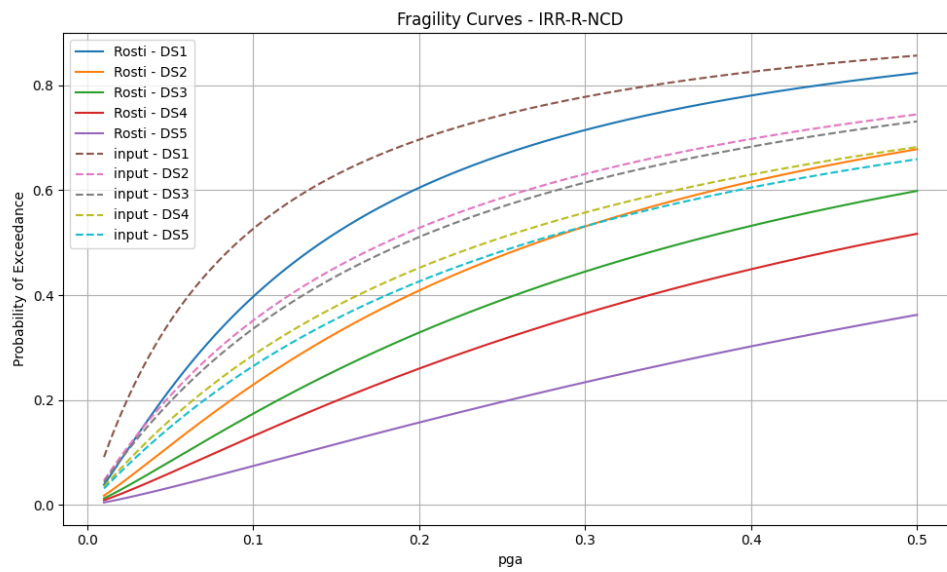


Figure 48. IRR-R-NCD cumulative distribution functions (CDFs) and comparison between input data and Rosti figures

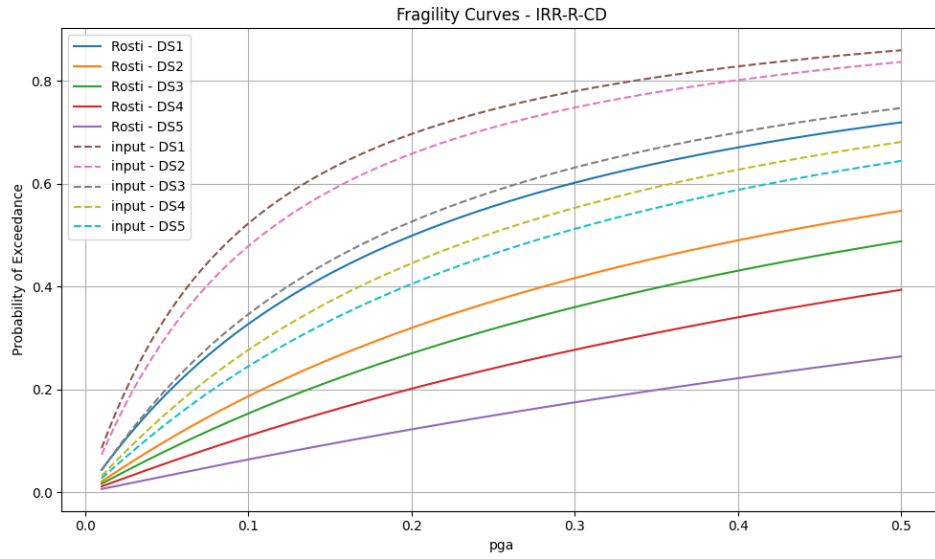


Figure 49. IRR-R-CD cumulative distribution functions (CDFs) and comparison between input data and Rosti figures

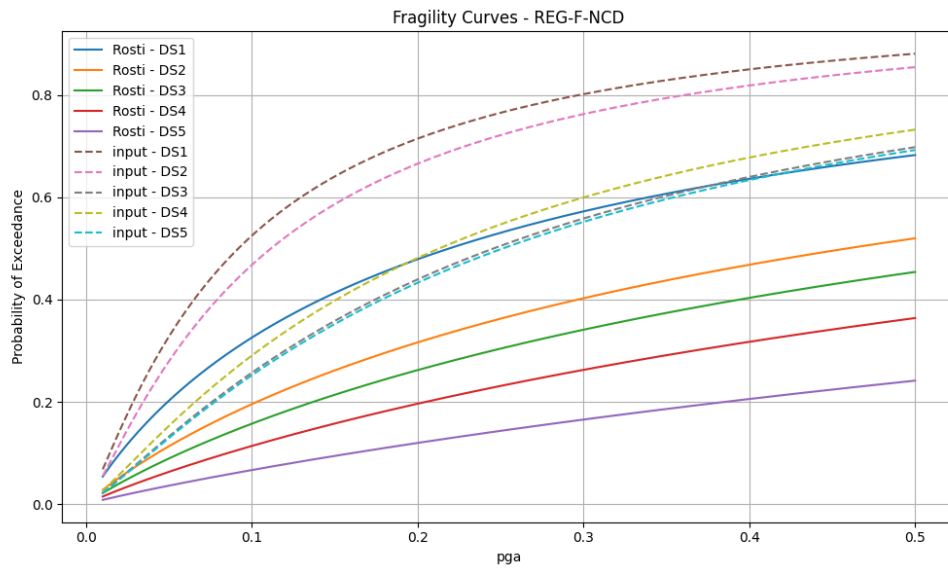


Figure 50. REG-F-NCD cumulative distribution functions (CDFs) and comparison between input data and Rosti figures

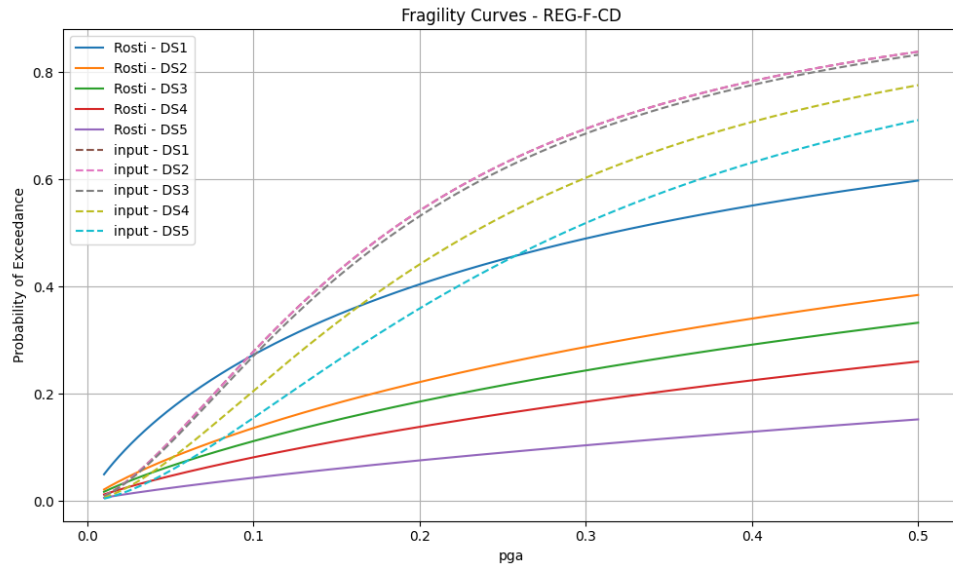


Figure 51. REG-F-CD cumulative distribution functions (CDFs) and comparison between input data and Rosti figures

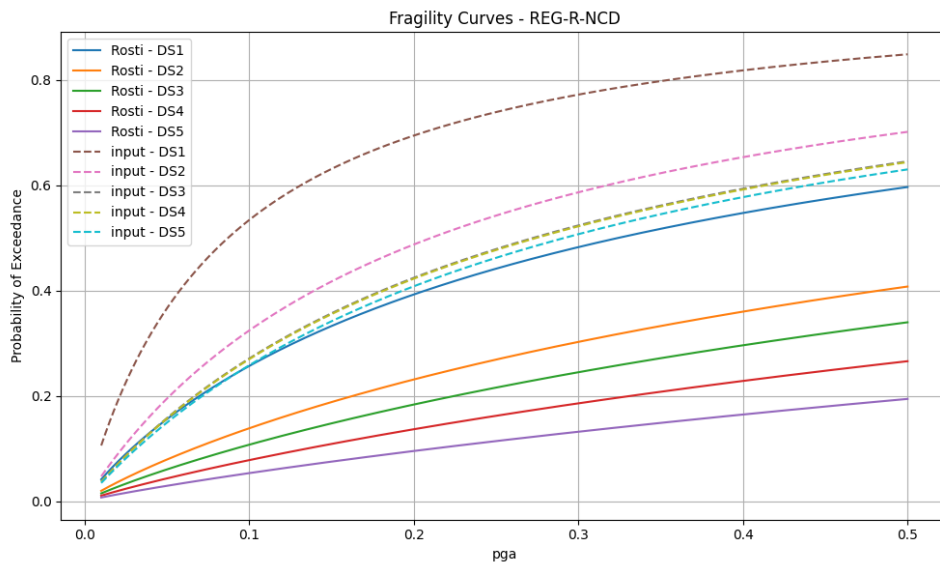


Figure 52. REG-R-NCD cumulative distribution functions (CDFs) and comparison between input data and Rosti figures

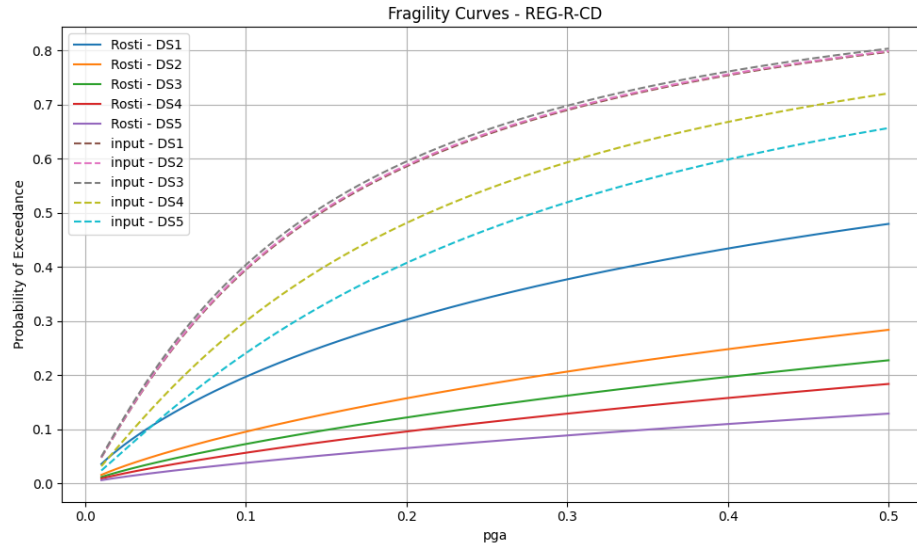


Figure 53. REG-R-CD cumulative distribution functions (CDFs) and comparison between input data and Rosti figures

Looking at the CDF distributions, the ordering of the damage levels in my results follows the correct trend, similar to what Rosti achieved. The progression from lighter to more severe damage states is preserved. However, the exceedance probability in my curves is consistently higher across all cases. This suggests that while the structure of the damage sequence is reliable, my filtering approach results in a more conservative assessment of vulnerability, likely due to the characteristics of the filtered dataset.

Comparison between methods

Both this study and the Rosti method focused on residential buildings affected by the 1980 Irpinia and 2009 L'Aquila earthquakes, using data from municipalities with a completeness ratio higher than 90%. However, a key difference lies in how we treated the data after selection. In our approach, we did not simply assume that all high-completeness-ratio (CR) data was accurate; instead, we took the extra step of checking each entry individually. This extra was particularly crucial because the Generalized Extreme Value (GEV) distribution we utilized is highly sensitive to outliers and inconsistent records—just one erroneous data point can lead to unrealistic spikes in the results.

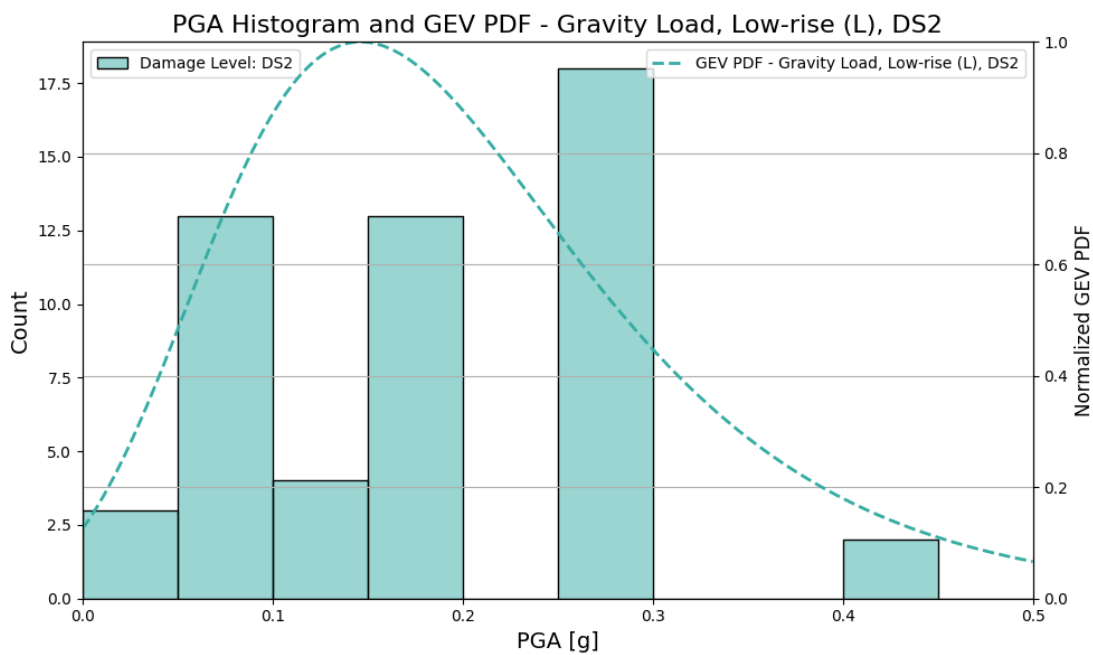
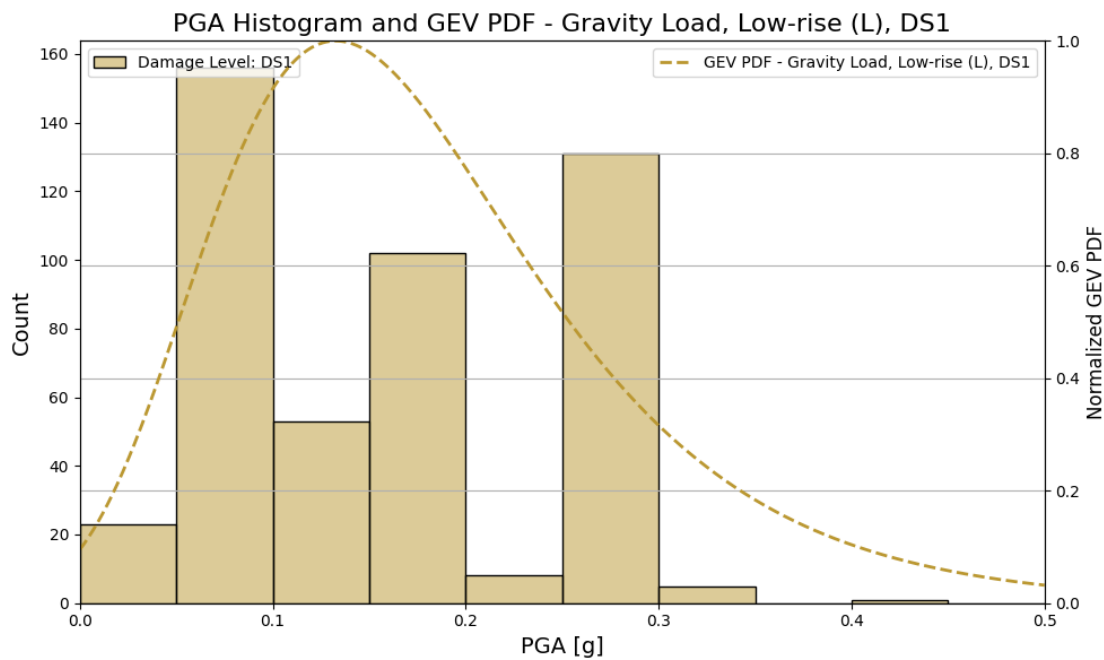
For buildings that had undergone multiple surveys, we always used the most recent version as the reference. If the latest survey was unavailable, we opted for the most complete alternative. In cases where surveys presented major contradictions—such as different reports providing completely opposing information—we excluded that data entirely. In summary, our filtering process was much stricter than that of Rosti's, which allowed us to develop cleaner and more reliable fragility curves. This level of care is especially vital when using advanced models like GEV, as the accuracy of the input directly impacts the quality of the outcome.

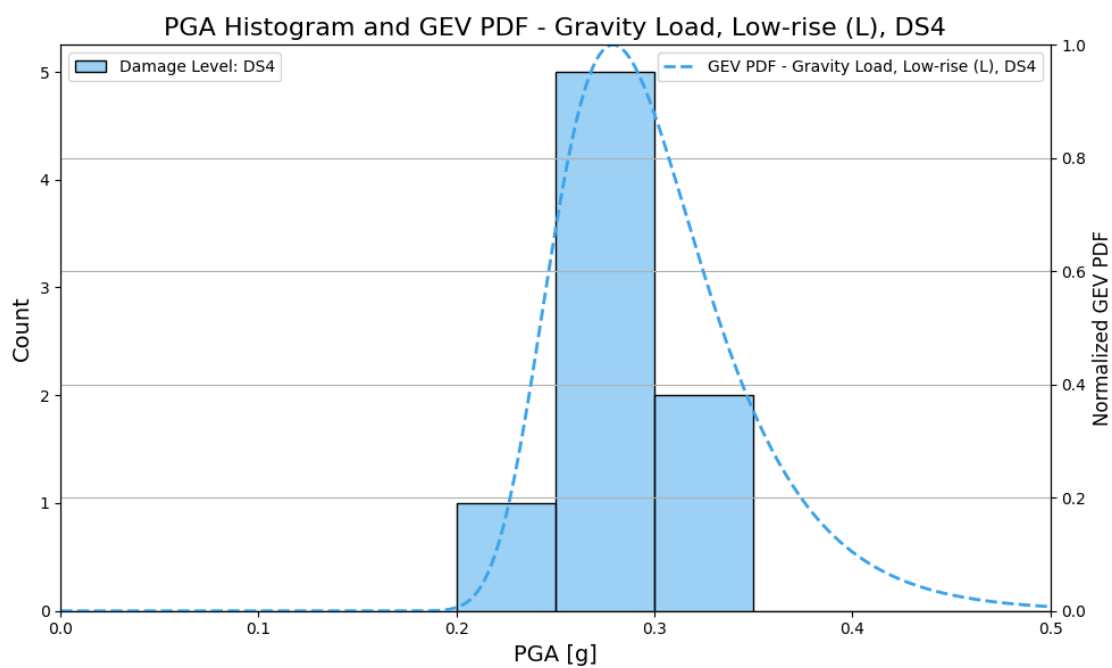
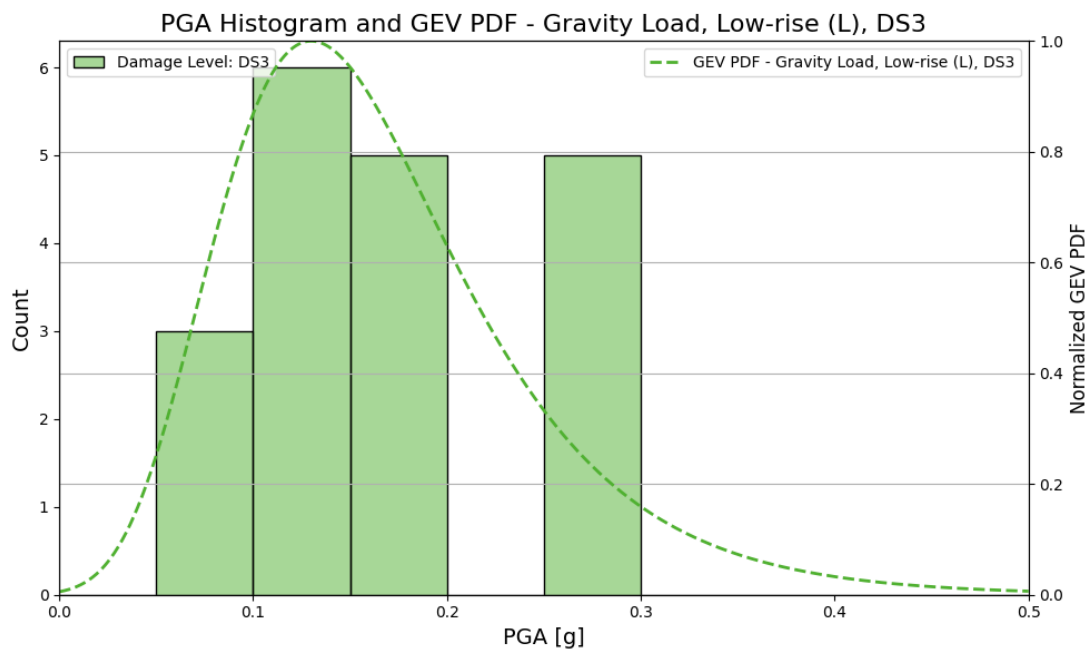
Histograms and GEV Distribution:

This section explores how the choice of statistical model—GEV or lognormal—can change how fragility is represented. Both models were applied to the same filtered dataset, directly comparing building heights and design categories. It helps highlight which model is more conservative or sensitive to rare but serious damage.

Histograms and the Generalized Extreme Value (GEV) distribution are key tools for exploring data and modeling extreme events. Histograms provide a visual overview of data distribution, helping guide the choice of suitable models. The GEV distribution is used to model the behavior of extreme values, with its parameters often informed by patterns observed in histograms. Together, these tools improve understanding of the data and support more informed decision-making across a wide range of applications.

Concrete buildings:





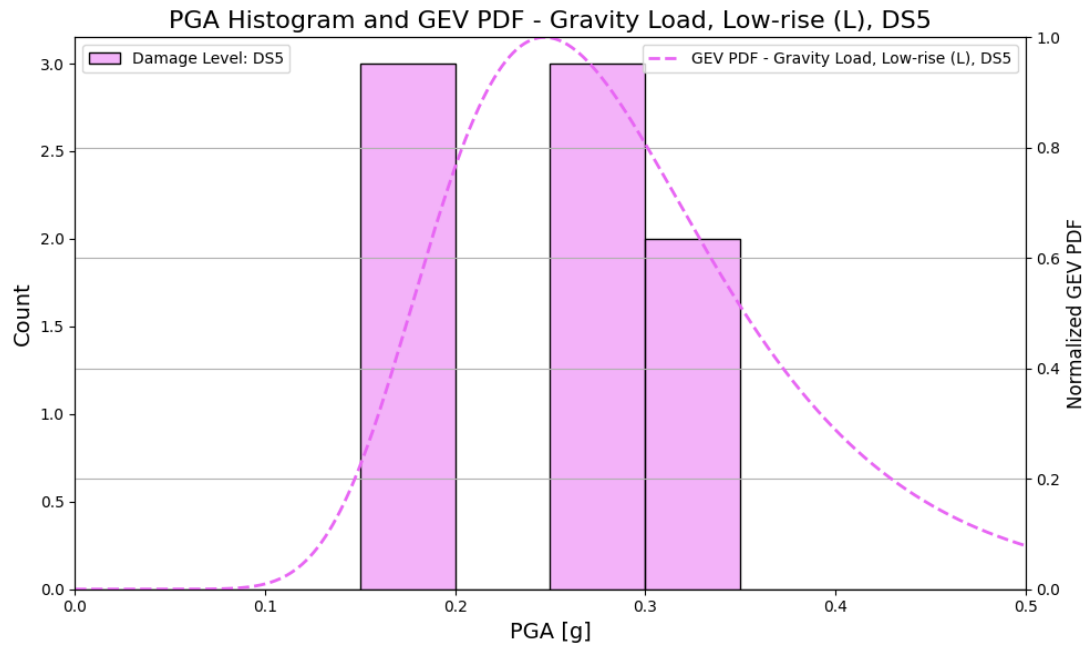
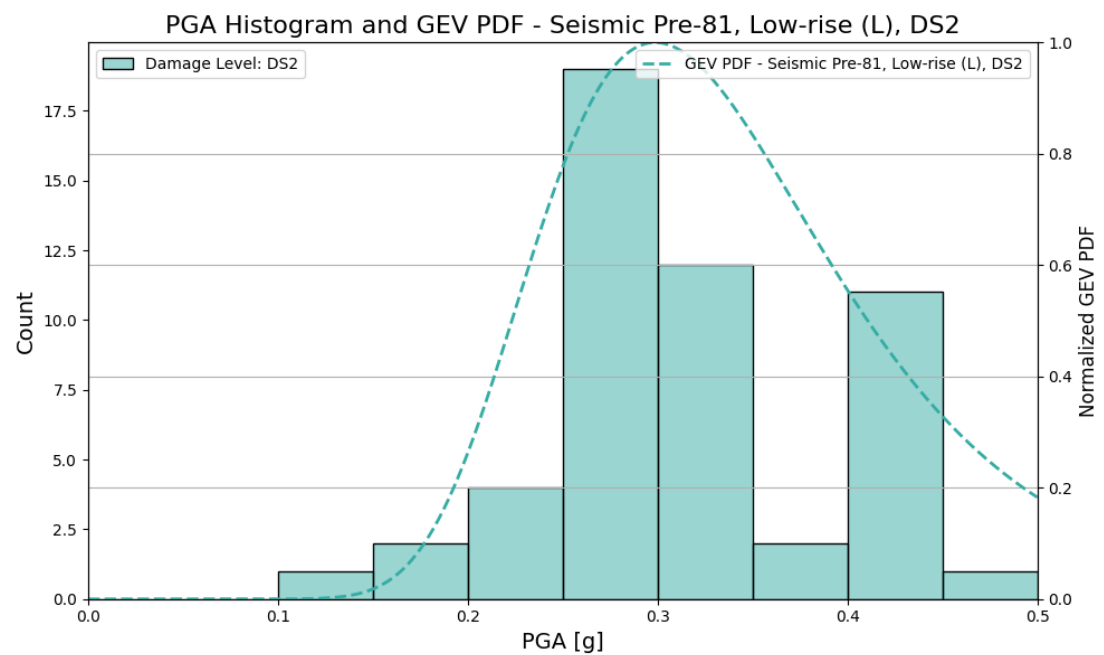
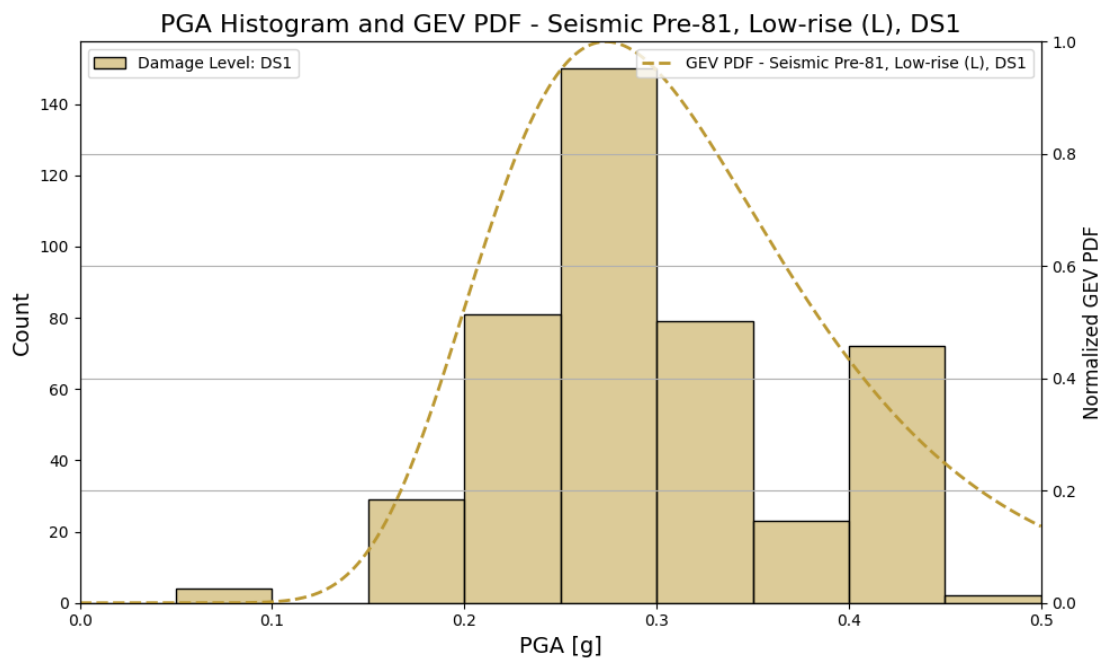
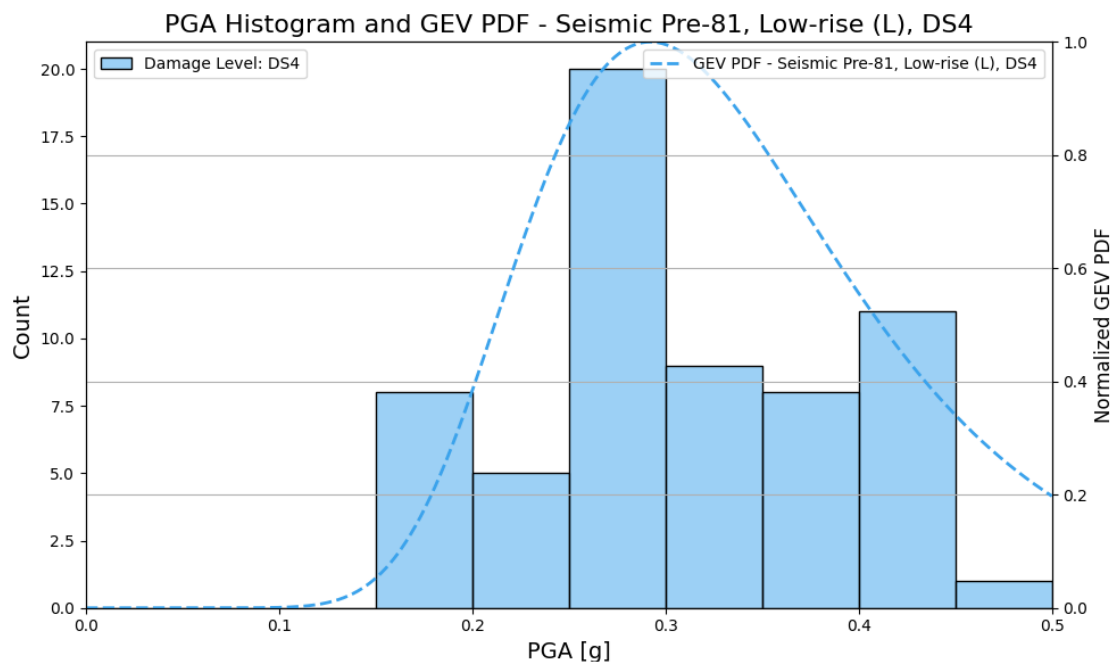
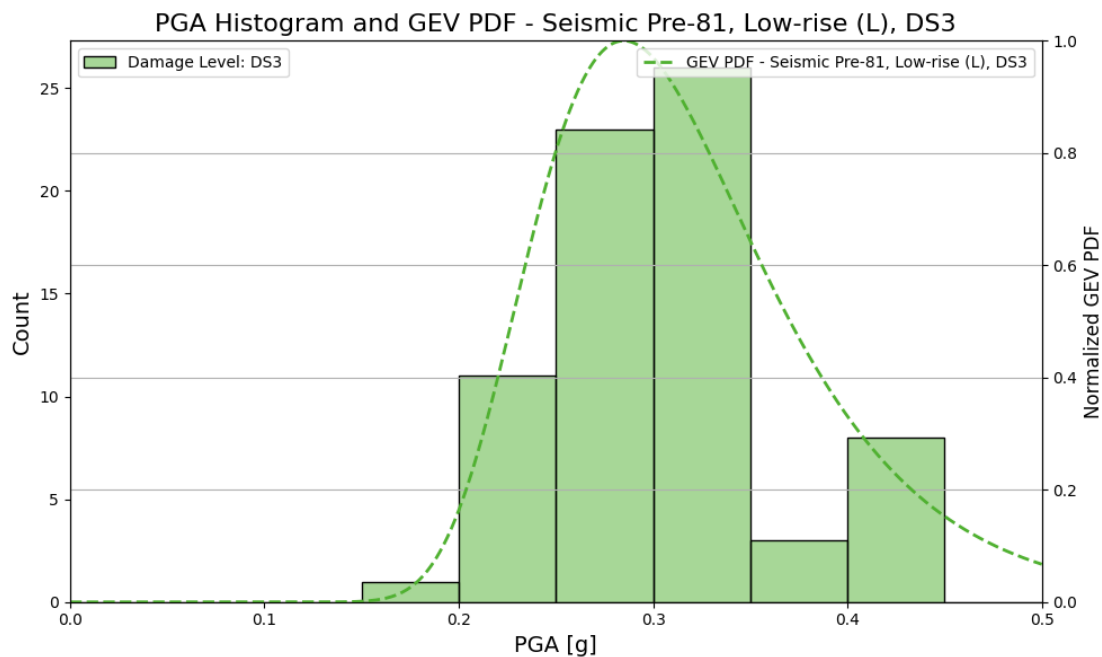


Figure 54. GEV distribution for low-rise gravity load concrete buildings across all damage levels





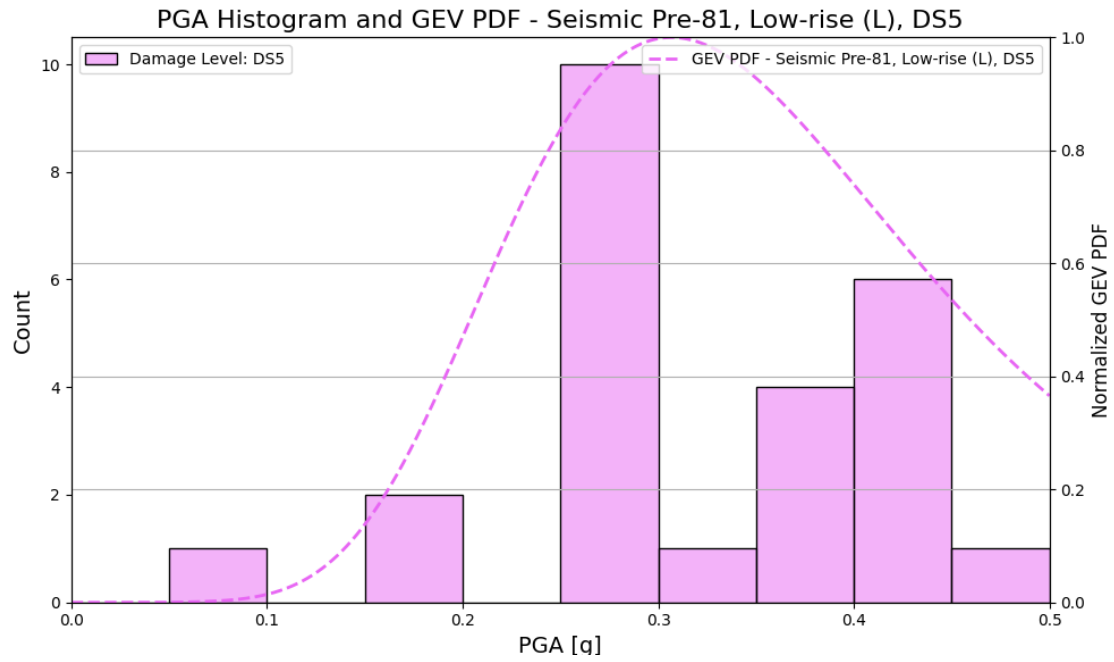
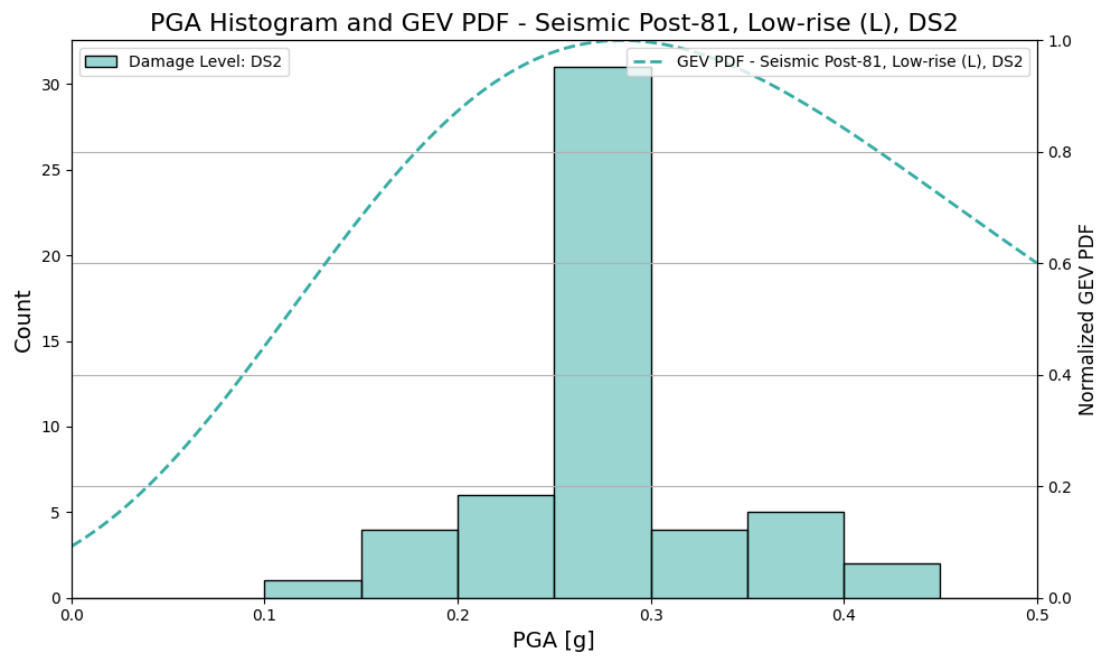
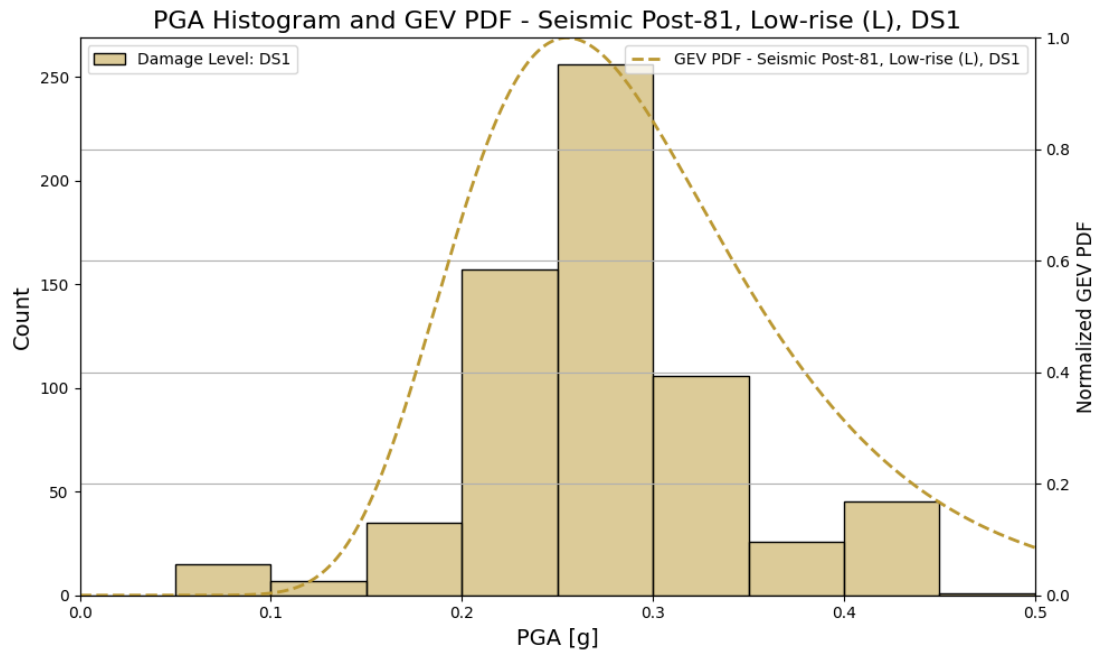
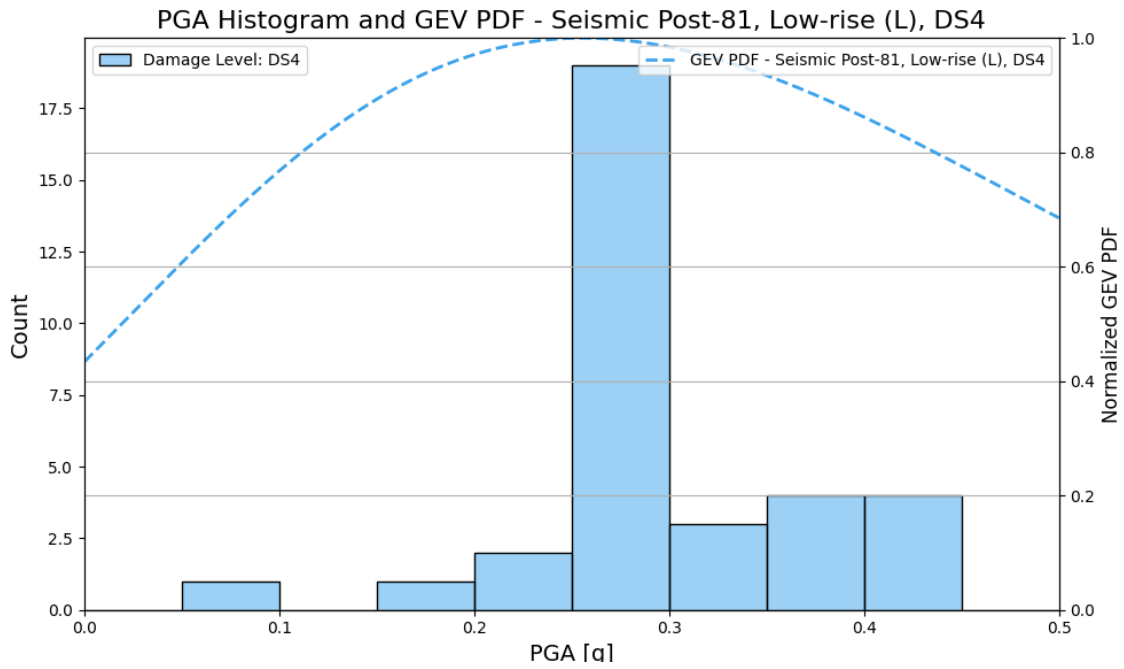
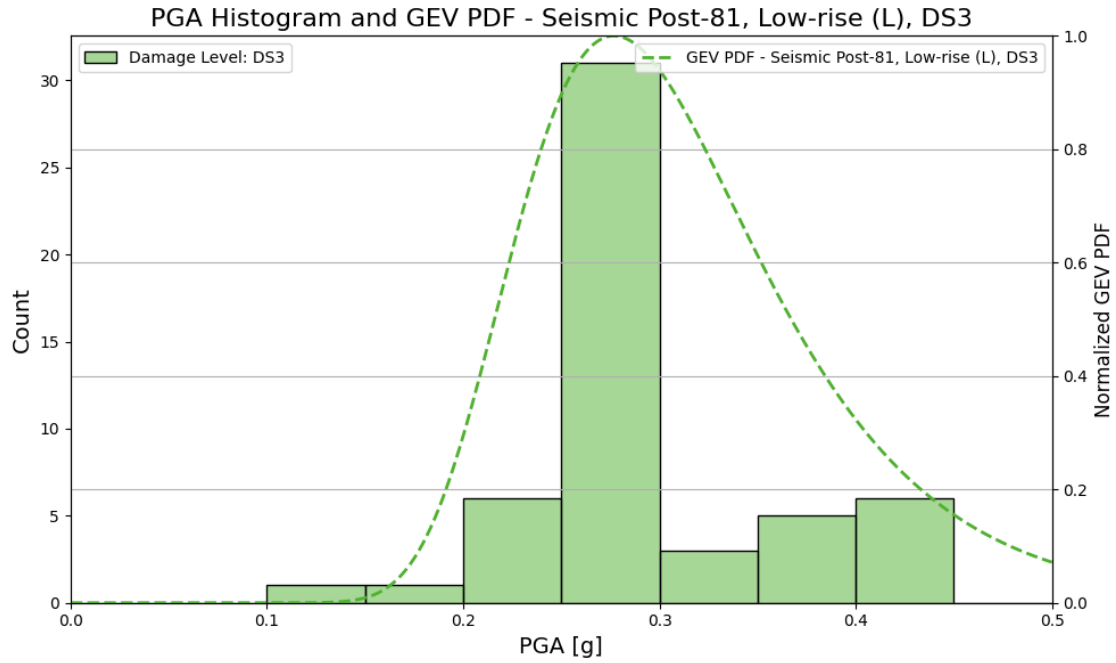


Figure 55. GEV distribution for low-rise seismic pre-81 concrete buildings across all damage levels





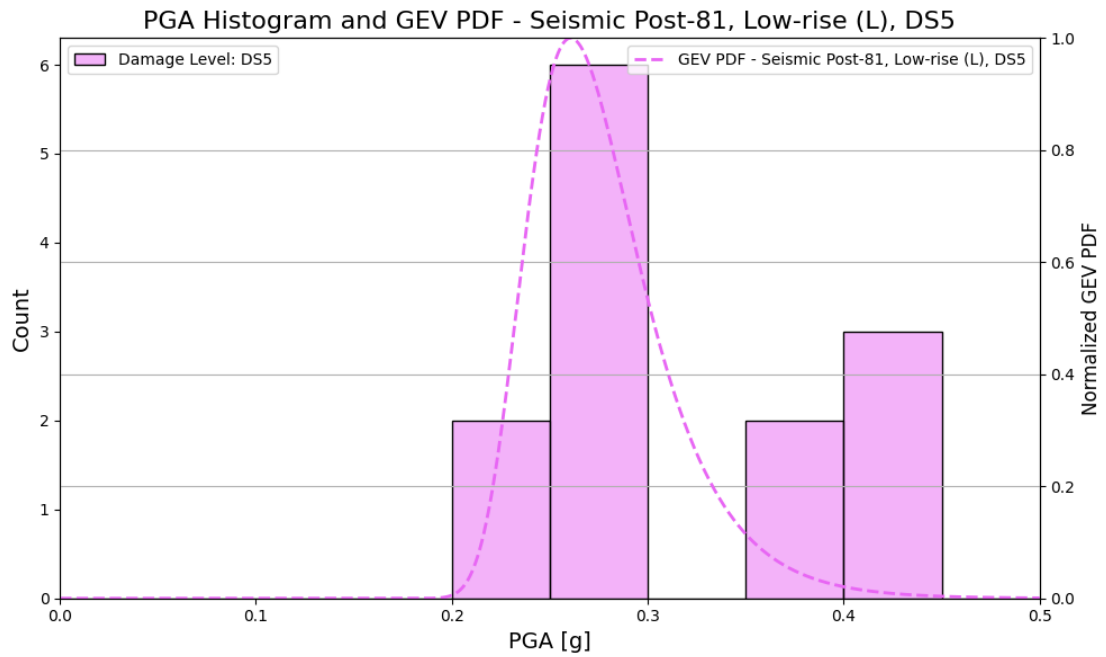
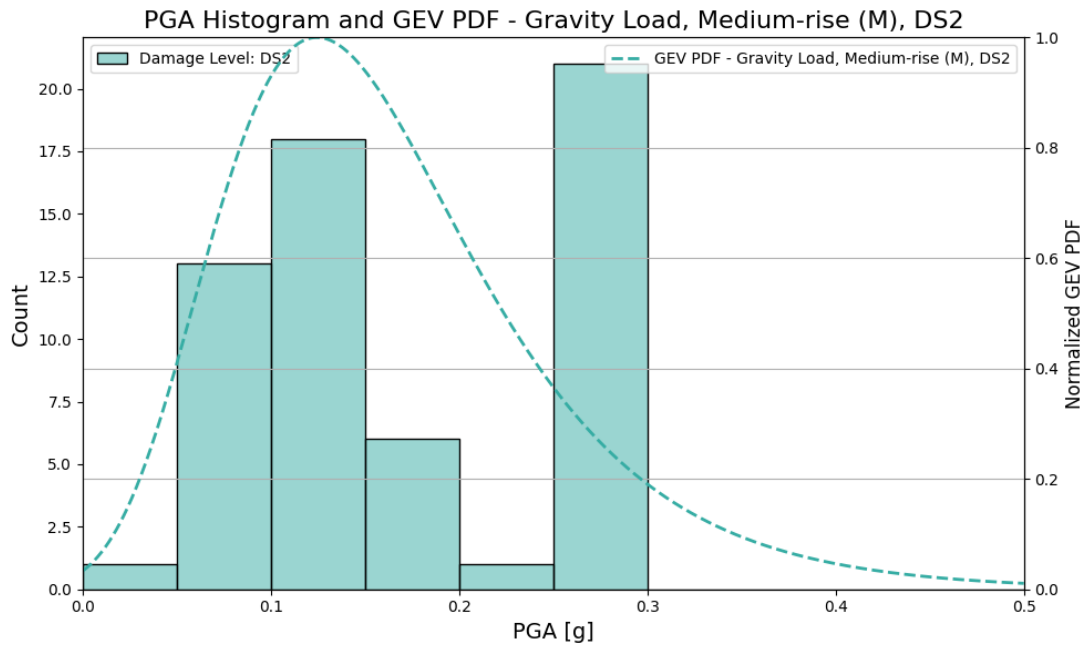
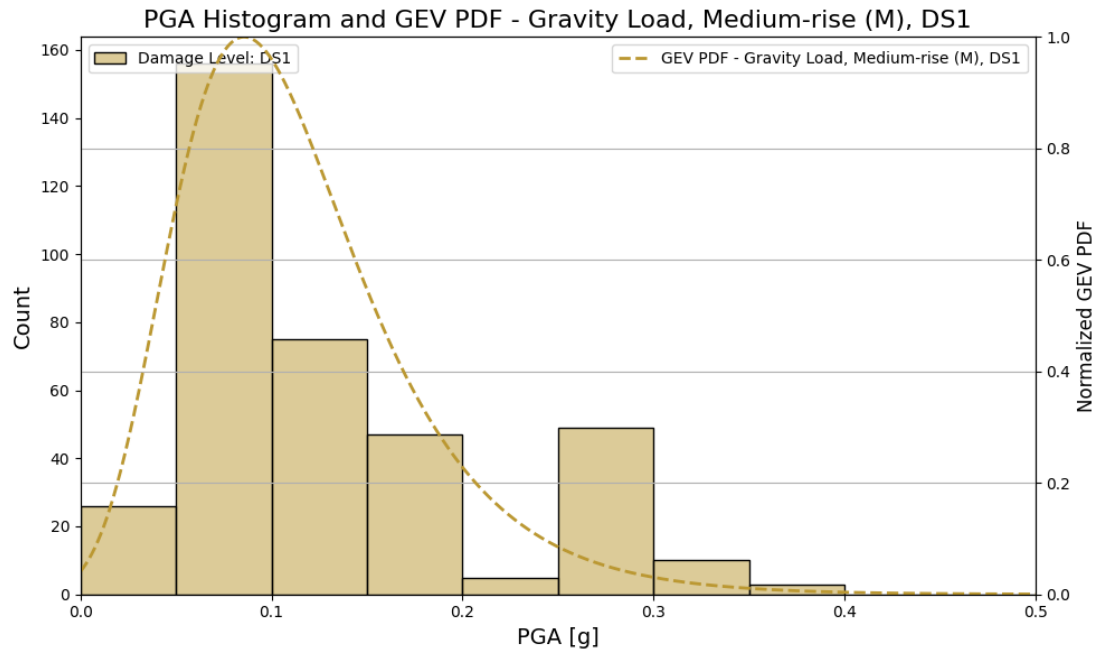
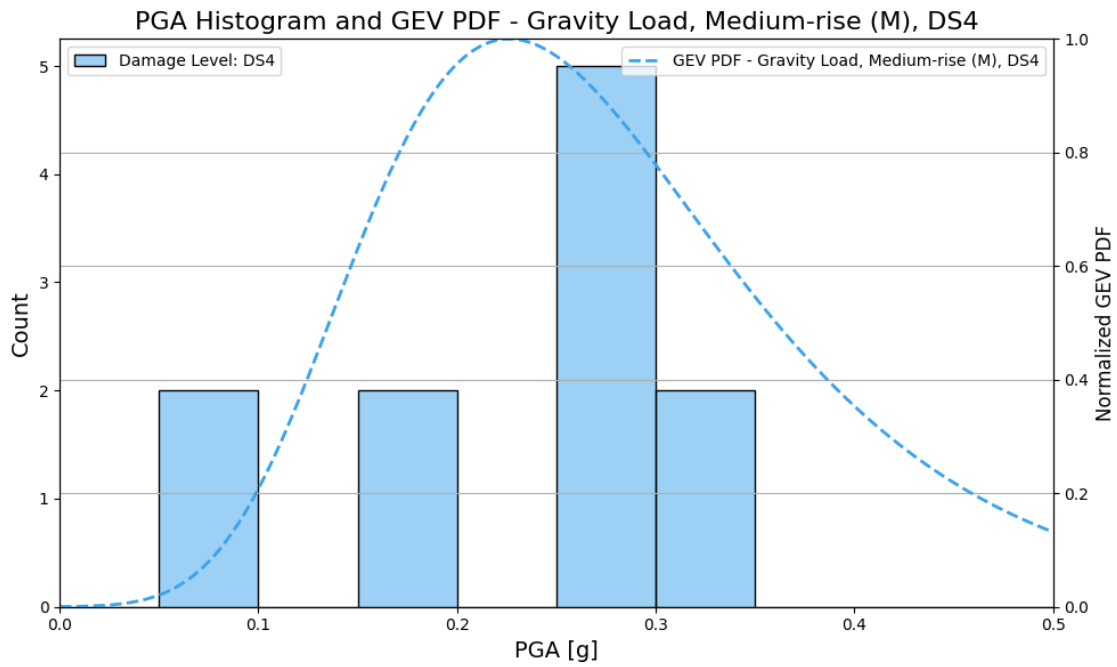
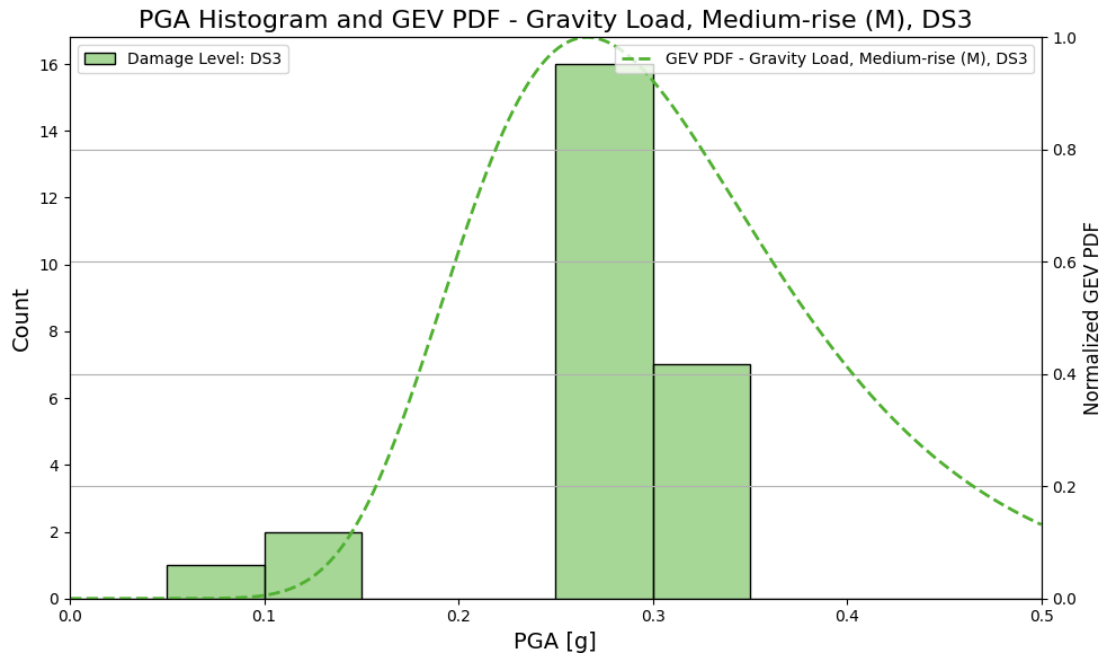


Figure 56. GEV distribution for low-rise seismic post-81 concrete buildings across all damage levels





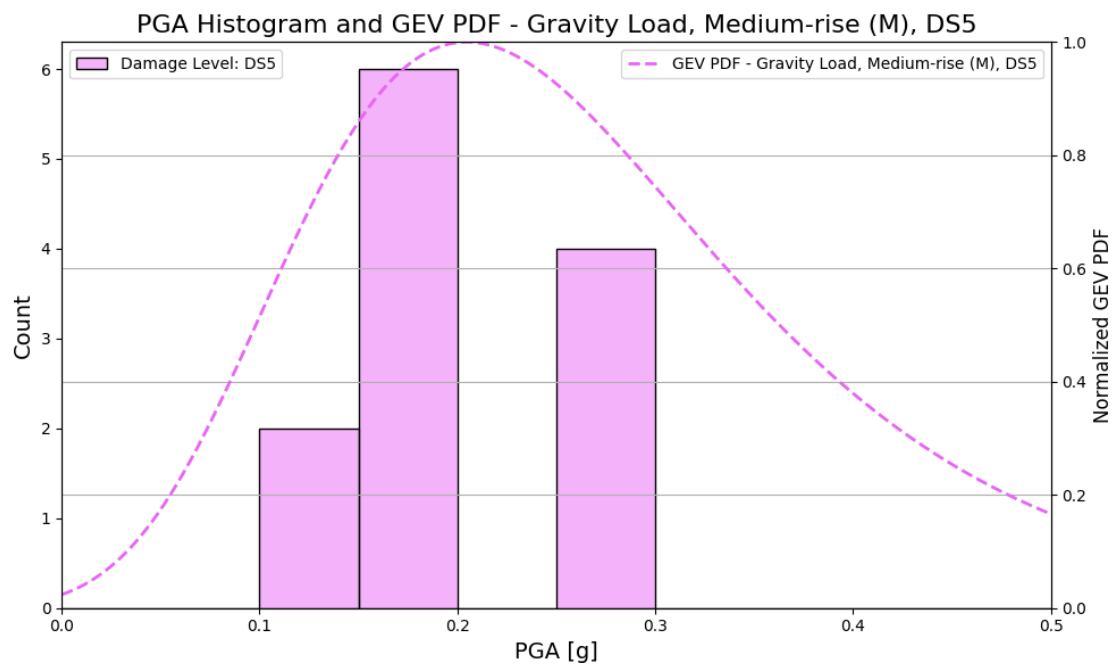
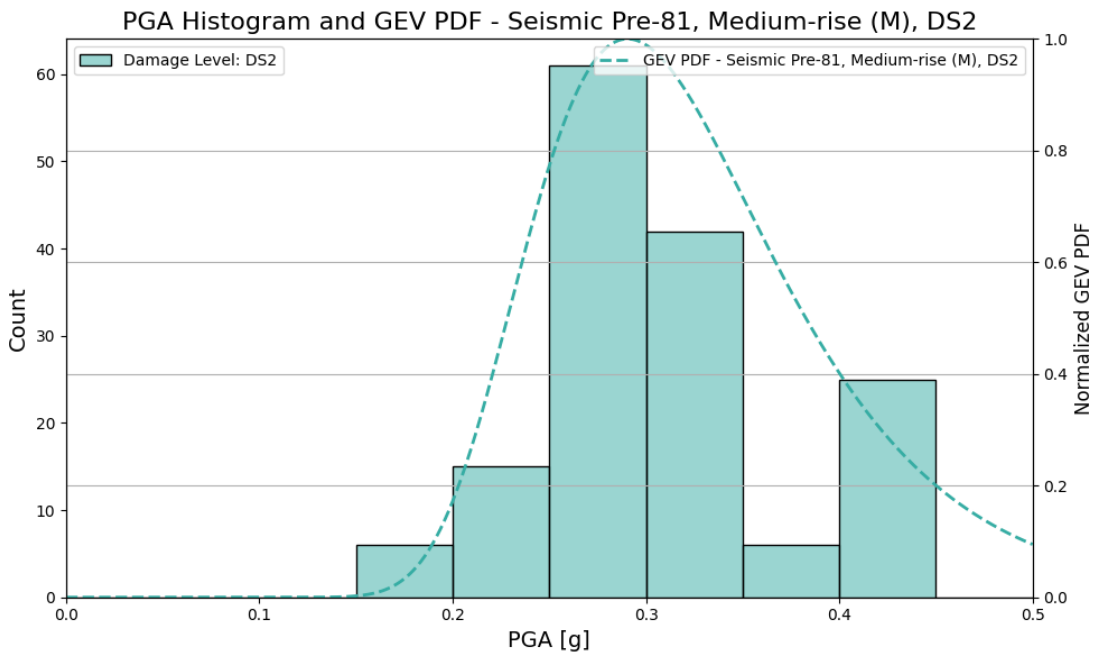
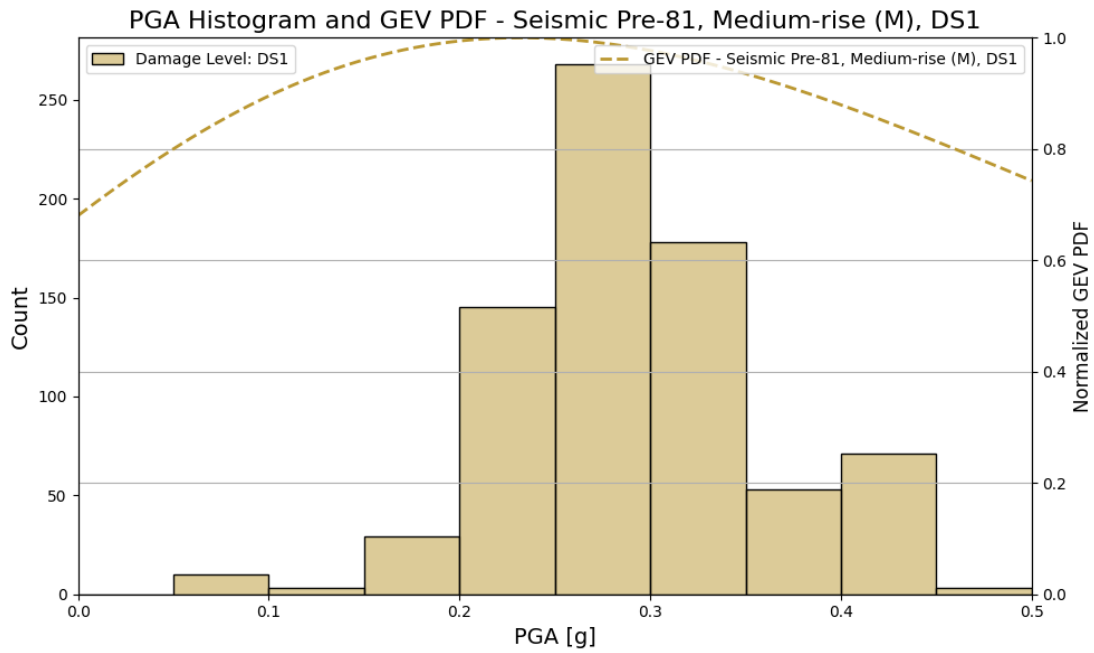
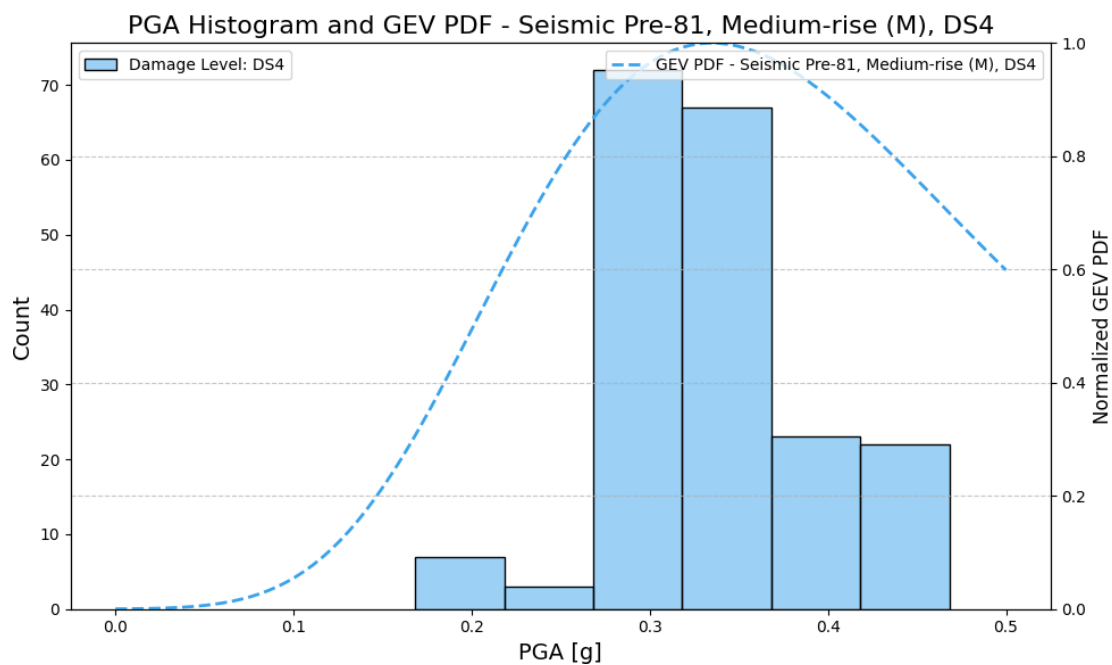
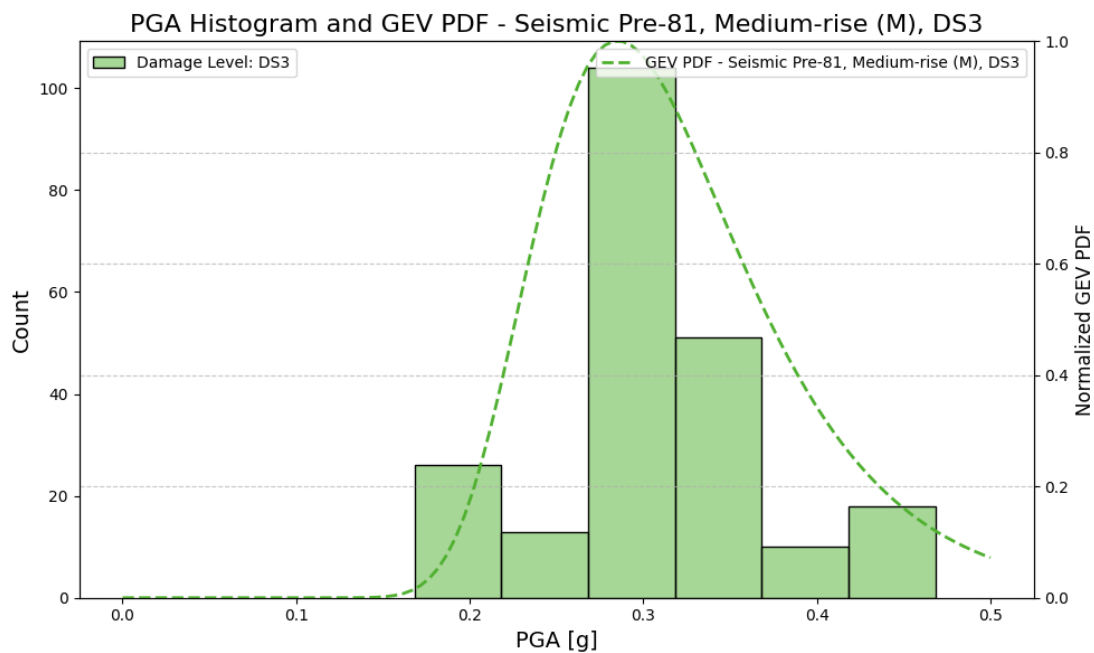


Figure 57. GEV distribution for medium-rise gravity load concrete buildings across all damage levels





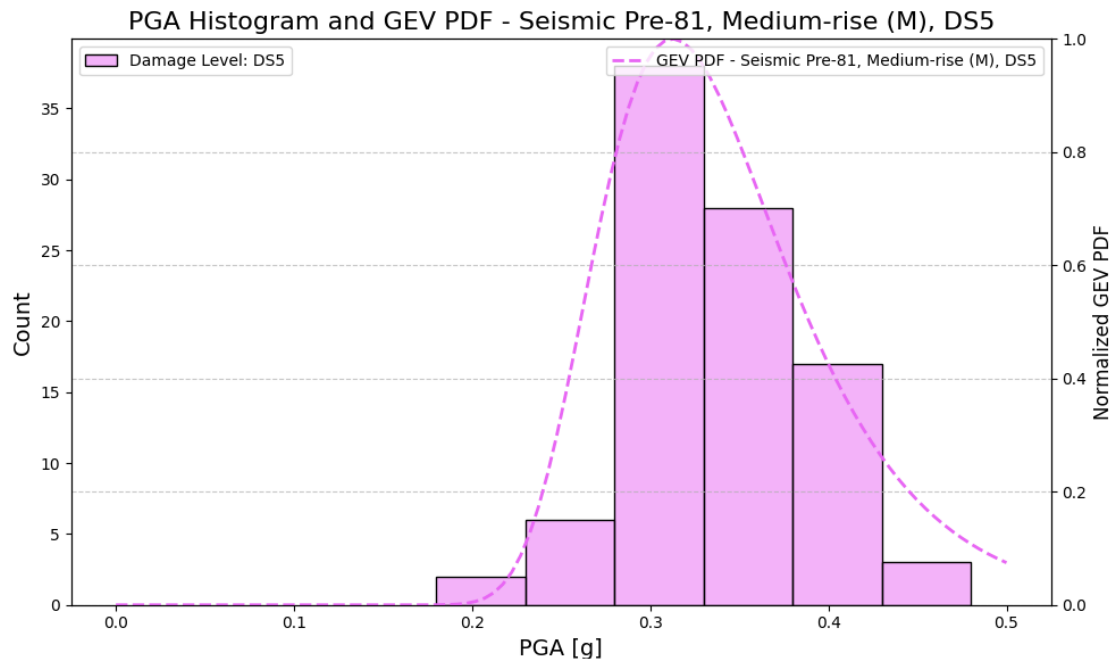
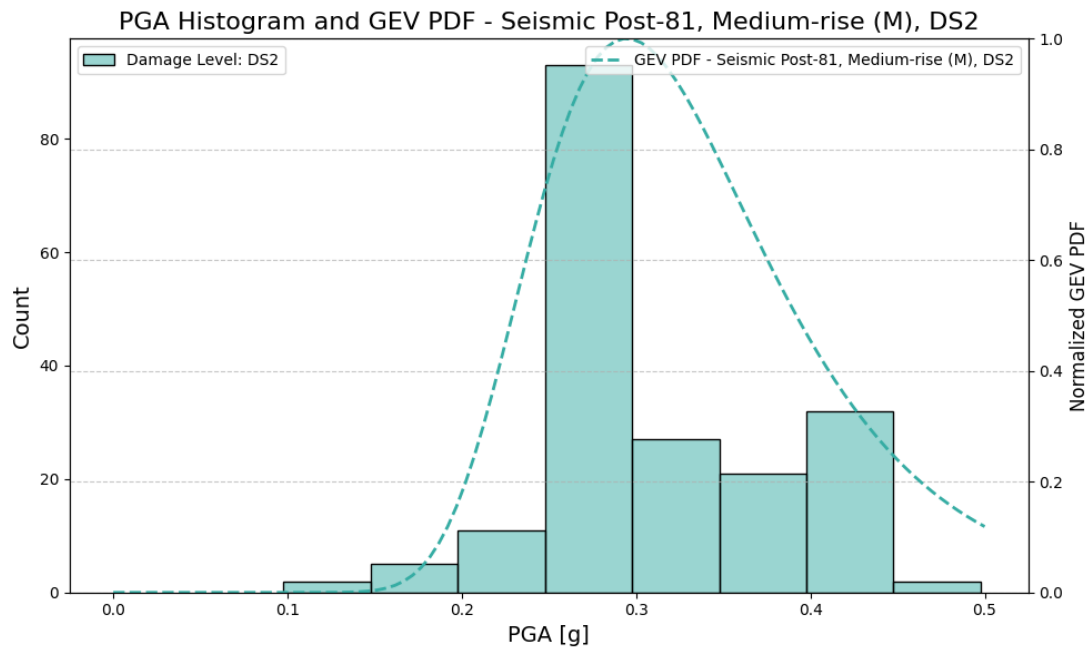
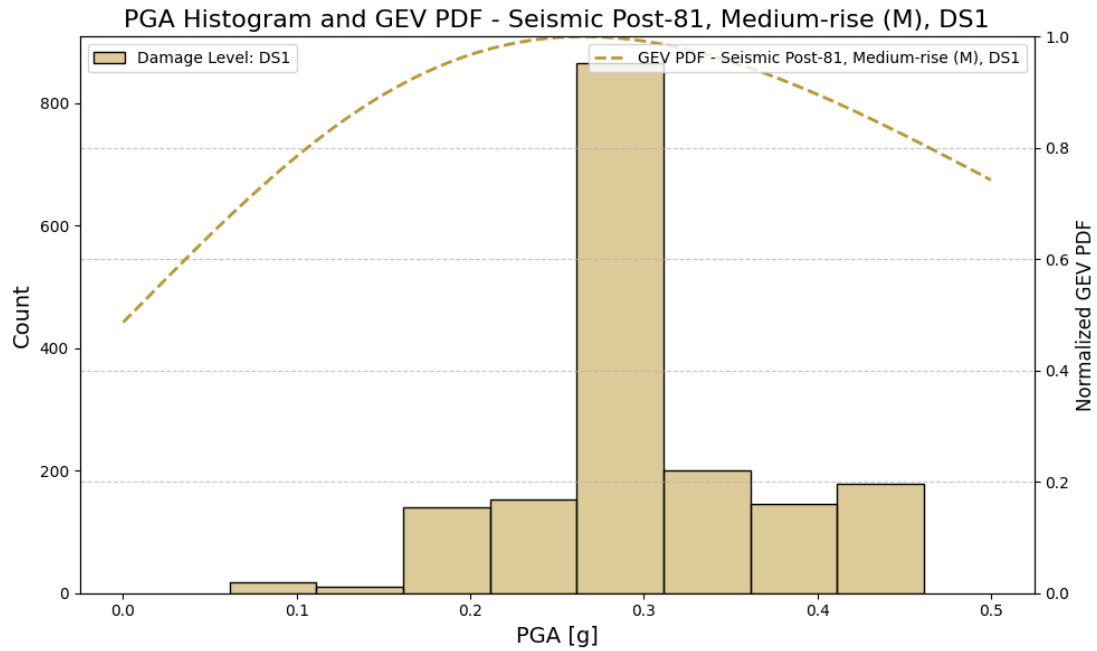
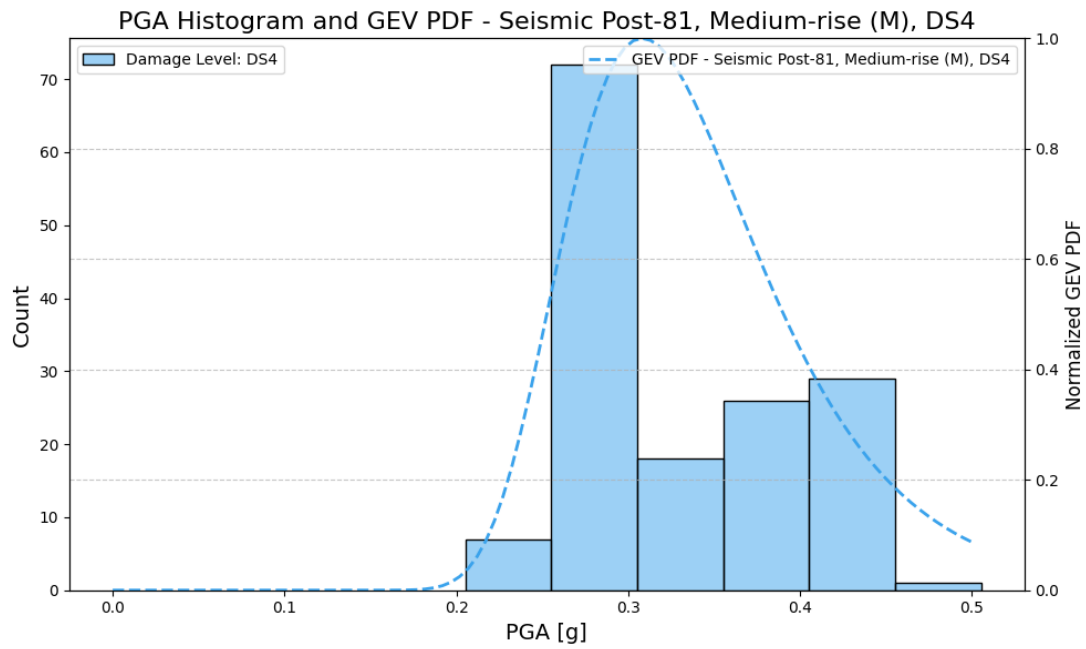
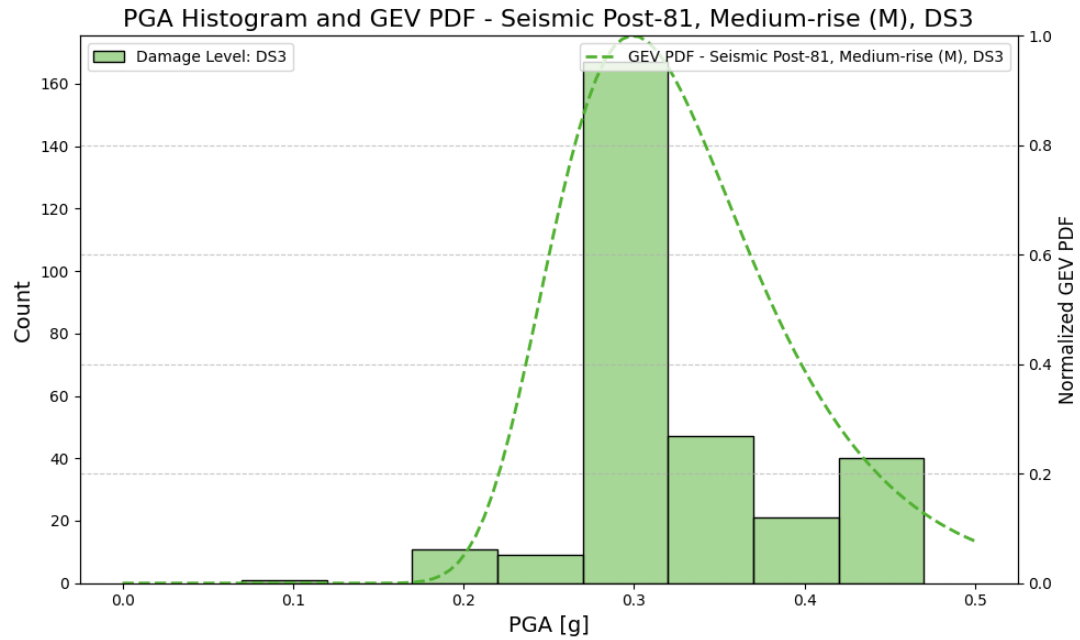


Figure 58. GEV distribution for medium-rise seismic pre81 concrete buildings across all damage levels





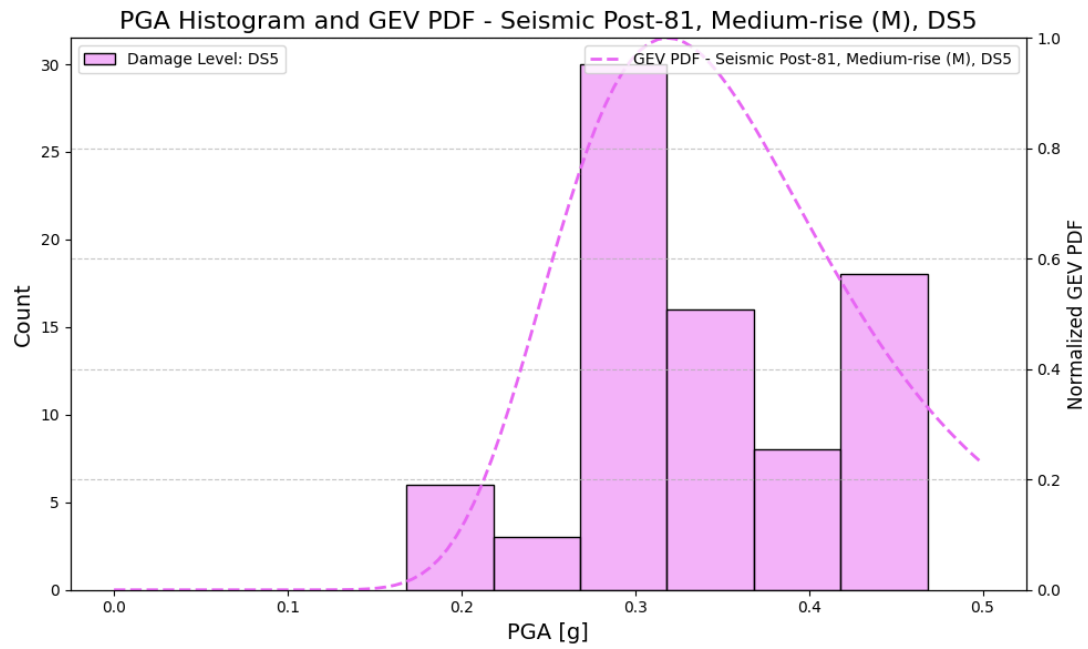
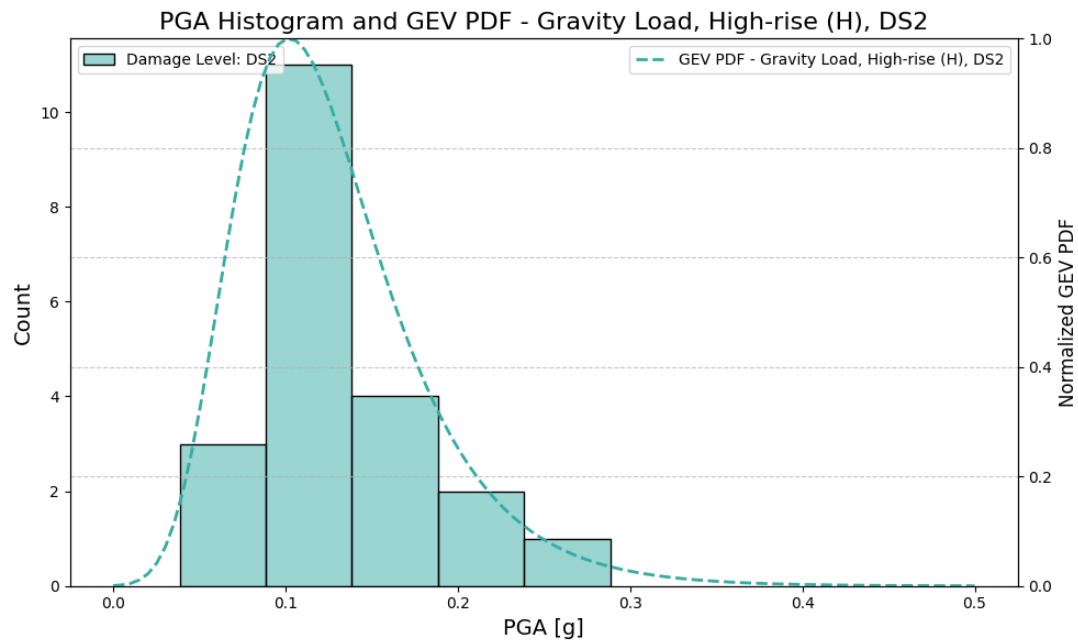
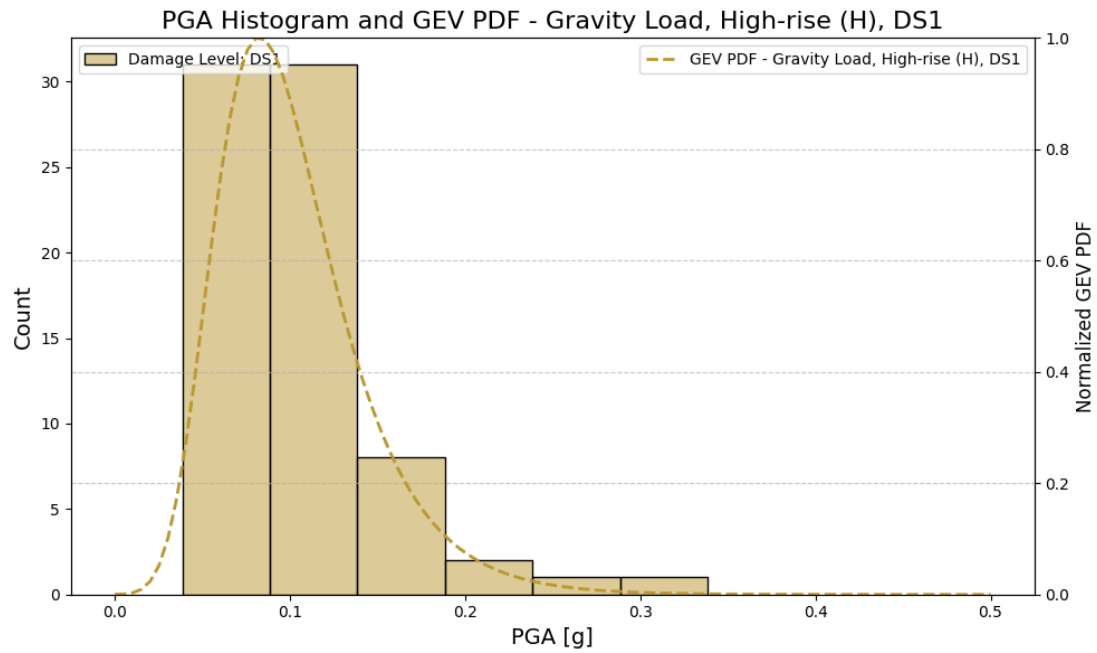
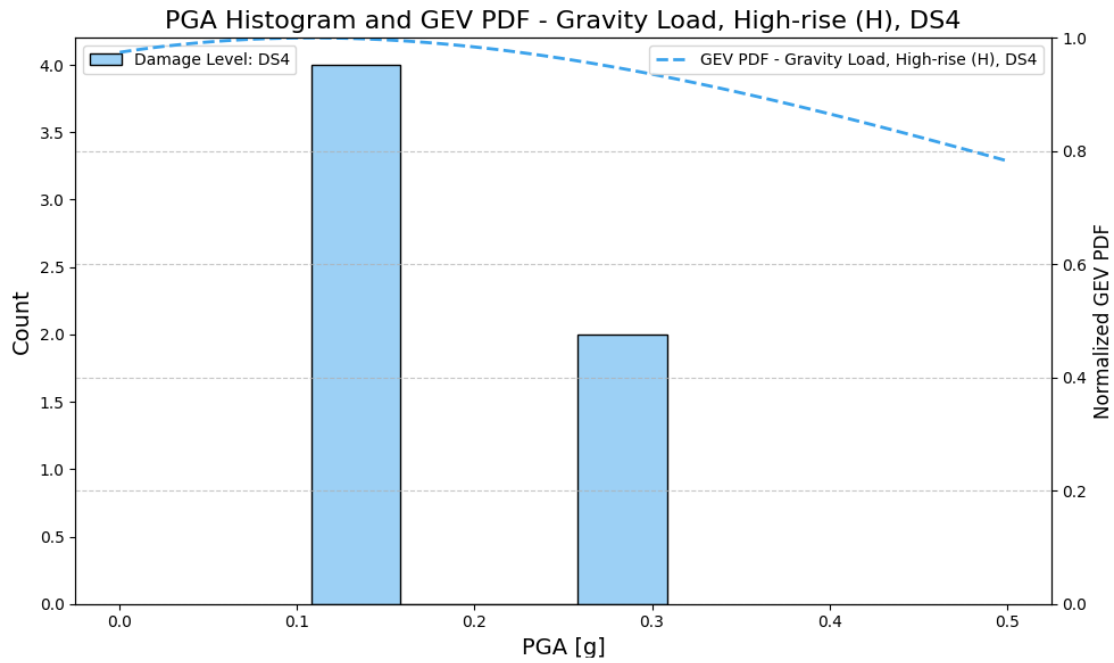
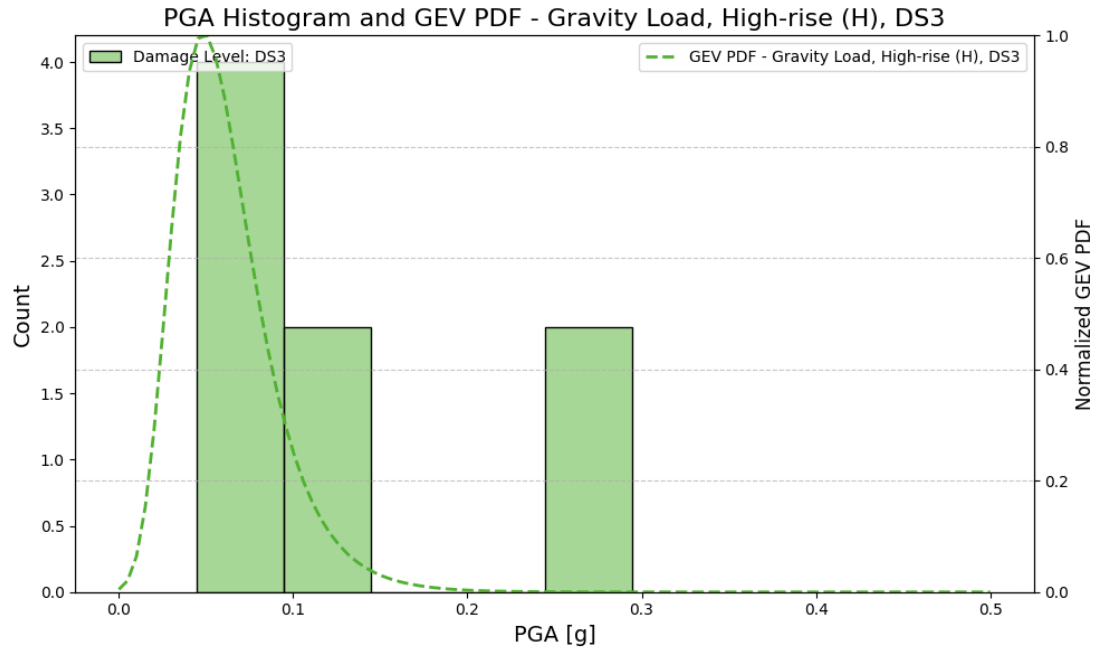


Figure 59. GEV distribution for medium-rise seismic post-81 concrete buildings across all damage levels





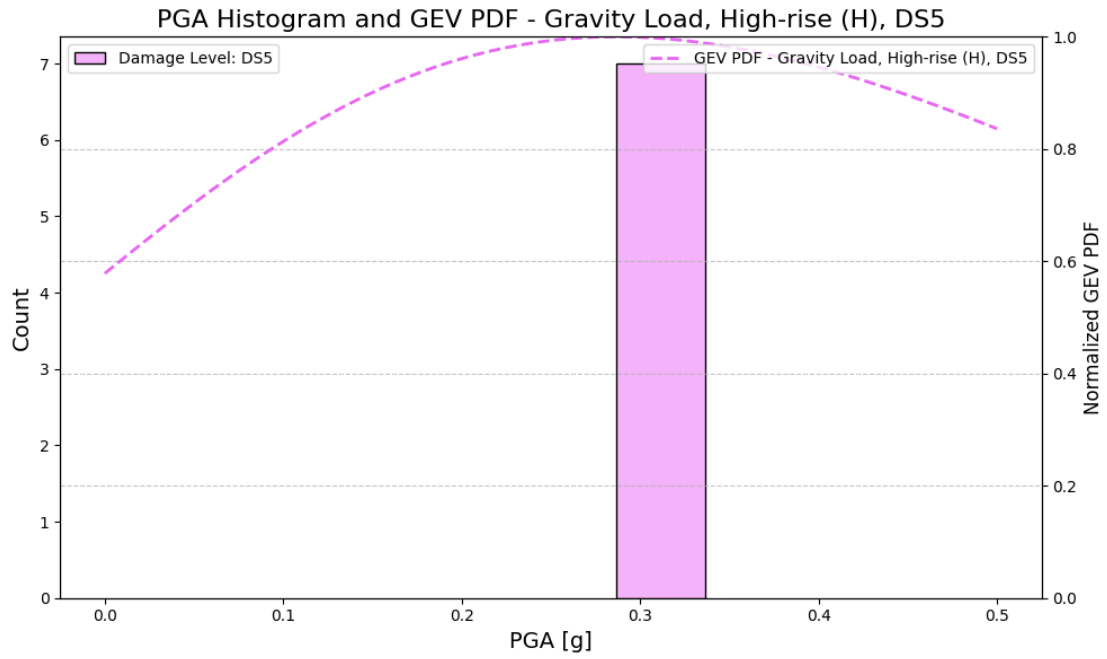
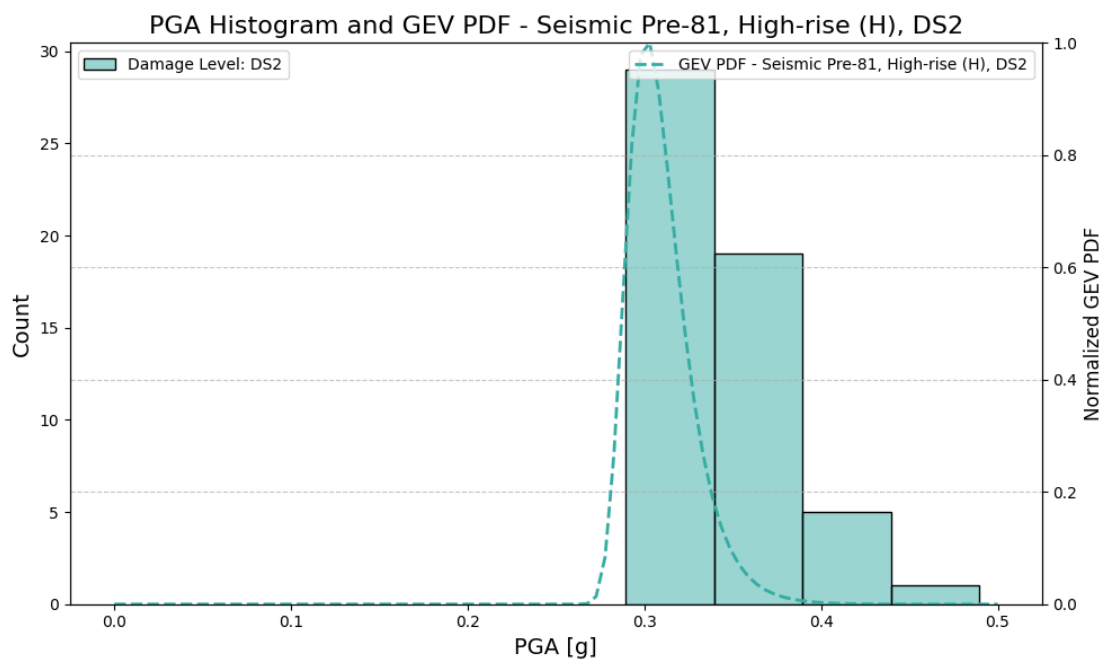
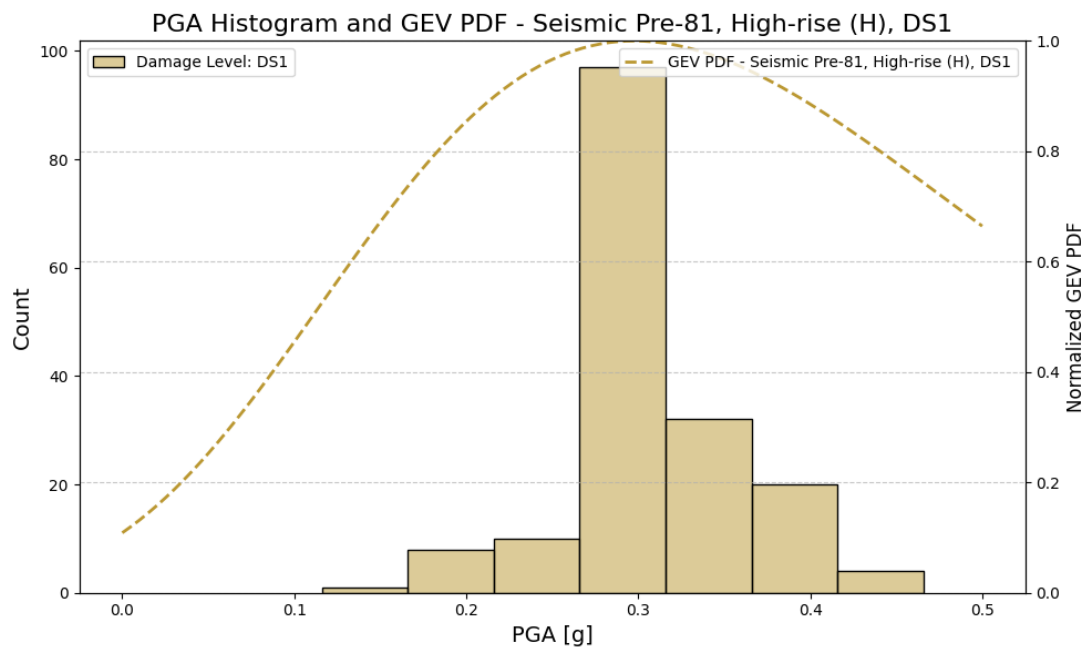
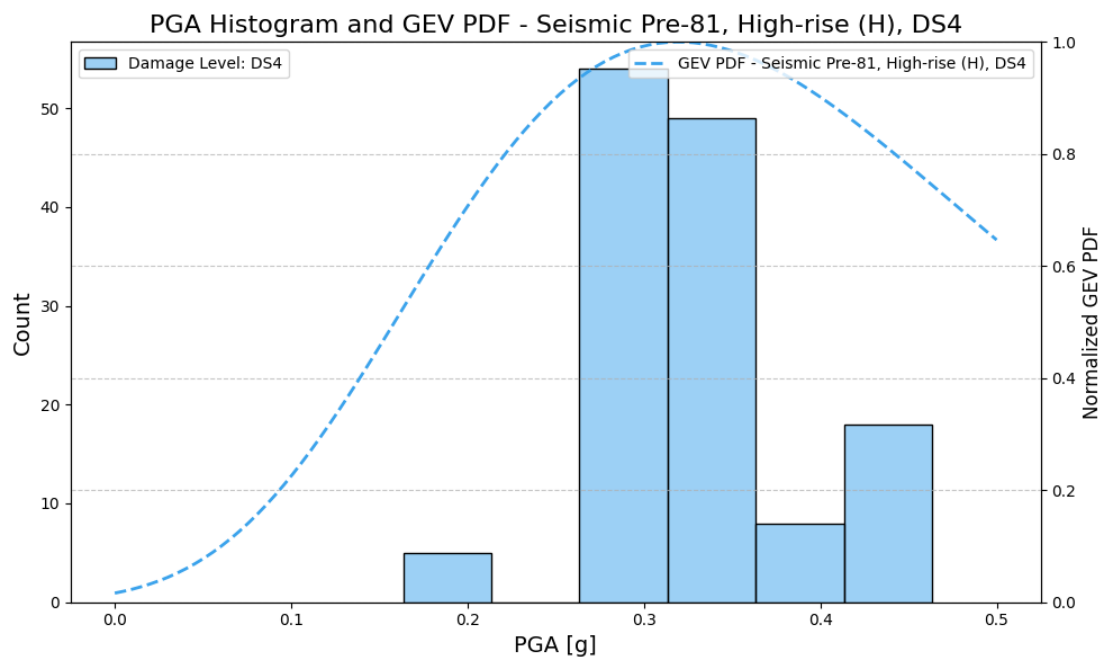
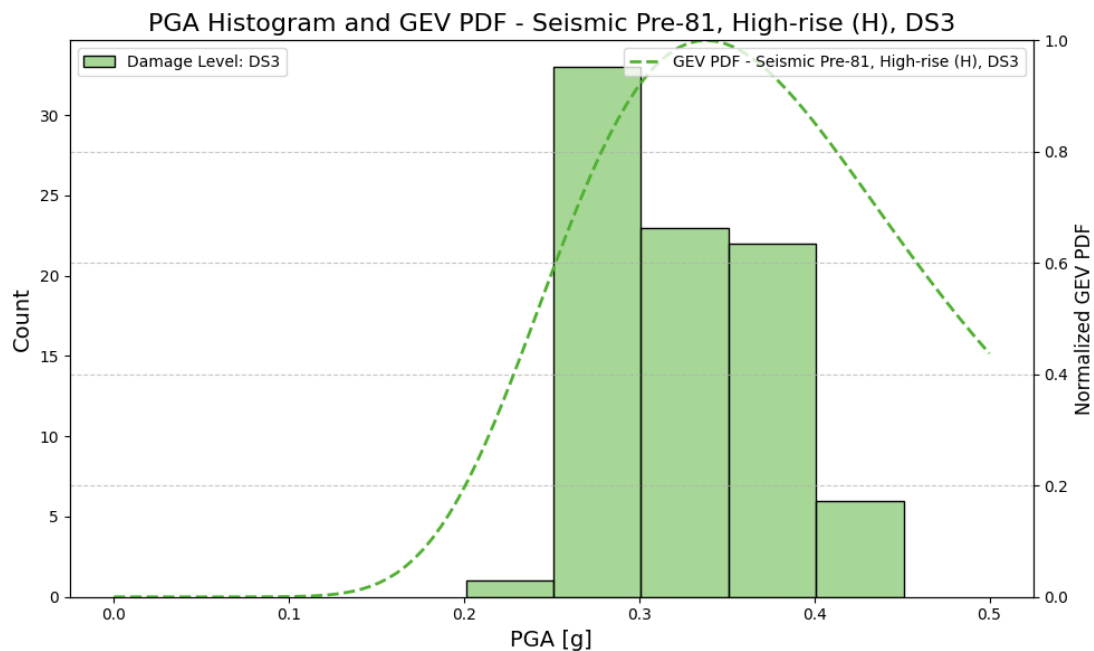


Figure 60. GEV distribution for high-rise gravity load concrete buildings across all damage levels





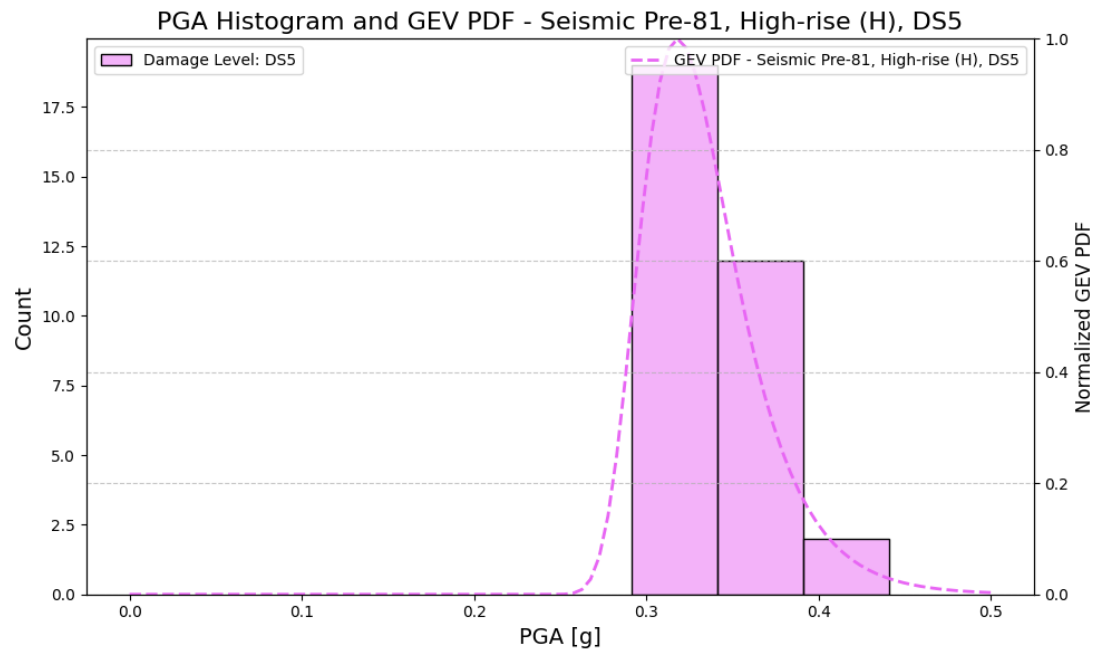
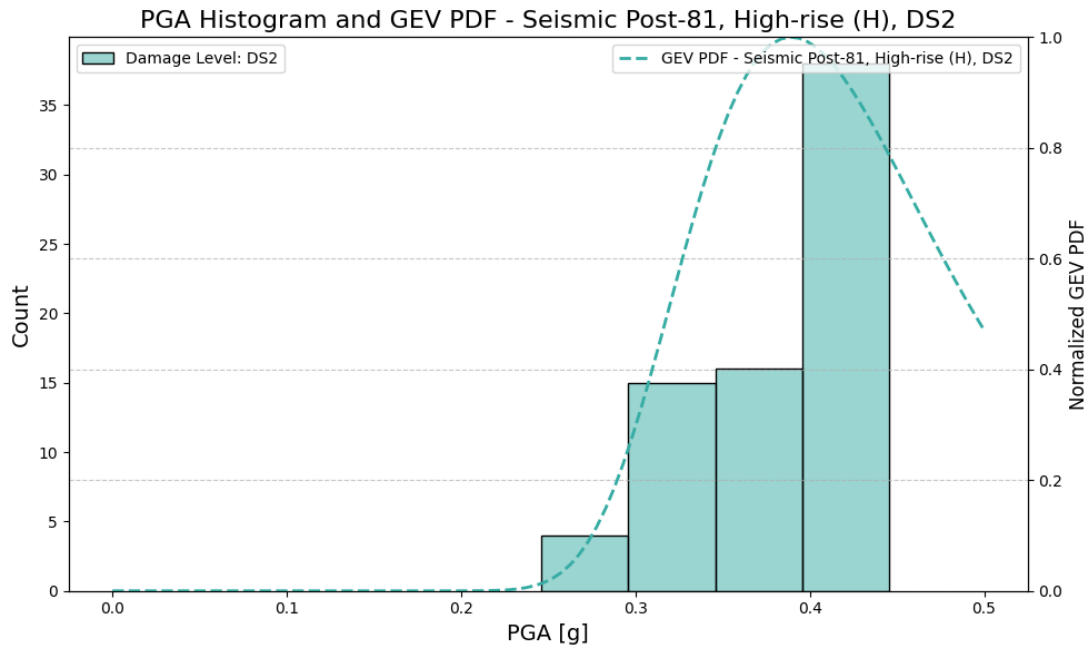
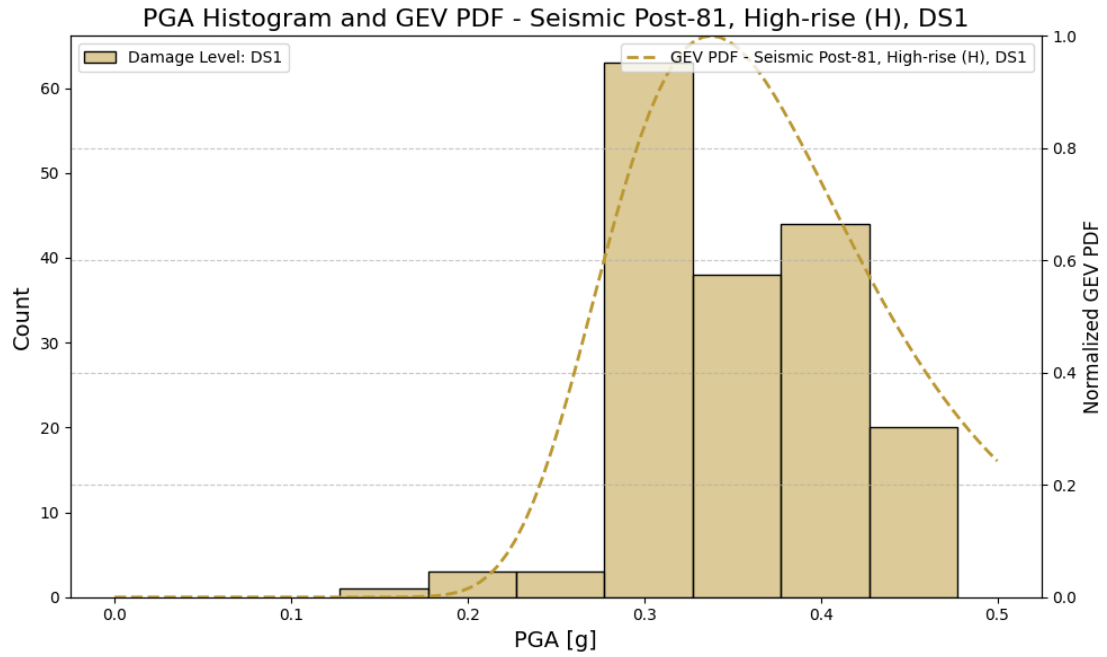
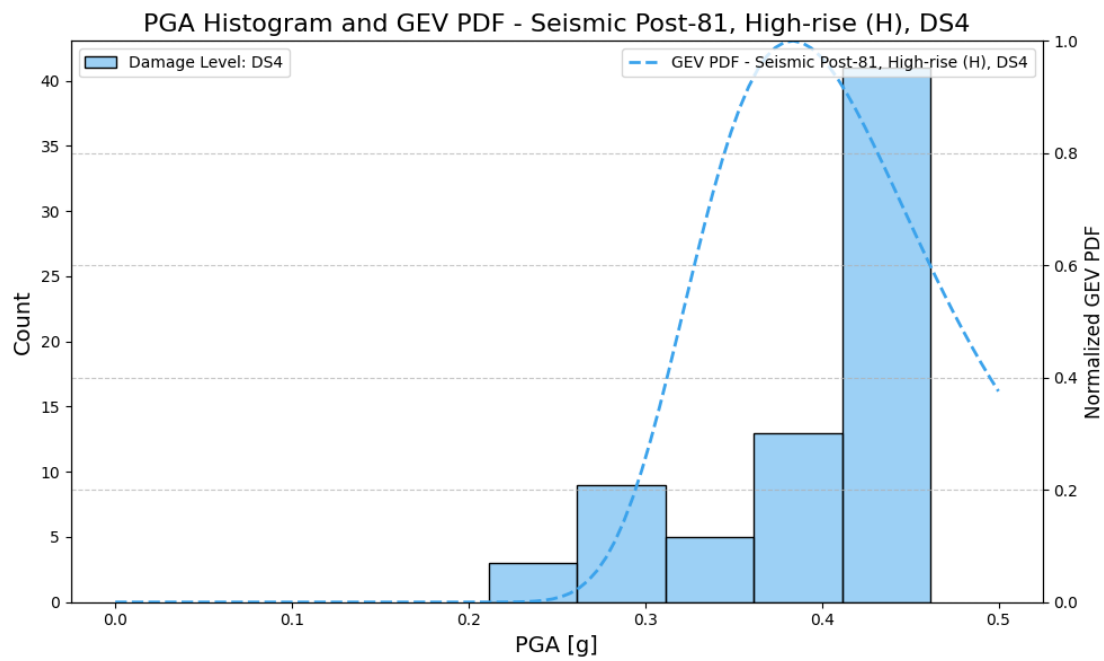
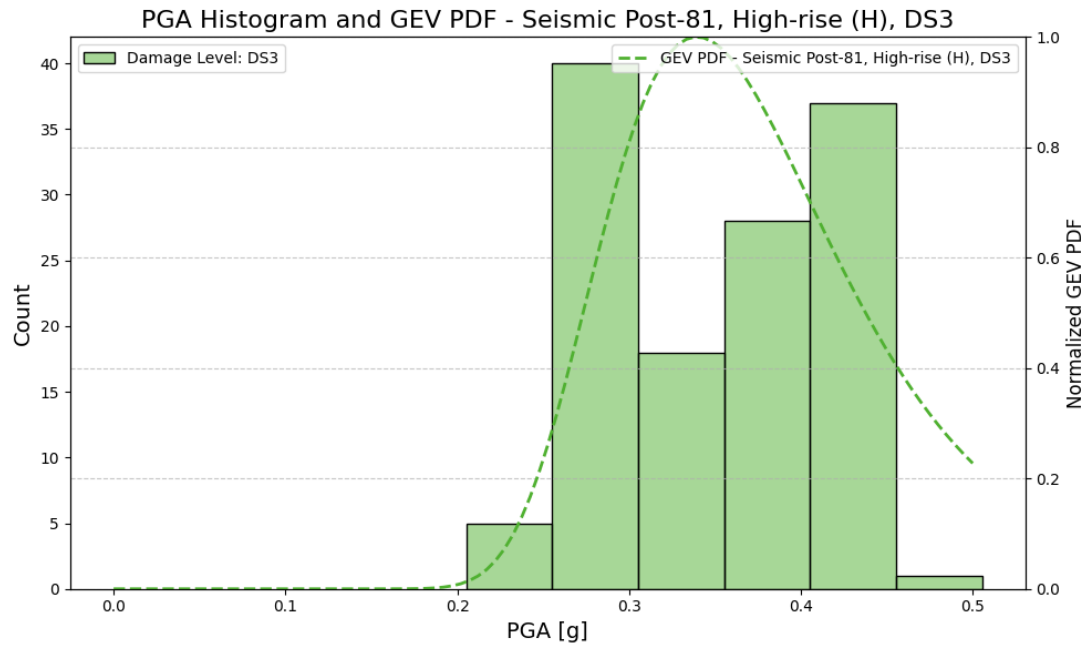


Figure 61. GEV distribution for high-rise seismic pre-81 concrete buildings across all damage levels





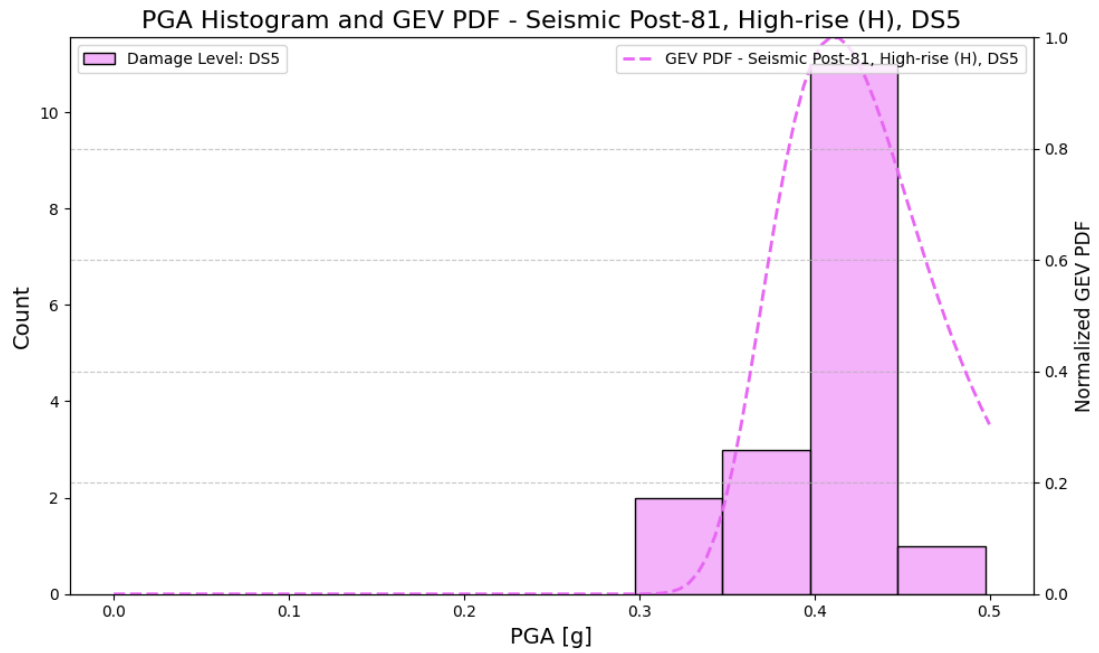
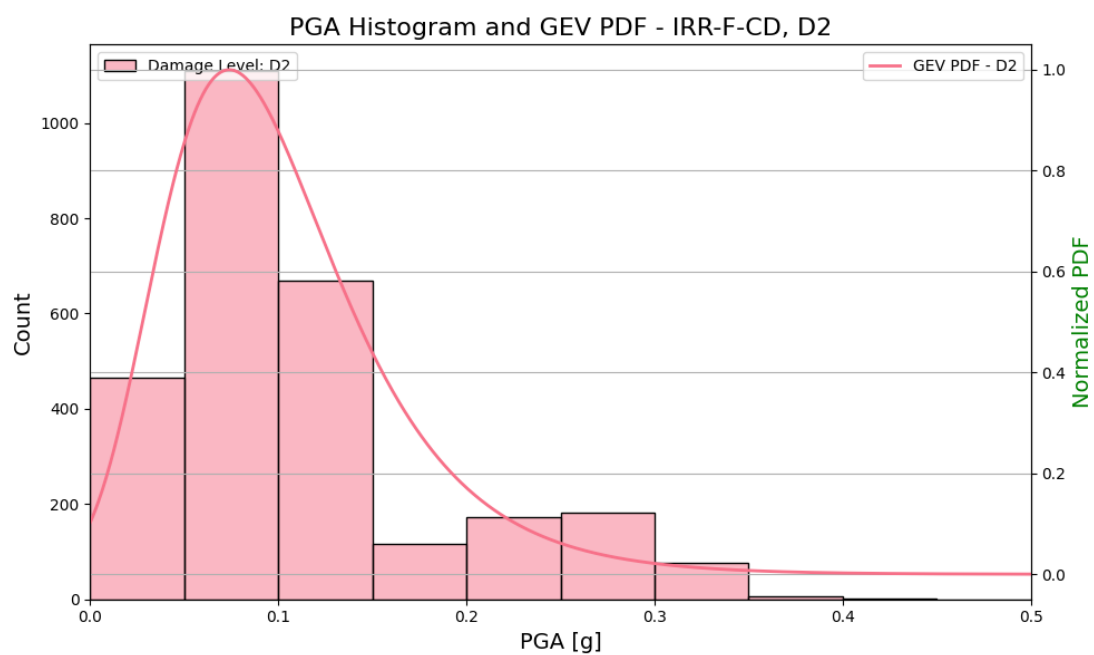
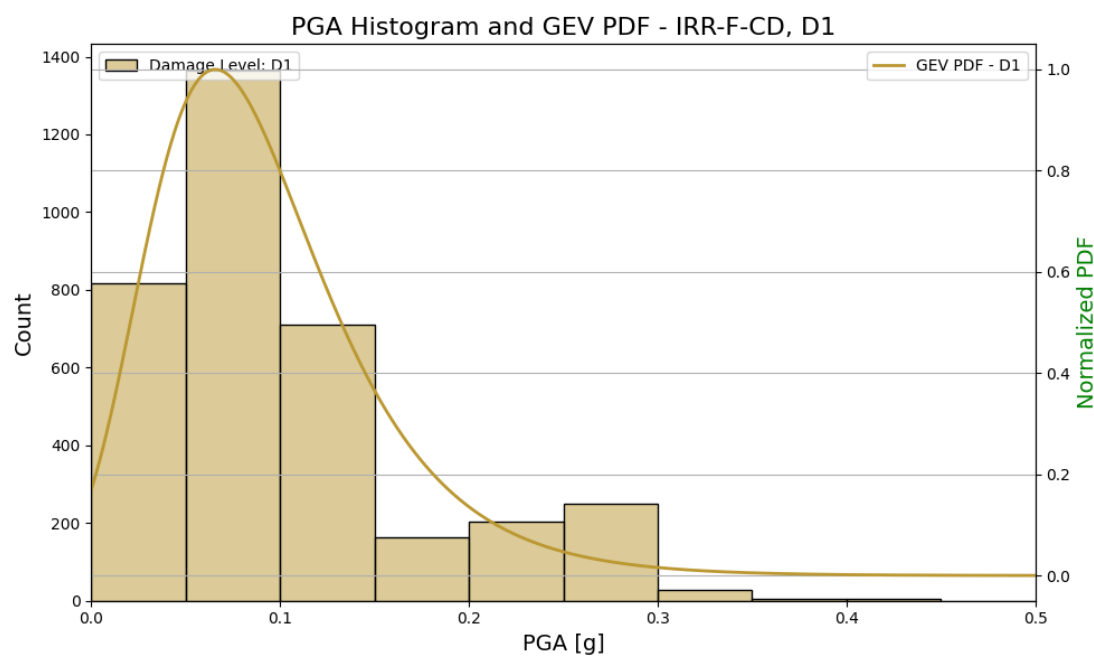
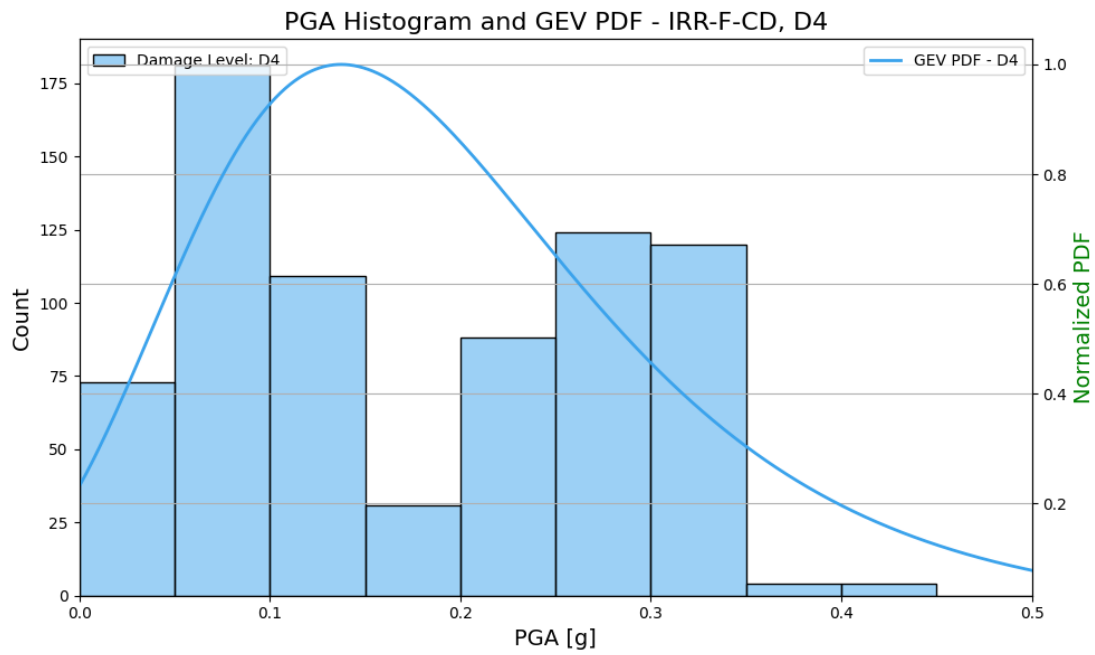
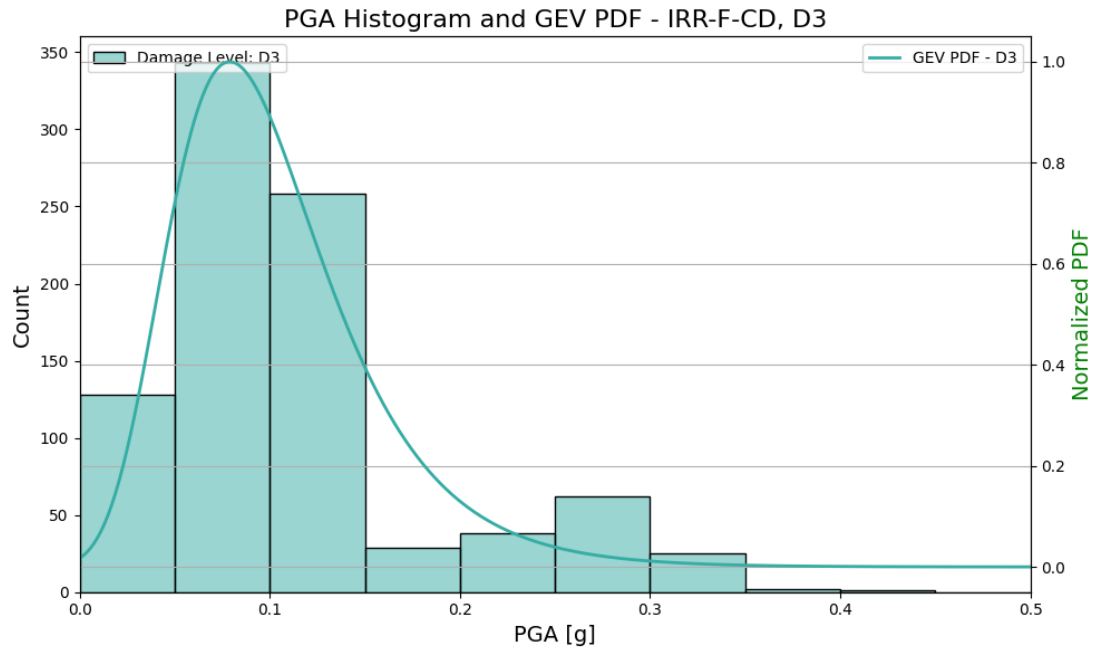


Figure 62. GEV distribution for high-rise seismic post-81 concrete buildings across all damage levels

Masonry buildings





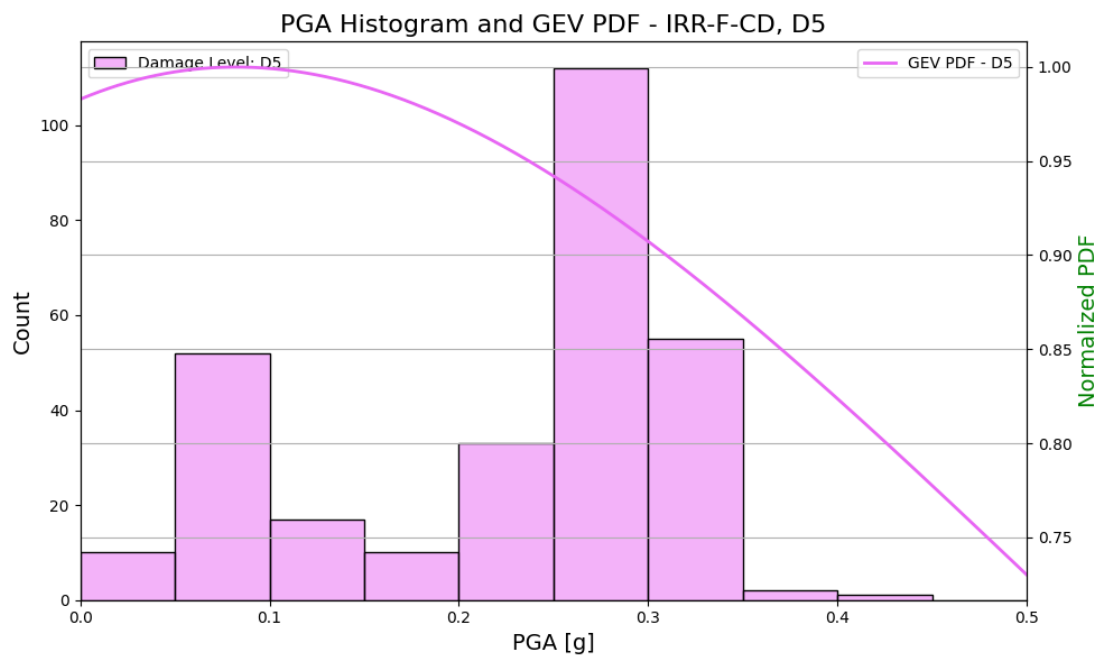
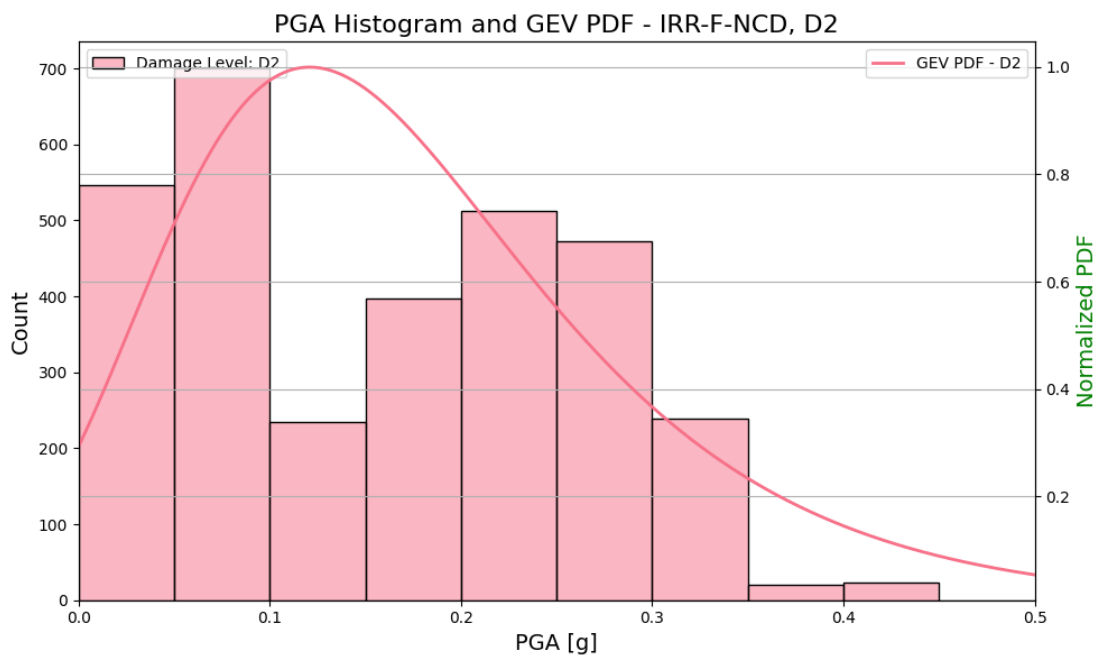
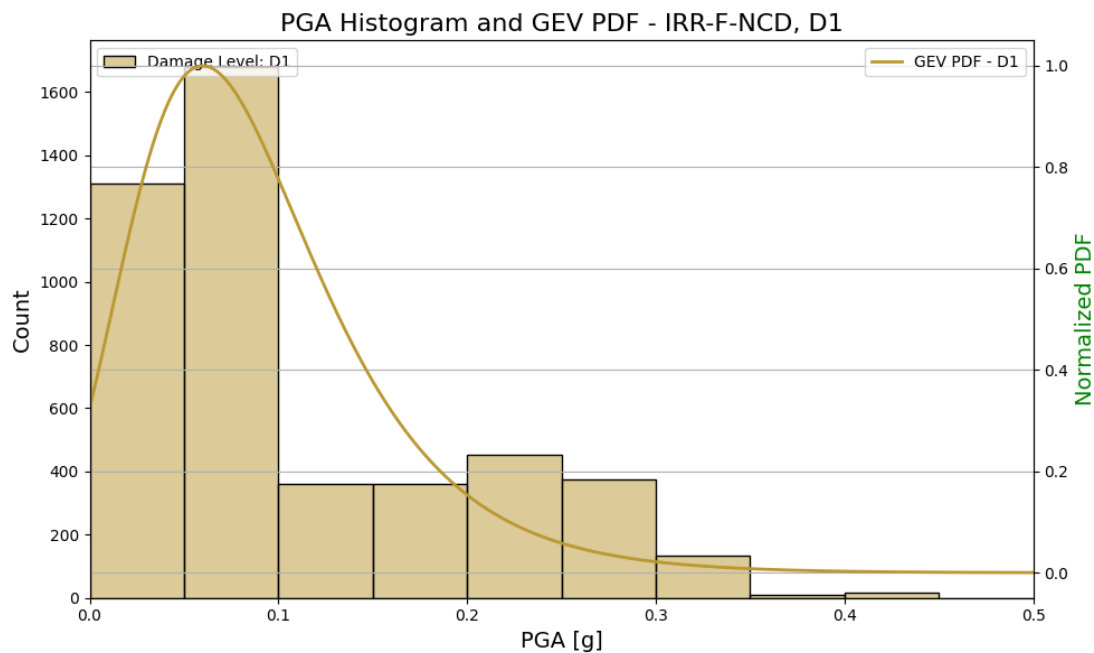
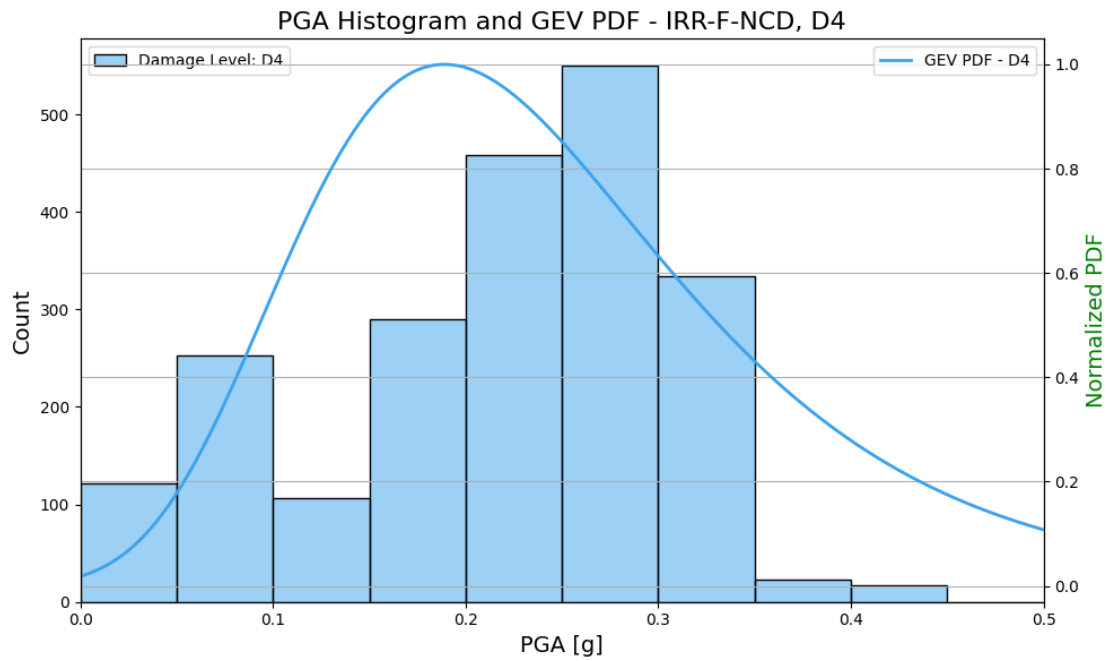
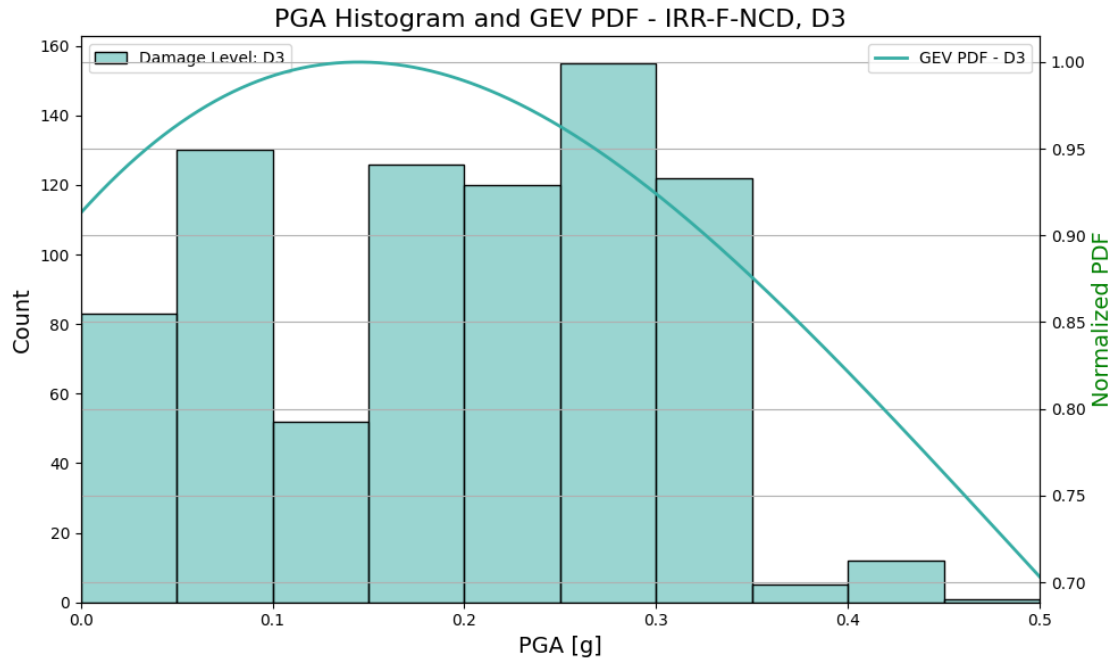


Figure 63. GEV distribution for IRR-F-CD masonry buildings across all damage levels





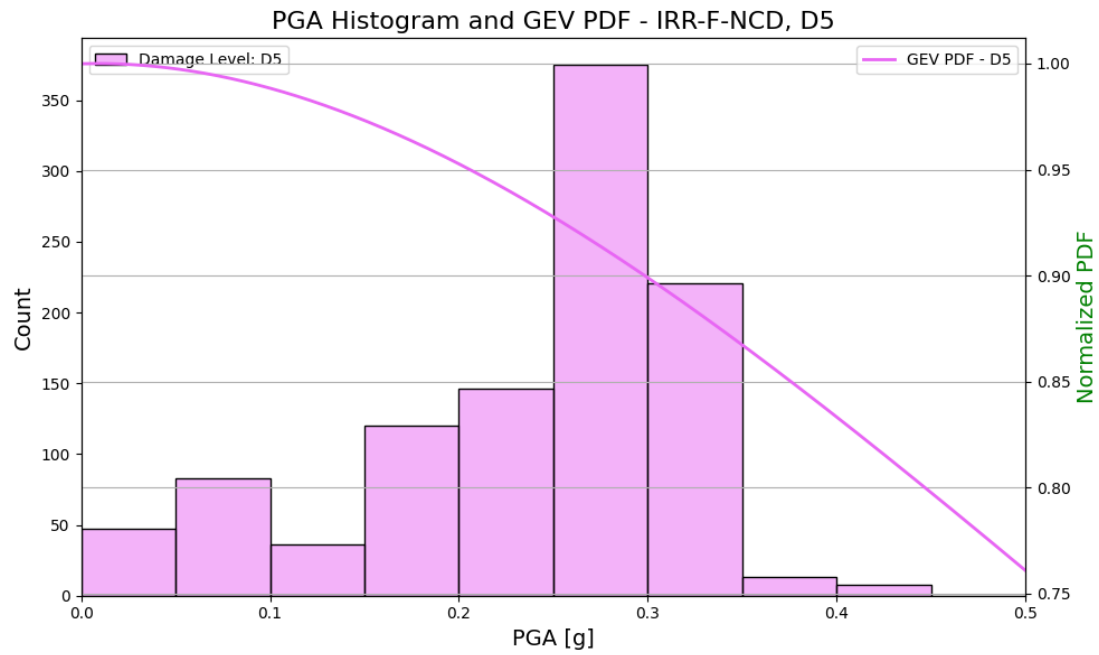
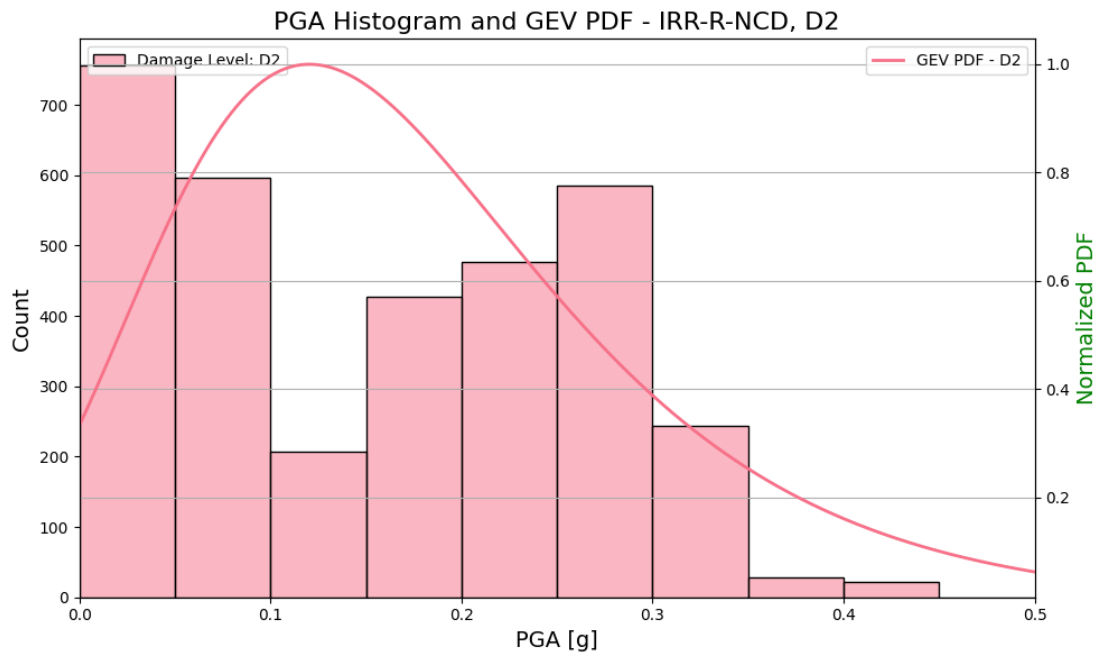
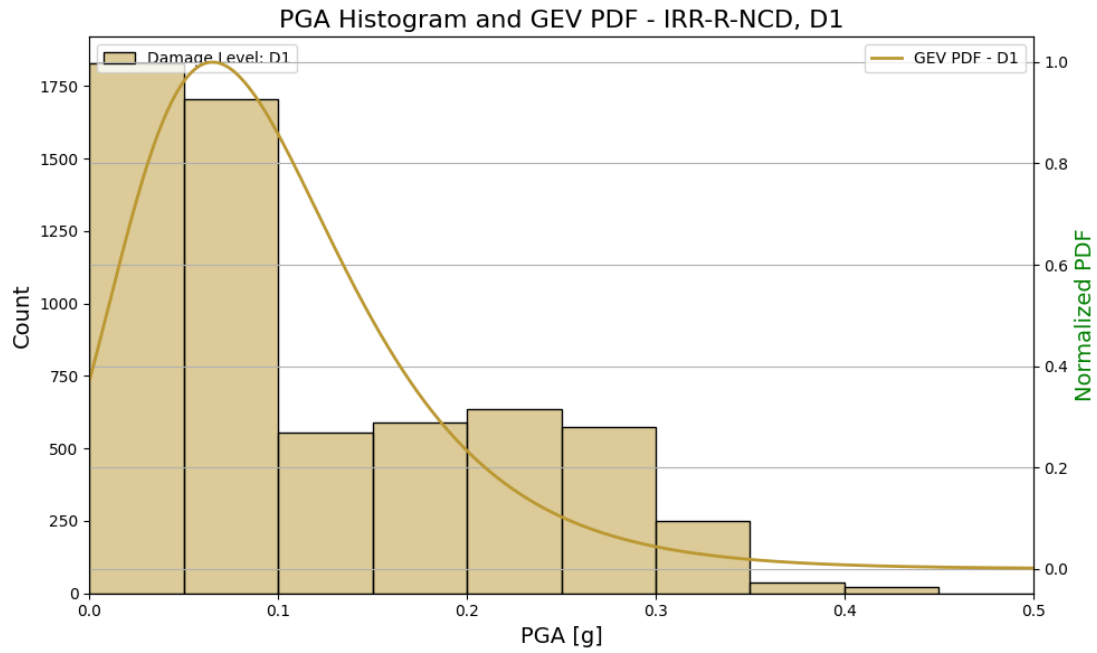
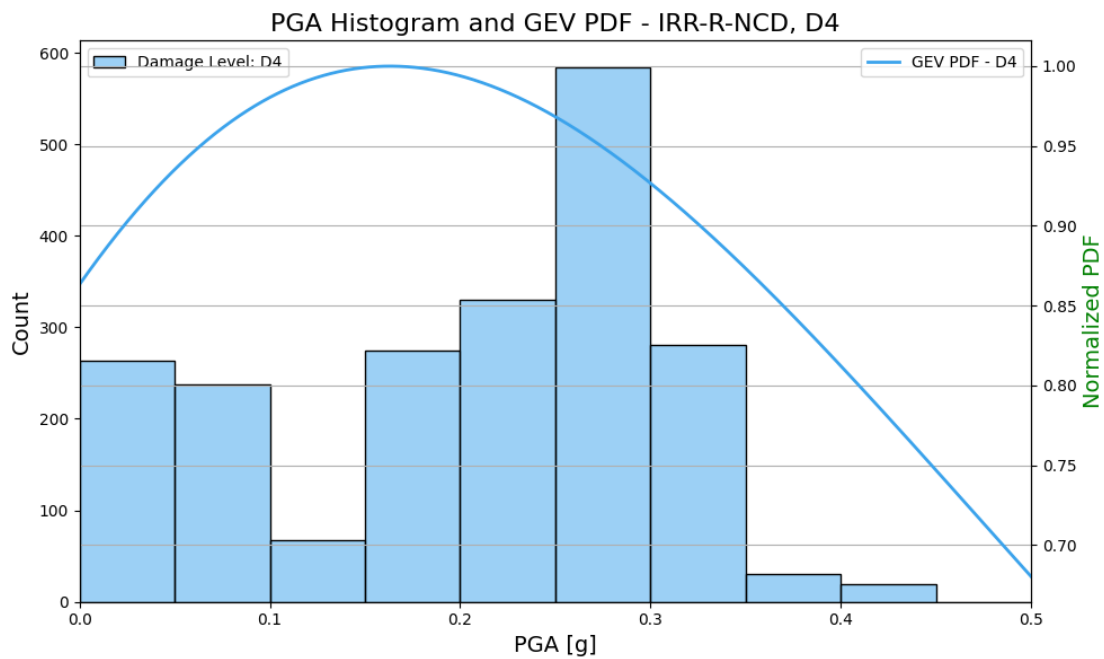
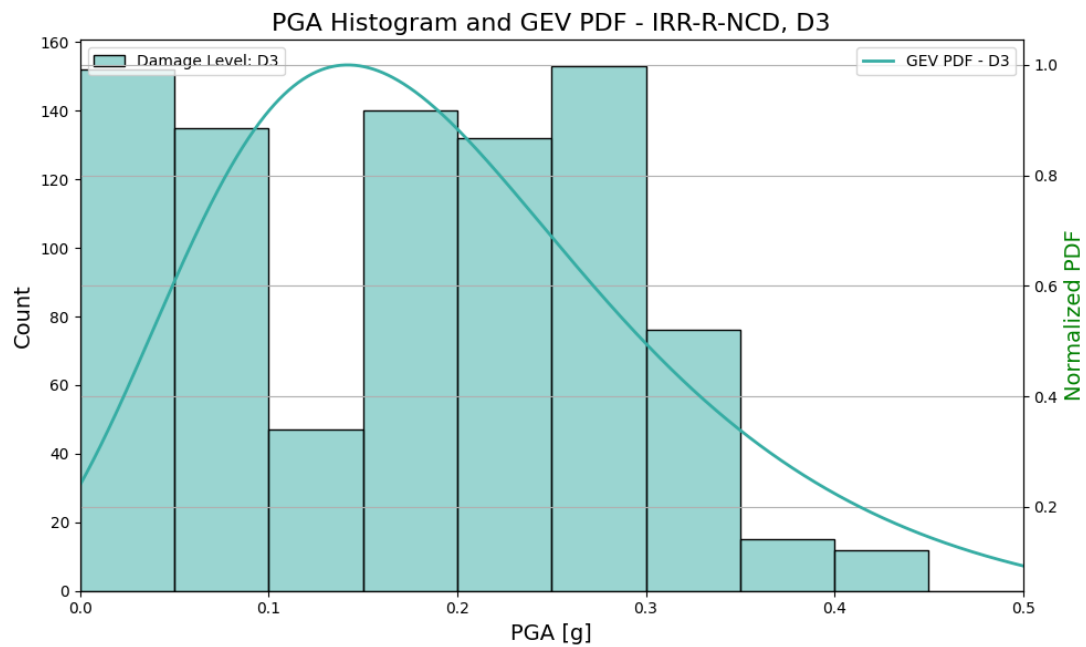


Figure 64. GEV distribution for IRR-F-NCD masonry buildings across all damage levels





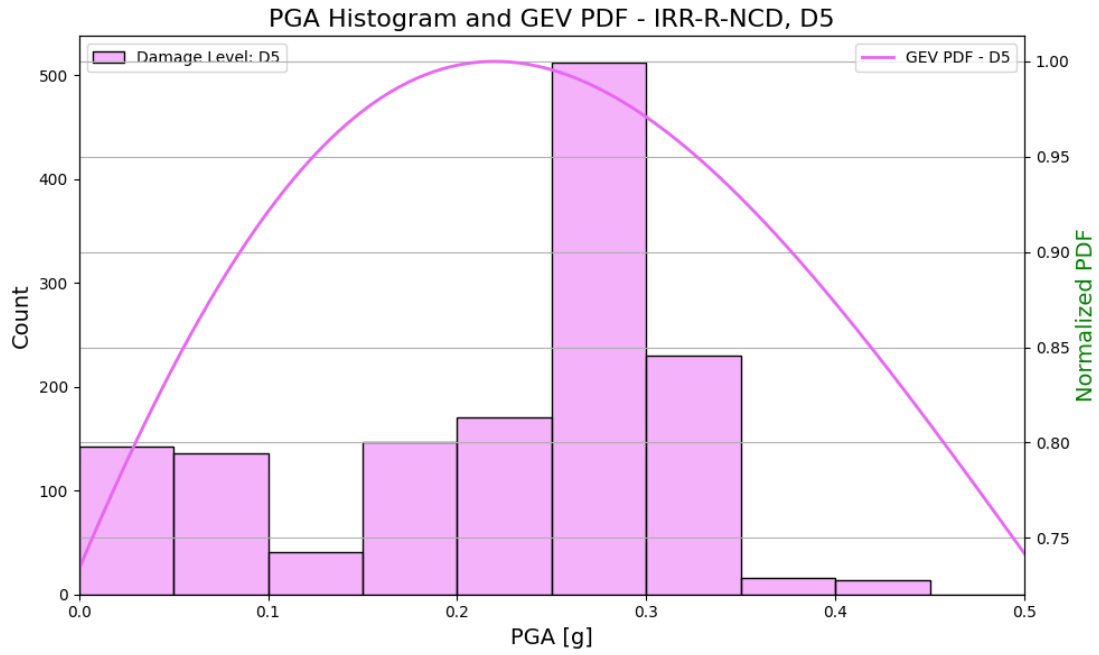
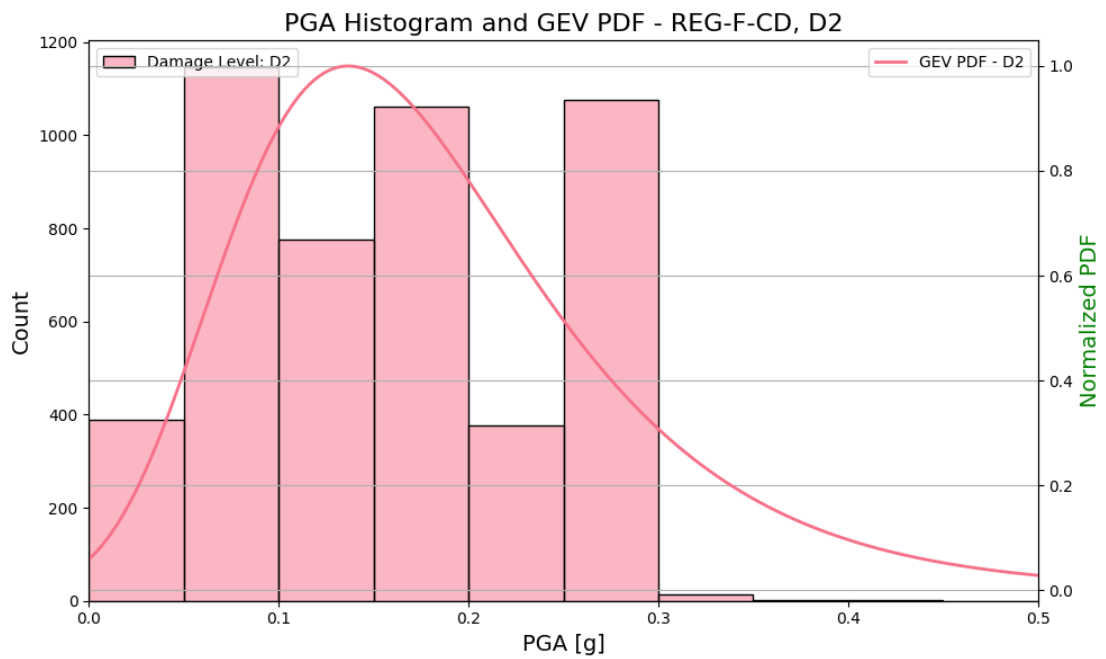
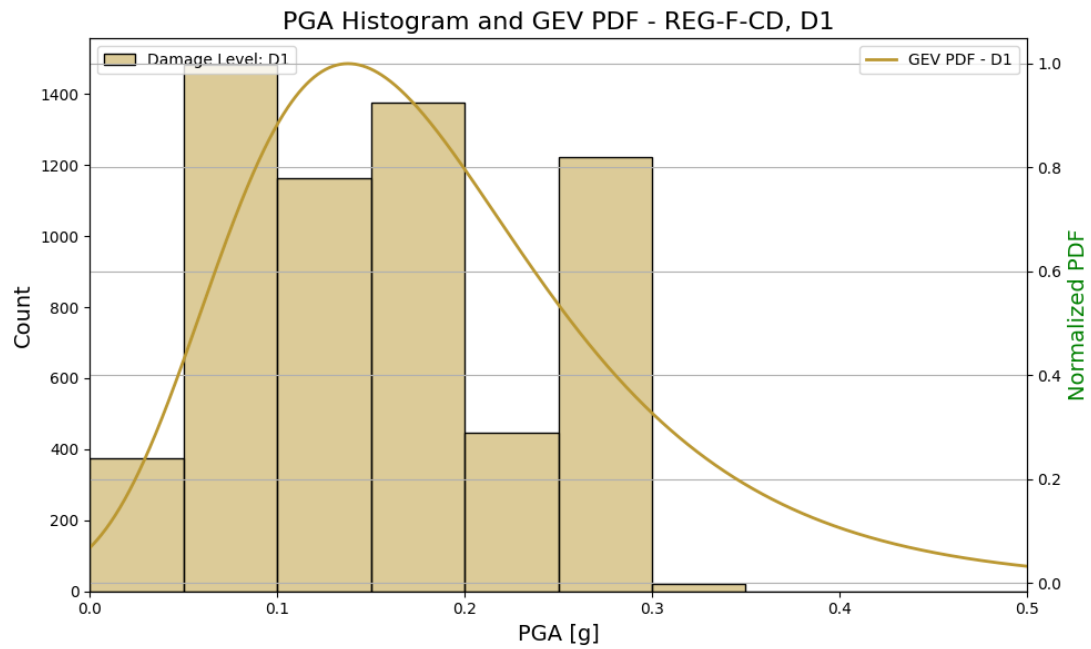
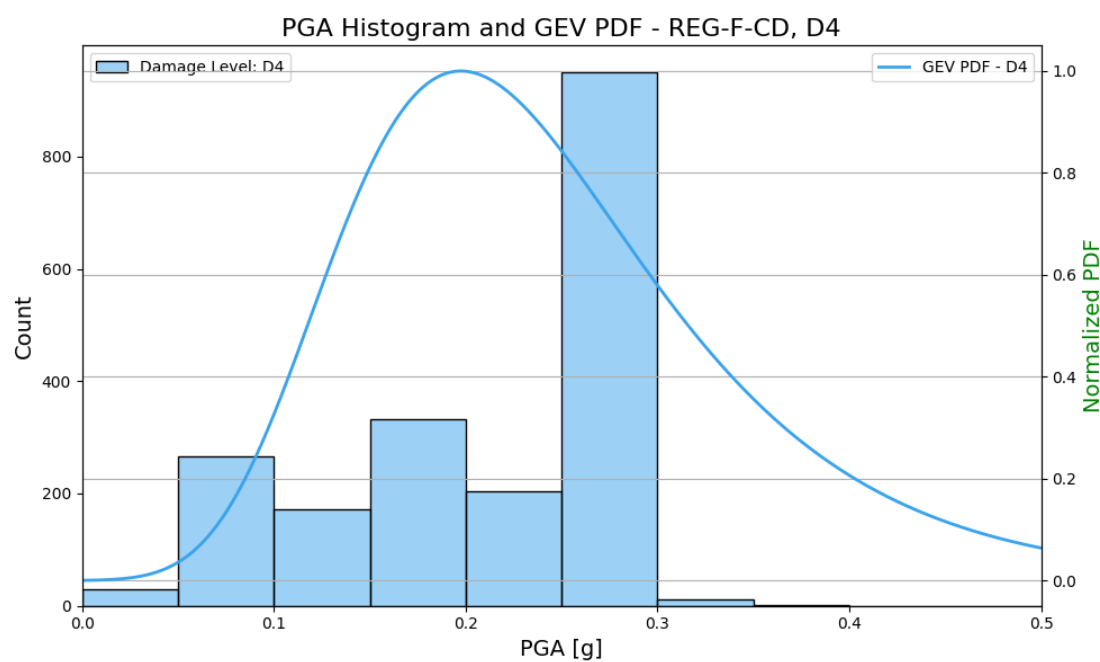
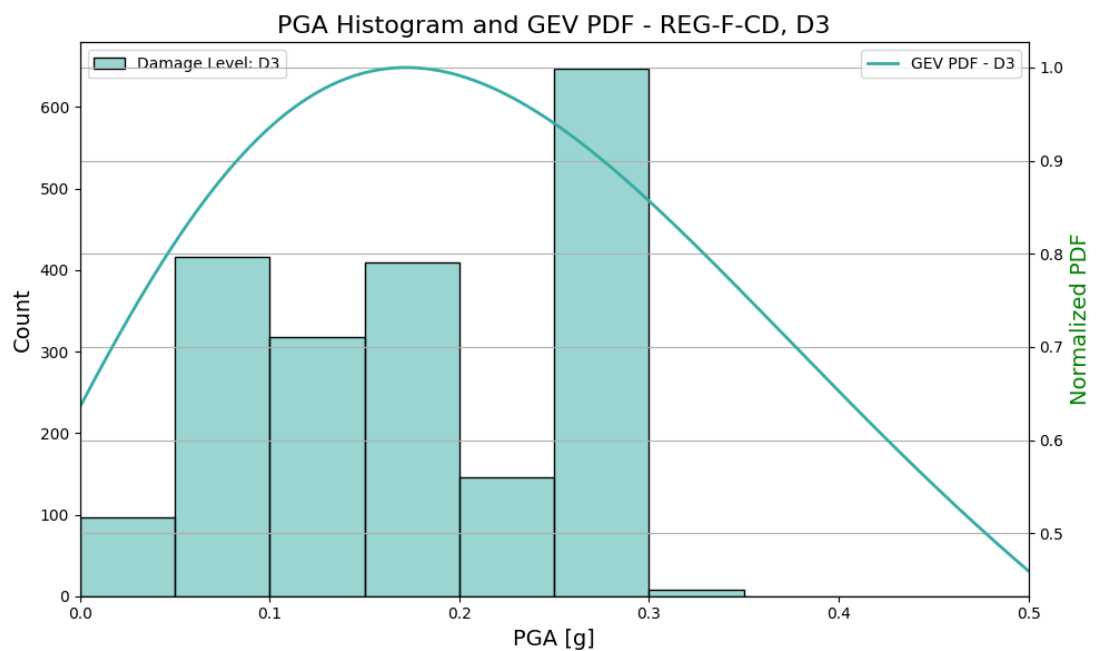


Figure 65. GEV distribution for IRR-R-NCD masonry buildings across all damage levels





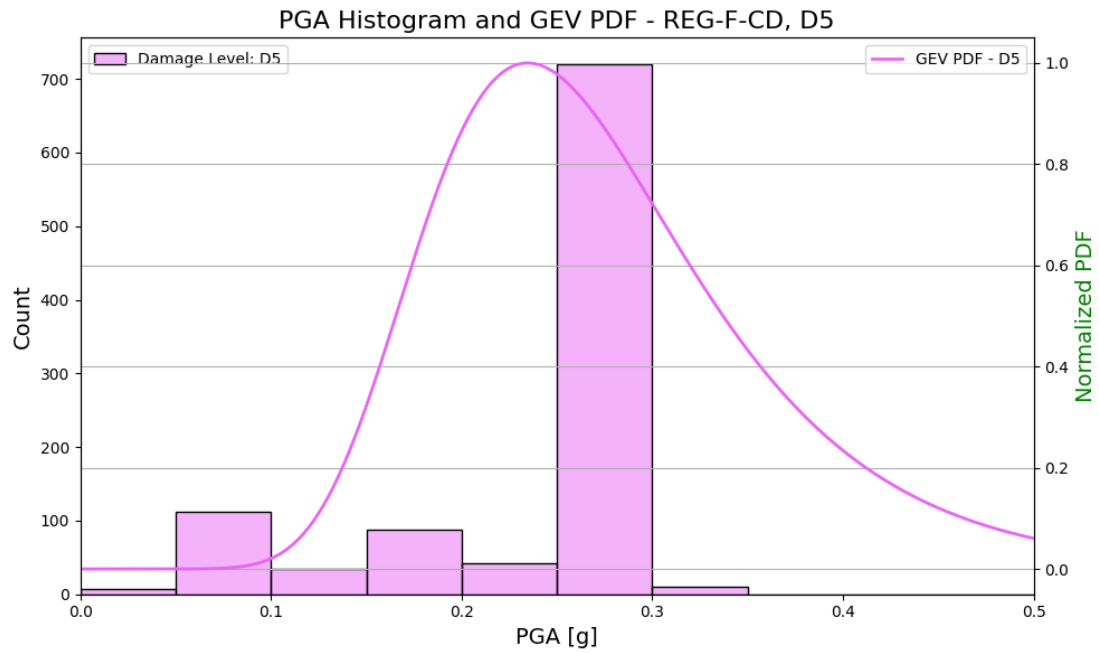
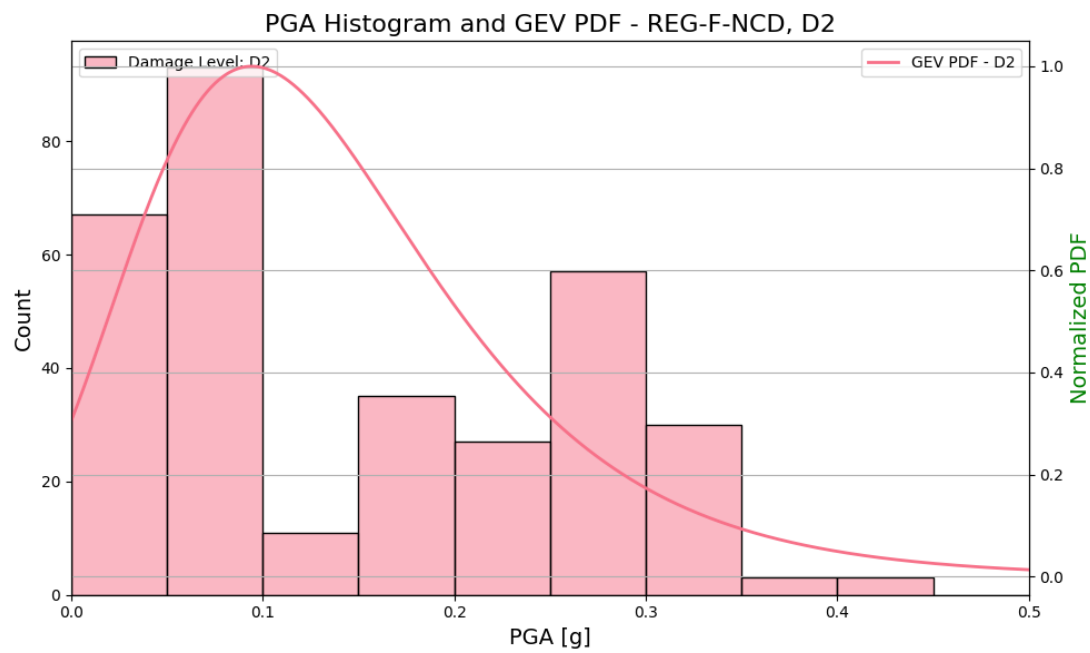
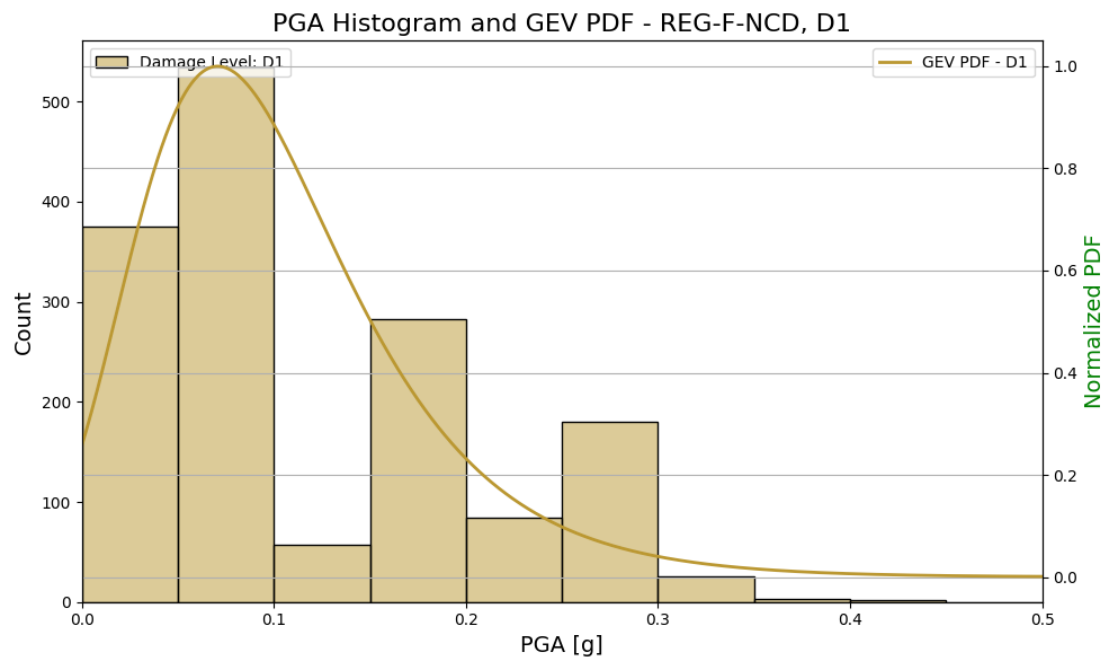
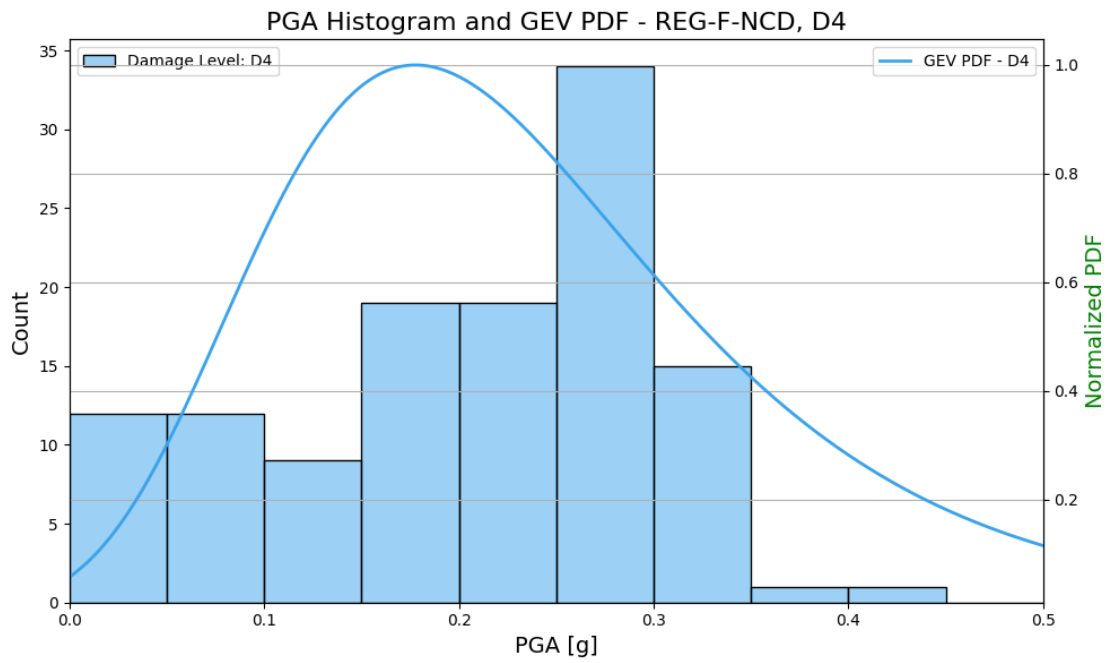
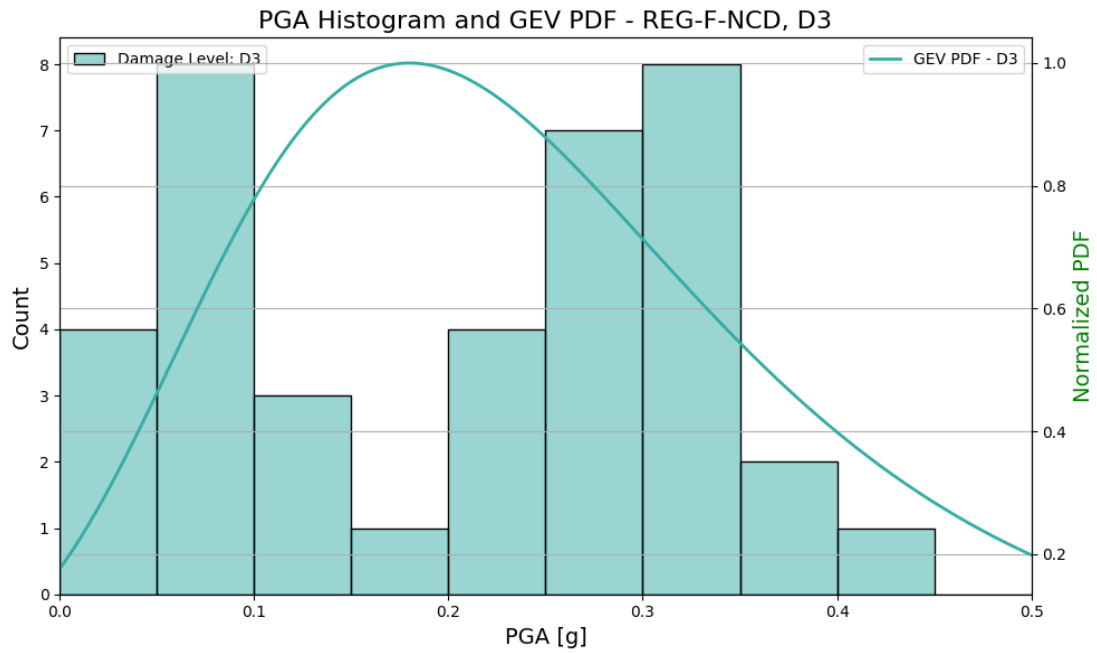


Figure 66. GEV distribution for REG-F-CD masonry buildings across all damage levels





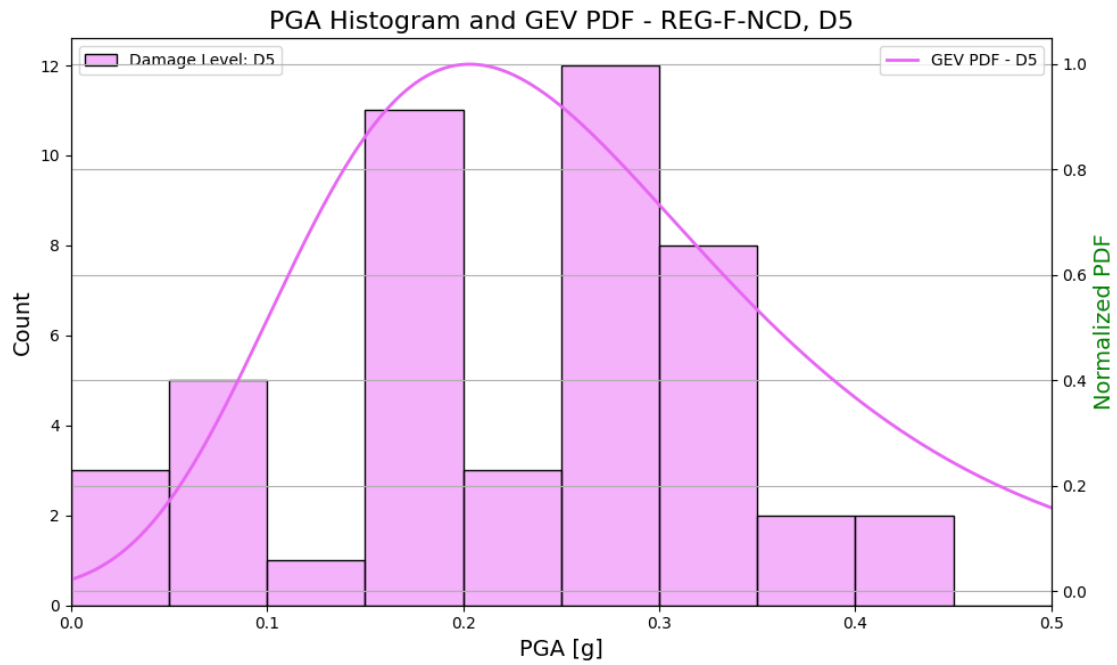
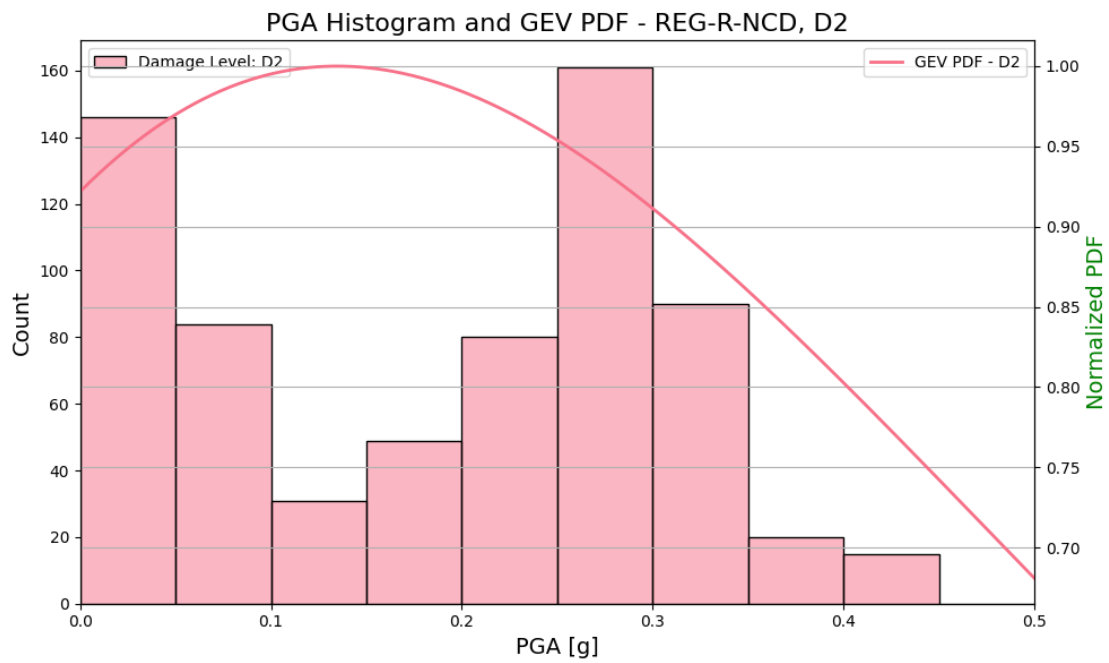
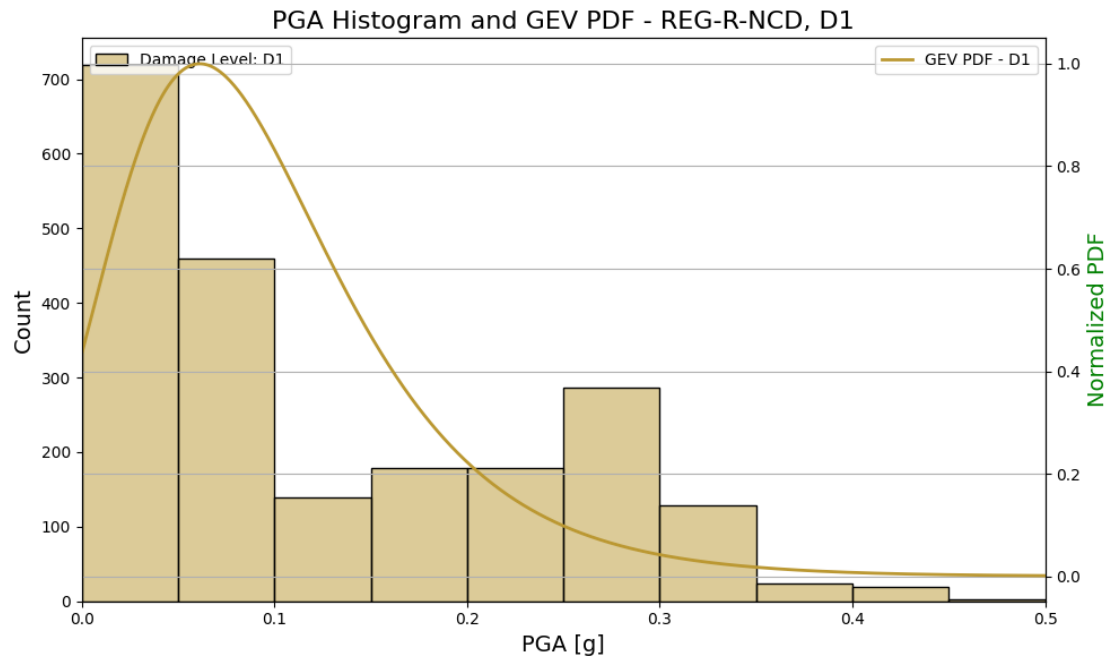
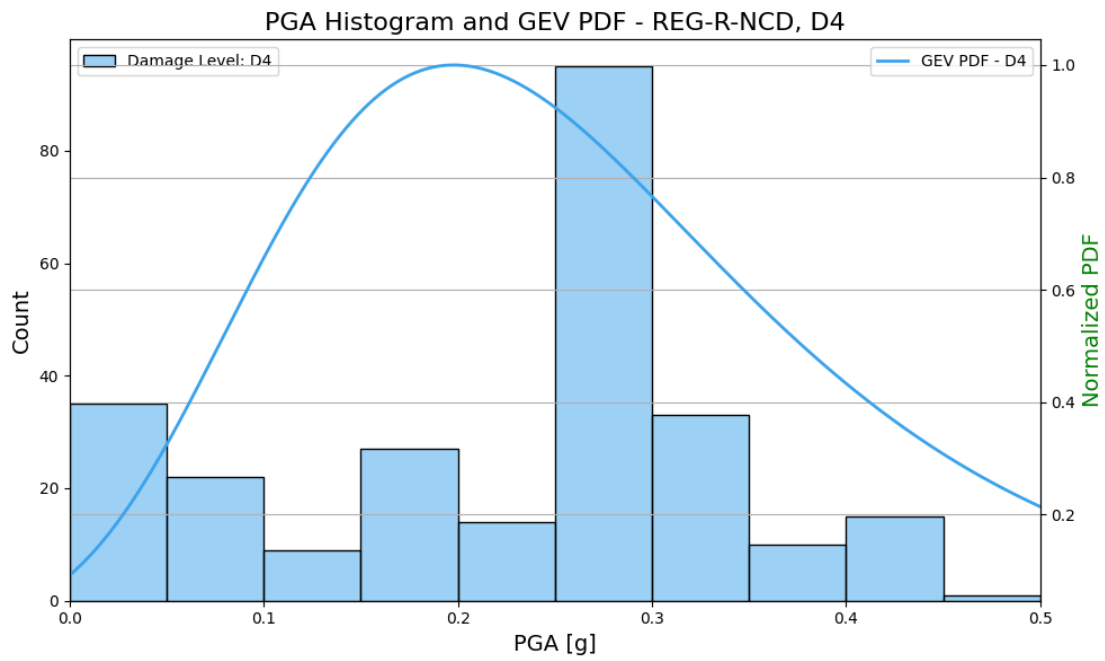
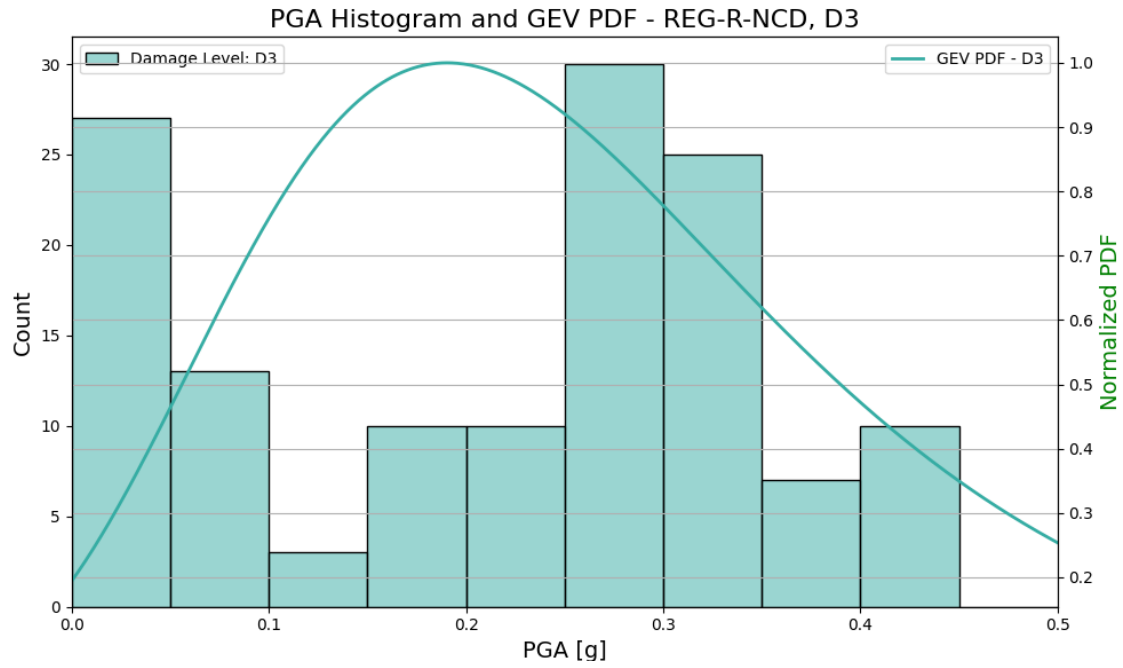


Figure 67. GEV distribution for REG-F-NCD masonry buildings across all damage levels





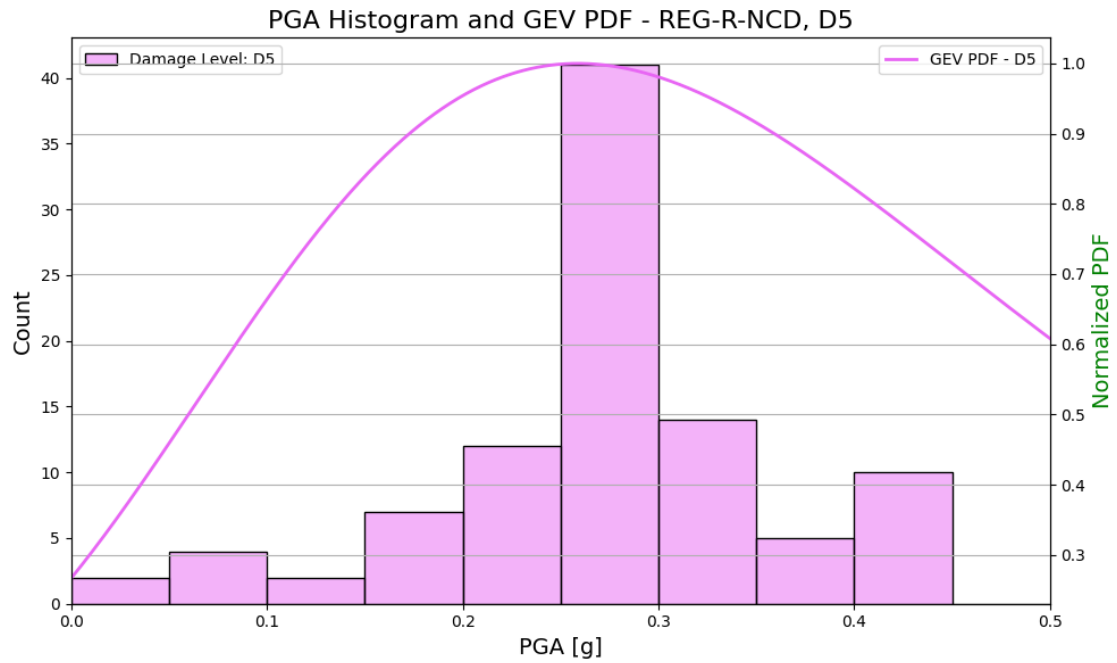
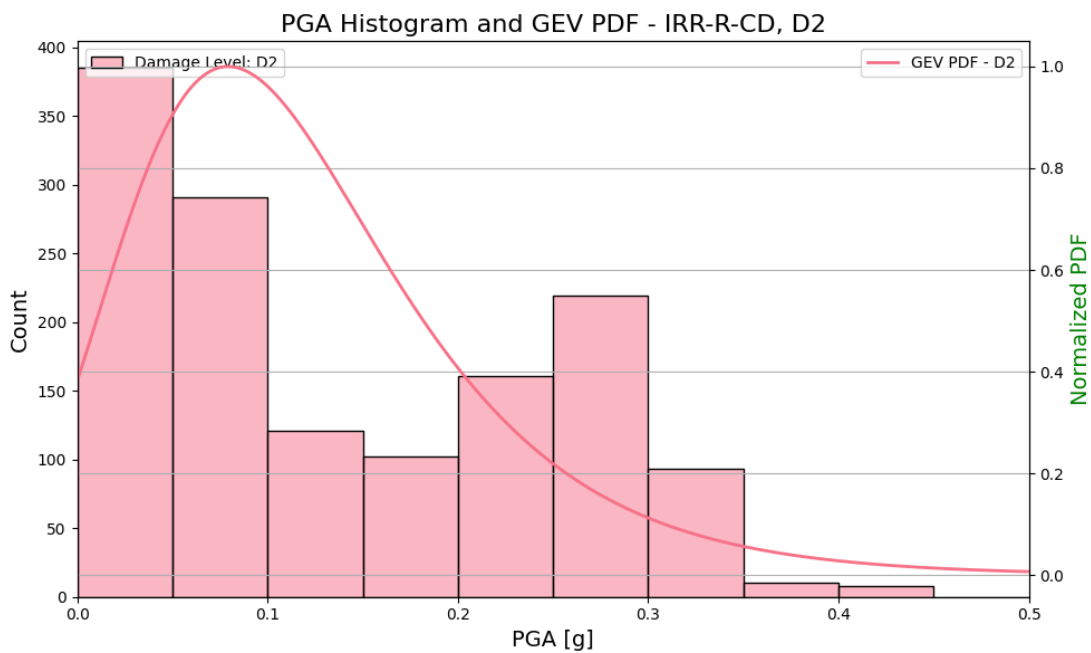
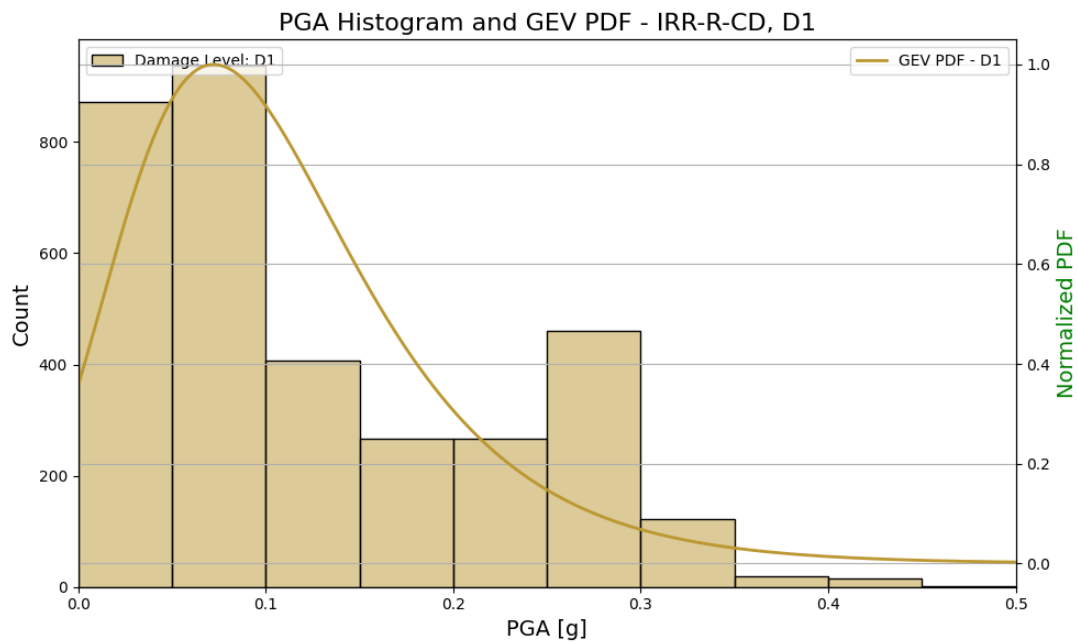
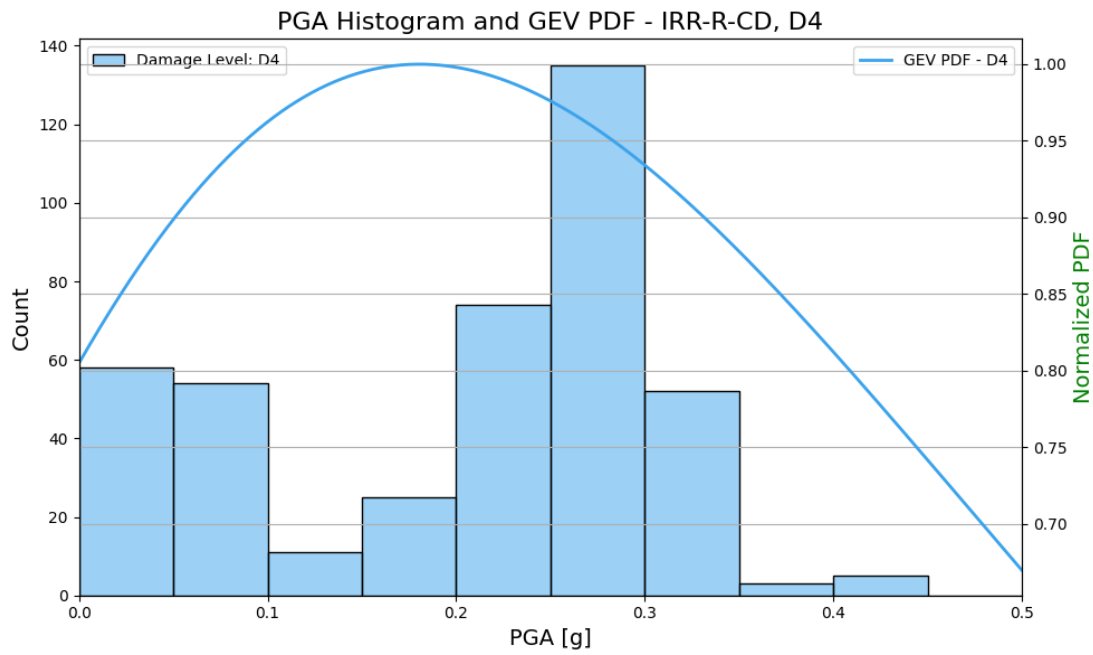
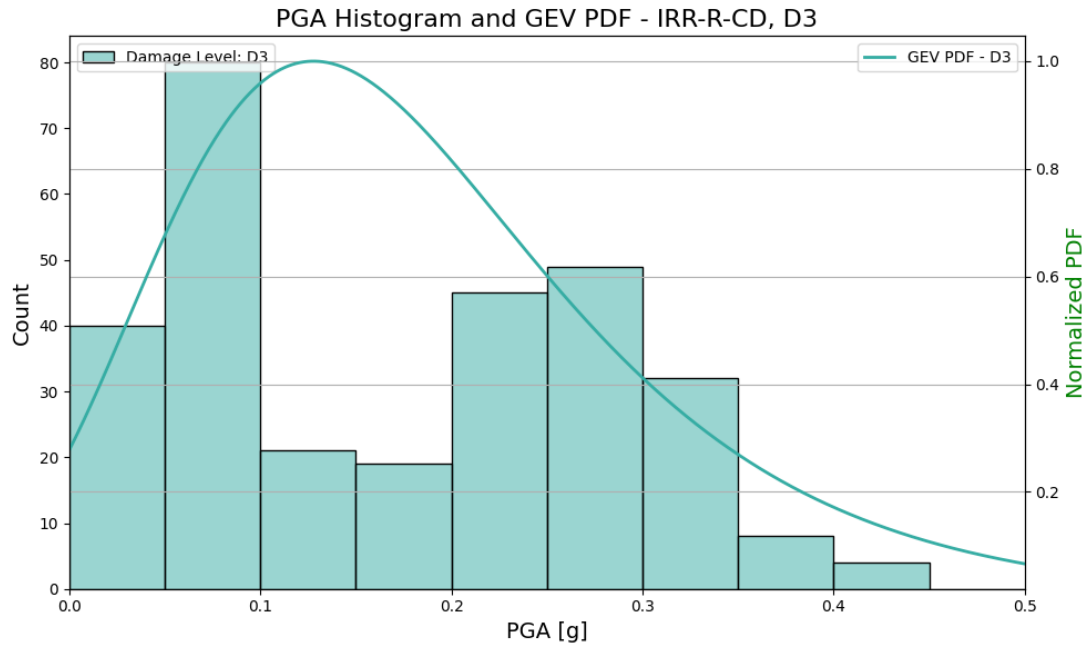


Figure 68. GEV distribution for REG-R-NCD masonry buildings across all damage levels





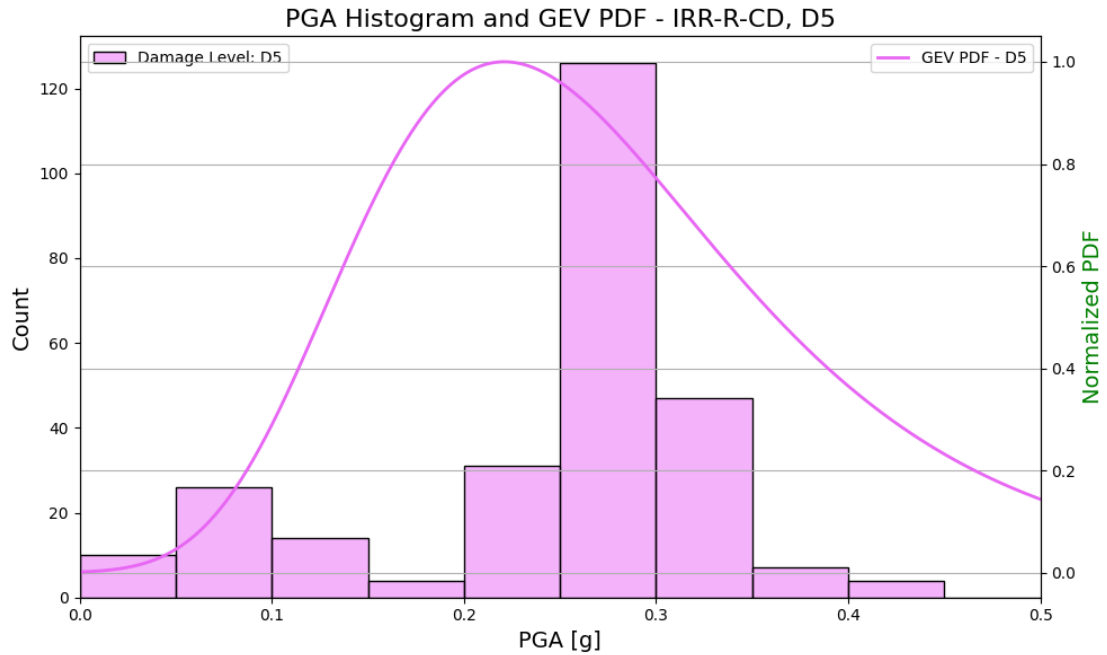
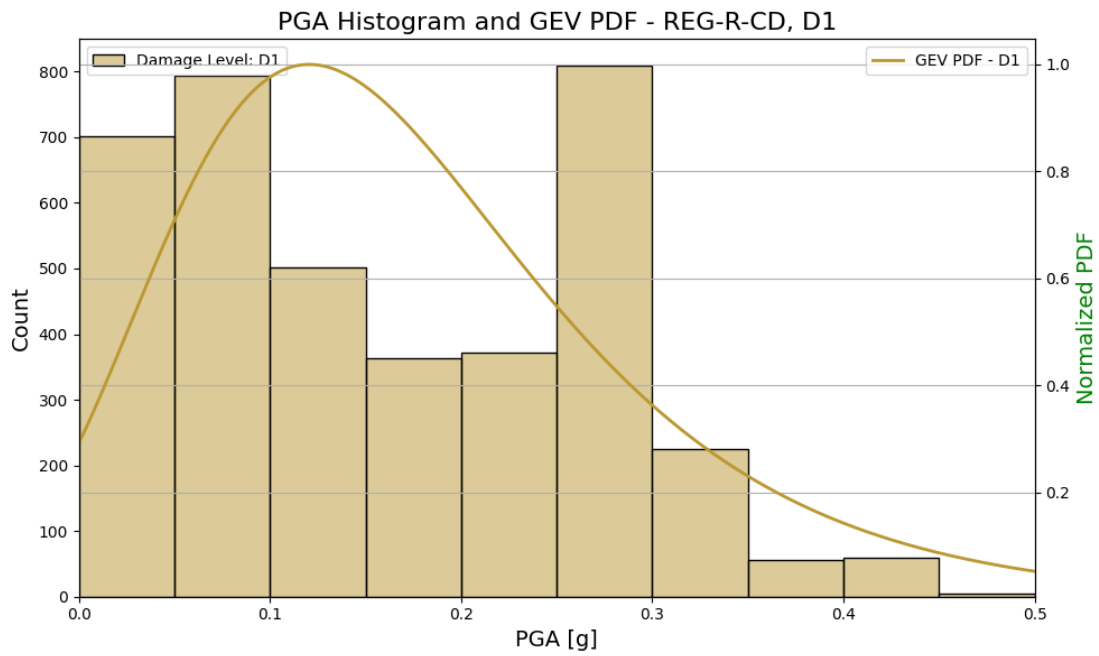
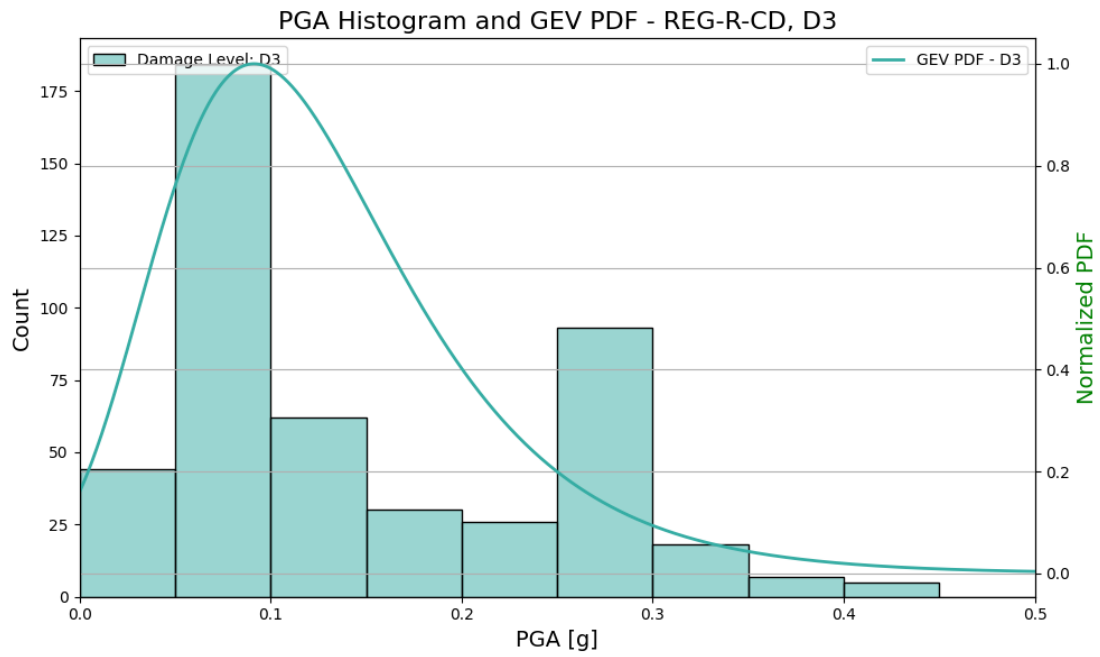
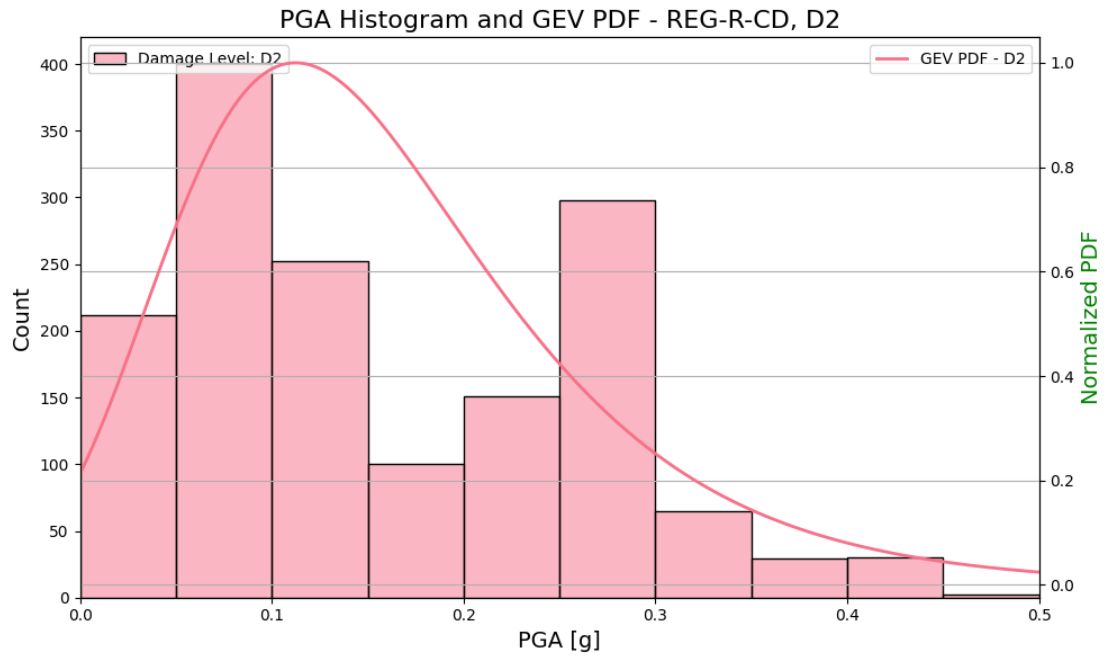


Figure 69. GEV distribution for IRR-R-CD masonry buildings across all damage levels





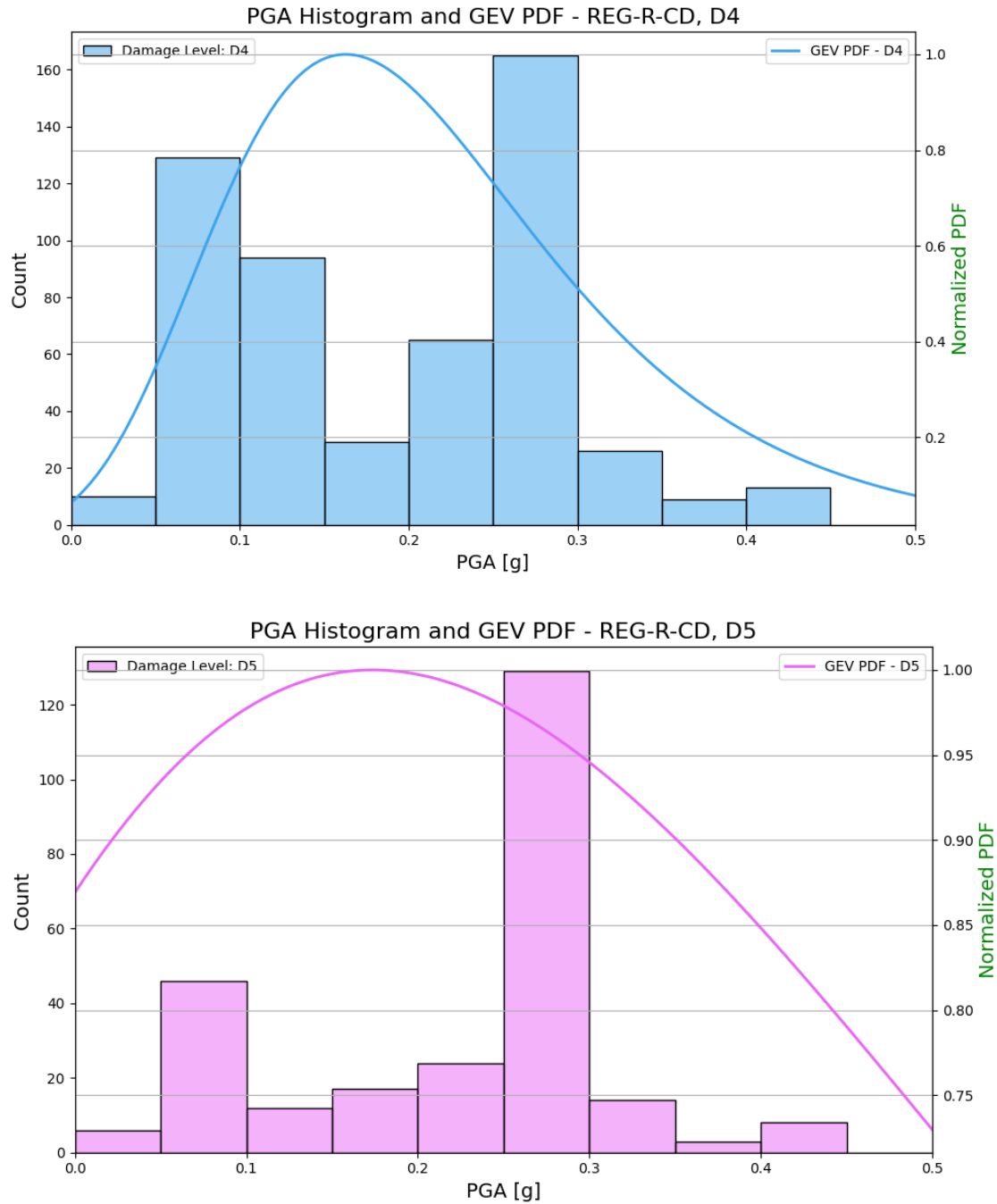


Figure 70. GEV distribution for REG-R-CD masonry buildings across all damage levels

The figures below show the Cumulative Distribution Function (CDF) of the Generalized Extreme Value (GEV) distribution, presented as an updated alternative to the CDF of the lognormal distribution.

For concrete buildings:

Cumulative Probability for Shape Parameter $\xi = -0.5$

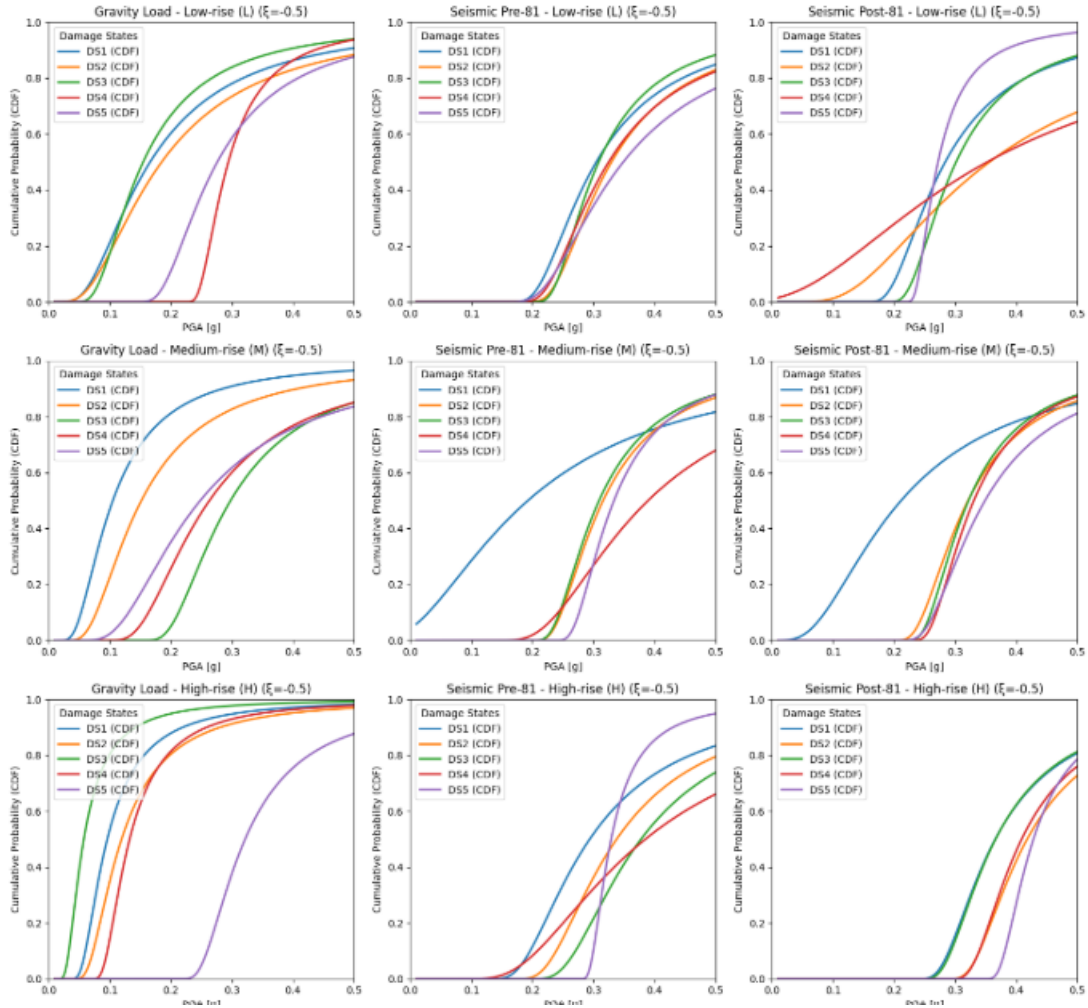


Figure 71. Cumulative distribution functions (CDFs) of the GEV distribution for concrete buildings with shape parameter $\xi = -0.5$

Cumulative Probability for Shape Parameter $\xi=0$

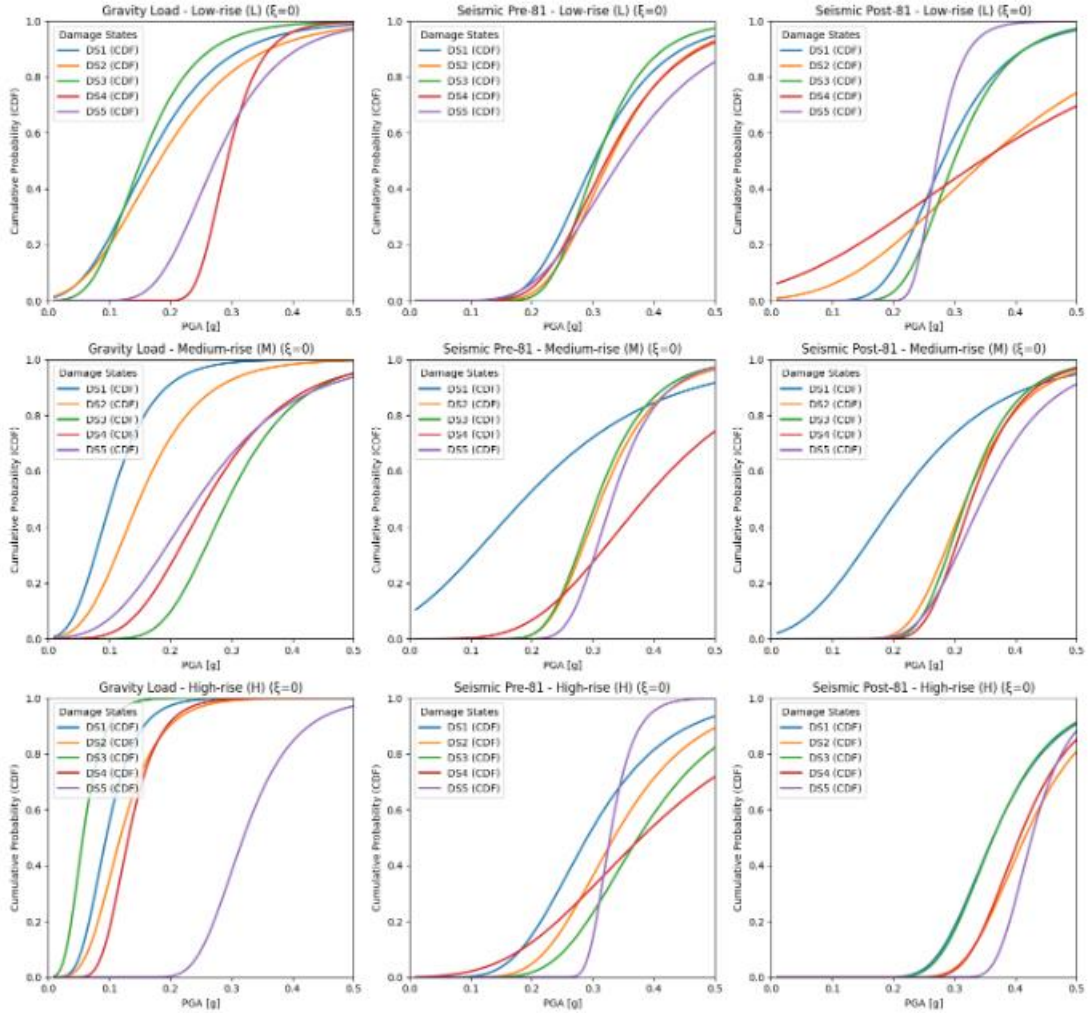


Figure 72. Cumulative distribution functions (CDFs) of the GEV distribution for concrete buildings with shape parameter $\xi = 0$

Cumulative Probability for Shape Parameter $\xi=0.5$

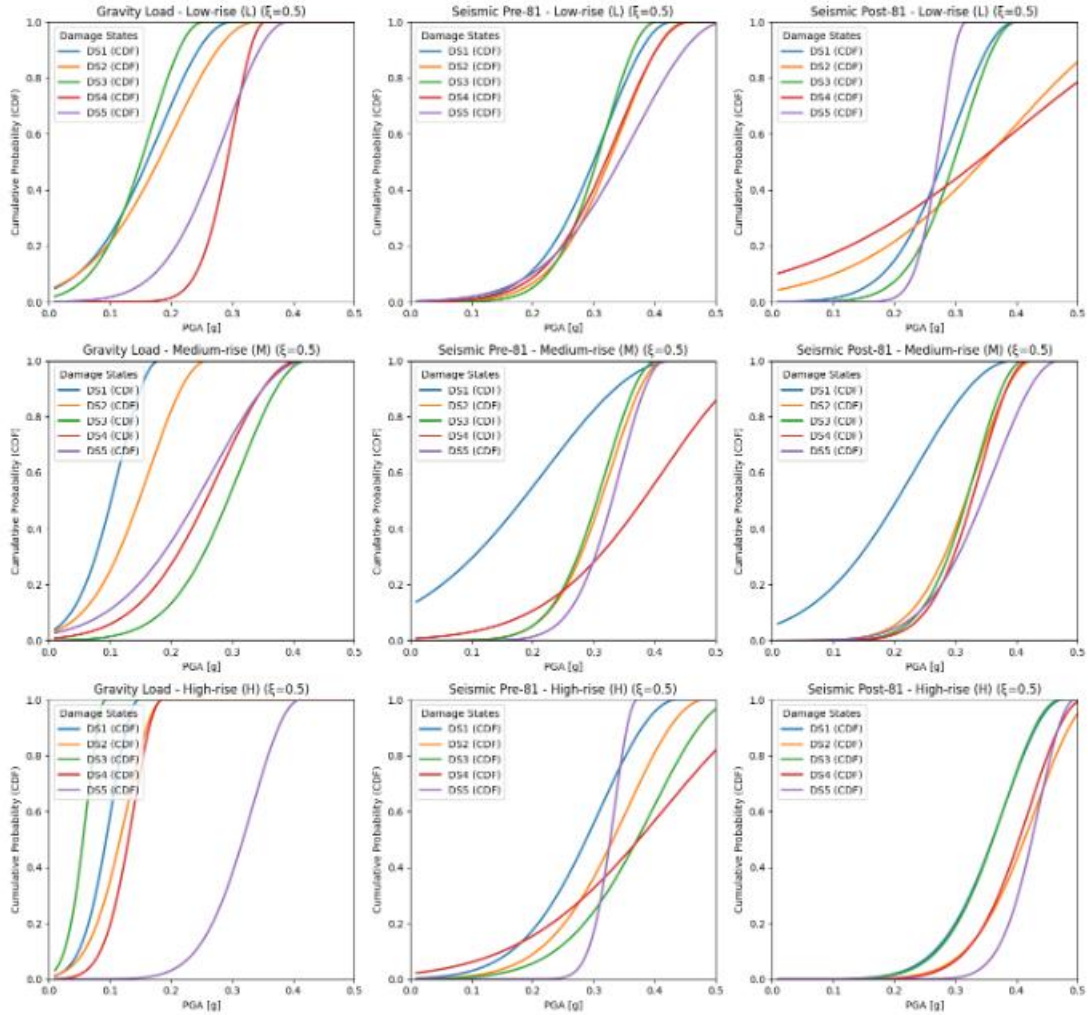


Figure 73. Cumulative distribution functions (CDFs) of the GEV distribution for concrete buildings with shape parameter $\xi = 0.5$

Several inconsistencies were observed in the original figures. For example, some CDF curves crossed over one another or did not follow the expected order based on damage severity. In a well-structured model, higher damage levels should consistently correspond to lower probabilities at

any given input value, since severe damage is less common. These irregularities pointed to possible issues in the underlying calculations.

One likely cause of these issues was the limited amount of input data. Small datasets can lead to highly variable results for the GEV distribution, making parameter estimates unstable or exaggerated. This can produce unrealistic or misleading outputs, as evident in some earlier plots.

The methodology was refined to address these problems. The input data was carefully reviewed, parameter estimation techniques were improved, and greater consistency was ensured across datasets. These changes were made to improve the CDF curves' reliability and readability.

The revised figure below shows the updated GEV and lognormal distributions CDFs. It highlights the improvements made, offering a clearer and more accurate representation.

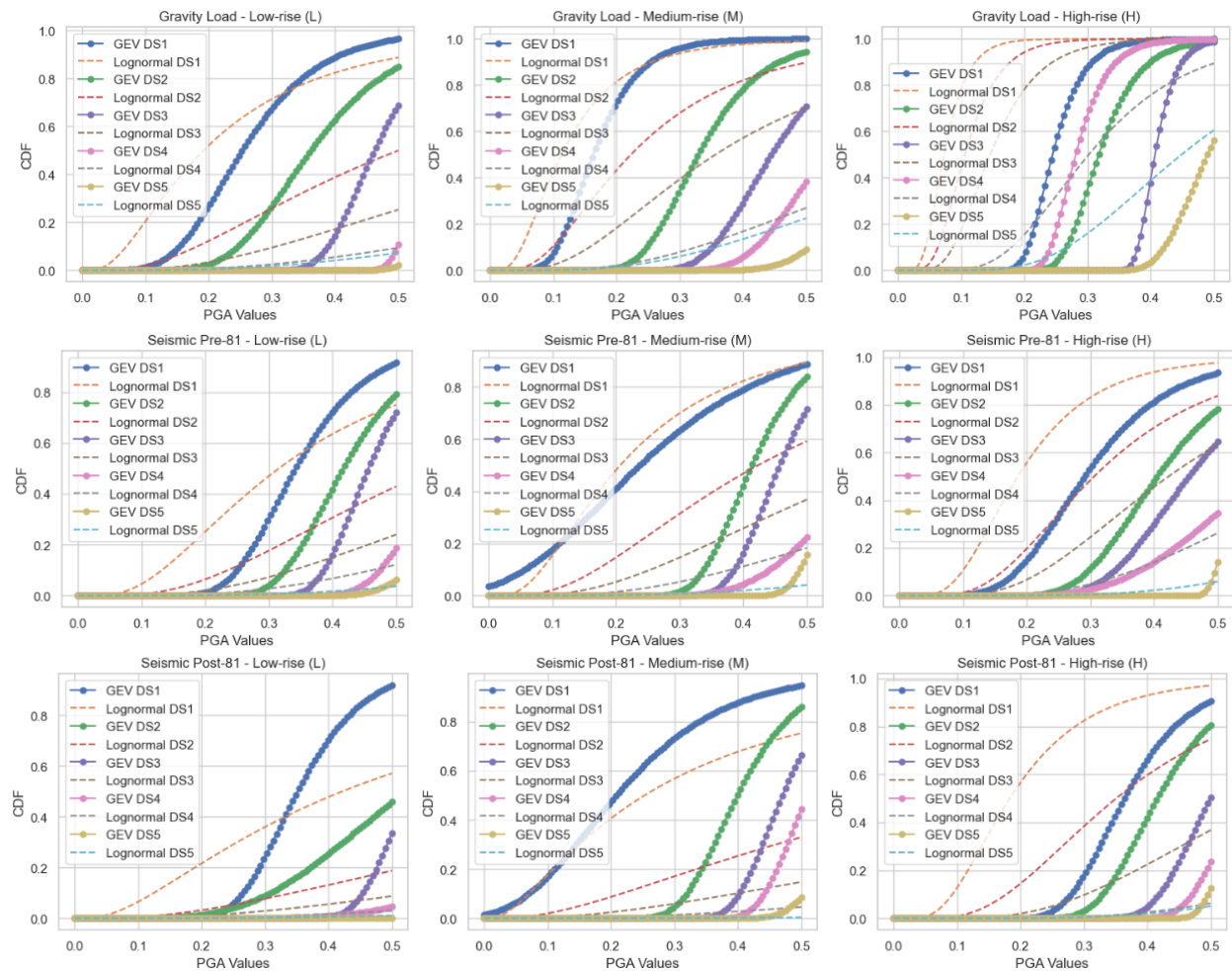


Figure 74. Adjusted Generalized Extreme Value (GEV) and lognormal CDFs for concrete buildings

In most cases, the GEV curves tend to rise earlier than the lognormal ones. This means that the GEV model usually predicts a higher chance of damage at lower ground shaking levels. This difference is especially noticeable in the lower damage states like DS1 and DS2, where the GEV curve often increases sooner and more steeply than the lognormal.

The updated plots show that the GEV model tends to be more conservative and responsive, especially as damage levels increase. While both models reflect the expected progression from light to severe damage, the GEV distribution better captures how quickly vulnerability can grow as seismic intensity increases. This makes it especially useful for identifying risk in more fragile or poorly designed buildings, or in situations where a more cautious assessment is needed.

For masonry buildings:

After analyzing GEV behavior in RC buildings, I applied it to masonry typologies. Since masonry is more irregular and damage-prone, it is important to see how the model behaves when the shape parameter (ξ) changes.

Cumulative Probability for Shape Parameter $\xi = -0.5$

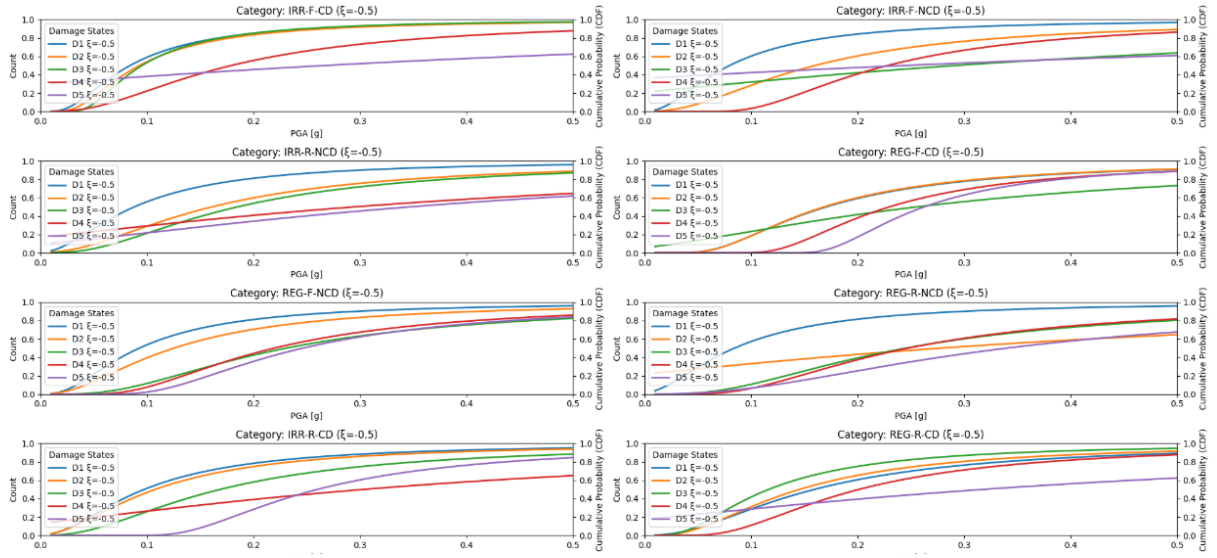


Figure 75. Cumulative distribution functions (CDFs) of the GEV distribution for masonry buildings with shape parameter $\xi = -0.5$

Cumulative Probability for Shape Parameter $\xi = 0$

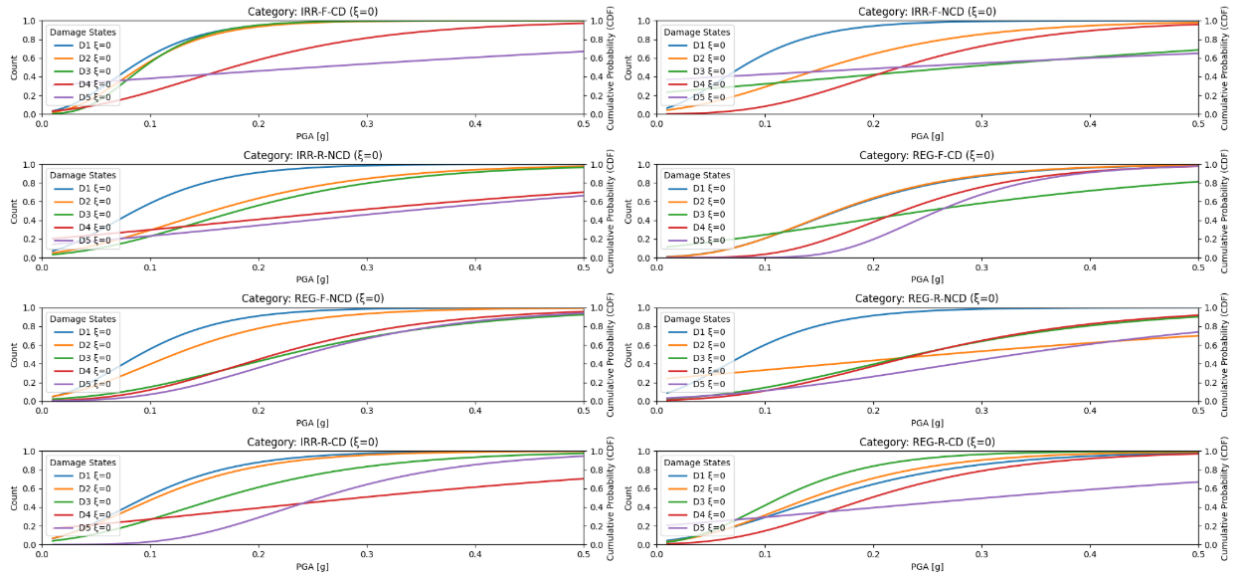


Figure 76. Cumulative distribution functions (CDFs) of the GEV distribution for masonry buildings with shape parameter $\xi = 0$

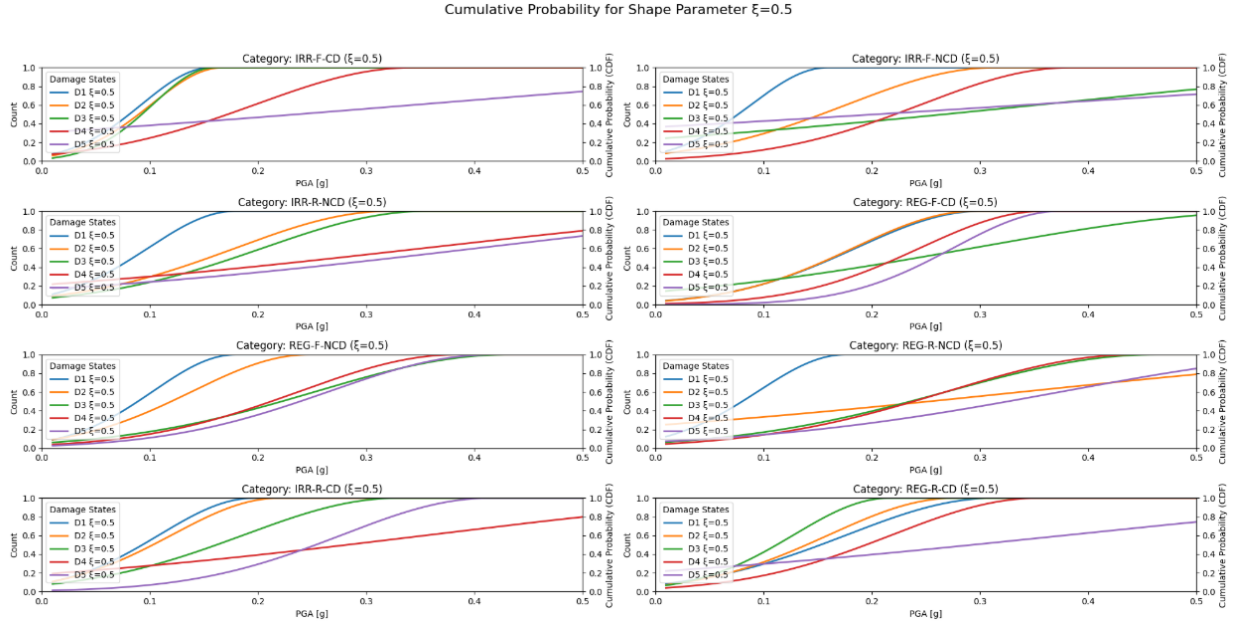


Figure 77. Cumulative distribution functions (CDFs) of the GEV distribution for masonry buildings with shape parameter $\xi = 0.5$

In the earlier CDF plots for masonry buildings using the GEV distribution, there were several problems. Some of the curves crossed each other or did not follow the correct order of damage levels. Normally, we expect more severe damage states to have lower probabilities at any given PGA value, since they happen less often. When this order is not followed, it suggests something went wrong with the calculations or the data.

One of the main reasons for these problems was the limited amount of input data. The GEV distribution is sensitive to how much data you have, and when the dataset is small or unbalanced, the model can give unstable or unrealistic results. This was visible in some plots where the curves were not smooth or did not make sense.

We improved the data and the method used to estimate the GEV parameters to fix this. The input data was cleaned more carefully, and the fitting process was made more stable.

The figure below illustrates the refined CDFs for the GEV and lognormal distributions for masonry structures, showcasing adjustments made to enhance accuracy and address inconsistencies observed in the initial calculations. These refinements provide a more accurate representation of the distributions specific to masonry buildings.

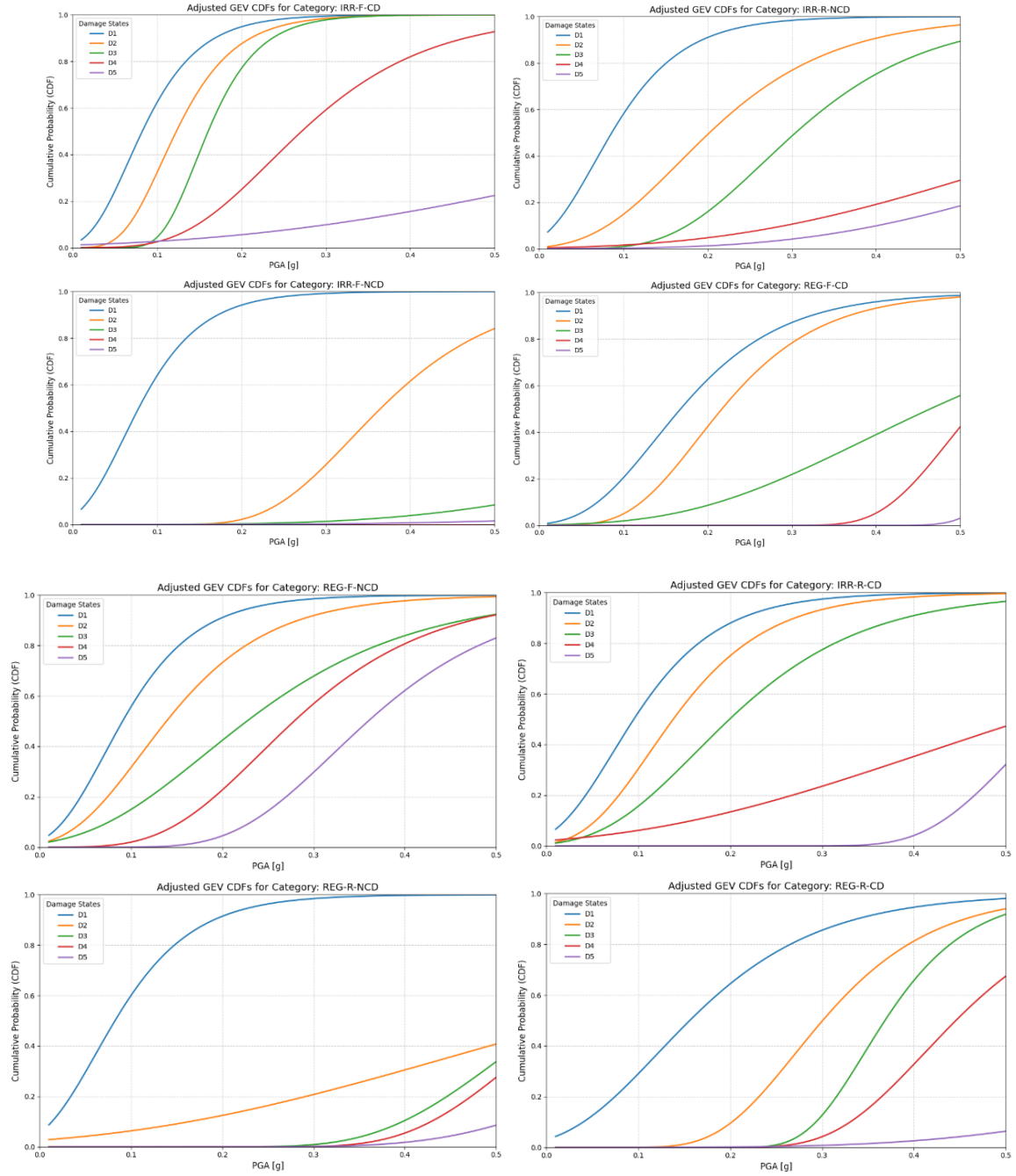


Figure 78. Adjusted Generalized Extreme Value (GEV) for masonry buildings

Study case

Torino is in an area with seismic activity, so assessing how well its buildings can handle earthquakes is important. This study examines the city's buildings to understand their vulnerability and create fragility curves based on local structural and environmental factors. Fragility curves help estimate the chance of damage to buildings at different earthquake strengths, making them useful tools for planning and risk reduction.

Modelling

The dataset includes important details about buildings in Torino, such as construction year, number of floors, location, and structural features. These factors are essential for understanding how buildings might respond to earthquakes and for creating reliable vulnerability models. However, because detailed structural data were limited, all buildings were grouped under the reinforced concrete category. While this simplification may reduce accuracy, it was a necessary step to organize and filter the data effectively.

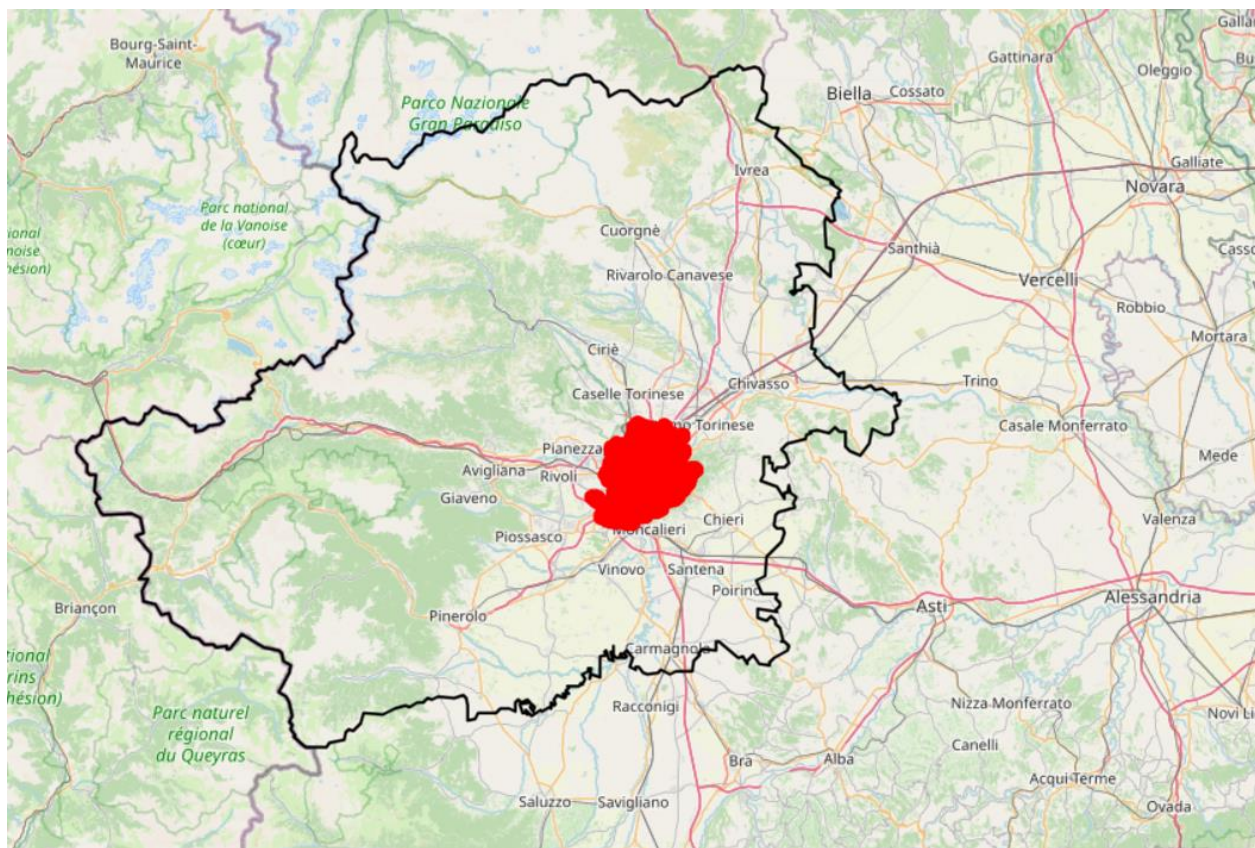


Figure 79. Building location distribution in Torino and Piemonte, Italy

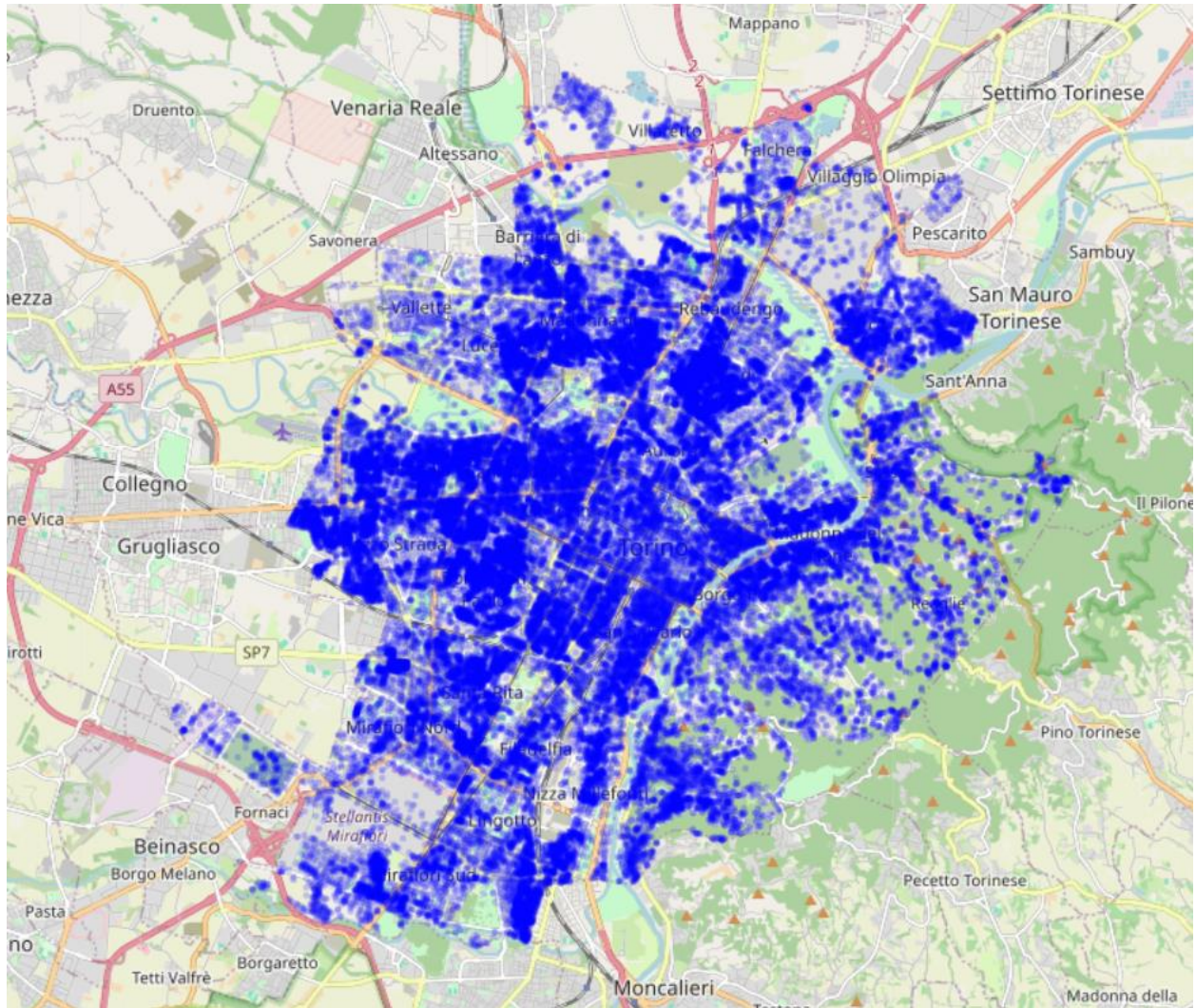


Figure 80. Map of input building data across Torino, Italy, showing spatial distribution of surveyed structures used in the analysis

To categorize the buildings, we can organize the results for each category as follows:

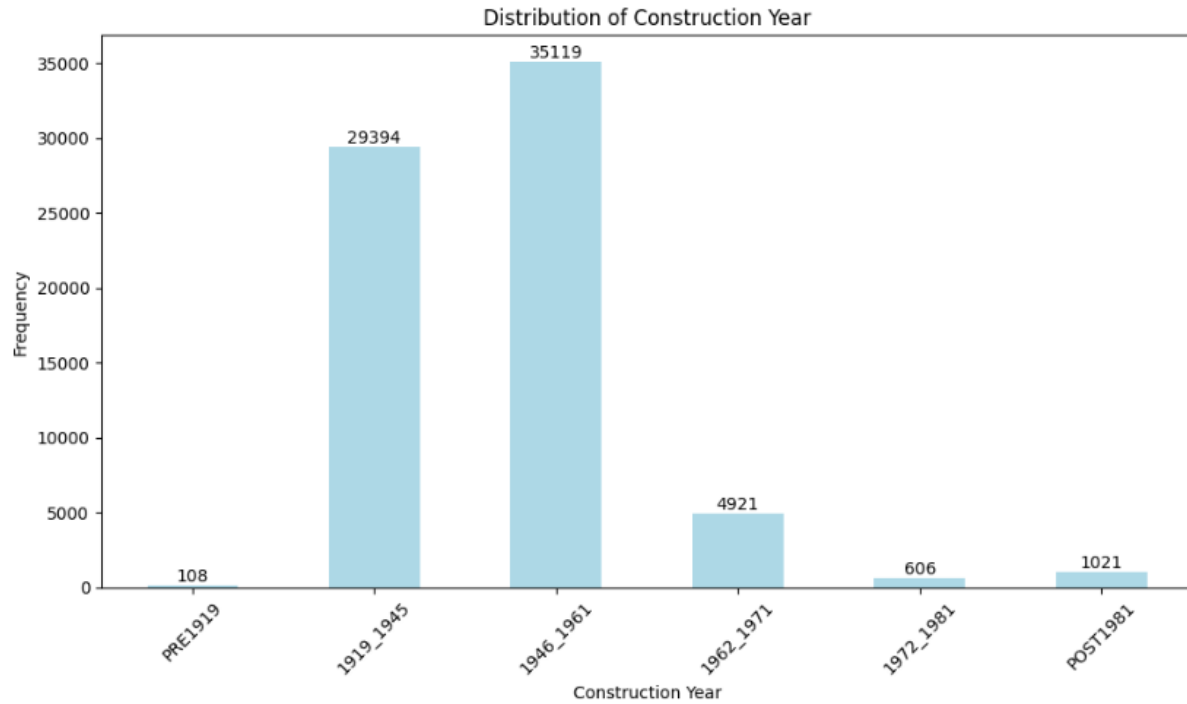


Figure 81. Torino construction year distribution based on the percentage of surveyed buildings

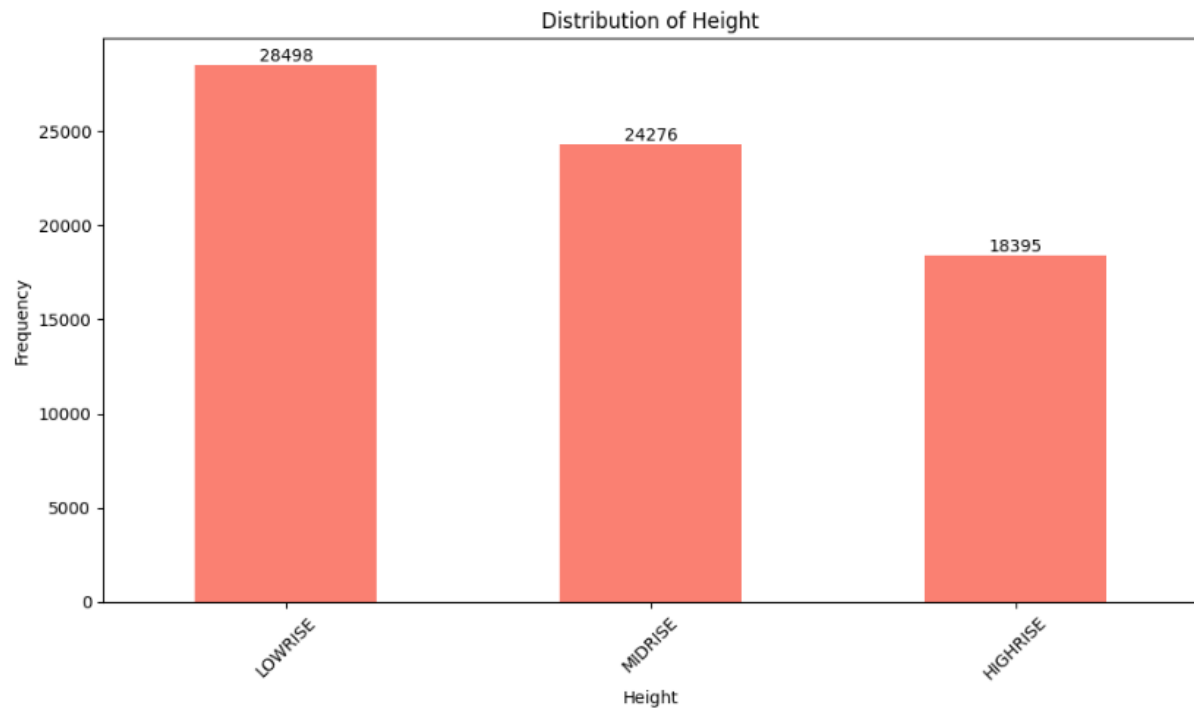


Figure 82. Torino building height distribution by percentage of low-, medium-, and high-rise structures

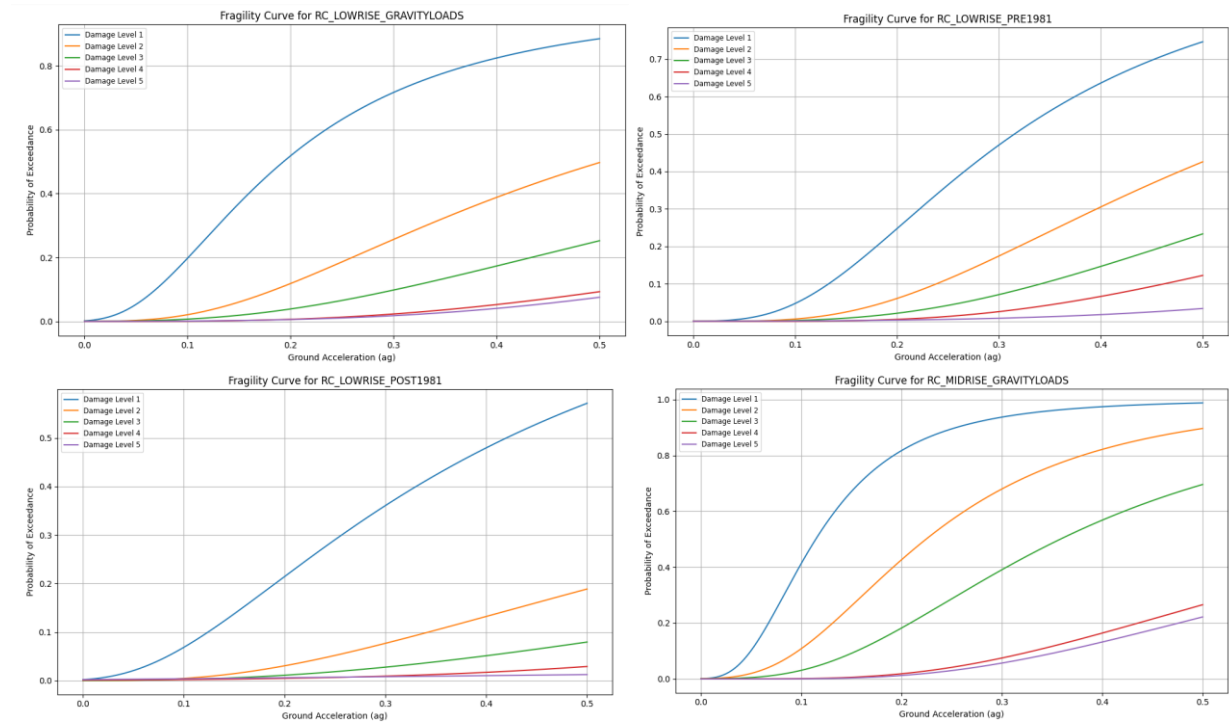
Different categories in the evaluation of the Torino data are presented:

Material	Building Class	Design Level
RC	LOWRISE	GRAVITYLOADS
		PRE1981
		POST1981
	MIDRISE	GRAVITYLOADS
		PRE1981
		POST1981
	HIGHRISE	GRAVITYLOADS
		PRE1981
		POST1981

Table 2. Different categories in the evaluation of the Torino data

Fragility curves

This study aims to develop fragility curves for the Torino to improve the accuracy of seismic risk assessments. This process involves using advanced statistical models—specifically the Generalized Extreme Value (GEV) distribution—and detailed data on the city’s building characteristics and seismic activity. The results will help shape risk reduction strategies, guide building retrofits, and support urban planning efforts to make Torino more resilient to future earthquakes.



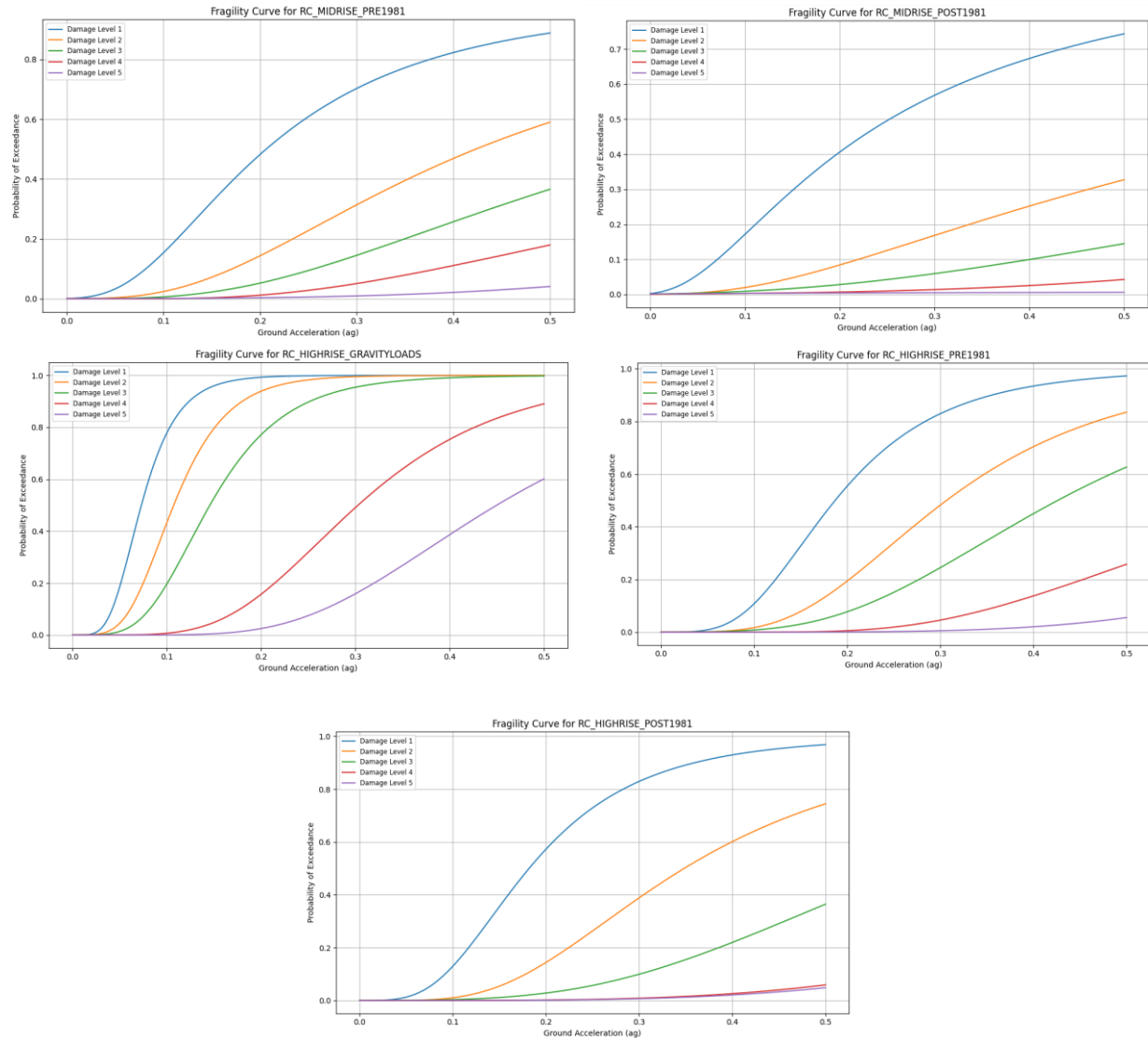


Figure 83. Fragility curves of Torino using the Generalized Extreme Value (GEV) distribution for reinforced concrete (RC) buildings across all heights, design levels, and damage levels

Conclusion

This study explored seismic vulnerability in a structured and practical way, focusing on developing accurate fragility curves to better understand how buildings respond to earthquakes. By using detailed datasets from Italy—particularly from the Da.D.O. platform—and applying advanced methods, the research produced fragility models tailored to different building types and local seismic conditions.

The Generalized Extreme Value (GEV) distribution was a major advancement. Compared to traditional lognormal models, the GEV distribution is better at capturing the likelihood of extreme damage, especially in high-risk scenarios. This improves the reliability of damage predictions and supports more informed decision-making.

The main contributions of this study include:

- Use of Real Data:

The models are based on actual damage data from post-earthquake surveys, which helps reduce uncertainty and makes the results more practical and applicable.

- Policy Support:

Fragility curves developed in this study can guide retrofitting priorities, help allocate resources effectively, and improve community resilience in earthquake-prone areas.

The case study of Torino showed how this approach works in a real-world setting, highlighting its flexibility and relevance for different urban environments.

Future research could build on this work by including more complex factors such as soil-structure interaction, real-time seismic monitoring, and the combined impact of multiple hazards. These additions would improve the accuracy of fragility models and support stronger, more resilient infrastructure planning worldwide.

References

- Banerjee, S, A Das, and R Roy. 2022. "A Probabilistic Framework for Fragility Curve Generation Using Numerical Simulation." *Engineering Structures* 254: 113832. <https://doi.org/10.1016/j.engstruct.2021.113832>.
- Baylon, Michael B, Maria Emilia P Sevilla, Miller D L Cutora, Rikki Mae S Villa, Princess Mherlene P Reynes, and Jhona May V Montemayor. 2022. "Development of Fragility Curves for Seismic Vulnerability Assessment : The Case of Philippine General Hospital Spine Building" 2 (4): 1–11.
- Bernardini, A, M Dolce, and A. Goretti. 2010. "Development of the Italian Damage Database: IRMA." *Bulletin of Earthquake Engineering* 8 (5): 1209–29.
- Caruso, M, M Di Ludovico, and A Prota. 2023. "Comparing Generic and Site-Specific Fragility Curves for Reinforced Concrete Buildings." *Engineering Structures* 277: 115527. <https://doi.org/10.1016/j.engstruct.2022.115527>.
- Cheikh, B. 1992. "Inelastic Response and Ductility Demand of Structures," no. 1991.
- Chopra, Anil K, and Chatpan Chintanapakdee. 2001. "Drift Spectrum vs. Modal Analysis of Structural Response to Near-Fault Ground Motions." *Earthquake Spectra* 17 (2): 221–34. <https://doi.org/10.1193/1.1586173>.
- Coles, Stuart. 2001. *An Introduction to Statistical Modeling of Extreme Values*. Springer. <https://doi.org/10.1007/978-1-4471-3675-0>.
- Commission, U S Nuclear Regulatory, Biswajit Dasgupta, and San Antonio. 2017. "EVALUATION OF METHODS USED TO CALCULATE Prepared for Biswajit Dasgupta Center for Nuclear Waste Regulatory Analyses San Antonio , Texas," no. May.
- Crowley, Helen, Rui Pinho, and Julian J Bommer. 2004. "A Probabilistic Displacement-Based Vulnerability Assessment Procedure for Earthquake Loss Estimation." *Bulletin of Earthquake Engineering* 2 (2): 173–219. <https://doi.org/10.1007/s10518-004-2290-8>.
- Elaiwi, Lect Sahar. 2023. "Structures A Review Article on the Performance Based Seismic Design of Structures Lect . Reem Hatem Ahmed.
- Everitt, B S, and A Skron dal. 2010. "Lognormal Distribution." In *The Cambridge Dictionary of Statistics*, 4th ed. Cambridge University Press. https://link.springer.com/10.1007/978-3-030-85040-1_441.
- Gaudio, C Del, P Ricci, G M Verderame, and G Manfredi. 2020. "Soil-Structure Interaction Effects on Seismic Fragility of Existing RC Buildings." *Soil Dynamics and Earthquake Engineering* 133: 106106.
- Haan, Laurens de, and Ana Ferreira. 2007. *Extreme Value Theory: An Introduction*. Springer. <https://doi.org/10.1007/978-0-387-34471-3>.
- Johnson, Norman L, Samuel Kotz, and N Balakrishnan. 1994. *Continuous Univariate Distributions, Volume 1*. 2nd ed. Wiley Series in Probability and Mathematical Statistics: Applied Probability and Statistics. New York: John Wiley & Sons.

- Khatiwada, Prashidha, Yiwei Hu, Elisa Lumantarna, and Scott J Menegon. 2023. "Dynamic Modal Analyses of Building Structures Employing Site-Specific Response Spectra Versus Code Response Spectrum Models." *CivilEng*. <https://doi.org/10.3390/civileng4010009>.
- Lee, Michael W., Teresa R. Johnson, and Jonathan Kibble. 2017. "Development of Statistical Models to Predict Medical Student Performance on the USMLE Step 1 as a Catalyst for Deployment of Student Services." *Medical Science Educator* 27 (4): 663–71. <https://doi.org/10.1007/s40670-017-0452-y>.
- Lucantoni, A, M Dolce, and C Moroni. 2001. "Fragility Curves for Masonry and RC Buildings Based on Damage Data." *Journal of Earthquake Engineering* 5 (S1): 201–18.
- Masi, Angelo, Sergio Lagomarsino, Mauro Dolce, and Vincenzo Manfredi. 2021. *Towards the Updated Italian Seismic Risk Assessment : Exposure and Vulnerability Modelling. Bulletin of Earthquake Engineering*. Vol. 19. Springer Netherlands. <https://doi.org/10.1007/s10518-021-01065-5>.
- Milutinovic, Z V, G Trendafiloski, and F Scherbaum. 2018. "Standardized Seismic Fragility Functions for European Buildings." *European Journal of Structural Engineering* 45 (3): 245–61.
- Nabilah, Abu Bakar, Raudhah Ahmadi, Noor Sheena Herayani Harith, Azlan Adnan, and Meldi Suhatri. 2023. "Development of Elastic Design Response Spectra with Emphasis on Far-Source Earthquakes for Low to Moderate Seismic Region." *Asian Journal of Civil Engineering* 24 (6): 1747–60. <https://doi.org/10.1007/s42107-023-00600-w>.
- "National Disaster Risk Reduction and Management Plan (NDRRMP)." 2011.
- Naumovski, Luka, Slovenian National Building, Slovenian National Building, Slovenian National Building, and Matija Gams. 2023. "PUSHOVER-BASED FRAGILITY ANALYSIS OF MULTI-STOREY CROSS- LAMINATED TIMBER PLATFORM-TYPE BUILDINGS," no. September.
- Park, Sung Y, and Anil K Bera. 2009. "Maximum Entropy Autoregressive Conditional Heteroskedasticity Model." *Journal of Econometrics* 150 (2): 219–30. <https://doi.org/10.1016/j.jeconom.2008.12.014>.
- Pasquale, G Di, G Orsini, and R W Romeo. 2005. "New Developments in Seismic Risk Assessment in Italy." *Earthquake Spectra* 21 (S1): 209–20.
- Rohmer, Jeremy, Pierre Gehl, Marine Marcilhac-fradin, Yves Guigueno, Nadia Rahni, Julien Clément, C Guillemin, and Orléans Cedex. 2020. "Non-Stationary Extreme Value Analysis Applied to Seismic Fragility Assessment for Nuclear Safety Analysis," 1267–85.
- Rosti, A, C Del Gaudio, M Rota, P Ricci, M Di Ludovico, A Penna, and G M Verderame. 2021. "Empirical Fragility Curves for Italian Residential RC Buildings." *Bulletin of Earthquake Engineering* 19 (8): 3165–83. <https://doi.org/10.1007/s10518-020-00971-4>.
- Rosti, Annalisa, Maria Rota, and Andrea Penna. 2021. "Empirical Fragility Curves for Italian URM Buildings." *Bulletin of Earthquake Engineering* 19 (8): 3057–76. <https://doi.org/10.1007/s10518-020-00845-9>.

- Rota, Maria, Andrea Penna, Claudio Luciano Strobbia, and Guido Magenes. 2011. "Typological Seismic Risk Maps for Italy Typological Seismic Risk Maps for Italy," no. May 2014. <https://doi.org/10.1193/1.3609850>.
- Shahi, Shrey K, and Jack W Baker. 2011. "An Empirically Calibrated Framework for Including the Effects of Near-Fault Directivity in Probabilistic Seismic Hazard Analysis." *Bulletin of the Seismological Society of America* 101 (2): 742–55. <https://doi.org/10.1785/0120100090>.
- Shao, Weiyi. 2024. "Derivation of Response Spectra and Hysteretic Energy: A Case Study on 2023 Turkey-Syria Earthquake in Consideration of Structural Ductility BT - Proceedings of the 3rd International Civil Engineering and Architecture Conference." In , edited by Marco Casini, 399–408. Singapore: Springer Nature Singapore.
- Silva, Vitor. 2014. "Development of the OpenQuake Engine , the Global Earthquake Model ' s Open- Source Software for Seismic Risk Assessment," no. May. <https://doi.org/10.1007/s11069-013-0618-x>.
- Wang, X, J Zhang, and H Li. 2024. "Ordinal Regression-Based Fragility Modeling of Bridge Structures Using Wenchuan Earthquake Data." *Earthquake Engineering & Structural Dynamics* 53 (2): 312–28. <https://doi.org/10.1002/eqe.3852>.
- Weisstein, Eric W. n.d. "Log Normal Distribution."
- Wikipedia contributors. n.d. "Log-Normal Distribution."
- Zentner, I, A Nadjarian N Humbert, and E Viallet. 2008. "NUMERICAL CALCULATION OF FRAGILITY CURVES FOR PROBABILISTIC SEISMIC RISK ASSESSMENT."